NOTICE

The quality of this microform is heavily dependent upon the quality of the original thesis submitted for microfilming. Every effort has been made to ensure the highest quality of reproduction possible.

If pages are missing, contact the university which granted the degree.

Some pages may have indistinct print especially if the original pages were typed with a poor typewriter ribbon or if the university sent us an inferior photocopy.

Reproduction in full or in part of this microform is governed by the Canadian Copyright Act, R.S.C. 1970, c. C-30, and subsequent amendments.

AVIS

La qualité de cette microforme dépend grandement de la qualité de la thèse soumise au microfilmage. Nous avons tout fait pour assurer une qualité supérieure de reproduction.

S'il manque des pages, veuillez communiquer avec l'université qui a conféré le grade.

La qualité d'impression de certaines pages peut laisser à désirer, surtout si les pages originales ont été dactylographiées à l'aide d'un ruban usé ou si l'université nous a fait parvenir une photocopie de qualité inférieure.

La reproduction, même partielle, de cette microforme est soumise à la Loi canadienne sur le droit d'auteur, SRC 1970, c. C-30, et ses amendements subséquents.

Title/Titre

Mechanosensitive ion channels

in the freshwater snail, *Lymnaea stagnalis*

Name/Nom

Wade Johannes Sigurdson

Thesis submitted to

School of Graduate Studies and Research

in partial fulfillment of the requirements for the Ph.D.

degree in Biology

NOTICE

The quality of this microform is heavily dependent upon the quality of the original thesis submitted for microfilming. Every effort has been made to ensure the highest quality of reproduction possible.

If pages are missing, contact the university which granted the degree.

Some pages may have indistinct print especially if the original pages were typed with a poor typewriter ribbon or if the university sent us an inferior photocopy.

AVIS

La qualité de cette microforme dépend grandement de la qualité de la thèse soumise au microfilmage. Nous avons tout fait pour assurer une qualité supérieure de reproduction.

S'il manque des pages, veuillez communiquer avec l'université qui a conféré le grade.

La qualité d'impression de certaines pages peut laisser à désirer, surtout si les pages originales ont été dactylographiées à l'aide d'un ruban usé ou si l'université nous a fait parvenir une photocopie de qualité inférieure.

ISBN 0-315-60539-1

UNIVERSITÉ D'OTTAWA
UNIVERSITY OF OTTAWA

This thesis is dedicated to my family

and to the memory of Johann Johannes Sigurdson

Abstract

Mechano-sensitive ion channels in cells isolated from the heart and circumoesophageal ganglia of a freshwater snail (*Lymnaea stagnalis*) were characterized as K^+ selective and sensitive to changes in cell membrane tension. Using the technique of single-channel recording, stretch-activated K^+ (SAK) channels (30 pS in physiological saline) were shown to have complex permeation properties indicative of multi-ion channels. SAK channels were blocked by milli-molar quantities of quinidine or tetraethyl-ammonium and exhibited selectivity ($Tl^+ > K^+ > Rb^+ > Na^+ > Li^+$) properties seen in many other K^+ channels.

SAK channels described in *Lymnaea* ventricular cells or neuron somas and growth cones were activated (increased open probability, P_o) by increases in membrane tension produced by suction on the cell membrane. Stretch-activation was a reversible and repeatable phenomenon, associated with a reduction in a long closed time separating bursts of openings, rather than by an increase in the open time. The SAK channel's stretch-sensitivity was variable between patches, a finding attributable to the inability to accurately determine membrane tension. In spite of this, kinetic analysis of heart SAK channels established the presence of at least two open and three closed states. Similar analysis of neuron SAK channels indicated at least two open and four closed states. In channels from both cell types, only the long closed time constant (τ_{C4}, extracted from closed time frequency distributions) showed sufficient mechano-sensitivity to produce the observed increase in P_o with increasing membrane tension (in one patch, when P_o increased by a factor of 77 times the zero pressure P_o, τ_{C4} decreased by a factor of 22).

In spite of the absence of specific SAK channel antagonists, attempts were made to establish a physiological role for SAK channels. Neurons and heart cells were shown to be resistant to severe hyposmotic insults. Hyposmotic shock resulted in hyperpolarization of the neuron soma resting potential and activation of SAK channels. These results suggested that SAK channels may contribute to osmotic-swelling limitation.

SAK channels were found in developing neuron growth cones as well as the cell body. Channel characteristics were similar in both structures and circumstantial evidence points to expression of new SAK channels during neurite development.

A new type of mechano-sensitive K^+ channel was found to coexist with SAK channels in neuron cell bodies and growth cones. These channels were in-activated (SIK) by increases in membrane tension and possessed a greater stretch-sensitivity than SAK channels. Decreased P_o was found to result from the lengthening of the long closed time in a fashion analogous but opposite to that seen in SAK channels, thus implying a common transduction mechanism. The differing stretch-sensitivities combined with similar permeation properties (6.6 pS in physiological saline; selectivity sequence, $Tl^+ > K^+ > Rb^+ > Na^+$) suggested that membrane tension could control cell resting potential and thus modulate voltage-activated Ca^{2+} channels and therefore the influx of Ca^{2+}, a known regulatory ion. SIK and SAK channels could therefore provide a mechanism for linking Ca^{2+} influx to tension during axonal outgrowth.

Résumé

Les canaux ioniques méchano-sensibles de cellules isolées dans le coeur et les ganglions circum-oesophagiens chez le gastropode d'eau douce (*Lymnaea stagnalis*) ont été identifiés comme étant sélectifs à l'égard du K^+ et sensibles aux changements de la tension de la membrane cellulaire. A l'aide de la technique d'enregistrement au canal unique, on observe, pour les canaux ionique K^+ activés par étirement (SAK), une perméabilité (30 pS dans la solution physiologique) qui indique une nature multi-ionique. Bloqués par des quantités millimolaires de quinidine ou de tetraethylammonium, les canaux SAK ont montré une séquence de qu'on retrouve des nombreux de canaux K^+ ($Tl^+ > K^+ > Rb^+ > Na^+ > Li^+$).

Les canaux SAK décrits sont activés, dans les cellules ventriculaires, les neurones et les cônes d'agrandir de *Lymnaea*, par une augmentation de la tension membranaire (accroissement de la probabilité de l'état ouvert, P_o) produite par une succion exercée sur la membrane cellulaire. L'activation par étirement est un phénomène réversible, et reproduisible associé à une réduction de la longue durée de fermeture du canal entre les brèves périodes d'ouverture plutôt qu'à une augmentation de la durée d'ouverture du canal. La sensibilité des canaux SAK à l'étirement varie d'une plaque à l'autre, phénomenè attribuable à l'impossibilité de mesurer la tension membranaire de façon précise. Malgré tout, l'analyse cinétique des canaux SAK du coeur a mis en évidence la présence d'au moins deux états ouverts et trois états fermés. Une analyse semblable des canaux SAK des neurones indique la présence d'au moins deux états ouverts et quatre fermés. Dans les canaux des deux types cellulaires, seule la constante de la longue durée de fermeture (τ_{C4}, dérivée de la distribution des durées de fermeture) a fait

preuve d'une mécano-sensibilité suffisante pour produire l'augmentation de P_o observée ainsi que celle de la tension membrainaire (à une endroit précis, lorsque P_o s'est accru par un facteur de 77 fois la pression zéro P_o, τ_{C4} a diminué par un facteur de 22).

Malgré l'absence d'antagonistes spécifiques des canaux SAK, nous avons tenté d'établir le rôle physiologique de ces derniers. Les neurones et les cellules cardiaques se sont montrés résistants aux traumatismes hypo-osmotiques graves. Les chocs hypo-osmotiques ont causé l'hyperpolarization du potentiel de repos du neurone et l'activation des canaux SAK. Ceçi qui laisse supposer que les canaux SAK contribuent peut-être à limiter l'enflure par osmose.

Les canaux SAK se situent aussi bien dans les cônes de croissance des neurones en développement que dans leur corps cellulaire. Les caractéristiques des canaux sont semblables dans les deux structures et des signes montrent l'expression de nouveaux canaux SAK pendant le développement du neurite.

Un nouveau type de canal K^+ mécano-sensible coexiste avec les canaux SAK du corps cellulaire et du cône d'croissance des neurones. Ces canaux sont inactivés (SIK) par l'augmentation de la tension membranaire et possédent une sensibilité à l'étirement supérieure à celle des canaux SAK. Un P_o moindre résulte de prolomgement de la longue durée de fermeture de façon analogue mais opposée à celle observée dans les canaux SAK, suggérant un mécanisme de transduction commun. Les sensibilites à l'étirement différentes accompagnées de perméabilités semblables (6.6 pS dans la solution physiologique; séquence sélective $Tl^+ > K^+ > Rb^+ > Na^+$) suggérent que la tension membranaire pourrait contrôler le potentiel de repos de la cellule et

ainsi moduler les canaux Ca^{2+} activés, par le potentiel et donc l'influx de Ca^{2+}, ion regulateur reconnu. Les canaux SIK et SAK pourraient par conséquent fournir un mécanisme pour lier l'influx de Ca^{2+} à la tension durant la croissance axonale.

Acknowledgements

I would like to thank my supervisor Dr. Cathy Morris who has unfailingly inspired me to think "biophysical". The transformation was at times rocky, but is now complete thanks to Cathy's guidance. Cathy has given generously of her knowledge, time and especially patience during the course of this work; it is a debt I cannot repay. Again, thank you.

To the members of my advisory committee, Drs. S. Jacobson, M. McBurney, D. Parry and J.-L. Schwarz, I thank for their suggestions and encouragement.

I thank the members of my examining committee, Drs. D.R. Gardner, G. Mainwood, T. Moon, J.-L. Schwarz and S. Sims, for their careful reading of this thesis.

To all those inhabitants of the Cube, past and present, I owe a debt of thanks for making the Cube, the Cube. It's a great place to spend (do) time as a graduate student. In large part this atmosphere is the product of Drs. Tom Moon, Jim Fenwick and Steve F. Perry who have all contributed to my academic education (and hockey skills). I am grateful to have known and to have as colleagues the students and post-docs I've met here. To name but a few, Glenn, Doug, Richard, Madeleine, Elaine, Rick, Michele, Phil and Diane and Mike; you've all made my sojourn in Ottawa memorable.

Finally I thank Lynn, who has always been there, unselfishly giving comfort and support, more often than not while engaging the trials of her own career. I could not have completed this work without you nor would I have wanted to.

Table of Contents

List of Figures

List of Tables

List of Abreviations

Akaike information criterion	AIC
Conductance	g, pS
Differential interference contrast optics	DIC
Goldman, Hodgkin, Katz	GHK
Hyposmotic shock	HOS
Mean burst duraton 1 and 2	τ_{B1}, τ_{B2}
Mean closed times 1-4	τ_{C1}, τ_{C2}, τ_{C3}, τ_{C4}
Mean interburst duration	τ_{IB}
Mean open times 1 and 2	τ_{O1}, τ_{O2}
MilliVolts (10^{-3} volts)	mV
Normal saline	NS
Offset pressure	P_{off}
Open probability	P_O
Patch perfusion solution	PPS
Pressure	mmHg
PicoAmperes (10^{-12} amperes)	pA
PicoSiemens (10^{-12} siemens)	pS
Pipette potential	V_p
Probability density function	pdf
Regulatory volume decrease	RVD
Resting membrane potential	V_{rest}
Reversal potential	V_{rev}
Simulated intracellular saline	IS
Standard deviation	std
Standard error of the mean	sem

Standard error of the slope	ses
Stretch-activated	SA
Stretch-activated cation channel	SACat
Stretch-activated K^+ channel	SAK
Stretch-inactivated	SI
Stretch-inactivated K^+ channel	SIK
Tetraethylammonium	TEA
Transmembrane potential	V_m

Chapter 1

Introduction

Mechanical forces are pervasive in our environment, and are experienced at the cellular level by all organisms whether they be animals, plants, fungi or bacteria. External and internal (intracellular and extracellular) mechanical stimuli, can therefore be thought of as a source of information which organisms can use to monitor their external environment and internal physiological processes. Evolution seems to have made widespread "use" of this source of information by producing mechanosensory structures that sense and transduce mechanical energy into meaningful cellular signals. Insofar as these forces consist of pressure or tension changes exerted primarily on the cell membrane and associated cytoskeletal structures, a logical location for the transducing elements is in the cell membrane itself.

Exteroreception

External mechanical stimuli are an important source of environmental information made use of by all organisms. Paramecia use a mechanosensory mechanism for modulating membrane potential; the resultant changes in intracellular Ca^{2+} then alter ciliary beating thus affecting swimming behavior (Eckert, 1972). Higher organisms have developed exquisite senses of touch by using mechanosensory projections [eg. a cat's whiskers (Nier, 1975) or cockroach tactile hairs (French, 1985)] or pressure sensitive receptors embedded in the skin [eg. Pacinian corpuscles (Lowenstein and Skalak, 1966), Merkel disks and Meissner's corpuscles (Vierck, 1975)]. Vertebrate auditory structures employ mechanosensitive stereocilia on hair

cells to transduce air pressure differences into membrane potential changes that modulate neurotransmitter release (Howard et al., 1988; Corey and Hudspeth, 1979; Hudspeth and Corey, 1977). In a similar fashion, the vestibular apparatus in vertebrates uses the mechanoelectrical transduction of hair cells to sense body orientation (Ohmori, 1987; Ohmori, 1984). In plants it is suspected that mechanosensitive ion channels are used as gravity detectors (Millet and Pickard, 1988) while magnetic field detection in some birds and fishes may have as a basis the sensing of the torque produced by magnetic particles (Sachs, 1988).

Proprioception and Interoception

Probably the least obvious, but most important aspects of mechano-transduction occurs within the organism itself in relation to self-monitoring. Musclo-skeletal mechanoreceptors such as muscle spindles, golgi tendon organs (Vierck, 1975; Leeson and Leeson, 1976), crustacean stretch receptors (Brown et al., 1978; Pasztor and Bush, 1987) and periodontal ligament mechanoreceptors (Byers, 1985) play central roles in sensing and coordinating limb position, posture, tension limiting and pain reception.

Blood pressure is continuously adjusted through both central regulation via output from various arterial baroreceptors (Brown, 1981) and locally by direct responses of the vascular endothelium to haemodynamic shear forces (Lansman et al., 1987; Nakache and Gaub, 1988; Olesen et al., 1988). Blood pressure and blood volume are inextricably linked; hence the regulation of diuresis by atrial natriuretic factor release from stretched atria (Flynn and Davies, 1985; deBold et al., 1981). Blood volume regulation goes hand in hand with osmotic homeostasis; hypothalamic osmotransducers (Abe and

Ogata, 1982) and osmotically sensitive cells in the kidney (juxtaglomerular apparatus) sense osmotic pressure and thereby measure the colligative properties of the extracellular fluids (Eckert and Randall, 1983). Cell swelling or shrinking caused by osmotic pressure changes will directly influence membrane tension.

Enteric mechanoreceptors sense filling of gut, bowel and bladder providing feedback during ingestion, imbibing and excretion.

Intrinsic cellular mechanoreception

The least understood aspect of mechanoreception is also probably the oldest in an evolutionary context. The first single-cell organisms were faced (as are modern ones) with volume regulation problems that required sensing of cell-swelling and mechanisms to mediate efflux of solutes and water to prevent lysis. Another basic problem is cell size regulation and division initiation in reproducing organisms, whether these are single cells or growing tissues. Motile cells or cellular structures interact with their environment in a very mechanical way and therefore would be expected to have mechanotransducers to provide feedback on their progress.

In all these examples mechanotransduction appears to originate at the single cell. This is seen even in complex transducers such as the cochlea where individual hair cells do the transducing; the accessory structures act only as amplifiers, or filters. It is quite likely then, that the plasma membrane is the site of the transduction event, since it is the one cell organelle which is affected by any mechanical perturbation and can control cell potential. What is the physical basis of these transduction events?

Ion channels as transducers of membrane tension

What are ion channels?

Ion channels are integral membrane proteins that span the plasmalemma thereby providing a diffusive passage for charged ionic species into or out of the cell. It is useful to view ion channels as enzymes catalyzing the transfer of ions from an aqueous medium across a hydrophobic barrier, the lipid bilayer. This barrier is energetically enormous for diffusion of small ions (250 kJ/mol); ion channels reduce this barrier to ,20 kJ/mol enhancing the diffusion rate by 10^{39} times (Latorre and Miller, 1983). Ion channels also resemble enzymes in their substrate specificity (ionic selectivity), reaction kinetics, competitive inhibition (by blockers) and the presumed changes in conformation that accompany the catalytic reaction (alterations between conducting and nonconducting states, "openings" and "closings" respectively). In this sense, ion channels are the most efficient enzymes known, passing 10^6-10^9 ions per second. The result of this high turnover number is a very small [on the order of several picoamperes (pA)], but measurable single-channel current (see reviews Hille, 1984; Auerbach and Sachs, 1984).

The *a priori* prediction that ion channels must exist stems from the observed macroscopic membrane conductance changes which occur during the action potential and chemically mediated receptor potentials, of which the best known is the acetylcholine induced conductance at the neuromuscular junction. Before Neher and Sakmann (1976) showed directly the presence of unit conductances in biological tissue, a good deal of indirect evidence had indicated that discrete microscopic conductance pathways formed the basis of macroscopic membrane currents (Hille, 1970; Anderson

and Stevens, 1973). In sublime understatement Hille (1970) suggested; "Many interesting questions concerning the opening and closing of ionic channels could be answered if unitary conductance changes could be resolved in a voltage clamp."

Although early experiments using lipid bilayers had shown that biologically derived factors could produce conductance changes of the size expected for ion channels (Mueller et al., 1962; Bean et al., 1969), it was not until the advent of the patch clamp technique that ion channel activity was directly demonstrated in biological membranes (Neher and Sakmann, 1976; Neher et al., 1978; Hamill et al., 1981). This technique has now become central in the study of ion channels (Sakmann and Neher, 1983).

Stretch-activated cation selective ion channels

The physical basis for the voltage- and chemically-dependent macroscopic membrane currents was anticipated quite early to be membrane pores with voltage or ligand-dependent behavior (see Hille 1984), but it was not until 1984 that Guharay and Sachs directly demonstrated ion channels could also be tension dependent. With the acuity of hindsight, ion channels would have seemed to be a natural choice for mechanoelectric transduction. Indeed, Katz (1950) had suggested that the basis of receptor potentials observed in the stretched muscle spindle, involved membrane permeability changes caused by the stretching of ionic pores. Much later, Hudspeth and collaborators (Howard et al., 1988) and Ohmori (1984) postulated that mechanotransducing channels were the displacement-sensitive elements in cochlear and vestibular hair cells.

The first stretch-sensitive ion channel described was found in embryonic chick skeletal muscle (Guharay and Sachs, 1984; Guharay and Sachs, 1985a, Guharay and Sachs, 1985b) and similar channels have been reported in *Xenopus* muscle and oocytes (Brehm et al., 1984; Methfessel et al., 1986; Yang et al., 1986; Yang and Sachs, 1987; Yang and Sachs, 1989), frog lens epithelium (Cooper et al., 1986), frog oocytes (Taglietti and Toselli, 1988), rat dorsal root ganglion cells (Yang et al., 1986), rat endothelium (Lansman et al., 1987), *Necturus* choroid plexus epithelium (Christensen, 1987), toad smooth muscle (Kirber et al.,1987; Kirber et al., 1988), *Amphiuma* erythrocytes (Yang and Sachs, 1987), human fibroblasts (Stockbridge and French, 1988), neuroblastoma (Falke and Misler, 1988), ascidian oocytes (Moody and Bosma, 1989) and non-ciliary membrane of guinea pig outer hair cells (F. Sachs, per. comm.).

All these channels exhibit an increase in activity, ie., probability of being open, in response to increased membrane tension and thus are referred to as being stretch-activated (SA). SA channels can be significantly activated when ~50 mmHg of suction is applied to the patch pipette. These channels all exhibit cation selectivity discriminating poorly between Na^+ and K^+ (P_K/P_{Na} = 3.9:1 for chick myocytes, Guharay and Sachs, 1984; P_K/P_{Na} = ~1:1 for lens epithelium and smooth muscle, Cooper et al., 1986 and Kirber et al., 1988 respectively) and will be referred to as SACat channels. The single-channel conductances range from 30 to ~50 pS picoSiemens (S = 1/Ω). The similarity of these channels and their appearance in a variety of vertebrate preparations lends support to the hypothesis that the SACat is the mechanotransducing ion channel found in vertebrate mechanosensory structures. This notion is further supported by

the similarity of selectivity characteristics seen in the cochlear hair cell mechanotransducing conductance and SACat channels (Howard et al., 1988; Sachs, 1988). Although the cochlear channels have not been studied at the single-channel level, it is likely that their permeability characteristics are essentially the same as the SACat channels.

The SACat channel's permeability to Na^+ means that under physiological conditions increased membrane tension would result in an inward Na^+ current. Thus, a depolarizing receptor potential is produced that would initiate action potentials (producing a spike train, as in Pacinian corpuscles) or modulate other voltage-dependent membrane conductances (Ca^{2+} channels which in turn modulate hair cell neurotransmitter release) in response to mechanical forces.

It is obvious that not all of the aforementioned cell types are afferent mechanosensory structures, so what other functions do the channels play? In most cases SACat function has not been demonstrated directly, but has been implied. For example, stretch-induced contraction in smooth muscle is expected to result from SACat activity producing a membrane depolarization followed by Ca^{2+} influx through voltage-dependent Ca^{2+} channels (Kirber et al., 1988). Christensen (1987) suggests that Ca^{2+} influx through SACat channels will activate Ca^{2+}-activated K^+ channels relieving internal osmotic pressure during hyposmotic shock. Lansman et al. (1987) proposes that endothelial SACat channels modulate endothelial relaxing factor (ERF) release. The presence of SACat channels in *Xenopus* (Methfessel et al., 1986), *Rana esculenta* (Taglietti and Toselli, 1988) and ascidian (Moody and Bosma, 1989) oocytes implicates them in a possible role in cell division during embryogenesis (Sachs, 1988).

K^+ selective stretch-activated ion channels

The cation selective SA channel is somewhat analogous to the acetylcholine receptor channel located at the neuromuscular junction; both are cation selective and have similar conductances. Activation of either channel produces a membrane depolarization[1] (Howard et al., 1988; Davenport and Thompson, 1987; Corey and Hudspeth, 1979; Brown et al., 1978) as a signal that some external event has transpired, be it mechanical or chemical. Imposing ionic selectivity on chemically mediated or mechanosensitive ion channels will however result in ion fluxes that may produce membrane potential changes opposite in effect, ie. hyperpolarization in the case of K^+ selective channels. Therefore, SA channels which exhibit selectivity to specific cations would potentially have different functions, not expected of the less discriminating SACat channels.

During recordings of isolated *Lymnaea stagnalis* (pond snail) ventricular cells, SA channels were observed only when the membrane potential provided an outward (out of the cell) driving force for potassium (Brezden et al., 1986). Subsequently, if the external K^+ concentration was raised (in the pipette) the reversal potential (V_{rev}) shifted in a depolarizing direction along the voltage axis, thus indicating a K^+ selective channel. The channel was also shown to be blocked by quinidine but not by other typical K^+ channel blockers such as tetraethylammonium and 4-aminopyridine. Because

---

[1]There have been no unequivocal demonstrations of SA channels acting directly to change membrane potential. However, there is compelling, albeit, indirect evidence (in the form of mechanically-induced membrane currents and voltage changes) for mechanotransducing channels acting to produce membrane potential changes in response to mechanical forces operating on the membrane.

the channel was not completely inactive in the absence of applied stimuli, it was suggested that it would contribute to the resting membrane potential of the cell. Specific functions related to its mechanosensitivity were suggested as well: it could function in an osmoregulatory role or to reduce membrane excitability during ventricular filling (Brezden et al., 1986). The stretch-sensitivity and kinetics of this channel, dubbed the SAK (stretch-activated K^+) channel, was later addressed by Sigurdson et al. (1987a) (see chapter 2).

An osmoregulatory role for SAK channels was, and still is, an attractive hypothesis, but requires the presence of the channel in all cell types of the snail. A survey of cell types revealed that neurons isolated from the circumoesophageal ganglionic mass and certain kidney cells contained a channel analogous to the ventricular SAK channel (Sigurdson et al., 1987b; Bedard, Sigurdson and Morris, unpublished results). This list of cells lends some weight to the notion that SAK channels are ubiquitously distributed in all cell types of *Lymnaea*, but a comprehensive survey is still required.

These observations have lead to the phylogenetic question; how widely distributed are SA K^+ channels? Do related snail species contain the channels? Do other invertebrates such as arthropods and annelids have similar channels? What about vertebrates? Bedard et al. (1988) examined neurons isolated from a snail in the Helicideae family, *Cepaea nemoralis*, and discovered a SA K^+ channel similar to that seen in *Lymnaea* neurons and heart cells. The channels were not found in cockroach or leech neurons, though preliminary patch data obtained from *Aplysia* neurons indicate the presence of SAK channels (Bedard et al., 1988; S. Siegelbaum, per. comm. to C. Morris). SAK channels have been found in at least one

arthropod however; Zagotta et al. (1988) found such a channel in embryonic *Drosophila* myotubes.

Recently, stretch-sensitive K^+ selective channels were found in *Necturus* kidney proximal tubule cells (Sackin and Palmer, 1987; Sackin, 1987; Sackin, 1989). This channel may play an osmoregulatory role similar to that suggested for the snail heart SAK channels (Brezden et al., 1986). During hyposmotic stress, increased membrane tension would activate the channels promoting net K^+ efflux with osmotically obliged water following. Sackin (1989) has shown that SAK channels can be activated during cell swelling, but it remains to be demonstrated whether this activation makes a significant contribution to the volume regulatory decrease seen in these cells.

It was suggested by Sachs (1988) that SACat channels found in *Xenopus* oocytes could regulate cell division during embryogenesis. Medina and Bregestovski (1988) recently described a SAK channel in embryos of the loach (a freshwater fish, *Misgurnus fossilis*). These authors were able to correlate membrane potential (V_m) oscillations with periods of channel activation during the cell cycle. As expected for a K^+ channel, during periods of channel activation V_m was more hyperpolarized than when the channels were quiescent.

In bovine endothelial cells, Olesen et al. (1988) identified an inwardly-rectifying K^+ current activated by haemodynamic shear stress. This current demonstrated desensitization at high flow rates. Olsen et al. (1988) were not able to identify individual SA channels, but the inward current closely resembled ensemble currents produced by inward rectifying K^+ channels with respect to the current/voltage relation and block by Ba^{2+} and Cs^+. The

inward rectification and desensitization are not typical features of the SAK channels so far described (see Sigurdson et al., 1987a; Sigurdson and Morris, 1989; Sackin, 1987; Medina and Bregestovski, 1988; Zagotta et al., 1988), so it is not clear if the presumed channels are a novel subtype of SAK channel or if activation of the current is a secondary product of an unidentified primary stretch sensitive component. Whatever the transduction mechanism, it is noteworthy that the stress-sensitivity of the current is closely matched to the measured haemodynamic stress produced by blood flow in small arteries and arterioles. The conductance may therefore modulate vessel smooth muscle relaxation via gap-junctional coupling or endothelial-derived relaxing factor release. The relation between these channels and the endothelial SACat channels described by Lansman et al. (1987) is not clear, but Olesen et al. (1988) suggested that at high flow velocities SACat activation would result in smooth muscle contraction, whereas low shear stress would cause relaxation. Independently, Nakache and Gaub (1988) have also shown hydrodynamic hyperpolarization of endothelial cells, but have not characterized the current in detail. Desensitization of mechanoreceptor current is not restricted to endothelial cells. Deitmer (1981) described a K^+ mechanoreceptor current in the ciliate *Stylonychia mytilus*, where receptor current amplitude was linearly dependent on stimulus strength, but current time course appeared phasic, ie. receptor current decay was independent of stimulus duration.

Recently several types of SA K^+ channels have been found in cultured astrocytes (Ding et al., 1988; F. Sachs, per. comm.).

All SAK channels so far described appear to have similar selectivity characteristics ie., under "physiological" conditions the channels are

outwardly rectifying, passing little or no inward Na^+ current. Beyond this similarity, the lack of detailed selectivity studies prevents further comparison.

Anion selective and non-selective SA channels

The diversity of species using SA channels is perhaps best exemplified by the anion selective and by the non-selective channels found in four different kingdoms. Anion selective SA channels observed in tobacco (Falke et al., 1987) and *E. coli* protoplasts (Martinac et al., 1987), while non-selective SA channels were shown in yeast spheroplasts (Gustin et al., 1988) and opossum kidney cells (Ubl et al., 1988a). The *E. coli* SA channel is notable in having a very high conductance, on the order of 1000 pS in a high salt (300 mM Cl^-) solution. Ubl et al. (1988a) suggest the opossum kidney SA channels, which have a much lower conductance, could play an osmoregulatory role, a function also put forward for the yeast and *E. coli* channels (Sami et al., 1988).

Stretch-inactivated K selective channels

A new mode of mechanosensitive ion channel gating has been recently found in *Lymnaea* neurons, namely stretch-inactivation. Here, spontaneously active K^+ channels are "turned off" when membrane tension is increased (Morris and Sigurdson, 1989). These channels coexist with SAK channels both in the cell body and growth cones. They possess differing stretch-sensitivities such that at intermediate tensions K^+ conductance is minimized. There is mounting evidence that intracellular Ca^{2+} levels play a role in regulation of growth cone motility and guidance (Kater et al., 1988). It is

suspected therefore that stretch-sensitive ion channels may influence Ca^{2+} levels in response to membrane tension changes that occur during motility (Morris and Sigurdson, 1989).

A biophysical model of stretch-sensitivity

Activation of ion channels by mechanical forces inevitability leads to questions concerning how the channels convert external mechanical energy (displacement of mass through space) into specific changes in protein conformation. Guharay and Sachs (1984) developed a model of stretch-sensitivity based on simple assumptions about the channel protein and about patch dimensions. The model led to some surprising predictions. Guharay and Sachs (1984) concluded that the observed stretch-sensitivity could only result from connections between the channel and the underlying cytoskeleton. The major tenets of their model (see below) have provided the impetus for ongoing experiments describing and quantifying this relationship.

A Hooke's law elastic model

The model developed by Guharay and Sachs (1984) (see also Sachs, 1988) is based on Hooke's Law which describes the proportionality of force to applied tension for solid elastic objects. This is the simplest description of how membrane tension acting on a channel could be converted into channel conformational changes. For "one-dimensional" objects such as wires or springs the relation between force and stretch is given by:

$$F = -K(x - l) \qquad (1.1)$$

where F is the force, K is the elastic constant, x the displacement from rest and l the rest length. The rest length is included since there is no way of knowing if the resting stress is zero when the applied force is zero. An example of non-zero resting stress is the case where the spring is stressed by its own weight.

This formalism can be applied to 2-dimensional objects like membranes by using tension rather than force and an area elasticity, K_A, instead of K (Helfrich, 1973). For no prestress (l = 0),

$$T = K_A \frac{\Delta A}{A} \qquad (1.2)$$

and the energy density (ergs per cm^{-2}) G_A (obtained by integrating the force over the area change) is:

$$G_A = K_A/2(\Delta A/A)^2 A \qquad \text{(Helfrich, 1973)}$$

or equivalently

$$G_A = \frac{T^2 A}{2K_A} \qquad (1.3)$$

where T is tension (dyn/cm), $\Delta A/A$ is the fractional increase in channel area produced by the tension, A is the closed channel area (πr^2) and K_A is the area elasticity constant (Guharay and Sachs, 1984; Sachs, 1988). Experimentally, membrane tension is increased by applying negative pressure (suction) to the membrane patch. Assuming a hemispherical patch, Laplace's Law relates the tension of a thin-walled elastic sphere to pressure, P, and patch diameter, d by

$$T = Pd/4 \qquad (1.4)$$

Combining equations 3 and 4, thereby accommodating the realities of pressure and patch diameter, we obtain

$$\Delta G = \frac{(Pd)^2 A}{32K_A} \qquad (1.5)$$

Thus, equation 1.5 relates the free energy change to the pressure applied to a membrane patch of a specific curvature and area and to the area and area elasticity of the channel. In practice, we can only accurately determine P, the one parameter the experimenter controls, but realistic estimates of patch diameter can be made. Channel area and K_A can only be given limits (see below).

Although this model seems formally correct, how can we relate it to SA channel data? Guharay and Sachs (1984) were fortunate to obtain a single-channel patch on which they collected data at several pressures. Thus, channel open probability as a function of pressure could be related to changes in the channel kinetics. The model in its simplest form, ie. a 2-state kinetic model, would have at most two transition rate constants showing stretch-dependency (a two state kinetic model implies that only one energy barrier need be crossed between open and closed conformations). When Guharay and Sachs (1984) analyzed the open and closed dwell times for their single channel patch, they found the channel occupied at least 3

closed states and 1 open state, of which only the long closed dwell time (C_1) was stretch-dependent. By assuming a simple linear reaction scheme,

$$C_1 \underset{k_{21}}{\overset{k_{12}}{<\!\!-\!\!-\!\!-\!\!-\!\!>}} C_2 \underset{k_{32}}{\overset{k_{23}}{<\!\!-\!\!-\!\!-\!\!-\!\!>}} C_3 \underset{k_{43}}{\overset{k_{34}}{<\!\!-\!\!-\!\!-\!\!-\!\!>}} O_4$$

they reached the conclusion that only the rate constant for leaving C_1, k_{12}, was stretch-sensitive. This allows the free energy change associated with membrane stretch, ΔG, to be equated with a measurable quantity. If the rate constant for crossing a single energy barrier is (Guharay and Sachs, 1984)

$$k_{12} = k_0 \exp(-\Delta G/kT) \qquad (1.6)$$

Combining equations 1.5 and 1.6 gives

$$k_{12} = k_0 \exp(-\Theta P^2) \qquad (1.7)$$

where

$$\Theta = \frac{d^2 A}{32 K_A kT} \qquad (1.8)$$

and k is the Boltzmann constant, T is absolute temperature and k_0 is a constant representing the rate when the open probability (P_o) is 0.

Therefore the stretch-sensitive rate constant is dependent on the pressure squared rather than pressure, as is the channel P_o. Θ, which embodies all the physical characteristics of the channel and patch, is given by the slope of ln P_o *vs* P^2 and is a measure of the stretch-sensitivity.

The maximum sensitivity will place restrictions on the channel area ($A = \pi r^2$) and its area elasticity, K_A. Equation 1.8 reduces to

$$\theta = \frac{1.73 \times 10^{-3} r^2}{K_A} \qquad (1.9)$$

if the patch diameter, d is 2 μm (kT = 4.04×10^{-14} dyn/cm at 20°C) and where r is the channel radius in Å. Guharay and Sachs (1984; 1985a) established for a series of patches, sensitivities that averaged 0.66 $cm^{-2}Hg$ under normal conditions and 4.34 $cm^{-2}Hg$ for cytochalasin-treated cells. Using the larger value as a maximum sensitivity, the ratio

$$\frac{r^2}{K_A} > 2.5 \times 10^3 \qquad (1.10)$$

permits inserting values for K_A that puts limits on the channel radius, r. For bilayers, erythrocyte and chick skeletal muscle membranes, area elasticity constants range from 3 to ~500 dyn/cm (Guharay and Sachs, 1984) which, if we assume the channel protein has the same K_A as the membrane, means the channel radius ranges from 87 Å to ~1100 Å, a huge protein. It seems unrealistic that the stiffness of proteins are as low as that of membranes, but protein K_A's are unknown. They were therefore estimated from polymers (nylon and rubber), silk (Guharay and Sachs, 1984) and protein bulk elasticities (Sachs, 1986). These values of K_A ranged from 3,000 to 60,000 dyn/cm making their estimate of protein radius much larger (as much as 12,000 Å) and seemingly unreasonable for a single molecule. The logical conclusion was that an energy gathering area sufficient for

collecting the mechanical tension could only result from a distributed cytoskeletal network in which the channel was embedded. The channel would harness the membrane tension by being placed at the node of a network of cytoskeletal strands.

Predictions of channel density

The whole cell mechanotransducing current (I) is the product of channel density (N), single-channel conductance (g), membrane potential (V_m) and open channel probability (P_o) for a given membrane tension;

$$I = gNP_oV_m \qquad (1.11)$$

Channel open probability is related to θ by,

$$P_o = 1/(1 + K_{eq}\exp(-\theta P^2) \qquad (1.12)$$

where, K_{eq} is the ratio of opening and closing rates at zero tension for a simple two state system (Cooper et al., 1986).

The channel sensitivity, θ is dependent on the area of tension collection as defined by "channel" radius r and K_A (equation 1.9; in the following discussion K_A is assumed to remain constant; i.e., the channels do not change their elasticity as a function of tension). As the radius is made smaller θ becomes smaller because there is less area/per channel for collection of tension. If "channel" radius (r) is equivalent to the internode spacing, then as channel density increases (radius decreases), sensitivity decreases (Sachs, 1986; 1988). Therefore the model predicts a optimal

channel density for any given operating tension and channel K_A (see Appendix 1). Large operating tensions provide more energy per unit area of membrane and thus allow high channel densities. Low tensions require larger collection areas resulting in low channel densities. Sachs (1986) predicted an optimal density of between 1 to 10 μm^{-2} which is similar to values described by Guharay and Sachs (1984), Sigurdson et al. (1987a), and Howard et al. (1988).

Evidence for cytoskeletal involvement

In order to optimize the tension transmitted to each channel, the channels must be evenly spaced. Channel insertion into a cytoskeleton network not only transfers tension to the channels but would also stabilize the channels spatially creating a homogeneous distribution. This in fact appears to be the case; the number of channels observed per patch in snail heart cells is almost always greater than one (very few single channel or zero channel patches) and seems to rarely exceed ~10 (Sigurdson et al., 1987a). A randomized channel distribution would be expected to produce zero channel and single-channel patches with a frequency greater than that observed.

Disruption of the cytoskeleton should interfere with SA channel function. Expecting to find a loss of stretch-sensitivity, Guharay and Sachs (1984) treated chick skeletal muscle cells with cytochalasins to disrupt α-actin filaments. They found instead an large increase in sensitivity, which suggests that actin filaments are in parallel with the channels (not directly connected) and normally relieve much of the tension in the membrane. Removal of the filaments allowed the channels to "see" more of the

membrane tension. Treatment with microtubule inhibitors and actin stabilizing agents had no effect on the channels (Sachs, 1988)

Recent evidence for channel/cytoskeleton interactions point to spectrin and ankyrin as possible candidates for the submembranous cytoskeleton involved in tension collection. These elements appear to control the density of Na^+ channels and glutamate receptors by anchorage to these proteins (Siman et al., 1985; Srinivasan et al., 1988). In erythrocyte membrane preparations, spectrin has been observed to form meshworks with internode spacings of ~2,000 Å (Byers and Branton, 1985). If SA channels were "hooked into" the intersections of such filaments, the diameter of 4,000 Å is in line with estimates for the collection area radius defined above (see Sachs, 1988). This also correlates with a channel density of about 1 to 2 μm^{-2} (r = 2,500 to 5,000 Å). However, it remains to be shown if such an interaction occurs between SA channels and the cytoskeleton.

Characterization of *Lymnaea* Stretch-sensitive K^+ channels

SA channels are a relative novelty compared to ligand and voltage dependent ion channels which have been studied in detail for more than thirty years. Although the vertebrate SACat channels were the first described and have been presented as the proto-typical SA channel, the existence of stretch-sensitive channels displaying K^+ specificity implies possible functions other than production of excitatory mechanosensory currents. Activation of SAK channels would hyperpolarize the cell, thereby stabilizing the resting potential (V_{rest}). A stretch-inactivated K^+ channel would produce the opposite effect, i.e., make the membrane susceptible, upon stimulation, to any depolarizing leakage currents.

It was now necessary to characterize the biophysical features of stretch-sensitive K^+ channels with respect to their stretch-sensitivity, kinetics, pharmacological responses and ionic selectivity. This will not only allow comparison with other SA channels, but perhaps give some clues to the functional mechanisms of SA channels and the physiological function(s) they perform.

Lymnaea heart SAK channels

Initially the limited experience with SA channels, prompted a certain degree of skepticism (among channel biophysicists) regarding the possibility of artifactual activation of any channel with membrane stretch[2]. An important question then, was, is there only one channel type affected by stretch and are the kinetic characteristics of this channel consistent from patch to patch and cell to cell? Consistency would be a strong indication of a specific process or mechanism. Additionally, it was important to determine if Ca^{2+} had any effects on the channel since Ca^{2+}-activated K^+ channels are present in molluscan tissues (Adams et al., 1980; Ewald et al., 1985). It was quite possible that a SA channel permeant to Ca^{2+} or a generalized Ca^{2+} leak during suction would specifically activate a K^+ channel of this sort, which would then erroneously be considered a SAK channel.

The characterization of SAK channels, initiated in *Lymnaea* heart cells (Brezden et al., 1986) left many unanswered questions concerning their stretch-sensitivity and kinetics. Did SAK channels respond to the same

---

[2]It should be noted that applying pressure to the membrane patch during single-channel recording was not, and is still not, a normal procedure for fear of loosing the gigaseal.

range of pressures as SACat channels? Did the channel respond with a monotonic increase in P_o or was the response perhaps sigmoid or hyperbolic? What is the kinetic basis of channel activation; are the changes in channel P_o as a function of pressure due to changes in specific open or closed dwell times? From the initial observations it was clear the channel openings appeared as bursts; i.e., openings punctuated by brief closings. Was this behavior modified by membrane tension and if so, could it be related to the kinetic parameters? These questions are addressed in Chapter 2.

***Lymnaea* neuron SAK channels**

The question of SAK channel distribution in the various cell types of *Lymnaea* lead to their discovery in the neurons composing the circumoesophageal ganglionic mass. This provided the opportunity for comparison with the SAK channels found in the ventricular cells and an opportunity to profit from the advantages of isolated neuron cultures.

The preliminary selectivity data collected from the heart SAK channels (Brezden et al., 1986) needed elaboration, but the isolated ventricular cells were difficult to work with; gigaseals were of poor quality, low in number and cells were spontaneously contractile. The initial work with the circumoesophageal neurons indicated an ease of patching that might accelerate the work.

More importantly, molluscan neurons have been used extensively in determining the biophysical and cell physiological relations of ion channels, the best example being that of the Kandel group's work on identified neurons in *Aplysia* (see Siegelbaum et al., 1982; Belardetti et al., 1987;

Piomelli et al., 1987; Shuster and Siegelbaum, 1987). Their elucidation of the modulation of a K^+ channel (the S channel) by serotonin [downregulation by phosphorylation via a cAMP-dependent protein kinase (Shuster et al., 1985)] and the neuropeptide FMRFamide [up regulation by arachidonic acid metabolites (Piomelli et al., 1987)] has created a basis for comparison with other molluscan systems.

Lymnaea neurons have been examined by a number of investigators who have described circumoesophageal ganglion anatomy (Allison and Benjamin, 1985), basic electrophysiological properties (Kostenko et al., 1973; Sattelle, 1974; Moreton and Gardner, 1976; Byerly and Moody, 1984) and ion channel types (Kazachenko and Geletyuk, 1984; Geletyuk and Kazachenko, 1985; Morris and Sigurdson, 1989; Sigurdson and Morris, 1989; Yazejian and Byerly, 1989). This background of knowledge will make the inclusion of stretch-sensitive channel data much easier in regard to channel function in specific neurons. Future use of isolated identified neurons will permit examining possible relations between neuromodulators and stretch-sensitive ion channels. This could in turn be related to the function of that specific neuron.

Neurons in culture can undergo neurite outgrowth and synaptogenesis, processes whose underlying molecular mechanisms are difficult to elucidate *in vivo*. Kater's group and others have shown snail neurite elongation, growth cone motility and synaptogenesis are modulated *in vitro* by electrical activity and serotonin (Haydon et al., 1984; Cohan and Kater, 1986) which in turn modulate intracellular Ca^{2+} levels (Cohan et al., 1987; Mattson and Kater, 1987; Kater et al., 1988; Goldberg, 1988; Smith, 1988). By definition, motility is a mechanical process. This immediately raises the question, what

role do stretch-sensitive ion channels play in motility? The potential presence of stretch-sensitive K^+ channels in or near the motile regions of neurites would indicate a possible regulatory function for the channels not previously recognized.

Such factors motivated a switch to isolated neurons for the remainder of the project. This necessitated some repetition of work already completed on heart cells. Comparison of channels in two cell types warranted this approach in any event.

Course of study of *Lymnaea* stretch-sensitive ion channels

Experimental technique

Single-channel recording is the only electrophysiological technique available that permits study of the properties of single ion channels. The technical aspects of this approach have been developed principally by Neher and Sakmann and collaborators (see Hamill et al., 1981; Neher and Sakmann, 1983). Briefly, the technique relies on the formation of a high resistance (gigaohm) electrical seal between the cell membrane and the walls of a glass micropipette (tip diameter 1 - 3 μm). The gigaohm resistance forces all current flow to occur across this patch of cell membrane and consequently through ion channels. The current amplitudes (picoAmperes) although small, can be detected by a high gain current/voltage converter whose output voltages can be further amplified, frequency boosted and filtered by the patch clamp amplifier electronics. The transmembrane field potential (V_m) across the membrane patch can be clamped (hence patch

clamping) by adjusting the pipette voltage (V_p). The experimenter can therefore control the ionic driving forces by voltage or by the composition of the pipette solution.

There are two single-channel recording configurations typically used; cell-attached recording, where the patch pipette remains attached to the cell (patch V_m is the result of V_p and the resting potential of the cell (V_{rest}) and excised patch recording where the mechanical stability of the gigaseal permits removal of the patch from the cell. In the latter configuration, there is complete control over V_m and the ionic composition on both sides of the membrane.

Since what we observe during single-channel recording, are the ionic currents which pass through ion channels, we can study these permeation properties by asking what kinds of ions are passed (selectivity), the current amplitudes (channel conductance), and the blocking of current flow by pharmacological agents.

The activity of the channel, i.e. the probability the channel is open, is dependent on the channels' gating kinetics. Ion channels open and close in a stochastic manner, meaning that the durations of openings and the intervals between openings (closings) are random variables. If the channels' kinetics are stationary, i.e. have transitions *rates* which are invariant in time, the generation of open and closed dwell times is described as a time homogeneous Markov process (Colquhoun and Hawkes, 1983). The distributions of open and closed dwell times will be described by a probability density function (pdf) composed of the sums of exponential terms. For

example, if the kinetic model has one open state and two closed states, the open time distribution will be described by

$$\text{pdf} = a\tau_{O1}\exp(-t/\tau_{O1}) \qquad (1.13)$$

and the closed time distribution by

$$\text{pdf} = a_1\tau_{C1}\exp(-t/\tau_{C1}) + a_2\tau_{C2}\exp(-t/\tau_{C2}) \qquad (1.14)$$

where t is a time interval, τ_{O1}, τ_{C1}, and τ_{C2} are time constants (mean dwell times; inverse rate constants) and a, a_1, and a_2 are the areas of each exponential term under the pdf. Values for the areas and time constants are estimated by fitting equations such as 1.13 and 1.14 to frequency histograms of open and closed times (see Material and Methods in Chapters 2 and 5).

Most channels display bursting behavior, i.e. openings are punctuated with several brief closings producing a burst. Analysis of burst kinetics (estimation of mean burst duration and interburst closed interval) proceeds in the same way as for open and closed times, except that some way must be developed for delineating a burst. An empirical method was worked out to do this and is described in detail in the Chapter 2 material and methods section.

Channel selectivity and pharmacology

In order to compare and contrast stretch-sensitive K^+ channels with other K^+ channels, basic biophysical information is required. Ion selectivity is pertinent to any proposed function and so must be clearly established. Selectivity sequences can help identify possible permeation mechanisms and allow comparisons with other K^+ channels.

1. Under conditions of cell-attached and excised (inside out) patches, I/V curves (single-channel current amplitudes as a function of transmembrane voltage) were made to determine the dependence of conductance and reversal potential on the concentrations of external test ions.

The *in vivo* conductance characteristics were approximated by using cell-attached patches with physiological saline (NS, normal saline) in the bath and inside the patch pipette. This would demonstrate under "normal" conditions the polarity of current flow and the effect of channel activation on the cell's resting potential (V_{rest}).

The shift in reversal potential (V_{rev}) due to the external K^+ concentration changes was correlated with the expected equilibrium potential (Nernst potential). Estimates of internal $[K^+]$ (Sattelle, 1974) will allow calculation of the Nernst potential for any external $[K^+]$.

Although a depolarizing V_{rev} shift in response to increased external $[K^+]$ is good evidence for a K^+-selective channel (Hille, 1984), the precise amount of shift will depend on permeability to other cations, such as Na^+, which the Nernst equation does not address. A better approach is the use

of the Goldman-Hodgkin-Katz (GHK) current (1.15) and voltage (1.16) equations, originally derived for the calculation of permeabilities (for single ion species) and reversal potentials (for multiple ions) for whole cells (Hille, 1984);

$$I = P_S z^2 \frac{VF^2}{RT} \frac{[S]_i - [S]_o \exp(-zFV/RT)}{1 - \exp(-zFV/RT)} \qquad (1.15)$$

$$V_{rev} = \frac{RT}{F} \ln \frac{P_K[K]_o + P_{Na}[Na]_o + P_{Cl}[Cl]_o}{P_K[K]_i + P_{Na}[Na]_i + P_{Cl}[Cl]_i} \qquad (1.16)$$

where I is single-channel current, P_S permeability coefficient of ion S, V transmembrane voltage, F the Faraday constant, R the gas constant, T absolute temperature, z the ionic valence, $[S]_i$ and $[S]_o$ the ionic concentration on the inside and the outside of the membrane, respectively, and P_K, P_{Na} and P_{Cl} the permeabilities of K^+, Na^+ and Cl^- respectively (Hille, 1984). By using the GHK current equation (1.15), P_S, which is independent of ion concentration, may be found. This permits direct comparisons among different channels regardless of the ionic concentrations used during recording. The GHK voltage equation (1.16) can be simplified for biionic conditions, ie. one ion type on each side of the membrane, and thus give a permeability ratio between two ions (in this case between the test cation and K^+);

$$V_{rev} = \frac{RT}{F} \ln \frac{P_X[X]_o}{P_K[K]_i} \qquad (1.17)$$

where V_{rev} is the biionic reversal potential, P_X and $[X]_o$ are the per-

meability and concentration of the test cation respectively (Hille, 1984; Benham et al., 1986).

Permeability ratios cannot be obtained from cell-attached patches since the internal [K^+] is not accurately known. Excised patches (inside out, outside out) allow control of the ionic conditions, and for a series of test cations, enable construction of selectivity sequences (permeabilities of other cations relative to K^+).

2. What common K^+ channel blockers affect stretch-sensitive K^+ channels? Identification of specific blockers would be a boon in the determination of channel function. It was shown that among three common K^+ channel blockers, tetraethyl ammonium (TEA), 4-aminopyridine (4-AP) and quinidine, only quinidine blocked *Lymnaea* heart SAK channels (Brezden et al., 1986). Later attempts to block heart SAK channels with the Ca^{2+}-activated K^+ channel antagonists, cetedil and apamin were also unsuccessful (Sigurdson et al., 1987a). The effects of quinidine, TEA, barium and cadmium were therefore tested on neuron SAK channels to determine if a similar blocking profile was present. This is not a comprehensive list of potential blockers, but should be large enough to determine if classical K^+ channel blockers will be of use in cell physiology studies of channel function.

3. The ubiquitous nature of Ca^{2+}-activated K^+ channels requires testing the Ca^{2+} sensitivity of stretch-sensitive K^+ channels to be sure that stretch-induced activation is not an artifact of Ca^{2+} entry through non-selective SA channels (see Christensen, 1987). This was tested on cell-attached patches, where the pipette contained 10^{-8} M Ca^{2+} and on inside-

out patches where the cytoplasmic side was perfused with saline containing 10^{-8} M Ca^{2+}.

Osmoregulation as a possible channel function

As suggested in Brezden et al. (1986) a feasible role of SAK channels is that of cell volume regulation during hyposmotic shock. K^+ efflux during hyposmotic shock has been observed in vertebrate (Gilles, 1983; Sarkadi et al., 1984; Tivey et al., 1985) and invertebrate preparations (Kevers et al., 1979; Treherne, 1980; Kevers et al., 1981). Presumably K^+ efflux is followed by osmotically obliged water thereby relieving swelling.

Net K^+ efflux through SAK channels during cell swelling or mechanical stimulation can be expected to hyperpolarize the cell. Changes in V_{rest} were monitored with intracellular microelectrodes during such perturbations. A more direct test of the role of SAK channels in osmoregulation was also made by monitoring SAK P_o during a hyposmotic shock. Cell swelling could then be correlated with changes in P_o. These experiments can help assess if channel activation can occur during nondestructive mechano-stimulation. The implication of positive results is that channel mechanosensitivity could be used in a physiologically relevant way.

Stretch-sensitivity and kinetic analysis

What happens when the channel is mechanically stressed? Kinetic analysis provides an extremely sensitive approach to this question. When coupled with a physical model, channel kinetics can give additional insights

in structure/function relationships (see Sachs, 1988). Examination of *Lymnaea* stretch-sensitive K^+ channels from this perspective is central in understanding not only how SA channels work in general, but also whether the tensions needed to activate the channel are physiologically relevant.

Channel stretch-sensitivity was characterized by applying calibrated suction to the recording pipette. The resulting changes in channel open probability and the underlying kinetic changes could then be observed for comparison with stretch-sensitive channels from other cell types. At its most rigorous, kinetic analysis requires single-channel patches; these were rarely, if ever, observed. Even so, examination of this data has provided insights useful for answering some basic questions. How does the stretch-sensitivity of heart and neuron SAK channels compare? Are the channel kinetics similar in the two cell types? Are the kinetic schemes similar to those observed in other systems; i.e., is only one dwell time stretch-dependent and is it an open or closed time? Do the mechanosensitive changes in P_o follow the pressure-squared relation described in the model of SA channel activation discussed above? Are there other channel types that display stretch-sensitivity? Are SAK channels voltage-dependent?

Channel spatial distribution

Determination of channel function is a major goal for future stretch-sensitive channel research, but will be hindered severely until an specific channel blocker is found. Still, a good deal of correlative information can be found from relatively simple observations of channel density and spatial distribution. SAK channel distribution was shown to be quite uniform in *Lymnaea* heart cells (Sigurdson et al., 1987a). *Lymnaea* neurons have a

more complex and interesting morphology, featuring extending neurites tipped with motile growth cones (Sigurdson and Morris, 1989). The presence of both SAKs and SIKs in growth cones will permit comparison of channel properties in membrane regions far removed from each other in terms of distance and age.

Chapter 2: Stretch-activated K^+ channel in *Lymnaea* heart cells

Introduction

The ventricular muscle cells found in the freshwater snail *Lymnaea stagnalis*, exhibit a resting membrane potential (V_{rest}) determined primarily by a resting K^+ permeability (Brezden and Gardner, 1984). During the course of single-channel recording from these isolated cells, a K^+-selective ion channel was routinely observed, and a role for the channel in setting the resting K^+ permeability was postulated (Brezden et al., 1986). Interestingly, the channel displayed a mode of gating different from typical voltage- and ligand-gated ion channels described in many cell types (see Hille, 1984), namely activation induced by increases in membrane tension. The channel is to some degree, spontaneously active at zero membrane tension; though not observed at V_{rest}, appropriate ionic conditions in the patch pipette (high $[K^+]$) or the pipette holding potential (set to provide a sufficient driving force for K^+) reveals its zero-tension activity (Brezden et al., 1986). The proposed contribution to V_{rest} by the channel is therefore quite plausible, but my main interest has now focused on its gating behaviour, and on functions which might relate to its stretch-sensitivity.

Stretch-activated (SA) ion channels were first described by Guharay and Sachs (1984) in chick embryonic skeletal muscle cells and have subsequently been seen in other vertebrate cell types (Brehm et al., 1984; Cooper et al., 1986). These channels discriminate poorly between Na^+ and K^+ and may function as mechanoreceptors in exteroception, proprioception and enteroception (Sachs, 1986).

The K^+ selectivity of the cardiac SA channel suggests a different sort of function for this channel, one that could involve a stretch-induced

negative feedback on contractility or a volume-induced activation to relieve hyposmotic swelling. The former suggestion, though feasible in a tissue undergoing repeated stretching and contracting, remains to be tested. The latter hypothesis is supported by a body of evidence (mostly non-electrophysiological) which describes volume-induced increases in K^+ permeability both in vertebrates and invertebrates (Treherne, 1980; Gilles, 1983; Grinstein et al., 1984). Under hyposmotic stress, cell-swelling would increase membrane tension thereby activating the SA channels. The increased K^+ permeability then allows K^+ efflux (observed in many instances of hyposmotic stress; see Kevers et al., 1981; Kevers et al., 1979; Gilles, 1983) followed by osmotically obliged water. This model also assumes an existing Cl^- permeability to maintain electro-neutrality. The role of SA ion channels in this process is not clear at this time.

Only the non-selective cation, SA channel (SACat) has had its stretch-sensitivity extensively characterized (Guharay and Sachs, 1984). Therefore I have began characterizing the snail ventricular cell, stretch-activated K^+ (SAK) channel by examining the effects of membrane tension on channel gating.

Materials and Methods

Cell isolation for patch recording followed the enzymatic dispersion technique described by Brezden et al. (1986). Pieces of ventricle (1 mm cubes) were treated with 0.25% trypsin (Sigma, type XII-S) for 30 min, followed by a 1-2 h 0.1% collagenase digestion. All enzyme treatments took place with gentle agitation and at room temperature (19-25°C). After

dispersion, cells were gently centrifuged and resuspended in normal saline (NS) (see Table 1) supplemented with glucose and antibiotics.

Patch electrodes were made from Corning 7052 glass (1.6 mm o.d. and either 1.15 mm or 0.8 mm i.d.) and coated with Sylgard prior to fire polishing. The side port of the electrode holder was connected to a mercury manometer with valving allowing application of suction or equilibration with the atmosphere. Recordings of cell-attached or excised (inside-out) patches were made using standard techniques (Hamill et al., 1981) with List EPC-5 or EPC-7 patch-clamp amplifiers at gains of 50 mV/pA or 100 mV/pA.

The kinetic properties of the channels were quantified in two ways. Open probability as a function of suction was determined from time averaged current measurements. A cursor driven computer program was used to determine zero current baseline (corrected for baseline drift) and the single channel current level in digitized data. Integration of the current record and division by the single channel amplitude results in an average current level. If the true number of channels was known, probability of being open (P_o) would be known directly, but since I do not known the channel number the results are presented as a index of P_o, representing the average number of channels open. Ideally, at large pressures all channels would be open and the index P_o will represent the total number of channels in the patch, i.e. the P_o *vs* pressure curve will saturate. Even at non-saturating pressures bursts of activity often reveal many more channels than the index P_o reports. At higher pressures, when zero current sections were absent, index P_o was determined by integrating the current record played out on chart paper.

Table 1. Composition of salines

	KCl	NaCl	$CaCl_2$	$MgCl_2$	Hepes	EGTA
Normal saline	1.6	50.0	3.5	2.0	5.0	0
30 mM K^+ saline	30.0	50.0	3.5	2.0	5.0	0
IS[a]	60.0	0	0.2	2.0	5.0	2.2

Concentrations given in mM. pH was adjusted with concentrated NaOH or KOH. For bath solutions, 5 mM glucose, 50 i.u. ml^{-1} penicillin and 50 μg ml^{-1} streptomycin were added.

[a] Intracellular saline.

Analysis of open and closed durations was made on records containing few multiple openings and which had been digitized at 5 times the filter cutoff frequency (50 μs point^{-1}; eight pole Bessel filtering at 4 kHz). Event durations were obtained from automatic event detection software which used event thresholds set at half the single-channel amplitude (from baseline) and opening durations greater than 100 μsec. Frequency histograms of open and closed durations were produced and used to extract time constants by regression of the sum of exponential probability density functions. The Marquardt non-linear least-squares algorithm (Schreiner et al., 1985) was modified according to Guharay and Sachs (1984); data were compared over the integral of each bin of the appropriate function (i.e., the sum of one, two or three exponentials), with bin widths adjusted to contain at least five events (a minimum number to allow for the assumption that errors have a Gaussian distribution). The squared residuals were weighted with the inverse variance (expected value; see equation 39, Colquhoun and Sigworth, 1983). Discrimination of the best fit function was based on the minimum chi-squared value derived from the fitting routine (see Colquhoun and Sigworth, 1983).

A characteristic feature of SAK channels is their apparent bursting behaviour; i.e., openings punctuated by several brief closings. Burst analysis provides an independent test of which kinetic parameters are affected by suction. The basis of the analysis is as follows. A series of increasing interburst intervals; i.e., channels are closed, are used to demarcate the start and finish of a burst. For example, for a very short interburst interval of 0.1 msec, all openings would be considered bursts and the burst duration is simply the average of all open events, proportion of time within

a burst spent open will approach one and closings per burst approach zero. As the interburst interval is increased, open events separated by brief closures will be grouped as a burst. If the channel activity is best described as a burst of activity separated by a relatively long closed time, then for a range of interburst intervals, the burst duration should not change. Further increases in interburst interval results in bursts being grouped together causing the duration to rapidly increase, proportion of time spent open to fall and closing per burst to increase. If channel events are closely spaced (P_o is large or the patch has many active channels), between-bursts closed events cannot be distinguished from within burst closings and burst durations cannot be determined.

The analysis proceeded as follows. (1) Idealized records of event durations were derived from raw data (see above). (2) The idealized record was sequentially processed with increasing interburst intervals and the average burst duration, closing per burst and proportion of time spent open calculated for each interval. Inspection of the plot of burst duration against interburst interval indicated if the channel exhibited bursting behaviour (presence of a plateau region where burst duration remains unchanged). (3) An appropriate interburst interval was empirically selected from the middle of the plateau region and used as a cutoff (i.e., all closing less than the cutoff were suppressed) in the creation of new idealized record that was then treated in the same way as open and closed times. Mathematical criteria for choosing the interburst interval have been derived by Magleby and Pallotta (1983) and Colquhoun and Sakmann (1985).

Results

SAK channels are stretch-sensitive under a wide range of conditions

SAK channels (Fig. 1a), although the most frequently observed, are not the only channels present in heart cell membranes (Fig. 1b-e). SAK channel currents can easily be distinguished by their amplitude, flickery (bursty) kinetics and stretch-sensitivity. The other channel types (Fig. 1b-e) have not been thoroughly characterized, but none exhibited activated currents. In all patches examined, the presence of SAK channels was confirmed by application of uncalibrated suction.

SAK channels were observed under a number of different holding potentials and ionic conditions, the most physiological being cell-attached with normal saline (NS) in the pipette and bath. Under these conditions SAK channels were not seen at V_{rest} (about -60 mV for isolated cells; Brezden et al., 1986), but upon increasing the driving force by depolarization to 20 mV or more, they became apparent as stretch-activated outward current (Fig. 2a). Stretch-activation of SAK channels under these relatively "normal" conditions implies that mechanical effects on channel gating are not unusual observations, distorted by extremes in voltage or ionic constituents, but are physiologically relevant phenomena.

SAK channels could be observed as inward current at V_{rest} by addition of high K^+ (30 mM K^+ saline) to the pipette (Fig. 2b). As with NS in the pipette, suction elicited channel activation. Although SAK channels were ubiquitous in cell-attached patches, excised patches were void of SA current when symmetrical NS was present. This was not an artifact of vesicle formation since other channels' currents were seen (Fig. 1d,e; 100 pS currents which are probably Cl^- channels described by Geletyuk and

Figure 1. Single-channel recordings from *Lymnaea* ventricle muscle. **a)** SAK channels record under cell-attached conditions with 30 mM K^+ saline in the pipette and = +40 mV. In this and all subsequent figures, upward deflections from the baseline represent outward membrane current. For purposes of calculating V_m, the resting potential is assumed to be -60 mV (see Brezden et al., 1986). No pressure was applied for these records. Scales: horizontal, 25 ms; vertical, 2.5 pA. **b)** A channel seen in about one-third of the patches. This channel has a smaller conductance than the SAK channel and produces prolonged burst of outward current under ionic and voltage conditions at which SAK channel current is also outward. The activity of this channel is sporadic but showed no evidence of increasing with applied stretch. Cell-attached patch, 30 mM K^+ saline in pipette, V_m= +40 mV. Horizontal arrowhead indicates position of the zero current baseline. Scale: 5 s, 2.5 pA. **c)** SAK channels (small deflections upward from the baseline) and a channel which I surmise must be passing inward Na^+ current (there is no driving force on Cl^- and Na^+ is the only other ionic species available in the pipette to carry an inward current). Channel activity with these characteristics was only noted in one patch. Inside-out patch, normal saline in the pipette, intracellular saline in bath, V_m= 0 mV. Scales: 250 ms, 2.5 pA. **d)** A large, long-lived channel seen in a few inside-out patches when Ca^{2+} was present on the intracellular side. This channel has a conductance of about 100 pS in symmetrical normal saline. It is not known which of the two predominant ion species (Na^+ or Cl^-) is responsible for this current. V_m= +70 mV for this trace. Scales: 5 s, 5 pS. **e)** Events recorded in symmetrical normal saline inside-out patch at V_m= +100 mV. This channel activity differs from that in **d** in that a number of open states are seen. This may correspond to the multiple-conductance Cl^- channel described in *Lymnaea* neurones under similar recording conditions (Geletyuk and Kazachenko, 1985). Scales: 5 s, 25 pA

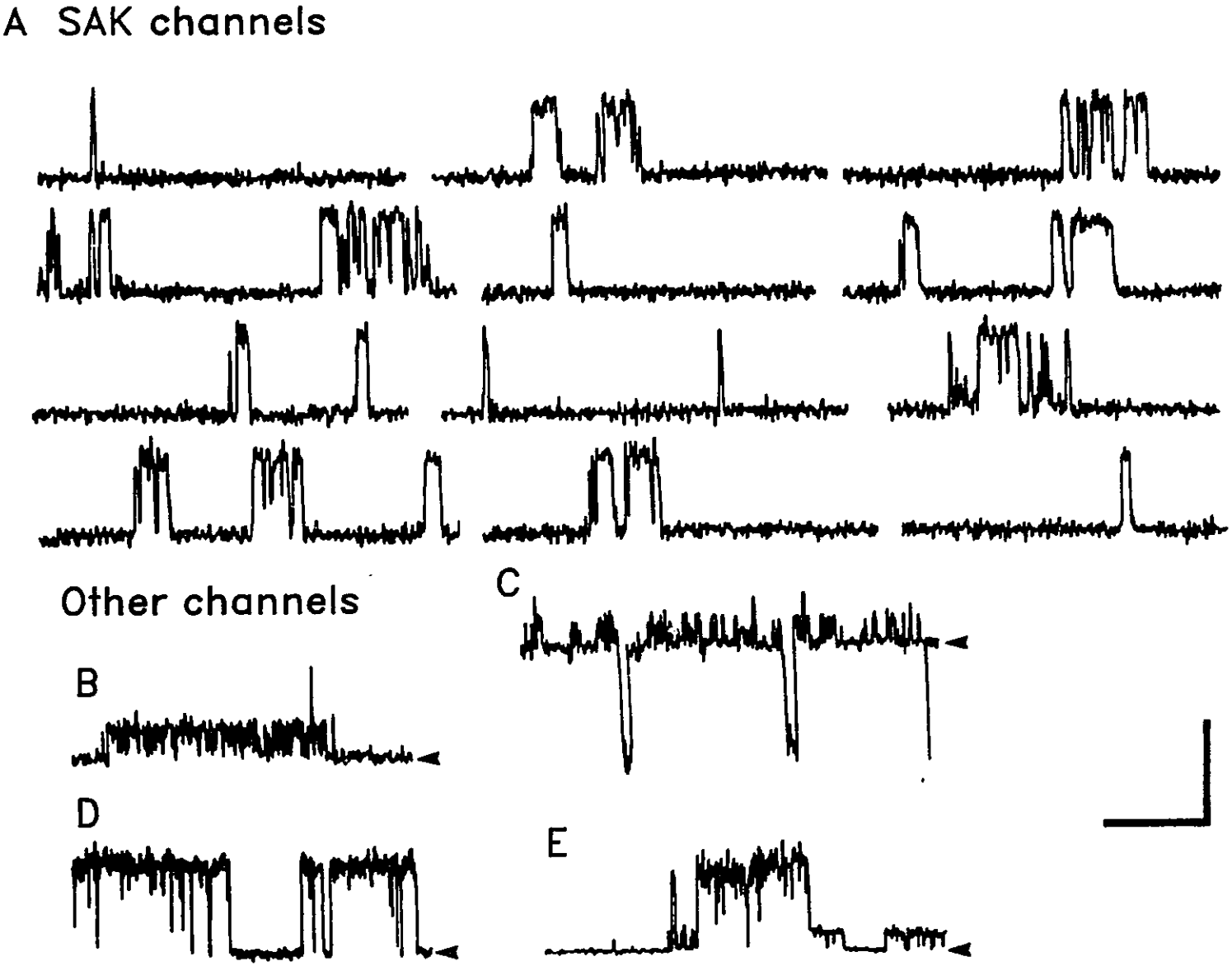
A SAK channels
Other channels
B
C
D
E

Figure 2. SAK channels are stretch-sensitive under a wide range of conditions. **a)** Cell-attached, NS in pipette, V_m = -20 mV. Scales: 5 s, 5 pA. For this trace, as well as **b**, **d** and **e**, application of suction is indicated by bar. **b)** Cell-attached, 30 mM K^+ saline in the pipette, V_m = +60 mV. Scales: 5 s, 5 pA. **c)** Inside-out patch, NS in the pipette, intracellular saline perfused over inner side. The high background (e.g. at 0 mm Hg) level of SAK channel activity may be due to pressure exerted by the flowing saline of the perfusion pipette. Channel activity increase when -3 mm Hg and -5 mm Hg are applied. Scales: 5 s, 5 pA. **d)** Cell-attached, intracellular saline in the pipette, V_m = -60 mV. Scales: 5 s, 2.5 pA. **e)** Inside-out, intracellular saline in the pipette, NS in bath, V_m = -60 mV or +60 mV. Although large outward currents flow through the SAK channel when K^+ is the cation on the inner side of the membrane, it is not possible to force an outward Na^+ current through the channel. Scales: 5 s, 2.5 pA.

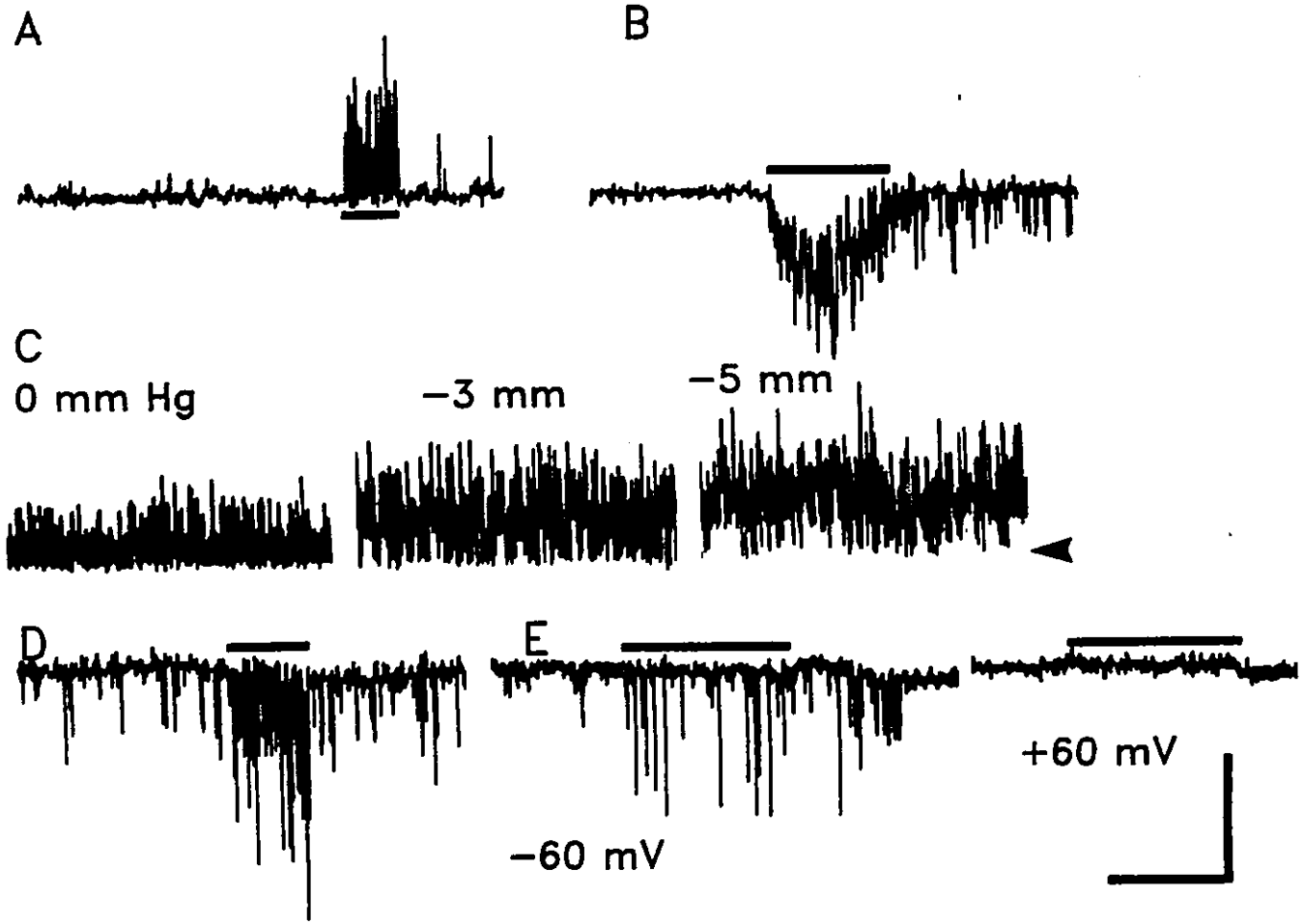
A
B
C
0 mm Hg
−3 mm
−5 mm
D
E
+60 mV
−60 mV

Kazachenko (1985)). The observation is best explained by assuming that the stretch-activated channel is K^+ selective and the low $[K^+]$ (1.6 mM) in NS prevents measurable K^+ currents from being detected. This was confirmed in Fig. 2c where outward SA currents were observed in inside-out patches (NS in pipette) when "intracellular" saline (Table 1; $[K^+]$= 60 mM) was perfused on the cytoplasmic side of the membrane patch.

Ca^{2+}-activated K^+ channels are ubiquitous ion channels found in a large number of cell types including snail neurons (Meech and Strumwasser, 1970; Adams et al., 1980; see Latorre and Miller, 1983) and since there is good circumstantial evidence for mechanically activated Ca^{2+} channels (Eckert, 1972), it is possible that SAK channels are being activated by Ca^{2+} influxes through mechanosensitive Ca^{2+} channels. I tested this possibility in the following ways.

(1) SA currents were observed in cell-attached patches (NS or 30 mM K^+ in pipette) at large depolarizations (V_m= +90 mV) where the driving force for Ca^{2+} influx should be small.

(2) Using excised, inside-out patches (NS in pipette), "intracellular" saline (Table 1; $[Ca^{2+}]$= 10^{-8} M) was perfused over the inner membrane surface. SAK channels were observed under these conditions (Fig. 2c).

(3) In cell-attached patches with "intracellular" saline in the pipette, SAK channels were seen (Fig. 2d); the $[Ca^{2+}]$ on both sides of the membrane would be presumably less than 10^{-7} M.

(4) When Ca^{2+} was present at 3.5 mM on the inner side of the membrane (inside-out, intracellular saline in pipette, NS in bath) stretch-activated current was observed (Fig. 2e). Any Ca^{2+} fluxes across the

membrane during suction would not affect [Ca^{2+}] on the cytoplasmic side of the patch.

Additionally, two drugs, apamin and cetiedil (10^{-6} M and 10^{-5} M applied respectively to patch pipette), known to block or antagonize Ca^{2+}-activated K^+ conductances were tested. Apamin which blocks Ca^{2+}-activated K^+ channels in cultured muscle cells (Hugues et al., 1982) and cetiedil which abolishes volume induced Ca^{2+}-dependent K^+ conductances in lymphocytes (Sarkadi et al., 1984) were both ineffective in modifying SAK channel conductance, stretch-sensitivity or kinetics.

SAK channel conductance is insensitive to membrane tension

SAK channel current/voltage (I/V) curves were made with and without suction being applied (Fig. 3). The slope conductances were essentially the same; suction did not affect channel amplitude and I can conclude that membrane tension does not distort the structural regions of the channel which are involved in ion permeation. It also indicates that significant amounts of channel bearing membrane are not being drawn up against the sidewalls of the pipette, since I would expect a reduction in channel amplitudes as the membrane approaches the wall (due to permeant ion depletion effects).

Effect of membrane tension on the probability that the channel is open

When a series of increasing static negative pressures were applied to a patch, SAK channels were activated as shown by the appearance of open and multiple open events. At higher pressures the multiple openings became fused until individual events could not be distinguished (Fig. 4). This

Figure 3. A comparison of current/voltage relationships for SAK channels without pressure (square) and with -10 mm Hg (diamond). Data were obtained on a cell-attached patch with NS in the pipette. The slope conductance for both regression lines is 33 pS.

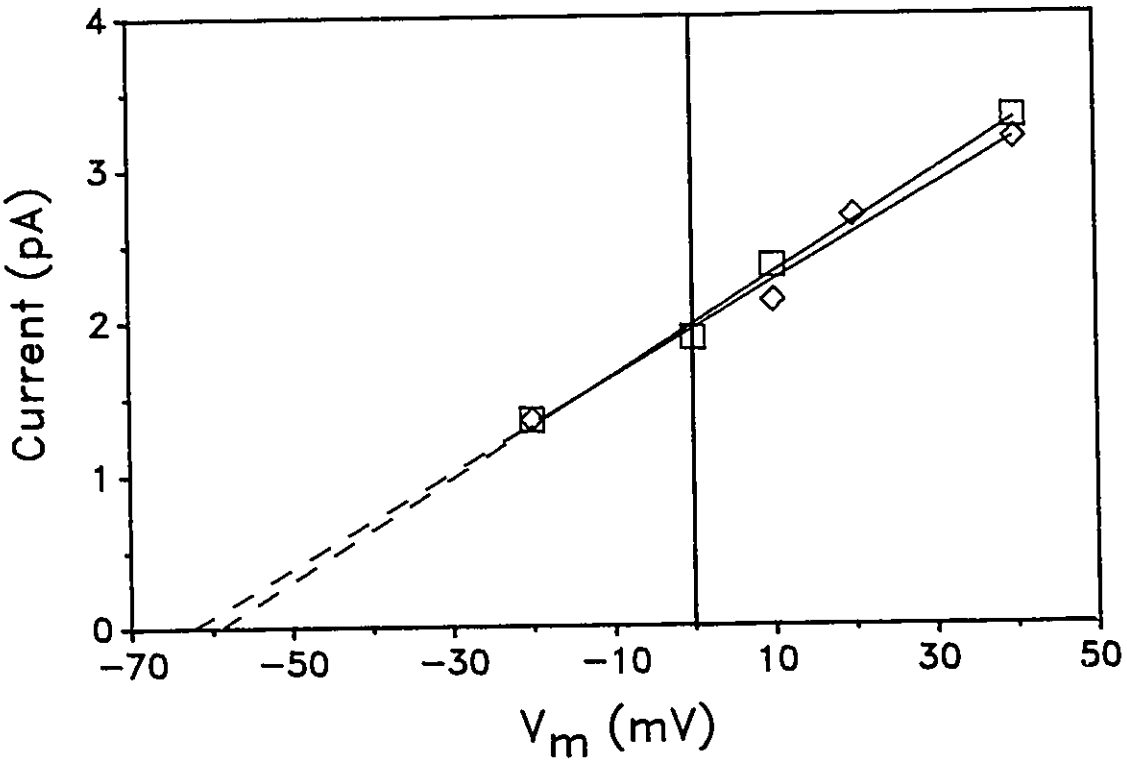
4
3
2
1
0
Current (pA)
−70
−50
−30
−10
10
30
50
V_m (mV)

Figure 4. SAK channel activity at a series of negative pressures. Cell-attached patch, 30 mM K^+ in pipette, $V_m = +140$ mV. Arrowhead indicates release of suction. The continuous record at 0 mm Hg (following -25 mm Hg) is interrupted then continued 85 s after release of suction. (The limited time resolution of the x-y plotter accounts for the apparent variability in channel amplitudes which are, however, of unitary height, as shown in Fig. 1a.)

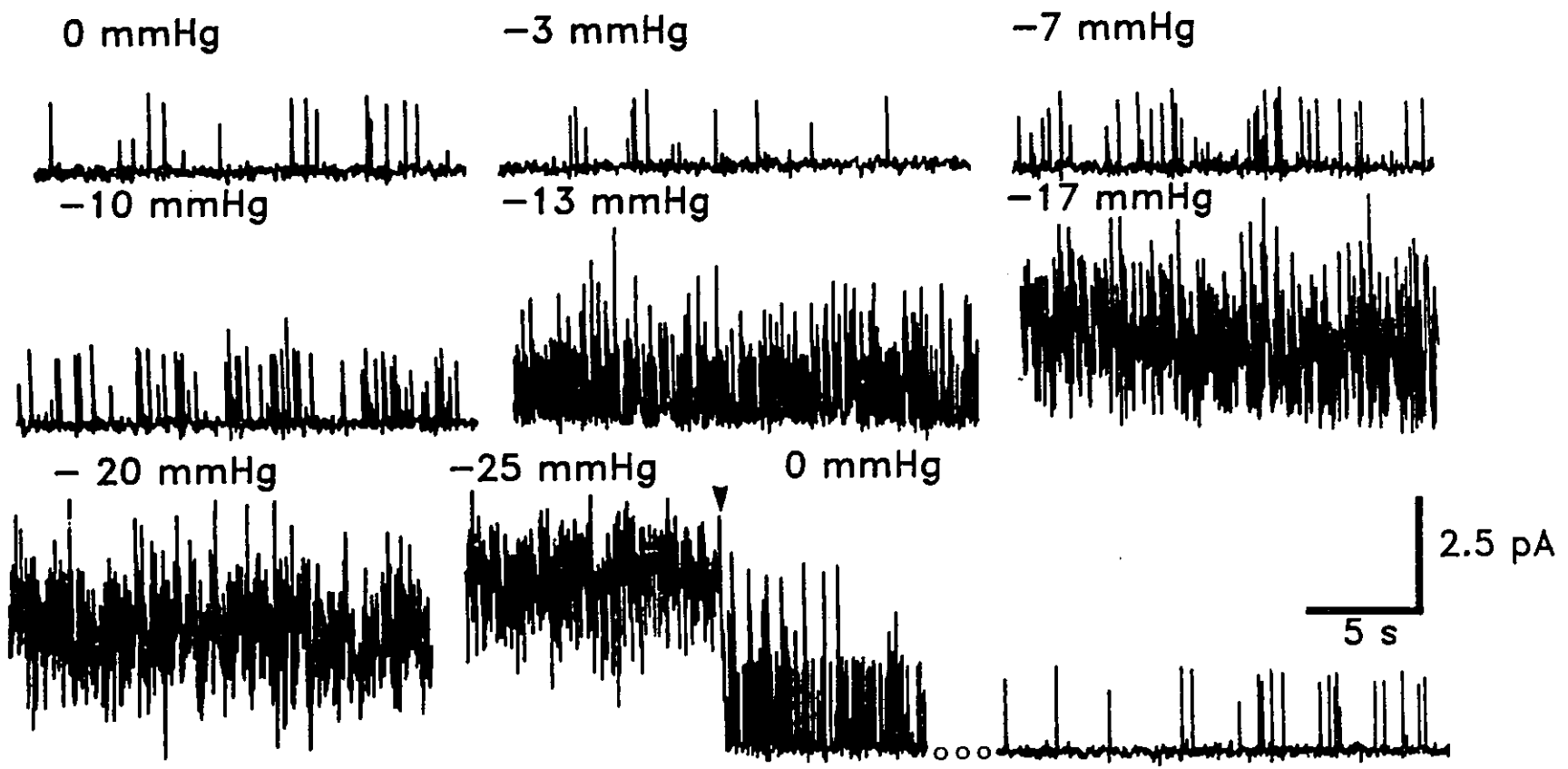
0 mmHg
−3 mmHg
−7 mmHg
−10 mmHg
−13 mmHg
−17 mmHg
− 20 mmHg
−25 mmHg
0 mmHg
2.5 pA
5 s

Fig. 1

increase in the open probability was reversible as seen by the immediate reduction in the number of current levels after release of calibrated (-25 mm Hg, Fig. 4) or uncalibrated suction (see Fig. 2). Typically, this turn-off after pressure release was immediate if pressure was applied for only a few seconds, but during long pressure series (Fig. 4) it often took several minutes for SAK channel activity to return to pre-suction levels. It is not clear whether this slow turn-off is caused by kinetic processes related to the length of time the membrane is under tension or is an artifact due to slow release of suction caused by capillarity within the pipette.

Plots of index P_o (time-averaged currents) against applied negative pressure (Fig. 5) were derived from records such as those shown in Fig. 4. In all cases the index P_o was a non-linear function of suction, but the pressure at which index P_o rapidly increased varied from patch to patch. When the patch was able to withstand higher pressures, the index P_o began to saturate (Fig. 4, see -25 mmHg trace; Fig. 5, squares). The saturation of index P_o denotes the lower limit of the total number of SAK channels present in the patch, which in the case of Fig. 4, is at least 3 channels. The total channel number cannot be found for a multi-state channel (see below) since the presence of stretch-independent rate constants prevents the channel from attaining a P_o equal to 1.

It should also be noted that as suction is increased, the current record becomes noisier (Fig. 4); i.e., the variance increases. This could result from bursts (see Fig. 1) of channel openings occurring more rapidly in succession, while intervening closed periods become smaller. The variance will be largest when $P_o \sim 0.5$, since on average the channels spend half their time

Figure 5. The effect of negative pressure on the probability that the SAK channel is open for different patches with 30 mM saline in the pipette. Ordinate: index of P_o, as explained in the text. Abscissa: applied pressure. Triangle, cell-attached, V_m = -80 mV; inverted triangle, inside-out, normal saline in bath, V_m = -40 mV (same patch as triangle); diamond, cell-attached, V_m = -120 mV; square, cell-attached, V_m = +40 mV.

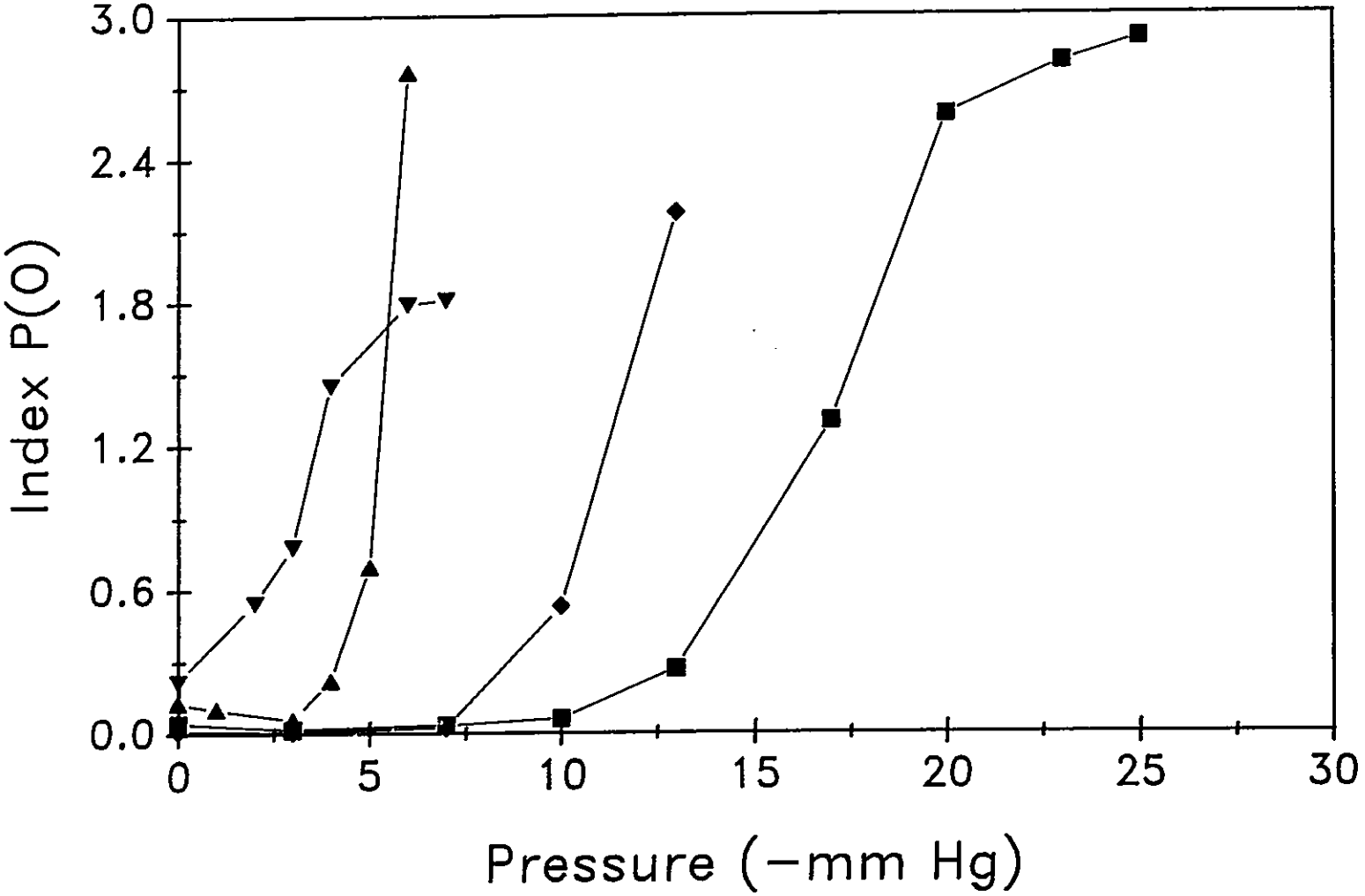
3.0
2.4
1.8
1.2
0.6
0.0
Index P(O)
0
5
10
15
20
25
30
Pressure (−mm Hg)

opened or closed. As P_o approaches 1, the variance will decrease (each channel spends more time open), but to a degree dependent on which of the kinetic components, i.e., openings or closings are stretch-dependent. If an open dwell time were stretch-dependent (open time increased as suction increased), the variance would approach the open channel noise level as P_o approached one (assuming one open state), but if a closed dwell time between bursts decreased as a function of pressure, the variance would only decrease to a point where the current record was made up of the remaining stretch-independent kinetic components. Application of suction sufficient to saturate SAK channel P_o, always resulted in variances in excess of the open channel noise. This is indicative then of a stretch-dependent closed dwell time.

The foot of the P_o curve might be thought of as a threshold region of channel activation, but only if pressure is directly acting on the channels and not through any intervening, complex compliancies in the patch. Using thin-walled pipettes and high magnification Nomarski optics, I have observed the membrane patch as pressure is applied. The patch appeared about 10 μm up the pipette where the walls are parallel. Initially the membrane was flaccid with a central "dimple". When suction ($\sim$ -5 mm Hg) was applied the membrane distended, the dimple disappeared and appeared to be under tension. There was a rough correlation between channel activity and the point of membrane distension. This was interpreted as evidence that channel activation depends on mechanical forces reaching the membrane and that suction does indeed exert these forces.

Open and closed states of the SAK channel

The increase in SAK channel P_o as a function of membrane tension could result from either a decrease in the rate of leaving an open state (mean open time increases) or an increase in the rate of leaving a closed state (decreasing closed dwell time). The observation that current variance is high at saturation suggests that a closed dwell time is decreasing. By examining the open and closed dwell time distributions as a function of pressure, this question can be addressed.

Ideally, open and closed time histograms used to study distributions should contain many thousand transitions and originate from a single-channel patch. Unfortunately, even after switching to heavily fire-polished thick-walled pipettes (to reduce patch area), single-channel patches were extremely rare and short-lived. As seen in Fig. 5, the rapid transition from low P_o (few events) to high P_o (many events and many doubles) made it difficult to obtain complete data sets encompassing a complete pressure series. It was possible however, to collect data over a range of 0 to -45 mm Hg in the cell-attached mode (V_m held at +30 to +60 mV) with either NS or 30 mM K^+ saline in the pipette.

Open time distributions consistently were best fit by the sum of two exponentials (Fig. 6a) rather than to one exponential. Closed time distributions required the sum of three exponentials for the best fit (Fig. 6b). The SAK channel therefore has at least five distinguishable kinetic states, two open and three closed.

In any known kinetic scheme, the mean dwell time for a particular state is the reciprocal of the sum of all rates for leaving that state. If we assume a simple linear kinetic scheme (see Guharay and Sachs, 1984),

Figure 6. Open- a) and closed-time b) histograms for SAK channels in a cell-attached patch held at -30 mm Hg and $V_m = +60$ mV. The time constants associated with the fitted function (continuous line drawn over the histogram bins) are indicated (O, open; C, closed). The tail of the third exponential fitted to the closed times is shown as an inset. Although data were rebinned for the fitting process (see Materials and Methods) they are displayed here with uniform-sized bin widths.

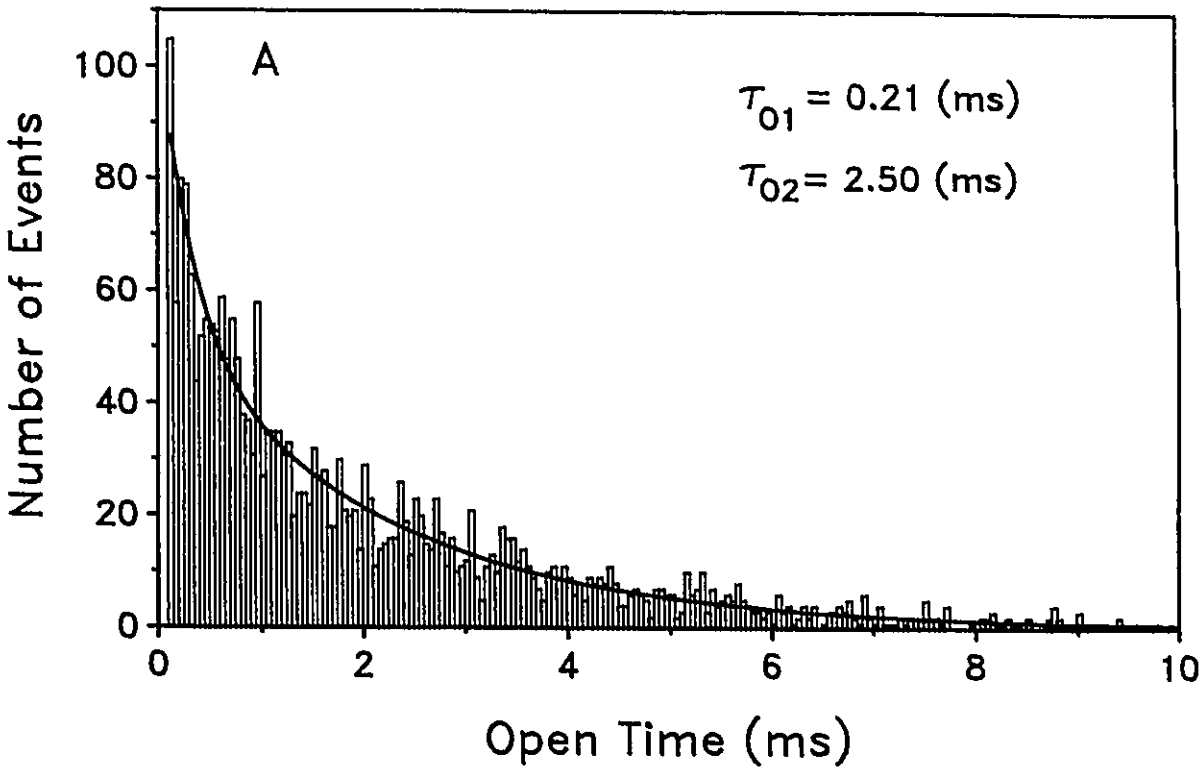
A
τ_{01} = 0.21 (ms)
τ_{02}= 2.50 (ms)
Number of Events
Open Time (ms)
0
20
40
60
80
100
0
2
4
6
8
10

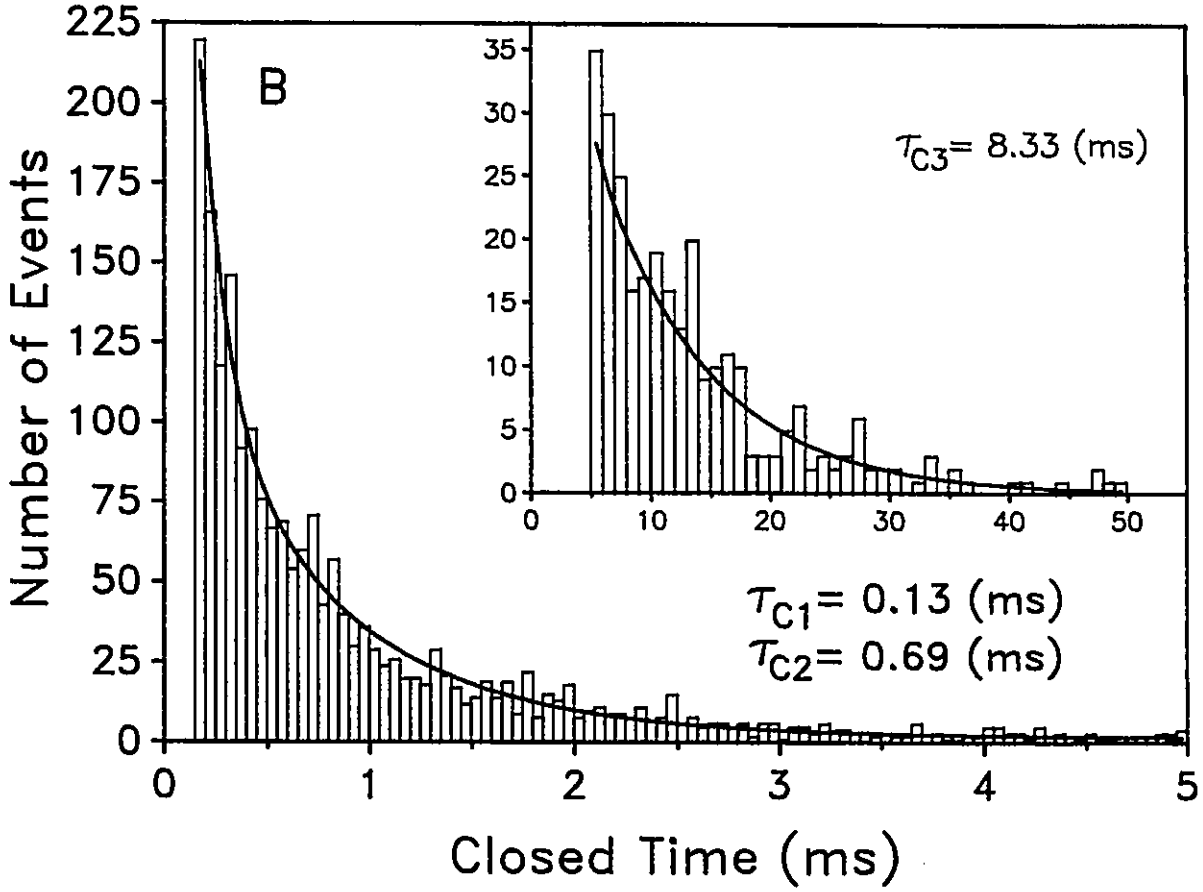
B
τ_{C3}= 8.33 (ms)
τ_{C1}= 0.13 (ms)
τ_{C2}= 0.69 (ms)
Number of Events
Closed Time (ms)
0
25
50
75
100
125
150
175
200
225
0
1
2
3
4
5
0
5
10
15
20
25
30
35
0
10
20
30
40
50

Figure 7. Time constants extracted from exponential fits as a function of pressure. The points connected by lines represent one cell-attached patch held at a constant potential (+30, +40 or +60 mV). a) square τ_{O1}, circle τ_{O2},; b) square τ_{C1}, diamond τ_{C2}; c) τ_{C3}. As explained in the text, the values for τ_{O1}, τ_{O2}, τ_{C1} and τ_{C2} reflect the true time constants, whcreas those for τ_{C3} are expected to scale inversely with increasing numbers of channels in the patch, and therefore are expected to vary widely from patch to patch. Inspection of the raw data indicates that τ_{C3} for the two rightmost patches in c continued to increase with decreasing negative pressure, but adequate three-exponential fits to the data could not be obtained because of the low relative density in the tail of the distribution.

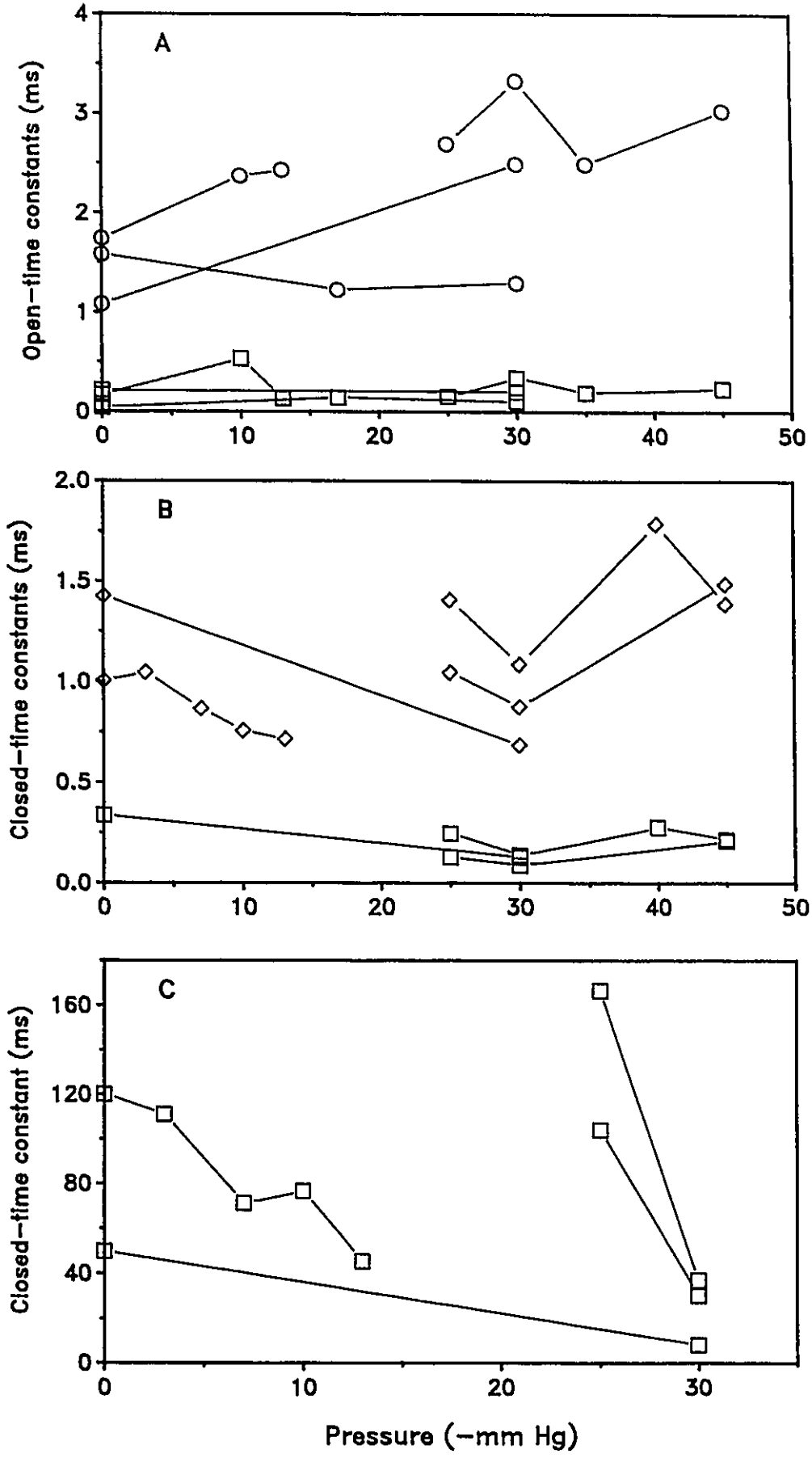
A
Open-time constants (ms)
4
3
2
1
0
0
10
20
30
40
50
B
Closed-time constants (ms)
2.0
1.5
1.0
0.5
0.0
0
10
20
30
40
50
C
Closed-time constant (ms)
160
120
80
40
0
0
10
20
30
Pressure (−mm Hg)

changes in one of the rates (presumably the stretch-sensitive rate) will be expressed by a change in one of the mean dwell times. Plots of open and closed time constants as a function of pressure (Fig. 7a and b) show that for the open times and short-lived closed times there are no consistent changes that would be responsible for the large P_o changes observed. So by elimination, the long closed time τ_{C3}, is the only time constant which should change and this is born out in Fig. 7c.

Multi-channel patches do not permit an unequivocal estimation of long closed time constants since once a channel has closed, there is a high probability that another channel will open before the first channel reopens, thus interrupting the closed interval "belonging" to the first channel. There is no way to distinguish which closed event belongs to which channel so the closed time distribution will be heavily contaminated by truncated closed times. Provided that multiple openings are eliminated, open times can be unambiguously estimated because it is extremely unlikely that one channel, while open, would close simultaneously as another channel opens. The same reasoning holds for the short closures, τ_{C1} and τ_{C2}; i.e., after brief closures there is a low probability that another channel will open. I can therefore assume that the open times, τ_{O1} and τ_{O2}, and the short closed times, τ_{C1} and τ_{C2}, are accurately estimated. Kinetically, the SAK channel can be described as having periods of activity, open durations punctuated by brief closures, followed by long periods of closure. When membrane tension is low these long closures can extend for hundreds of milliseconds, but as tension increases the transition rate for leaving this closed state increases thereby reducing the average long closed time. Since none of the other closed dwell times (recall the linear kinetic scheme)

appear to be stretch-sensitive, I have no evidence for a pressure-dependent transition rate for entering the long closed state.

SAK channel bursts

Following the procedure outlined in Materials and Methods, SAK channel bursts were analyzed. In Fig. 8 average burst duration, proportion of time spent open in a burst and the average number of closings per burst (all against interburst intervals) are plotted for one patch (Fig. 8a) at 4 different pressures and for 3 different patches (Fig. 8b). These graphs were used to choose an interburst interval of 3 ms as the appropriate cutoff time (i.e., all closings shorter than 3 ms are ignored; see Material and Methods) on the basis that between 2 and 10 ms estimates of these parameters should not change significantly. Analysis using 6 ms as the cutoff was also made for comparison (Table 2).

On the basis of curves in Fig. 8, I conclude that SAK channels do burst (see plateaus between 1 and 10 ms indicative of an unchanging parameter as interburst interval increases), but that bursts do not cluster (no evidence for another plateau at large interburst intervals). These plots also show that one interburst interval will suffice for more than one patch and/or pressure. In Fig. 8b, there is an example of data (-30 mm Hg) which contains overlapping bursts due to the large P_o. This data shows no burst duration plateau and is not suitable for further analysis.

Figure 8. Determination of burst parameters using different interburst intervals as explained in the text. **a)** Data obtained from the same patch at four pressures, square 0 mm Hg, triangle -7 mm Hg, inverted triangle -10 mm Hg and diamond -13 mm Hg (patch 1 of Table 2). **b)** Data obtained at 0 mm Hg for three different patches (square 0 mm Hg from **a**, triangle patch 3 of Table 2, diamond patch 2 of Table 2) plus burst duration data (inverted triangle) for the same patch as diamond but at -30 mm Hg. Note that abscissae are logarithmic, as are the ordinates for burst duration and closings per burst.

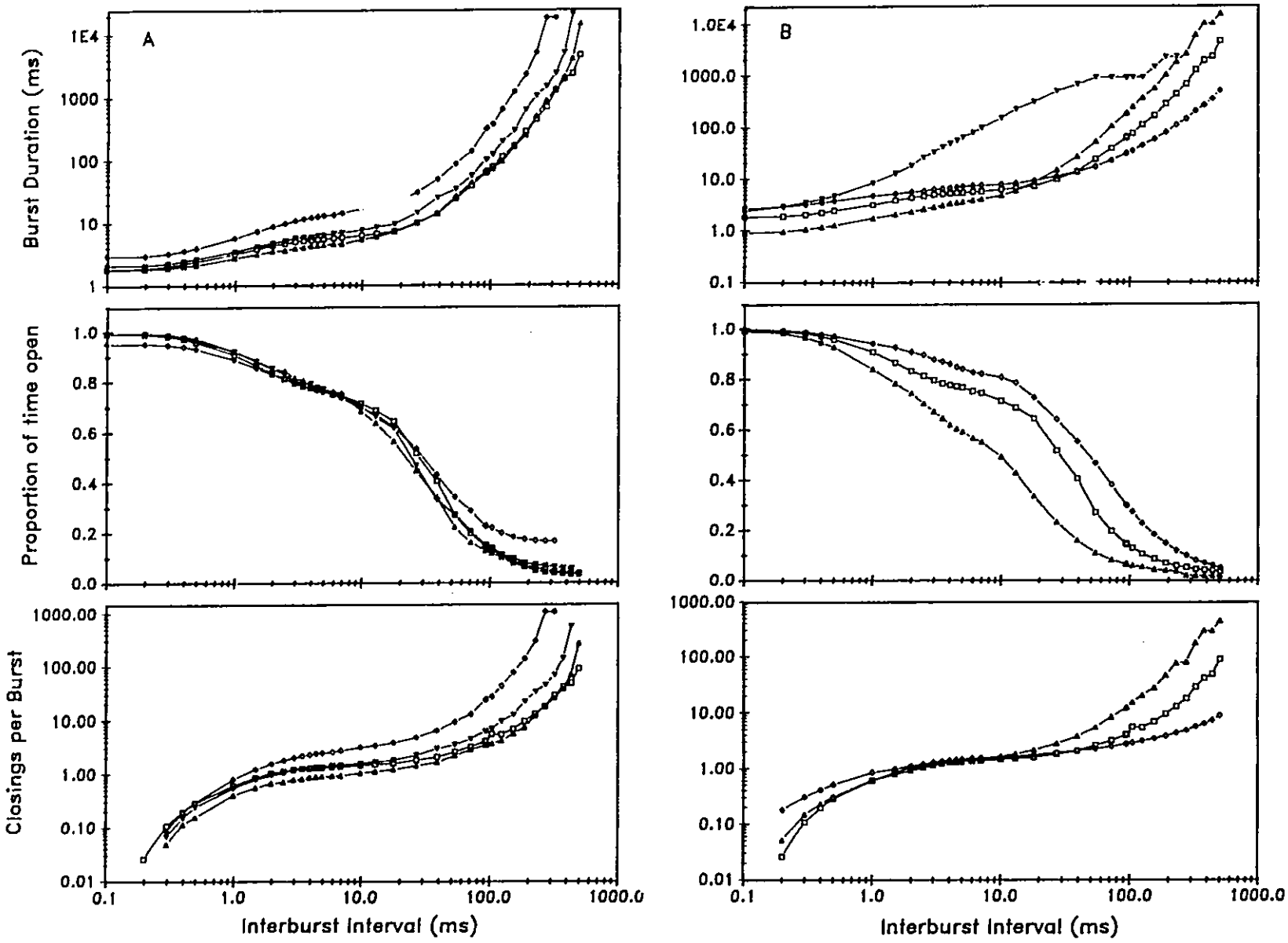
A
B
Burst Duration (ms)
Proportion of time open
Closings per Burst
Interburst Interval (ms)
Interburst Interval (ms)
1E4
1000
100
10
1
1.0E4
1000.0
100.0
10.0
1.0
0.1
1.0
0.8
0.6
0.4
0.2
0.0
1000.00
100.00
10.00
1.00
0.10
0.01
0.1
1.0
10.0
100.0
1000.0

Figure 9. Histograms for SAK channel burst activity. An interburst interval of 3 ms was used in this example, which is from a cell-attached patch held at 0 mm Hg and $V_m = +40$ mV. The burst distribution has been fitted to the sum of two exponentials whereas interburst intervals can be described by a single exponential.

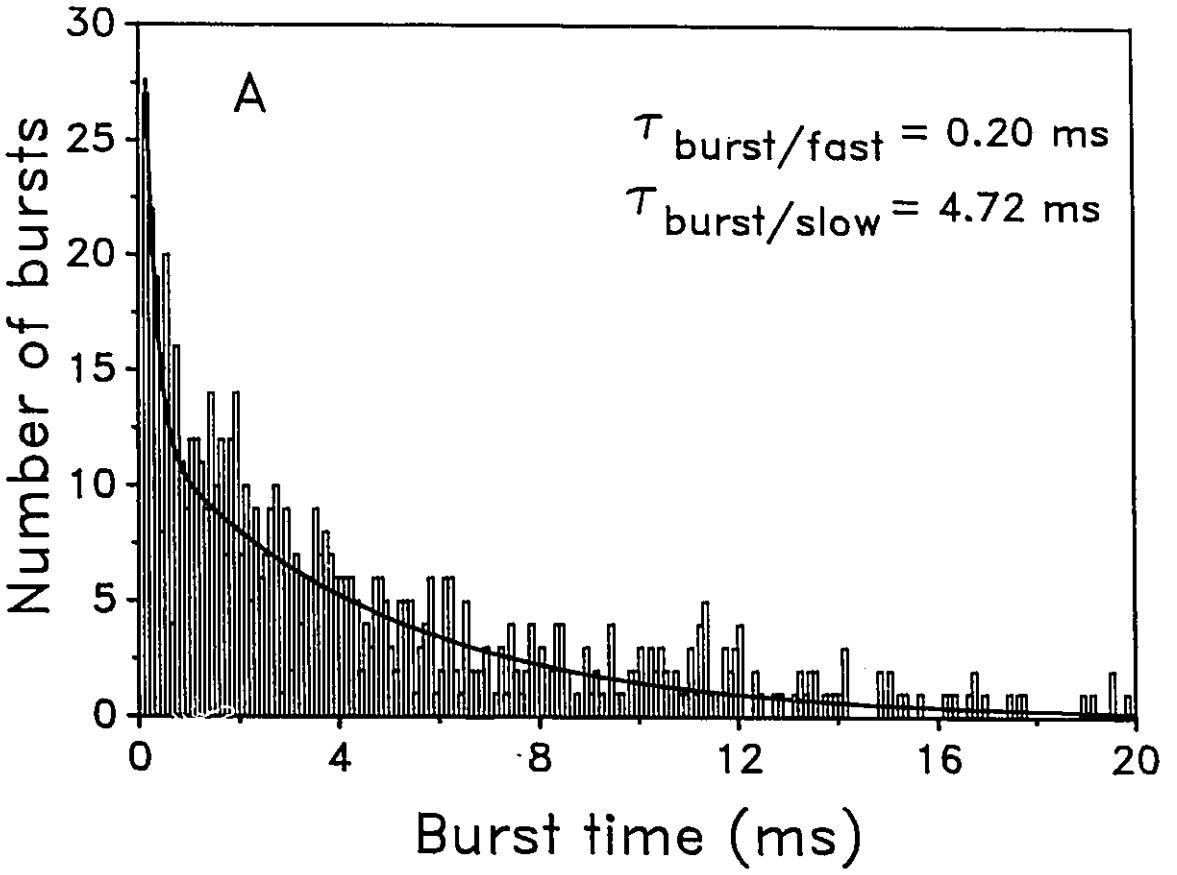
A
$\tau_{burst/fast}$ = 0.20 ms
$\tau_{burst/slow}$ = 4.72 ms
Number of bursts
0
5
10
15
20
25
30
0
4
8
12
16
20
Burst time (ms)

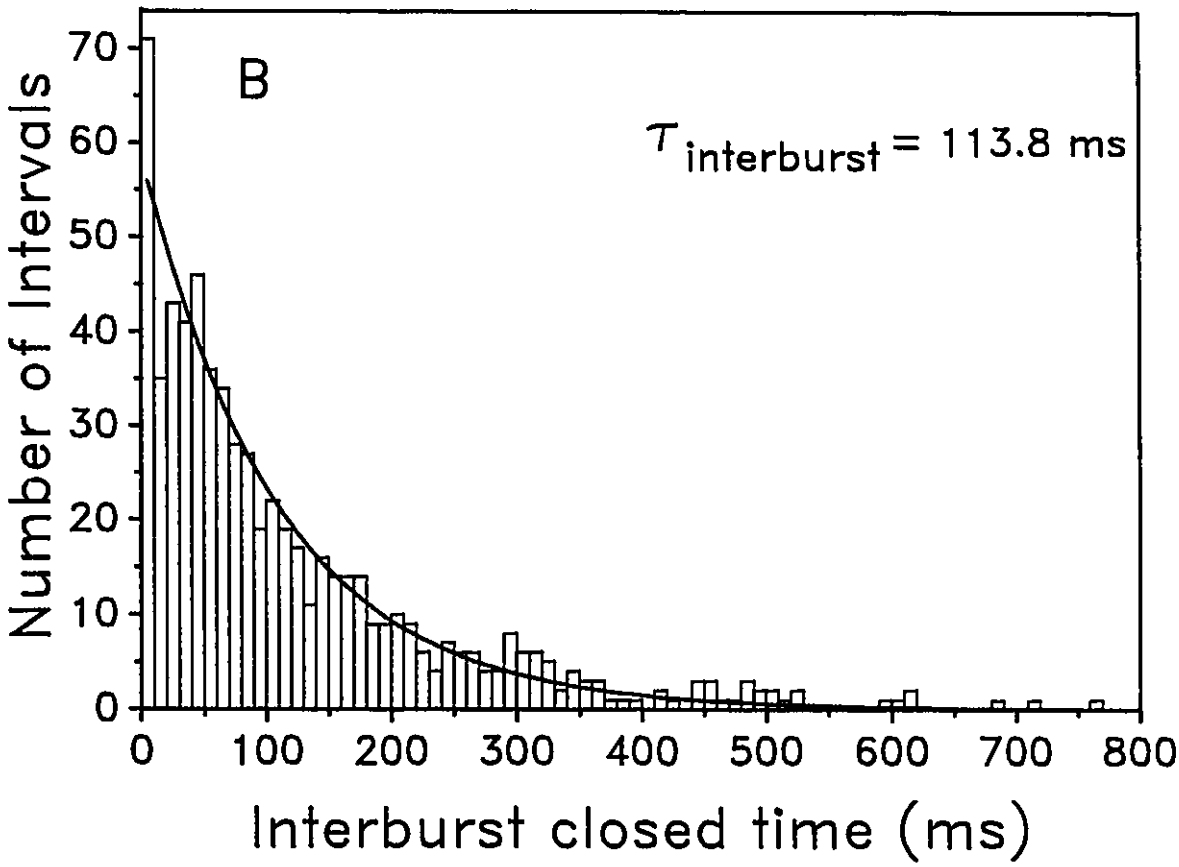
B
$\tau_{interburst}$ = 113.8 ms
Number of Intervals
0
10
20
30
40
50
60
70
0
100
200
300
400
500
600
700
800
Interburst closed time (ms)

We now used the empirically derived interval or cutoff (3 ms) to create histograms of burst and interburst durations (Fig 9). Burst durations were best fit to a sum of two exponentials; the fast time constant (presumably individual openings of short duration) represented only 10-15% of events in

Table 2. Heart SAK channel burst kinetics

Parameter	Applied pressure 0 mmHg	-7 mmHg	-10 mmHg	-13 mmHg
Patch 1				
Index P_o	0.04	0.03	0.06	0.27
$\tau_{burst/fast}$ (ms)	0.02 (0.19)[a]	0.44 (0.46)	0.39 (0.59)	0.2 (0.25)
$\tau_{burst/slow}$ (ms)	4.7 (5.2)	4.7 (5.6)	6.0 (7.1)	11.1 (14.9)
$\tau_{interburst}$ (ms)	113.8	111.0	65.8	40.4
τ_{C3} (ms)	120.5	111.4[b]	77.9	45.5
Closings per burst	1.4	1.0	1.4	2.2
Proportion of time open	0.79	0.81	0.8	0.8

	0 mmHg	0 mmHg
Patches 2 and 3		
$\tau_{burst/fast}$ (ms)	0.14	0.12
$\tau_{burst/slow}$ (ms)	2.6 (3.8)	3.5 (4.2)
$\tau_{interburst}$ (ms)	46.1	397.7
τ_{C3} (ms)	50.0	323.5
Closings per burst[c]	1.7	1.9
Proportion of time open	0.66	0.88

[a] The values in parentheses were obtained using an interburst of 6 ms whereas all others are based on a 3 ms interburst interval (both fit to a sum of two exponentials).

[b] This value was obtained from a single exponential fit to all closed times $\geq$ 5 ms, whereas other τ values are obtained from multiple exponential fits.

[c] Closings per burst pertain to slow bursts only, as explained in the text. All data are from cell-attached patches. Patch 1, 30 mM K^+ saline in pipette, V_m = +40 mV; patches 2 and 3, NS in pipette, V_m = +60 and +30 mV.

the distribution, but would contaminate the burst part of the distribution. Better estimates of proportion of time open and closings per burst were made by eliminating all "bursts" shorter than 0.7 ms (Table 2). At 0 mm Hg the mean proportion of time spent open in a burst was 0.78 $\pm$ 0.11 (N= 3) and the mean number of closings per burst was 1.66 $\pm$ 0.26 (N= 3). Using 3 ms as the interburst interval cutoff, the mean burst duration ($\tau_{burst/slow}$) was 3.6 $\pm$ 1.1 ms for these three patches. It is apparent that the burst duration for this patch does increase as pressure increases (see Fig. 8a upper panel; Table 2). This may be due to small increases in open dwell times occasionally seen in some patches (see Fig. 7a).

The interburst interval (the closed intervals between bursts) for each of the pressures was well fitted to a single exponential. $\tau_{interburst}$, the extracted time constant, was similar to τ_{C3} in terms of magnitude and changes in magnitude as suction was increased (Table 2). Thus there seems to be little uncertainty that $\tau_{interburst}$ and τ_{C3} are essentially equivalent and that the burst analysis can provide an independent measure of this kinetic parameter.

Discussion

The *Lymnaea* cardiac SAK channel is at least as sensitive to membrane tension as the chick skeletal muscle stretch-activated cation channel described by Guharay and Sachs (1984). Between 0 and -50 mm Hg suction, the latter channel showed a non-saturating, linear (ln P_o) dependence on the pressure squared. Presumably, the stretch-activated cation channel would eventually saturate at higher pressures; pressures at which the heart SAK channels had already saturated (two patches saturated below -25 mm

Hg) or were well into the steepest part of the P_o curve. The SAK channels are if anything more stretch-sensitive than the chick muscle channels. This increase in stretch-sensitivity could result from the adjustment of the underlying transduction machinery (increased gain) or to an intrinsic difference between the two channels. Another possibility is that the intrinsic membrane tension was higher in the heart cell membrane causing the channels to reach their "operating" tension at lower applied pressures. (In essence, the foot of the P_o *vs* pressure curve would be shifted to the right in the case of the chick cells.) Guharay and Sachs (1984) showed that cytochalasin B treated muscle cells were 30 times more sensitive than untreated cells. They concluded that inherent membrane-tension was being relieved by underlying actin-containing structures and removal of these elements by cytochalasin resulted in the stretch-sensitive channels "seeing" more tension. Physically this could be represented by the reduction of membrane slack or compliance. An intrinsic adjustment of similar structures in the cardiac cells, could account for the increased SAK channel stretch-sensitivity and/or differing sensitivities between patches.

Kinetically the SAK channel and the chick stretch-activated cation channel are somewhat similar. The SAK channel open time distribution contains an additional fast component not seen in the chick channel, but both channels have at least 3 closed dwell times. Both channels exhibit bursting behavior with bursts dominated by channel openings. The consistency of closings per burst and proportion of time spent open as a function of pressure is indicative of the stretch-insensitivity of the fast kinetic parameters that produce the bursts. (As noted in the results the rise in burst duration as suction is increased may be due to small increases in τ_{O2},

but these changes are minor and too inconsistent between patches to account for the large increases in P_o.) Guharay and Sachs (1984) were able to show directly that the transition rate for leaving the long-lived closed state was stretch-sensitive. Although I have had to use data that was not ideal for closed-time determinations, I feel confident my estimate of the long closed-time also reflects changes in the stretch-sensitive transition rate because of the qualitative agreement with the estimate of the inter-burst interval. Therefore in both channel types it is the average closed-time between bursts that is stretch-sensitive, decreasing with increasing pressure.

A further similarity between SAK channels and stretch-sensitive chick channels is a low and apparently homogeneous membrane density. It is difficult at best to obtain SAK channel density estimates so it's only possible to put limits on the channel density and distribution. A homogeneous channels distribution (with a density not greater than 1 μm^{-2}) is expected for the following reasons. Random sampling of the cell membrane would produce a Poisson distribution of channel density if the channel was randomly distributed and had a low mean number of channels per patch. Single-channel recording is a random sampling of membrane patches and so I would have expected to find one-channel or zero-channel patches. Even using small orifice pipettes I consistently found patches with at least two or three channels (as many as 10 channels in larger pipettes). Estimates of membrane patch area (made by observing patches in thin-walled pipettes) were about 8 μm^{-2} thus giving a density less than 1 μm^{-2}. In comparison, Na^+ channel density ranges from $\sim$100 μm^{-2} in *Myxicola* axons to 3000 μm^{-2} in frog node of Ranvier (Hille, 1984). The non-random distribution of SAK

channels may be explained by cytoskeletal interactions that limit channel lateral diffusive mobility (Almers and Stirling, 1984). This is in keeping with the model formulated by Sachs (1986) which requires cytoskeletal elements to be part of the transduction machinery.

Is it necessary to postulate a specific transduction mechanism for the SAK channels? Is stretch-activation an artifact? If membrane tension acted non-specifically on channel kinetics (in the same way as an increase in thermal energy, i.e. by increasing all rates), it would be unlikely to find only one stretch-sensitive kinetic parameter in a collection of at least five distinguishable states. A non-specific effect of membrane tension should also result in other channels being stretch-sensitive. This was not observed (see the low conductance channel in Fig. 1b). Another potential artifact is the drawing up of new channel-bearing membrane into the pipette exposing additional spontaneously active channels. Based on channel densities, a 20 fold increase in membrane area would be needed to account for the observed P_o increase. Since stretch-activated currents are observed in excised patches this is impossible.

The physiological role of the *Lymnaea* cardiac SAK channel is not clear, but their hypothesized role in osmoregulation (Brezden et al., 1986) is a promising one. Preliminary studies of cells isolated from *Lymnaea* kidney indicates the presence of channels apparently similar to SAK channels. These cells also exhibit a quinidine sensitive pathway that limits cell swelling during hyposmotic shock (Morris et al., 1989). Quinidine blocks SAK channels (Brezden et al., 1986) so investigation of the volume-regulating behavior in *Lymnaea* ventricular cells may shed light on SAK channel function.

Chapter 3: Ionic selectivity of stretch-activated ion channels in snail neurons

Introduction

The ubiquity and diversity of K^+ selective ion channels have made these channels the object of intense study in attempts to understand the physical basis of ion channel permeation. Previous work has centered on K^+ channels whose gating modalities involve voltage and ligand activation. Recently another mode of channel gating has been described that involves the transduction of mechanical energy, in the form of membrane tension, into channel activation (see Sachs, 1988).

Based on selectivity criteria, stretch-activated (SA) channels of animal cells appear to be of three types (see Kullberg, 1987). There are the cation selective channels originally described by Guharay and Sachs (1984), (common in many vertebrate preparations) and a K^+ selective stretch-activated (SAK) channel described in pond snail ventricular cells (Brezden et al., 1986; Sigurdson et al., 1987a), land snail neurons (Bedard et al., 1988), amphibian kidney (Sackin, 1987; Sackin, 1989), *Drosophila* muscle (Zagotta et al., 1988) and fish embryos (Medina and Bregestovski, 1988). Recent reports of a SAK channel in glial cells now extends this distribution to mammals (Ding et al., 1988). A third type of SA channel, found in kidney (Ubl et al., 1988a) does not distinguish between cations and anions.

Any function proposed for an ion channel is directly tied to its ionic selectivity which must therefore be unequivocally determined. Previous reports on SAK channels have established a clear preference for K^+ over Na^+, but generally have not quantified this selectivity relative to other monovalent cations. Selectivity sequence data and absolute permeability

measurements permit comparison with voltage- and ligand-gated K^+ channels and allow inferences to be drawn about permeation mechanisms.

Investigation of the SAK channel's physiological role would be fostered by pharmacological tools that interfere with channel function. Earlier attempts to find a suitable SAK channel blocker met with limited success since only quinidine was found to be effective (Brezden et al., 1986; Sigurdson et al., 1987a). This has prompted further examination of quinidine and other K^+ channel blockers.

Here we report on the selectivity and on its sensitivity to K^+ channel blockers of a SA channel found in isolated *Lymnaea* neuron cell bodies. This channel is evidently similar to the SAK channel described earlier (Brezden et al. 1986; Sigurdson et al., 1987a) in *Lymnaea* heart cells.

Materials and Methods

Animals

Pond snails (*Lymnaea stagnalis*) were collected locally (Rideau River) or purchased from Blades Biological, Edenbridge, England. Snails were housed either in tanks with flow-through dechlorinated water or in aquaria fitted with charcoal filters and aeration. Temperature was maintained at 15-18° C by water mixing or immersion heaters. Snails were fed on Romaine or iceberg lettuce *ab libitum*.

Cell isolation and culture

Neurons were isolated from the circumoesophageal ganglionic ring which included the right and left pedal, pleural, parietal, cerebral ganglia as well as the visceral ganglion. The ring was placed in sterile isotonic normal saline (NS, see Table 3) supplemented with 5 mM glucose. Connectives between the individual ganglia were severed and neurons from individual ganglionic masses isolated by first loosening the connective tissue sheath in 0.25% protease (Sigma) (40 min agitation) followed by mechanical dispersion in glass-bottomed recording chambers or culture dishes containing glass coverslips. Chambers were detergent-washed, rinsed thoroughly with distilled water, surface sterilized with 70% ethanol and then dried in a 60° C oven for at least 2 hours before use. Cell adhesion and spreading on the glass substratum was generally good provided the amount of cellular debris was minimized during dispersal. To improve adhesion, coverslips were sometimes acid/base washed with 1% HCl followed by 1% Na_2CO_3 and thorough rinsing with distilled water (Jacobson, 1977). Cultures were

maintained in sterile NS, supplemented with 5 mM glucose, penicillin (500 I.U. ml^{-1}) and streptomycin (500 μg ml^{-1}).

Recording solutions

NS was used as the standard bath saline and pipette solution to simulate physiological ionic conditions. Recording solutions used in the patch pipette, bath and perfusion pipette are listed in Table 3. Solutions used for comparison of relative K^+ and Na^+ permeabilities are referred to as 50K,10Na, 10K,50Na or 100K. For biionic experiments pipette solutions contained 50 mM of the test cation (counter ion either Cl^- or gluconate, except for Tl^+ whose counter ions were acetate or nitrate). The patch perfusion solution (PPS) and a simulated intracellular saline (IS) contained a calculated free Ca^{2+} concentration of 10^{-8} M. Quinidine and tetraethylammonium (TEA) (Sigma) in NS were used as patch pipette filling solutions as needed. The ionic strength of pipette solutions was kept approximately the same as NS except for those containing 100 mM KCl. All solutions were buffered with 5 mM Hepes with pH adjusted to 7.6 with either 0.1 M NaOH or KOH.

Cells were cultured and all recordings made at room temperature (18-23° C).

Table 3. Culture and Recording Solutions (in millimoles/liter)*

Solution	Na	K	Ca	Mg	EGTA
NS	50.0	1.6	3.5	2.0	
30K	20.0	30.0	3.5	2.0	
50K external		50.0	1.0	0.0	
100K external		100.0	1.0	0.0	
50K,10Na	10.0	50.0	1.0		
10K,50Na	50.0	10.0	1.0		
50K PPS		50.0	0.2		2.2
100K PPS		100.0	1.0		
IS		60.0	0.2	2.0	2.2

*All solutions adjusted to pH 7.6 with 0.1 M NaOH or KOH.

Recording Configuration

Standard single-channel recording techniques were employed (Hamill et al., 1981) to record from cell-attached or excised (inside-out) patch configurations. Patch electrodes were pulled (Kopf 750 pipette puller) from Corning 7052 capillary tubes (Garner Glass Co, Claremont, CA ID=0.8 mm, OD=1.65 mm) and fire-polished with a platinum/iridium heating element just before use. Pipette tip openings were estimated to be a maximum of 2 μm in diameter prior to fire-polishing and had a mean bubble number of 4 $\pm$ 0.6, n=5 (Sigurdson and Morris, 1989; see Corey and Stevens, 1983). Suction was applied to the patch pipette through the sidearm of the electrode holder and when required monitored by a Bio-Tek pressure transducer (Bio-Tek Instruments, Burlington, VT).

Single-channel currents were recorded using an Axopatch 1A (Axon Instruments, Burlingame, CA) or List EPC-7 (List Medical/Medical Systems, Greenvale, NY) patch clamp amplifier. Currents were filtered (8 pole Bessel, Frequency Devices Inc.) at 5 or 10 kHz and stored on either FM tape (Racal Store 4) or on video tape using a PCM-1 (Medical Systems, Greenvale, NY) digitizing unit. For analysis of current amplitudes, data were filtered at 1 or 2 kHz, displayed on a digital storage oscilloscope and the amplitudes of at least 10 individual events directly measured from the display. Alternatively, current records were filtered at 2.5 or 5 kHz, digitized at 10 kHz and amplitude histograms generated point by point on a DEC LSI 11/23 computer. Mean channel current was obtained by manually selecting the midpoint of such histograms.

To facilitate rapid solution changes during biionic recordings, the recording pipette was placed in the flow of large >50 μm diameter perfusion

pipette (Yellen, 1982). Flow rate was hydrostatically controlled and could be monitored by observing schlieren lines during mixing of the bath and PPS. The SAK channels were sensitive to the perfusion flow rate; too great a flow tended to activate the channels. To balance channel activity with a flow rate sufficient to exclude the possibility of bath contamination of the perfusion stream, the hydrostatic pressure head was adjusted using the coarse controls of a micromanipulator. It was possible to change the internal bathing solution of the patch in less than one second and, given the appropriate ionic conditions, observe changes in channel amplitude and polarity.

Current/Voltage Relations

Current/voltage (I/V) curves were constructed from single-channel amplitudes of SAK channel currents during application of negative pressure (usually uncalibrated, but sufficient for identification). For cell-attached I/V relations the membrane voltage (V_m) was taken to be:

$$V_m = V_{rest} - V_p \qquad (3.1)$$

where V_p is the pipette holding potential and V_{rest} the assumed resting potential of the cell. V_{rest}, obtained from intracellular measurements, was previously shown to be -50 mV $\pm$ 1.9mV (sem, n = 32) (Sigurdson and Morris, 1989).

V_{rev} (zero current potentials) were determined either directly from the current record or by interpolation of the I/V curves. In cases where currents were too small to be observed, such as for Na^+ and Li^+,

approximate V_{rev}'s were obtained by extrapolation of the K^+ quadrant (outward current) of the I/V curves.

Permeability ratios were determined under biionic conditions by use of a simplified Goldman-Hodgkin-Katz (GHK) voltage equation

$$V_{rev} = \frac{RT}{F} \ln \frac{P_X[X]_o}{P_K[K]_i} \qquad (3.2)$$

where F is the Faraday, R the gas constant, T the absolute temperature, V_{rev} the biionic reversal potential, P_X, $[X]_o$ and P_K, $[K]_i$ the permeability and concentration of the test cation on the outside of the membrane and K^+ on the inside of the membrane respectively (Hille, 1984; Benham et al., 1986). Rearranging equation 3.2 gives the P_X/P_K ratio directly from the reversal potential, V_{rev}.

$$\frac{P_X}{P_K} = \frac{[K]_i \exp(V_{rev}F/RT)}{[X]_o} \qquad (3.3)$$

Under the low ionic concentrations (relative to terrestrial or marine organisms) used in these experiments (see Table 3), Na^+ and Li^+ currents through the SAK channel were generally not seen. To more closely examine the relative permeabilities of Na^+ and K^+, a mixture of the two ions was chosen which resulted in I/V curves having measurable single channel currents on either side of the zero current potential. By assuming no Cl^- permeability, a modified GHK voltage equation gives the P_{Na}/P_K ratio directly from a mixture of two ions

$$\frac{P_{Na}}{P_K} = \frac{\exp(V_{rev}F/RT)[K]_i - [K]_o}{[Na]_o - \exp(V_{rev}F/RT)[Na]_i} \qquad (3.4)$$

where P_{Na}, P_K are the permeabilities of Na and K respectively, V_{rev} the zero current potential, $[K]_i$, $[K]_o$, $[Na]_i$ and $[Na]_o$ the concentrations of K and Na on the inside and outside of the membrane.

Absolute values for ion permeabilities permit comparison with other channels which are examined under different ionic concentrations. These are given by the GHK current equation for conditions of one ion on each side of the membrane (Hille, 1984; Benham et al., 1986)

$$I = P_X z^2 \frac{VF^2}{RT} \frac{[X]_i - [X]_o \exp(-zFV/RT)}{1 - \exp(-zFV/RT)} \qquad (3.5)$$

where I is the single-channel current, P_X the permeability of ion X (cm s^{-1}, derived from the limiting conductance), V the transmembrane voltage, z the valence, and $[X]_i$ and $[X]_o$ the concentrations of X on the inside and outside of the membrane. For symmetrical solutions, i.e. $[X]_i = [X]_o$, this reduces to

$$I = P_X z^2 \frac{VF^2}{RT} [X] \qquad (3.6)$$

or

$$P_X = \frac{IRT}{z^2 VF^2 [X]} \qquad (3.7)$$

(Benham et al., 1986). Therefore, I is linearly dependent on [X] thus allowing comparison of P_X in instances where [X] is not the same. P_K was determined in this way by using symmetrical K^+ solutions, constructing an

I/V curve, calculating a P_K for each current/voltage pair and averaging the P_K's.

Analysis of burst characteristics, duration and number of closings per burst, was performed using an empirical technique described in Sigurdson et al. (1987a) and Chapter 2. Briefly, to define a group of channel openings as a burst, a series of increasing interburst intervals are tested. For very short intervals, openings will be defined as a "burst". As intervals increase in length, short closings are ignored, thereby grouping openings together into bursts. If bursts are well separated, there will be a range of increasing intervals, for which burst durations do not increase as the interval increases. This "plateau" region of a plot of burst duration *vs* interburst interval can be used to give an estimate of true burst duration. The number of closing per burst was obtained in the same fashion.

The errors about means are expressed as standard deviations (std) or standard errors (sem), while errors about slopes are given as the standard error of the slope (ses). For comparison of 2 or more slopes, a F test for the discrimination of significant differences between slopes was used (Sokal and Rolf, 1981).

Results

A neuron soma ion channel activated by stretch

Under nominally physiological conditions, i.e., NS in the patch electrode and bath, the stretch-activated channel was observed as outward current. During the application of suction, the number of open events per unit time and the number of open channels increased, resulting in an eruption of activity (Fig. 10a). When high K^+ is present in the pipette SA

events can be observed at the resting potential of the cell (Fig. 10b) or at depolarized voltages (Fig. 10c). The presence of high concentrations of external Ba^+ and Cs^+ do not block SAK channel conductance and none of these agents, including TEA, affect channel stretch-activation (Fig. 10d, e, f). The channels are not sensitive to Ca^{2+} as shown in cell-attached and inside-out patches where Ca^{2+} has been buffered to 10^{-8} M (Fig. 10c, f). The activation of the channels is quite rapid (1 - 2 s), giving a quick diagnostic for the presence of the channel. The channel was seen in virtually every neuron and every patch (>200 patches) examined in this population of unidentified neuronal somata.

Figure 10. Neuron SAK channels activated under a variety of conditions. In these long time base records, channel openings appear as spikes. **a)** During application of suction (indicated by line below this and subsequent recording traces) both frequency of channel opening and the numbers of open channels increased. At least 3 channels were activated as shown by outward current levels. Simulated physiological recording conditions, i.e. cell-attached, NS in pipette and bath. V_m = +50 mV, assuming that V_{rest} = -50 mV (see Methods). **b)** In cell-attached patches, with 50 mM K^+ present outside (in pipette) and V_m at rest, suction elicits inward current as expected for a K^+ selective channel under conditions where E_K was approximately zero (assuming $[K]_i$ = 50 mM) and the driving force equal to V_{rest} (about -50 mV). **c)** SAK channels remained responsive to suction in the presence of intracellular levels (10^{-8} M) of external Ca^{2+}. Cell-attached patch with IS present in pipette. V_m = +70 mV. **d)** External TEA (10 mM TEA in NS in pipette) did not affect SAK channel stretch-sensitivity nor completely block outward SAK channel in cell-attached patches. Current amplitudes were reduced however, at V_m's in the physiological range (see Fig. 22a. V_m = +90 mV. **e)** At high external concentrations, Ba^+ had no effect on SAK stretch-sensitivity and did not block outward K^+ current or permeate the channel. Cell-attached patch; 50 mM Ba^+ in pipette. V_m = +70 mV. **f)** Excised patches (inside out) containing SAK channels were formed for determination of biionic permeability ratios. In this example (50 mM Cs^+ in pipette and 50 mM K^+ PPS perfusion) Cs^+ did not block outward stretch-activated K^+ current nor affect stretch-sensitivity. The low $[Ca^{2+}]$ in PPS demonstrated that SAK channel activity is not dependent on cytoplasmic Ca^{2+}. V_m = +80 mV. In all excised patches, SAK channels were activated by application of suction to ensure positive identification of the channels in what were usually quite noisy records. Suction was uncalibrated (~-40 mmHg) and manually applied. The increased noise (compared to cell-attached patches) arose (more often) from a decrease in seal resistance or as in this case from other lower conductance, non-stretch-sensitive channels. All records filtered at 1 kHz. Scales, all records 5 pA; **a** and **b** 1.25 s; **c**, 5 s; **d**, **e** and **f**, 2.5 s.

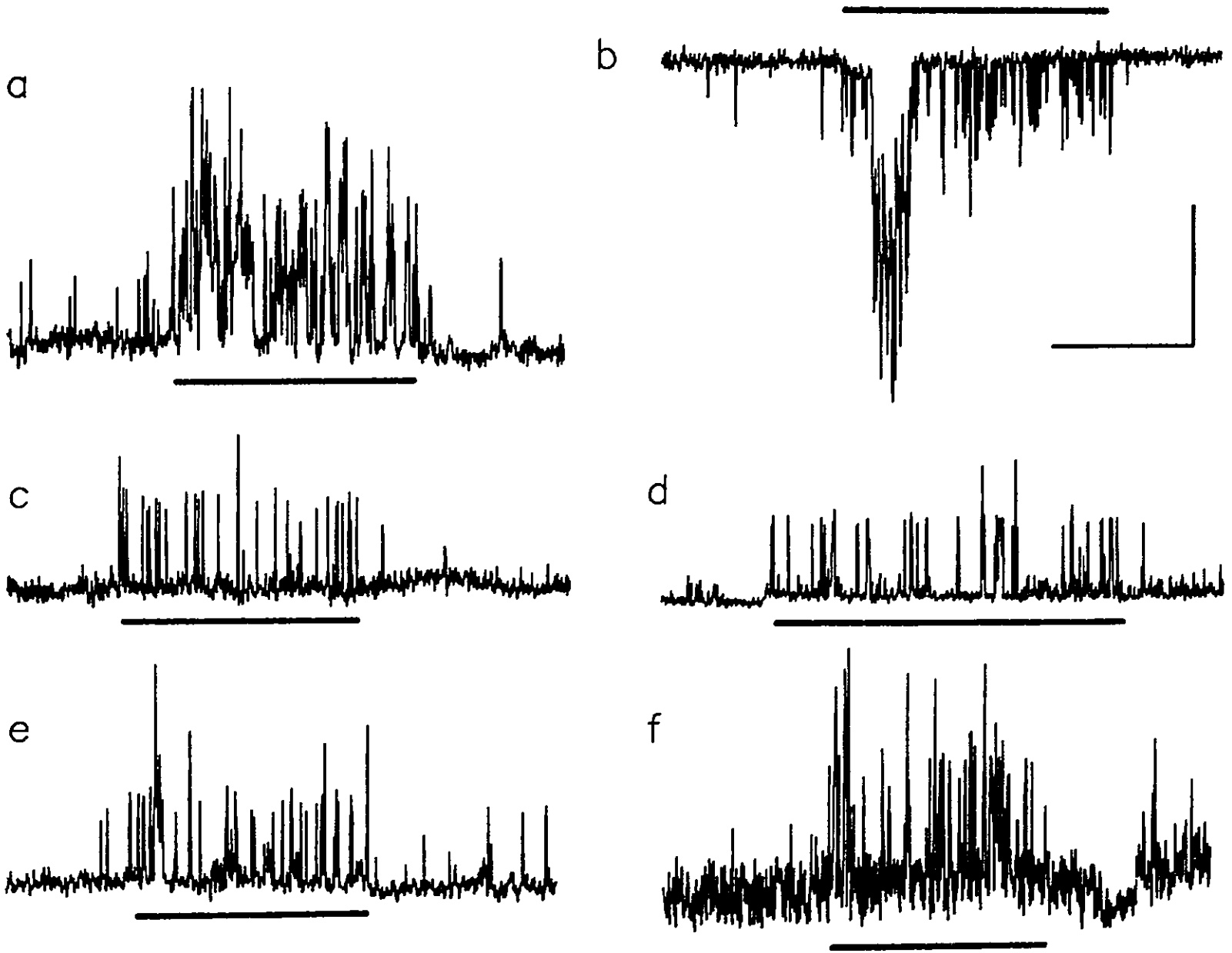
a
b
c
d
e
f

Channel conductance as a function of stretch

In a simple model of SAK channel gating, one could envisage membrane tension causing the channel pore to widen sufficiently to allow ions to permeate (the "rubber donut" model) (Sachs, 1988). Such a mechanism would have profound effects on the permeation properties of the channel, which would now be dependent on the degree of membrane tension. This possibility was tested by examining channel amplitudes and slope conductances as a function of pressure.

Fig. 11 is a point by point histogram of current for the same patch at 6 different pressures. It is clear for the first nonzero peak, representing one open channel, that channel amplitude is invariant as membrane tension is changed. When 2 or more channels are open, increased current variance makes it difficult to obtain long periods when amplitude can be precisely measured. Nevertheless, when the midpoints (determined by eye) of the distributions are averaged, the amplitude of two open channels is twice that of one open channel.

Figure 11 . Point by point amplitude histogram of SAK channel currents for 6 different pressures, ranging from 0 to -70 mmHg. Histogram peaks correspond to the zero current baseline, 1, 2 and 3 channels open simultaneously. The third peak was obtained only at -70 mmHg, during periods when 3 channels were open for significant periods of time. Amplitude means for 1 and 2 channels were found by selecting the midpoint of the respective histogram peak. Histogram peaks were arbitrarily scaled for display purposes. Cell-attached patch with NS in pipette and bath. $V_m = +70$ mV.

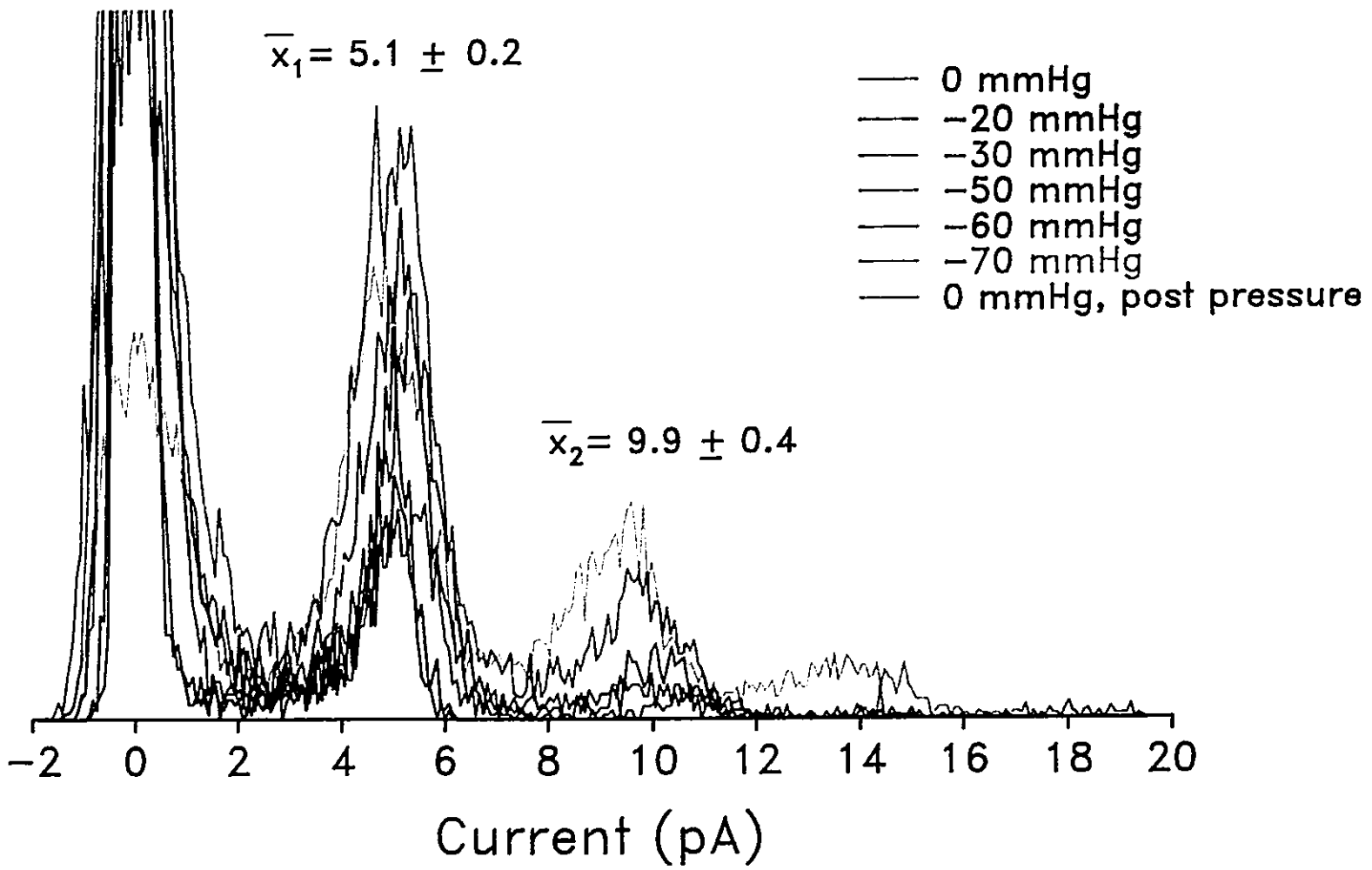
$\bar{x}_1$= 5.1 ± 0.2
$\bar{x}_2$= 9.9 ± 0.4
0 mmHg
−20 mmHg
−30 mmHg
−50 mmHg
−60 mmHg
−70 mmHg
0 mmHg, post pressure
−2 0 2 4 6 8 10 12 14 16 18 20
Current (pA)

Current voltage relations of cell-attached patches

Under physiological ionic conditions (NS in the patch electrode), inward SA current was never convincingly observed even at large hyperpolarizations. At extreme voltages, only currents associated with gigaseal breakdown were seen. This outward rectification of the single channel current therefore suggested a K^+ selective channel (Fig. 12). Substitutions of patch electrode solutions for those containing higher [K^+] demonstrated a shift in the depolarizing direction (Fig. 13, 14) consistent with K^+ selectivity. For cell-attached patches variation in the resting potential (V_{rest}) in a mixed population of neurons precludes accurate measurements of reversal potential (V_{rev}) shifts. Intracellular recordings indicated an average V_{rest} of -50 mV $\pm$ 1.9 mV (sem, n = 32) (Sigurdson and Morris, 1989; Sattelle (1974) reported a V_{rest} of -53.3 mV $\pm$ 2.7 mV with identical external K^+), but this encompasses much variation (V_{rest} ranged from -36 to -75 mV). Nevertheless, for convenience, transmembrane potentials reported here are based on an assumed V_{rest} of -50 mV when the bath

contains NS. The Nernst potential for a 1.6/50 mM (50 mM is a reasonable estimate of internal [K^+], see Sattelle, 1974) K^+ gradient is -87 mV, for 30/50, -13 mV and for 100/50, 17.5 mV. The observed V_{rev} shifts for 30 K^+ and 100 mM K^+ saline (Fig. 14) were -9.7 mV $\pm$ 3.7 mV (std, n = 4) and +24 mV $\pm$ 5.2 mV (std, n = 3) respectively, reflecting approximately the correct shift of 58 mV per decade concentration change for a K^+ electrode. The V_{rev} for 50 K^+ saline was +7 mV $\pm$ 13 mV (std, n = 5) which was close to the expected E_K of 0 mV, but displayed a variability which I cannot account for. Cell attached slope conductances increase as external K^+ increases (Fig. 14), in general agreement with the GHK current equation (equation 3.5).

Figure 12. Current/voltage relation for a cell-attached patch demonstrating outward currents of spontaneously active SAK channels under physiological ionic conditions (NS in pipette and bath). Zero current was observed when V_m was equal to V_{rest}, i.e. pipette holding potential equal to 0 mV. Inward current could not be elicited at larger hyperpolarizations. No suction was applied during these records, but stretch-sensitive channel current could be elicited throughout this voltage range (not shown). Filtered at 2 kHz; scales, 5 pA and 50 ms.

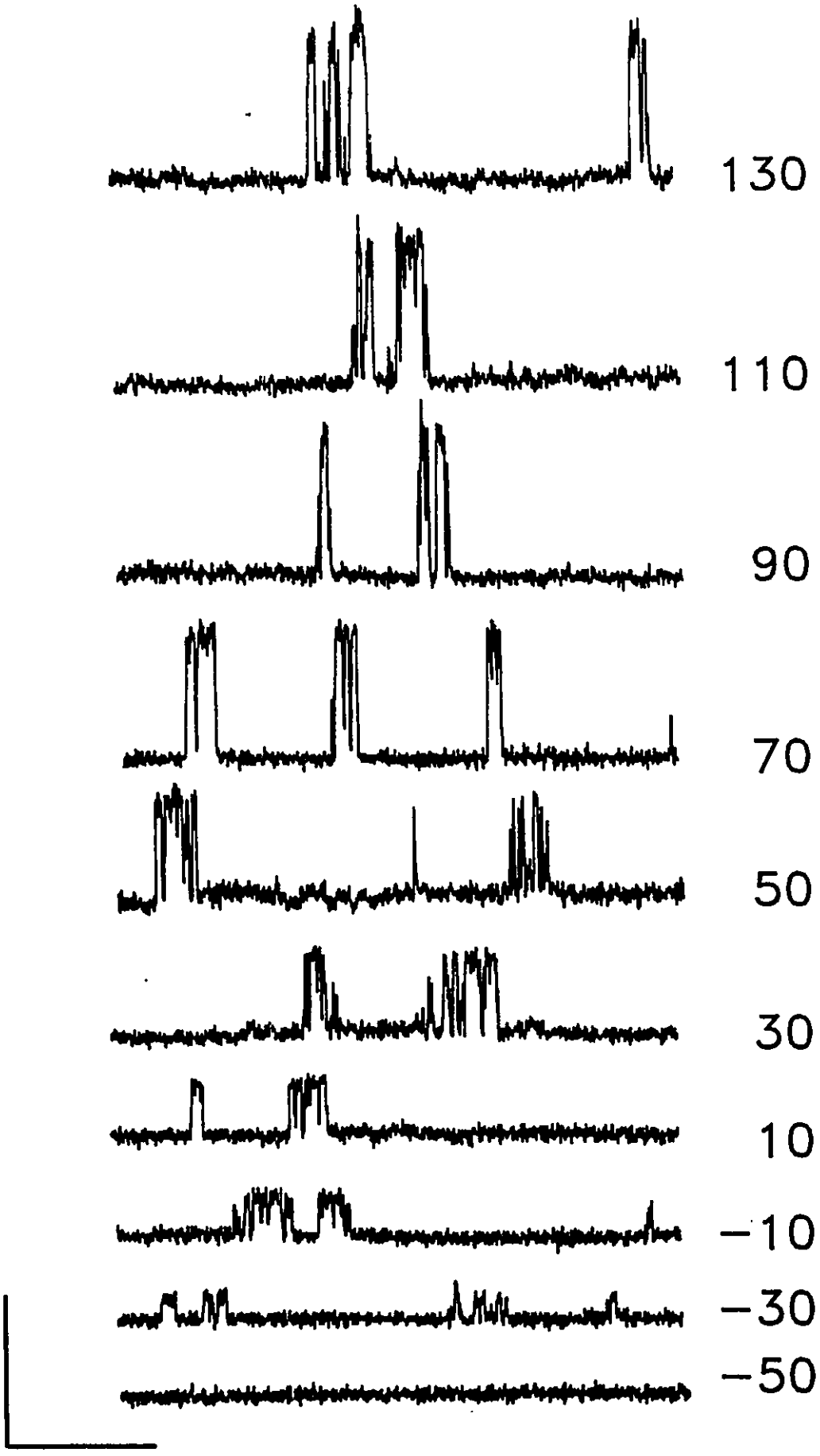
130
110
90
70
50
30
10
−10
−30
−50

Figure 13. Current/voltage relation for a cell-attached patch demonstrating inward and outward currents of spontaneously active SAK channels under conditions of high external K^+ (100 mM, NS in bath). Zero current potential was approximately 10 mV. No suction was applied during these records, but stretch-sensitive channel current could be elicited throughout this voltage range (not shown). Filtered at 2 kHz; scales, 5 pA and 50 ms.

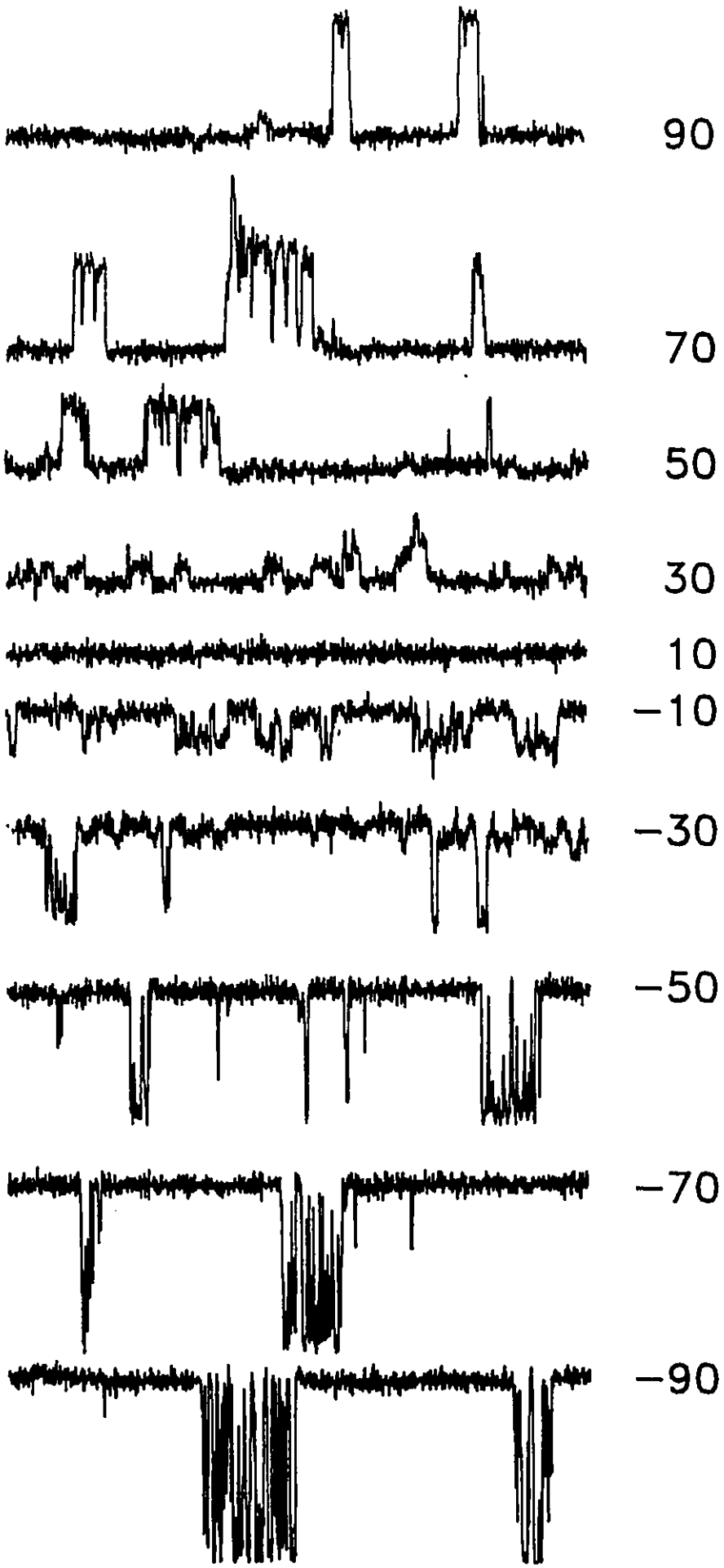
90
70
50
30
10
−10
−30
−50
−70
−90

Figure 14. Cell-attached I/V curves showing V_{rev} shift with increasing external [K^+]. For pipettes containing NS, inward current was not observed at large hyperpolarizations. Linear extrapolation of the NS curve therefore is an underestimate of the zero current potential (departures from linearity of the curve would be expected at greater hyperpolarizations, although outward current amplitudes would likely be too small for accurate measurement). Slope conductances increased as the concentration of external K^+ was increased. Under physiological conditions (NS in pipette) SAK channels had a conductance of 30 pS $\pm$ 7 pS (std, n = 7), which increased to 33 pS $\pm$ 3 pS (std, n = 4) with 30 mM K^+, 43 pS $\pm$ 5 pS (std, n = 4) with 50 mM K^+, and to 56 pS $\pm$ 6 pS (std, n = 3) when 100 mM K^+ was the external [K^+].

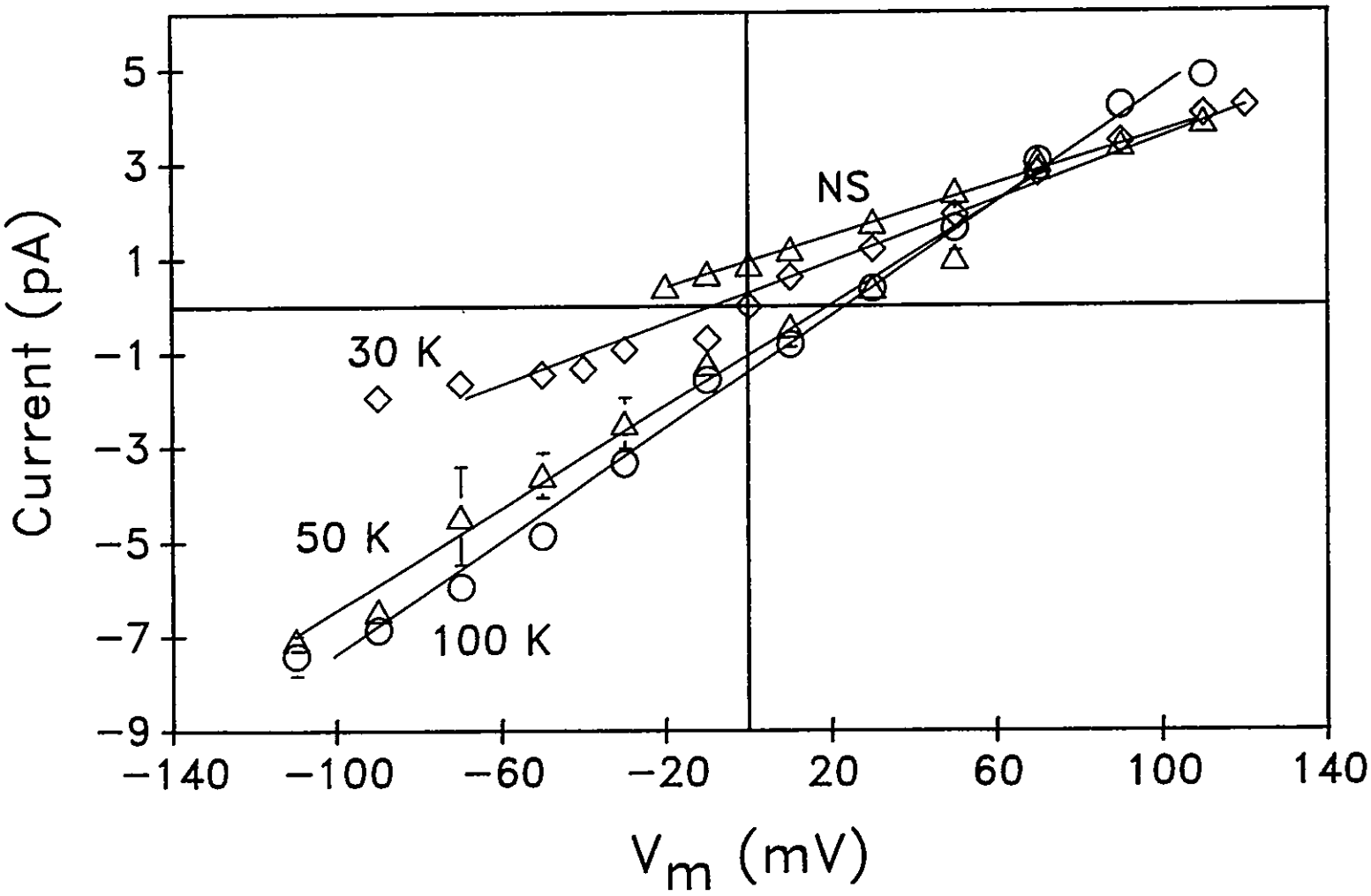
Current (pA)
5
3
1
−1
−3
−5
−7
−9
−140
−100
−60
−20
20
60
100
140
V_m (mV)
NS
30 K
50 K
100 K

Relative Na^+/K^+ permeabilities

To circumvent the problem of unknown resting potentials, excised patches were used to determine the relative permeabilities of K^+ and other monovalent cations. Na^+ is the major cation of the extracellular fluid in *Lymnaea* (Brezden and Gardner, 1983) and therefore a candidate for any inward current which might flow through these channels. However, during cell-attached recording, inward currents were undetectable with NS in the pipette making the reversal potential asymptotic. To provide a more accurate measure of V_{rev}, a new bathing solution containing a higher K^+ concentration (enough to produce detectable outward current) was used (50 mM Na^+, 10 mM K^+).

Excised patches, useful for this experimental purpose proved to be difficult to obtain. The channel's mechanosensitivity was often problematic in that upon excision, channels were activated to a point where single-channel amplitudes could not be measured accurately. The fact that excision followed by exposure to low Ca^{2+} solutions did not reduce the activity is good evidence against this being a Ca^{2+}-related effect (see Fig. 10c, f). Perhaps, the tension on the membrane and underlying cytoskeletal elements during and following excision disrupts the "normal" channel activity in an essentially irreversible way. In those patches where single-channel activity was more moderate, flow from the perfusion pipette often activated the channels (see Methods).

Fig. 15 presents the I/V curves obtained for one patch (50 mM K^+, 10 mM Na^+ in the patch electrode) under 3 conditions: cell-attached, inside-out and inside-out/perfusion. As expected for a K^+ selective channel (assuming V_{rest} is -50 mV and an intracellular $[K^+]$ of ~50 mM), V_{rev} is initially near

zero under cell-attached conditions. When the patch is excised into 10 mM K^+/50 mM Na^+, V_{rev} shifts to +33 mV (by linear extrapolation), approaching the K^+ equilibrium potential (E_K) of +41 mV. For three such patches, V_{rev} was +32.3 mV $\pm$ 3.6 mV (std), giving a P_{Na}/P_K ratio not greater than 0.083 (equation 3.4). When this patch electrode was placed in the flow of the perfusion pipette containing 100 mM K^+, V_{rev} shifted in a hyperpolarizing direction to -17.5 mV; i.e. to the K^+ Nernst potential (-17.4 mV). This represents a 50.5 mV shift in V_{rev} per 10 fold increase in $[K^+]$.

The channel has negligeable Cl^- permeability since V_{rev} in the cell-attached mode (presumably low intracellular $[Cl^-]$ and therefore a negative E_{Cl}) was near zero and a depolarized V_{rev} was observed under symmetrical Cl^- for the excised non-perfused patch.

Figure 15. I/V curves for one patch under 3 different ionic conditions. a) Cell-attached patch with 50K, 10Na in pipette. V_{rev} = -6 mV, slope conductance was 64 pS based on linear portion of curve. Data fit to 3rd order polynomial for display purposes. b) Excised (inside out) patch with 10K, 50Na in bath. Extrapolation of linear regression line to zero current gave V_{rev} as +33 mV (E_K = +44 mV for this K^+ gradient). Slope conductance was 27 pS. Curve represents calculation of GHK current equation (equation 3.5) using $[K]_i$ = 10 mM and $[K]_o$ = 50 mM (P_K determined from limiting conductance measurements in Fig. 16a). c) Internal solution changed to perfusion solution consisting of 100 mM K^+. I/V curve shifted in depolarizing direction as predicted for a K^+ selective channel. V_{rev} (estimated from 3rd order polynomial curve fit) was essentially identical to E_K (-17 mV) for a 50/100 ionic gradient. Slope conductance based on most linear portion of curve was 54 pS. Curve represents calculation of GHK current equation using $[K]_i$ = 100 mM and $[K]_o$ = 50 mM.

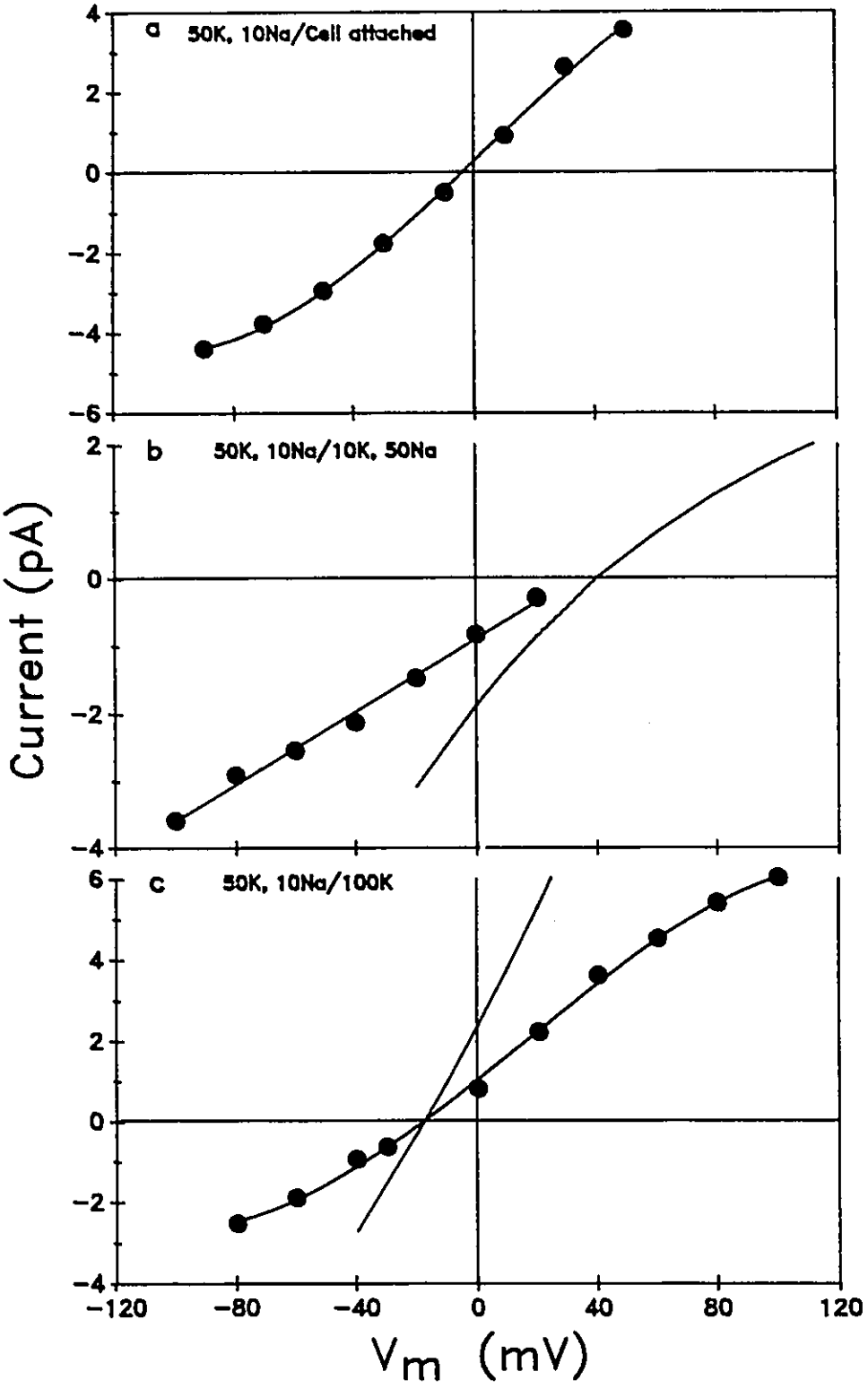
a 50K, 10Na/Cell attached
b 50K, 10Na/10K, 50Na
c 50K, 10Na/100K
Current (pA)
Vm (mV)
4
2
0
-2
-4
-6
6
-120
-80
-40
40
80
120

Absolute K^+ permeability

An absolute measure of SAK channel permeability to K^+ was determined (equation 3.7) under symmetrical K^+ (50 mM) using inside-out patches with the internal solution provided by a perfusion pipette. Based on four such patches, P_K was found to be $4.9 \times 10^{-13} \pm 0.76 \times 10^{-13}$ cm s^{-1} which is comparable to high conductance Ca^{2+}-activated K^+ channels (Latorre and Miller, 1983; Blatz and Magleby, 1984; Benham et al., 1986), but is about 3 times larger than the *Aplysia* S channel (Shuster and Siegelbaum, 1987; see Table 4). A large permeability can be reconciled with the relatively low slope conductance of 86 pS (Fig. 16a) by recalling the lower ionic strength of solutions used. In Fig. 16a, the deviation from linearity seen in the depolarizing quadrant is a consistent feature of I/V curves produced under symmetrical K^+ conditions.

Biionic selectivity

SAK channel permeability ratios were determined from V_{rev}'s obtained under biionic conditions for the monovalent cations, Na^+, Tl^+, Rb^+, Li^+ and Cs^+ (Figs. 16b, 17). V_{rev}'s for Na^+, Li^+ and Cs^+ were difficult to establish due to the very low current amplitudes and the increased baseline noise encountered in excised patches. Currents carried by Li^+ and Cs^+ were not detectable in either cell-attached or excised patches (test cation in the pipette and K^+ in the internal solution) so V_{rev}'s were estimated by linear extrapolation to zero current from the nearby portion of the I/V curve.

Figure 16. Determination of absolute K^+ permeability and Na/K biionic permeability ratios. **a)** I/V curve obtained for SAK channels under symmetrical K^+ (50 mM). Curve represents calculated GHK current equation based on mean of P_K's obtained at each voltage (over the range indicated by the line) for each of 4 patches. Mean P_K was 4.9 x 10^{-13} $\pm$ 0.76 x 10^{-13} cm s^{-1} (sem, n = 4). Average slope conductance was 86 $\pm$ 5 pS (ses, n = 4). **b)** Biionic I/V curves for symmetrical (50 mM) conditions of external (pipette) Na^+, internal (perfusion) K^+ (Na/K) and external K^+, internal (bath) Na^+ (K/Na). V_{rev}'s were obtained from the plot of averaged currents at each voltage from several patches. In some instances, where spontaneous channel activity was too large to allow I/V curve construction, V_{rev} was estimated directly from the current record, i.e. from the pipette holding potential where there was minimum stretch-activated current. P_{Na}/P_K ratios determined from V_{rev}'s (-47 mV, Na/K; +60 mV, K/Na) were 0.093 for K/Na (2 patches) and 0.154 for Na/K (6 patches). Curves are for the modified GHK current equation (equation 3.8), where current values are calculated from the external and internal ionic concentrations which have been multiplied by the P_{Na}/P_K ratio appropriate for that condition. For example, the curve for Na/K results from multiplying the external [K] by the P_{Na}/P_K ratio obtained under those conditions. This has the effect of reducing the concentration term by the fraction of the permeability of Na relative to K thus producing a rectification in the GHK current voltage relation.

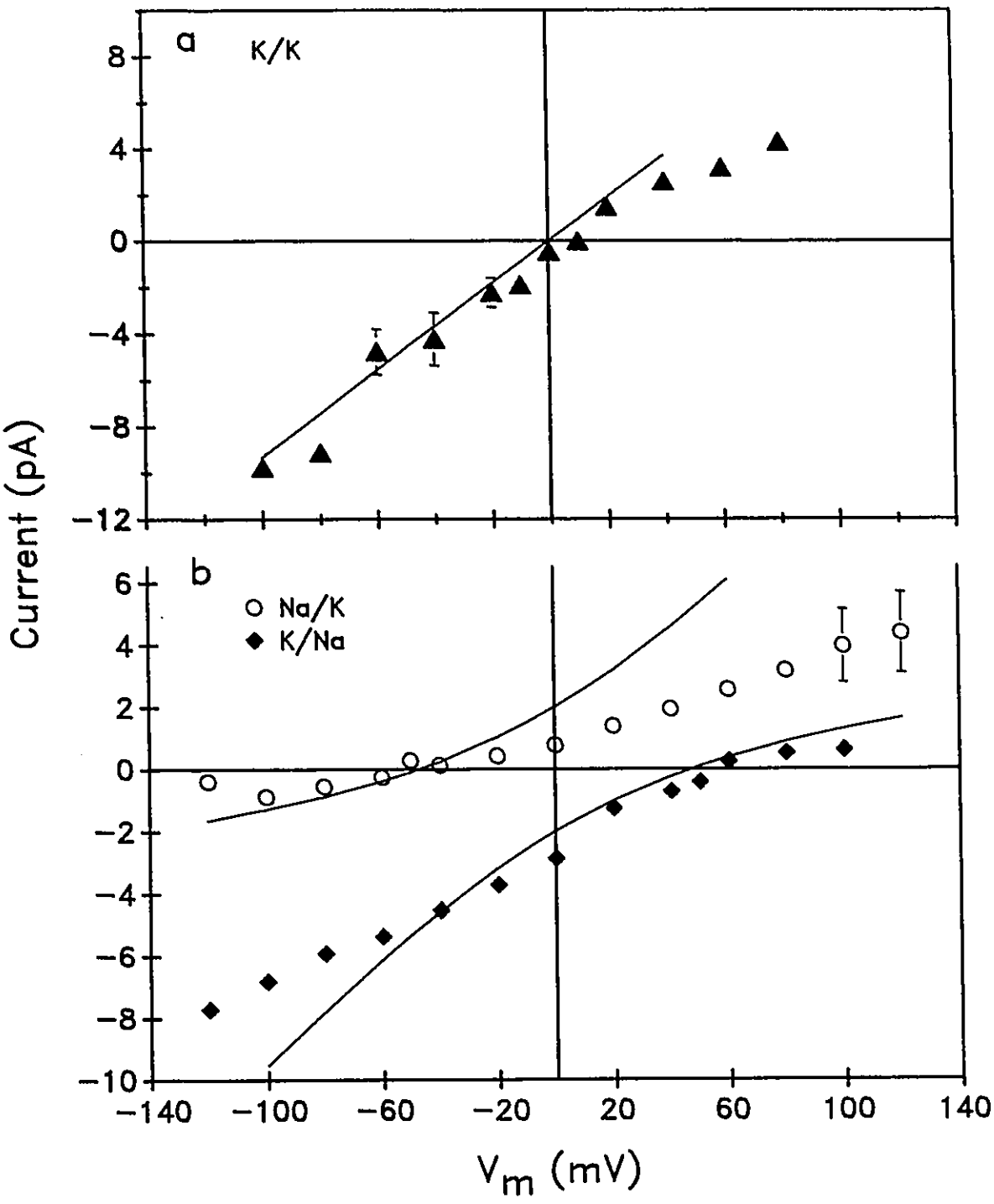
a
K/K
8
4
0
−4
−8
−12
b
Na/K
K/Na
6
4
2
0
−2
−4
−6
−8
−10
−140
−100
−60
−20
20
60
100
140
Current (pA)
V_m (mV)

Figure 17. Biionic I/V curves for symmetrical (50 mM) conditions where the external test ion was Tl^+, Rb^+, Li^+ or Cs^+ while the internal side of the membrane was perfused with K^+. **a)** Tl/K biionic I/V relation showing a positive V_{rev} (+12 mV, n = 2) and a slope conductance of 43.1 pS $\pm$ 3.7 pS (ses). **b)** Rb/K biionic I/V relation showing a negative V_{rev} (-18 mV, n = 3). Slope conductance of outward K^+ current part of the curve was 54 pS $\pm$ 5.4 pS (ses), while the inward Rb portion was 7 pS $\pm$ 1.1 pS (ses). Line drawn through points was a 3rd order polynomial fit to the data as an aid for interpolation of V_{rev}. **c)** Li/K I/V relation showing outward rectification of the stretch-activated K^+ current. Inward Li^+ current was never observed and as such, the estimated V_{rev} (-91 mV) is likely underestimated. Due to the curvature of the I/V relation, slope conductance (31.5 pS $\pm$ 2.5 ses, n = 4) was estimated from the middle part of the voltage range (+40 to +100 mV). **d)** Cs/K biionic I/V curve illustrating the discrepancy between the zero current potential (0 mV) indicating an equivalent permeability to K^+ and the lack of any inward Cs^+ current. Slope conductance was 50.3 pS $\pm$ 2.6 pS (ses, n = 3). Curves on each of these I/V relations represent the modified GHK current equation (equation 3.8) with the $[K]_o$ term adjusted by the appropriate permeability ratio (see Fig. 16b).

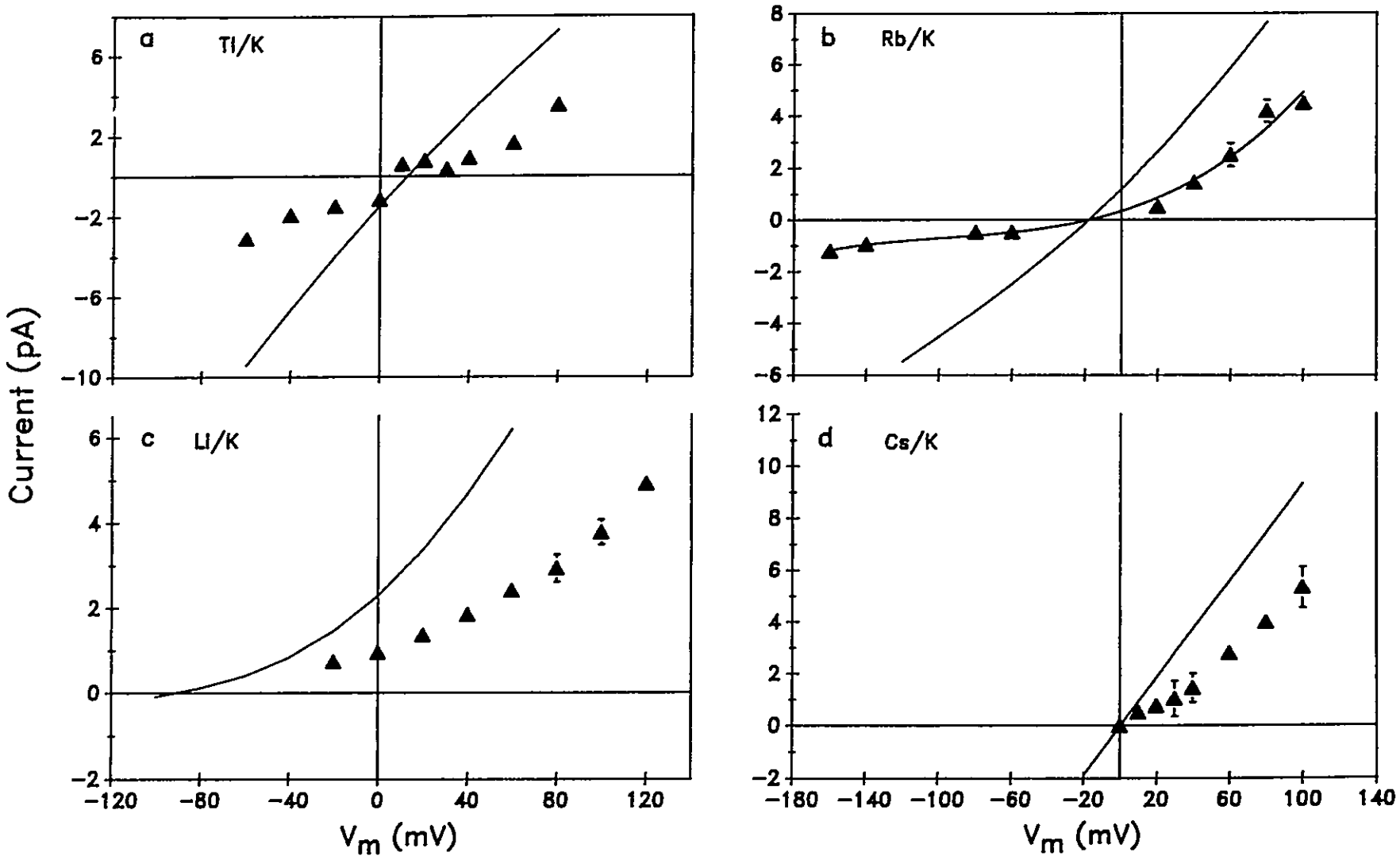
a
Tl/K
b
Rb/K
c
Li/K
d
Cs/K
Current (pA)
V_m (mV)
V_m (mV)

P_{Na}/P_K ratios were determined from biionic V_{rev}'s under two conditions; i.e. K^+ external and Na^+ internal (K^+/Na^+) and vice versa (Na^+/K^+) (Fig. 16b). Both conditions indicated a low Na^+ permeability relative to K^+ (0.093 for K^+/Na^+, n = 2 and 0.154 for Na^+/K^+, n = 6) in keeping with the result for the two ions under mixed conditions (see above).

The biionic reversal potential selectivity sequence was Tl^+ (1.61) > K^+ (1) > Rb^+ (0.49) > Na^+ (0.154) > Li^+ (0.027). The Tl^+/K^+ I/V curve (Fig. 17a) was approximately linear over the entire voltage range examined in contrast with the outwardly rectifying I/V relations found for Na^+, Rb^+ and Li^+ (Figs. 16b, 17b and c).

Although a Cs^+ current was never seen, and outward K^+ current rectification was observed, the I/V relation could be extrapolated to near 0 mV (Fig. 17d). The lack of inward Cs^+ current and the presence of K^+ current rectification demonstrates a low permeation rate for Cs^+ and presumably a small P_{Cs}/P_K ratio. This appears to be at odds with the indicated V_{rev}, and may have two alternative explanations. First, errors associated with extrapolating a non-linear I/V relation. Second, a small P_{Cs}/P_K should result in a V_{rev} shift similar to that of Li^+ (Fig. 17c). Since such a shift was not observed, this suggests a discrepancy between the GHK voltage and current equations. It is worth noting that Cs^+ did not block outward K^+ currents and that the slope conductance (50.3 pS $\pm$ 2.6 pS ses) was actually larger than that found for the "more permeable" Tl^+ (43.1 pS $\pm$ 3.7 pS ses).

The GHK current and voltage equations are based on the independence assumption, i.e. that permeation of a given species should be unaffected by addition of other ions or by an increase in the concentration of the same

species (Hille, 1984). This assumption can be tested by comparing the biionic I/V relation with that predicted by a modified form of the GHK current equation (Blatz and Magleby, 1984)

$$I = P_K z^2 \frac{VF^2}{RT} \frac{[K]_i - P_X/P_K[K]_o \exp(-zFV/RT)}{1 - \exp(-zFV/RT)} \qquad (3.8)$$

In this expression, the $[K]_o$ term is a product of the exponential and the observed permeability ratio (P_X/P_K, where X is the test ion). This results in rectification of I dependent on the difference between the $[K]_i$ term and the "adjusted" $[K]_o$ term. When equation 3.8 was plotted for each of the tested cations (Figs. 16b, 17), it was immediately obvious that none of I/V relations followed the independence assumption; i.e. all showed deviations from the GHK curve predicted on the basis of permeabilities determined from V_{rev}'s. Deviations primarily took the form of conductance reductions and included the Tl/K I/V relation (Fig. 17a), which according to its P_{Tl}/P_K, should exhibit a larger conductance compared to relations obtained under symmetrical K^+ conditions.

The channel is blocked by quinidine and TEA, but not Ba^+

Determination of SAK channel function will require pharmacological tools that, when applied externally, inhibit channel operation. Fortunately, the ubiquitous nature of the SAK channel allows comparison between different patches for control and drug-exposed effects. Three K^+ channel blockers, quinidine, TEA and Ba^+, were tested externally in cell-attached patches. Where partial or zero drug effect was observed, the presence of normally-functioning SAK channels was confirmed by application of negative

pressure to the pipette. The aim was to screen reagents for use under physiological conditions, rather than to examine the details of blocking action.

Quinidine produced significant changes, showing a dose-dependent reduction of conductance and a change in channel kinetics in the form of increase flicker (Fig. 18a). Stretch-sensitivity was unaffected (Fig. 18b). Reduction in the slope conductance (Fig. 19a) was significant for 100 μM and 1 mM quinidine ($p < 0.05$) with respect to the control. The degree of block encountered with 1 mM quinidine was variable, i.e. in half of the patches no SA currents were observable while other patches exhibited block as typified by Fig. 18a. 10 μM quinidine did not significantly reduce the slope conductance, but increased flicker was evident (Fig. 18a).

Figure 18. Block of SAK channels by external quinidine is dose-dependent and does not affect stretch-sensitivity. a) Comparison of single-channel currents from different cell-attached patches in the presence of three concentrations of quinidine. Channel flicker was increased at all quinidine concentrations and at 100 μM and 1 mM channel amplitude was reduced by ~50% and ~70% respectively. Accurate determinations of open channel amplitude were complicated by bandwidth attenuation of short duration open events (especially for 1 mM quinidine) and by imprecise knowledge of the true V_{rest} (for assessment of the driving force between patches). Here the pipette holding potential was -120 mV, resulting in V_m = +70 mV (V_{rest} assumed to be -50 mV). **b)** 1 mM quinidine did not affect SAK channel stretch-sensitivity. Cell-attached patch, V_m = +70 mV, filtered at 2 kHz. Scales, 5 pA and 50 ms for **a** and 2.5 s for **b.**

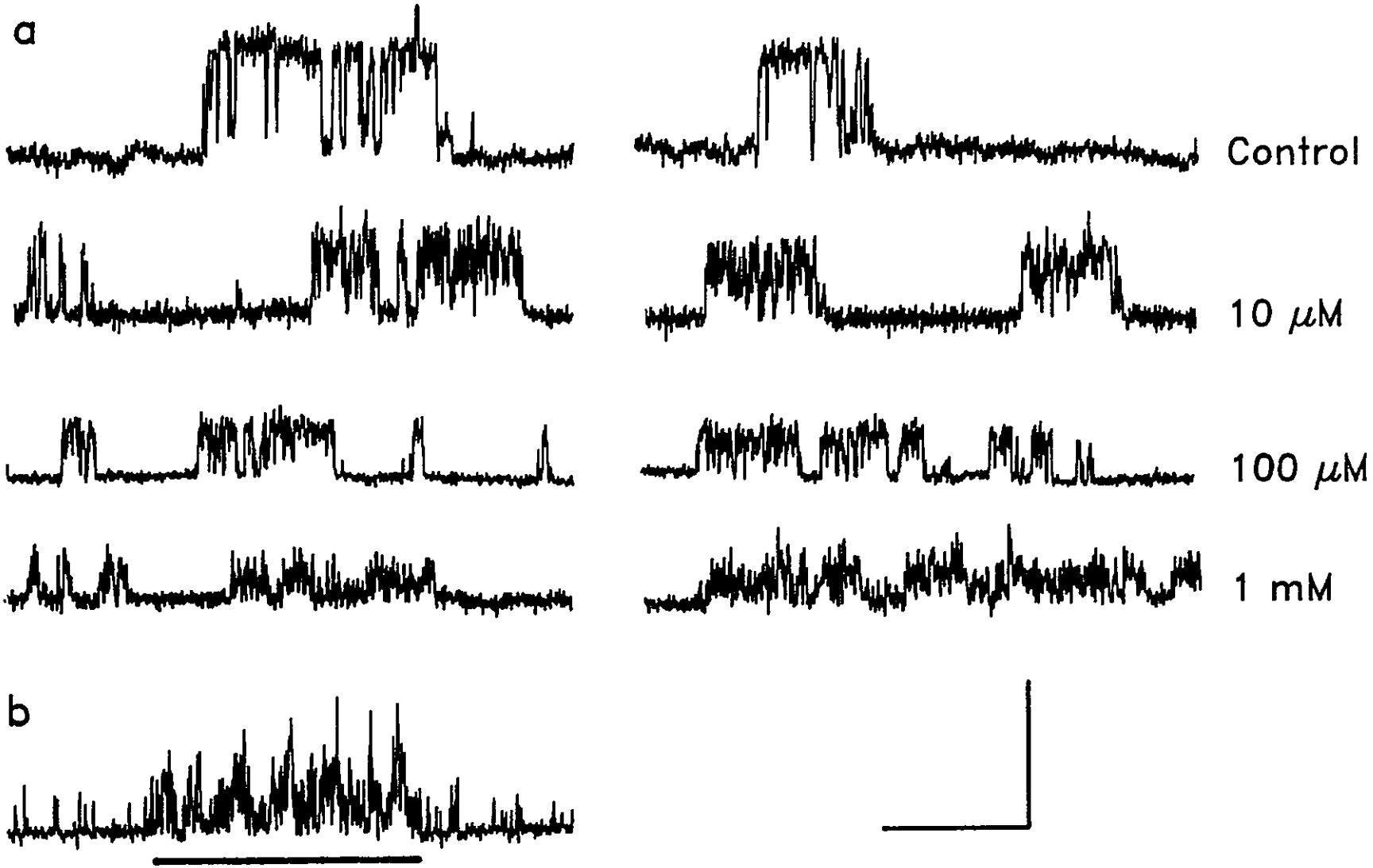
a
Control
10 μM
100 μM
1 mM
b

Figure 19. SAK channel block by quinidine is dose-dependent, but voltage-dependency of block is not consistent with a one-site model. **a)** Cell-attached SAK channel I/V relations in the presence of external quinidine (10 μM, circle; 100 μM, open triangle; 1 mM, square), demonstrating the reduction of slope conductance relative to control. 100 μM and 1 mM quinidine significantly reduced slope conductance (22 pS $\pm$ 1.6 pS and 8.4 pS $\pm$ 1.4 pS, ses, respectively, $p < 0.05$) relative to control (27 pS $\pm$ 0.4 pS, ses). 10 μM quinidine did not significantly reduce the slope conductance (23.4 pS $\pm$ 2.0 pS, ses), but increased flicker of the channels was noted (see Fig. 18a). **b)** Quinidine block is apparently voltage-dependent for all three quinidine concentrations (all slopes were significantly different from zero, $p < 0.05$), but δ was not constant with changing amounts of the drug. δ decreased from -0.46 for 10 μM to -0.2 for 100 μM to 0.07 for 1 mM (δ for 10 μM not significantly different from δ for 100 μM, but different from δ for 1 mM, $\alpha = 0.05$). Zero voltage dissociation constants, $K_d(0)$, (obtained from y-intercepts) were 13 μM, 78 μM and 700 μM for 10μM, 100 μM and 1 mM quinidine respectively.

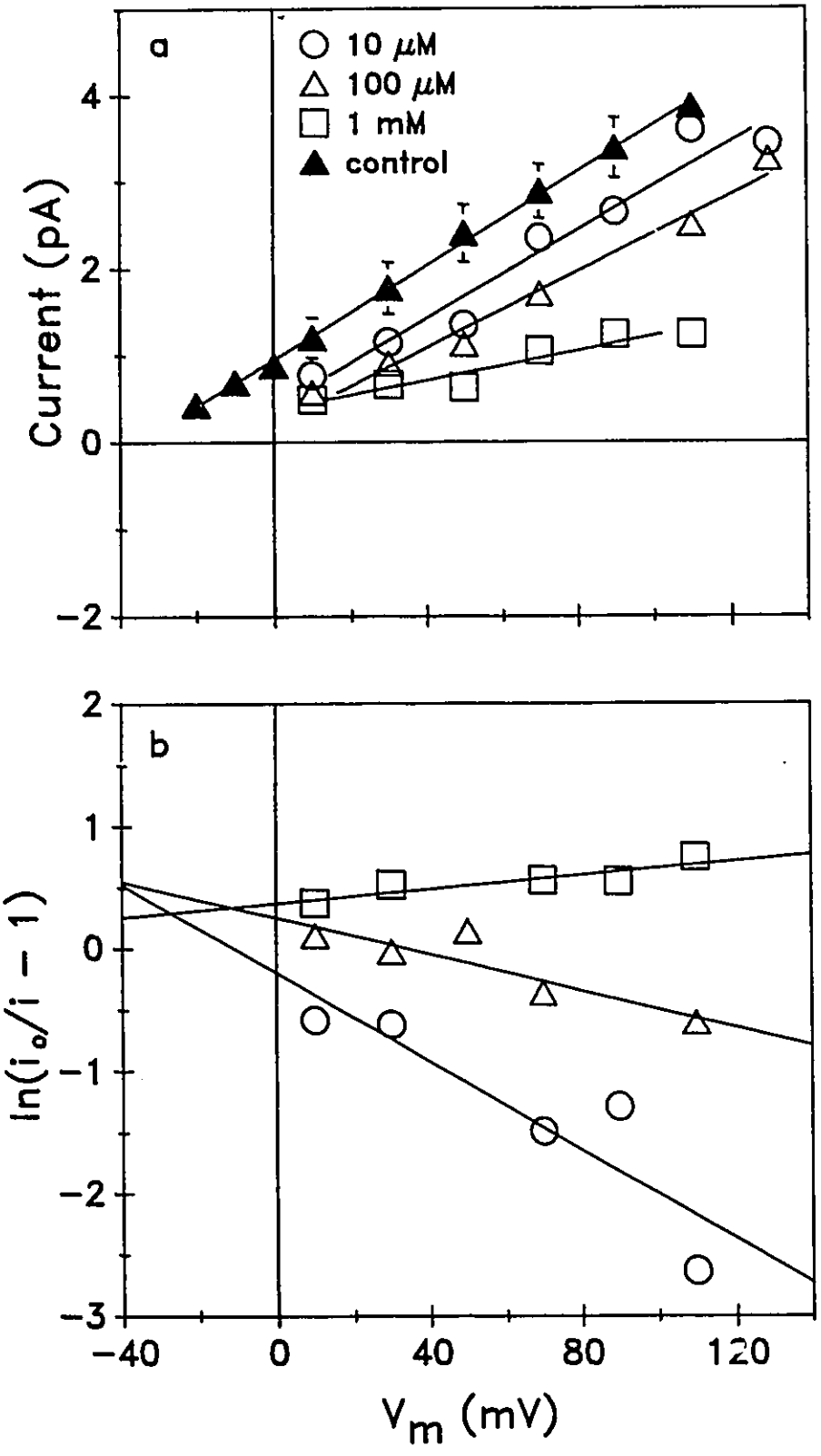
a
10 μM
100 μM
1 mM
control
Current (pA)
4
2
0
−2
b
ln(i₀/i − 1)
2
1
0
−1
−2
−3
−40
0
40
80
120
Vm (mV)

In these preliminary quinidine experiments, we examined only cell-attached patches using NS in the pipette and therefore observed only outward currents. Full examination of voltage-dependent block by quinidine (which might be expected if block depends on the charged species entering the channel) would require a range of hyperpolarizing and depolarizing potentials, and sufficient data for kinetic analysis of the voltage-dependence of blocking and unblocking rates (see Glavinovic and Trifaro, 1988). Another approach for detection of voltage dependence is, however, available that can be applied to the present data; it uses the relation described by Woodhull, (1973) (also see Coronado and Miller, 1979; Yellen, 1984a). Here, the fractional decrease in current (relative to control) is related to the zero voltage dissociation constant ($K_d(0)$) and an electrical distance term (δ). δ gives the fraction of the electric field which the blocker binding site actually is exposed to; for an external, positively charged blocking species it is a negative value (see Appendix 1). This model assumes a single blocker binding site on one side of the membrane and that the blocker has negligible permeability (Woodhull, 1973). Both $K_d(0)$ and δ can be obtained from a plot of the equation describing the single channel current in the presence of blocker as a function of voltage (Coronado and Miller, 1979)

$$i = \frac{i_o}{1 + [B]/K_d(0)\exp(zF\delta V/RT)} \qquad (3.9)$$

which, rearranged and linearized gives

$$\ln(i_o/i - 1) = \ln \frac{[B]}{K_d(0)} + \frac{F\delta V}{RT} \qquad (3.10)$$

where i_o is the unblocked single-channel current, i the blocked current, [B] blocker concentration, V the voltage, z the blocker valence and F, R and T have their usual meanings. A linear regression plot of $\ln(i_o/i - 1)$ *vs* voltage gives the slope as δ and the y-intercept which yields $K_d(0)$.

It is apparent that quinidine blockade is voltage dependent since non-zero values for δ were obtained for each of the 3 concentrations examined (all 3 slopes significantly different from zero, $p < 0.05$) (Fig 19b). However, if the blocker binding site within the electric field is accessible only from the external side of the membrane (a reasonable assumption if the externally applied blocker is membrane impermeant) then all 3 concentrations should provide the same negative value for δ. In fact each concentration gives a different δ (see Fig. 19b). The lowest concentration (10 μM) yielded the greatest voltage dependency, i.e. the largest δ, while the highest concentration (1 mM) displayed the smallest δ, which also was positive. Moreover, each decade change in concentration should shift the y-intercept by a factor of 10 if the $K_d(0)$ is to remain the same. This is clearly not the case in Fig. 19b. These results imply a more complicated blocking scheme than can be accounted for by the model.

Quinidine, even at the lowest concentration used, induces an increased flicker of the open channel events which increases as the concentration is increased (Fig. 18). For a single open state channel undergoing block, burst length should linearly increase with blocker concentration (Colquhoun and Hawkes, 1983). With 10 μM quinidine in the pipette, analysis of burst duration and number of closings per burst (using an empirical method; see Sigurdson et al., 1987a) revealed an approximately 1.3 fold increase in burst duration and 4 fold increase in the number of closings per burst compared to control (Fig. 20). Records from other patches containing SAK channels could not be analyzed in this way because they contained too many multiple openings.

Figure 20. Characteristics of SAK channel bursts in the presence of external 10 μM quinidine (open triangle). Plots of burst duration and closings per burst against interburst interval for two different patches at the same pressure (-40 mmHg) and similar P_o's (0.143 for 10 μM and 0.065 for control). In both plots, between interburst intervals of 1.2 and 10 ms (the midpoint of which gives an approximate value for average burst duration or closings per burst), quinidine increased both burst duration (from 9 to 12 ms) and closings per burst (from 3 to 11). Cell-attached patches, $V_m = +70$ mV.

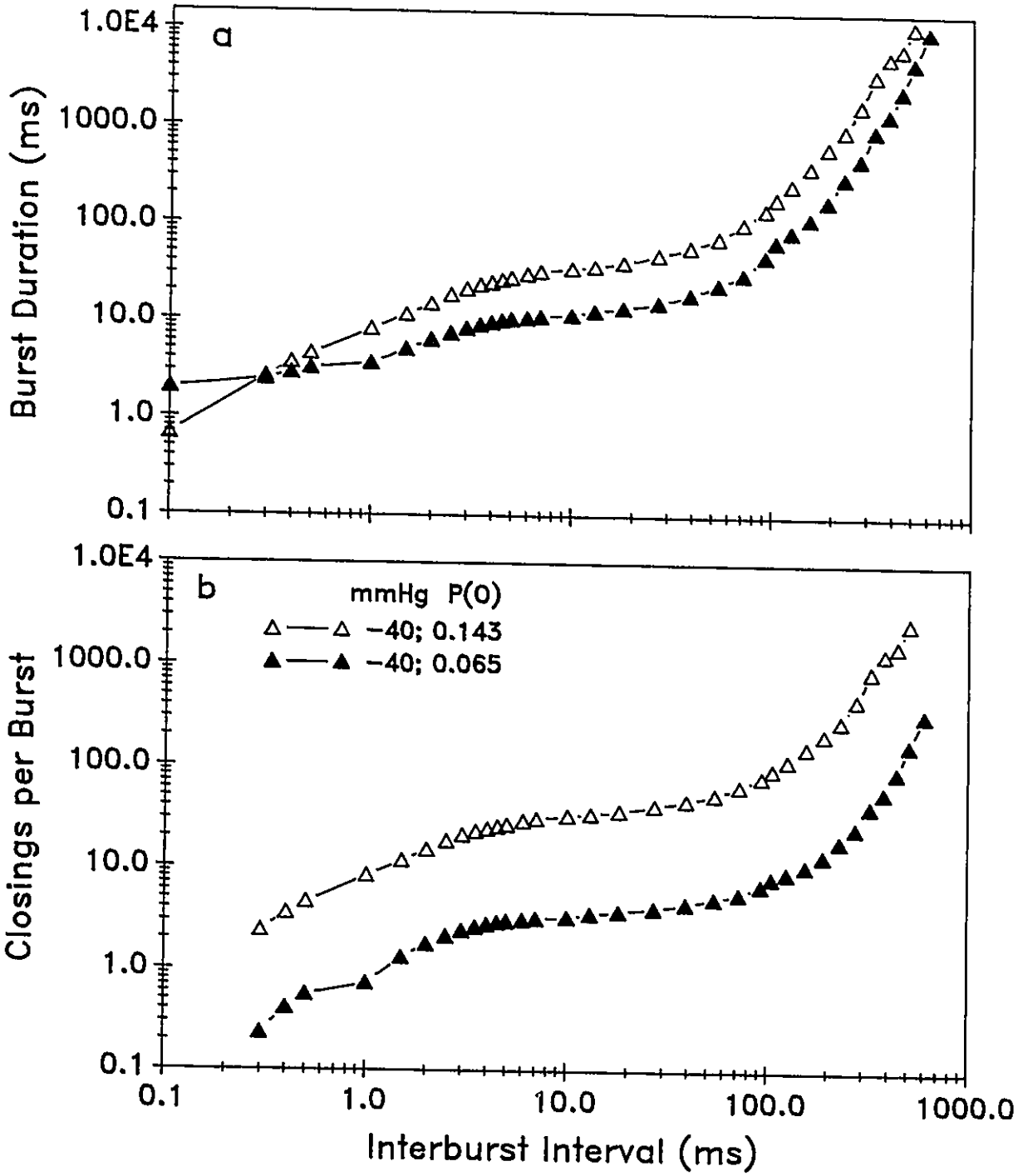
a
1.0E4
1000.0
100.0
10.0
1.0
0.1
Burst Duration (ms)
b
mmHg P(0)
−40; 0.143
−40; 0.065
Closings per Burst
0.1
1.0
10.0
100.0
1000.0
Interburst Interval (ms)

When TEA was added to the patch pipette there was no significant change ($p < 0.05$) in the slope conductance (over a V_m range of 0 to 110 mV), even with 10 or 20 mM TEA (Fig. 21, 13). It is evident however, that in the physiological voltage range (V_m = 0 to 30 mV), channel currents are reduced by approximately 50%. The absence of flicker (Fig. 21, compare with quinidine, Fig. 18) in the presence of TEA implies a rapid type of block; i.e. blocking and unblocking events too short to be detected, given the recording system bandwidth (see Yellen, 1984a). As seen in Fig. 19d, TEA did not affect SAK channel stretch-sensitivity. Block by TEA of *Lymnaea* neuron SAK channels is apparently similar to that observed in the *Drosophila* stretch-activated K^+ channel, which is also blocked (50% amplitude reduction) by external 10 mM TEA (Zagotta et al., 1988).

TEA block is voltage dependent as demonstrated by nonzero slopes for plots of $\ln(i_o/i - 1)$ *vs* V_m (Fig. 22b) at 10 and 20 mM TEA (slopes significantly different from zero, $p < 0.05$). Slopes of these plots were not significantly different from each other ($p < 0.05$), implying that the external TEA binding site is between -0.24 (δ for 10 mM) and -0.32 (δ for 20 mM) across the electric field. The zero-voltage dissociation constants were 25 and 16 mM for 10 and 20 mM TEA respectively.

High concentrations of Ba^+ (50 mM) had no significant effects on SAK channel conductance when applied externally (see Fig. 19e).

Figure 21. Single-channel currents at three depolarized (physiological) V_m's from cell-attached patches with NS or NS plus 20 mM TEA in the pipette. Channel amplitude was reduced by ~50% relative to control. TEA did not induce an increase in channel flicker, indicative of a fast type of block. V_m's range from +30 to -10 mV. Filtered at 2 kHz. Scale, 2.5 pS and 50 mS.

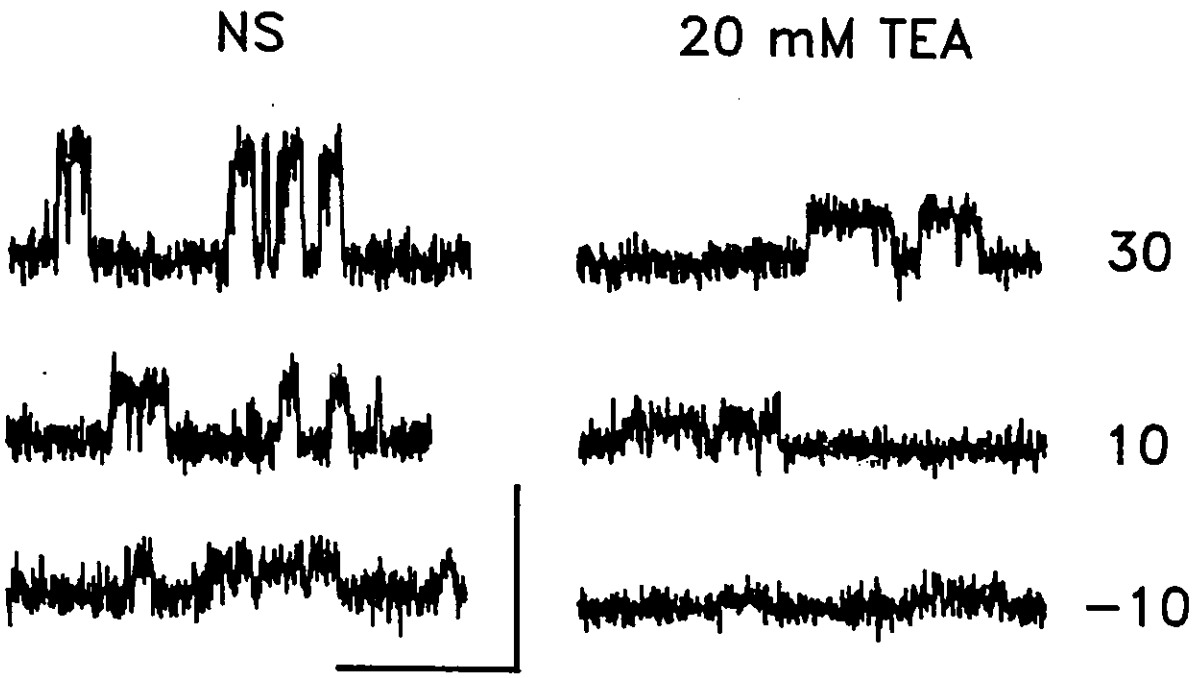
NS
20 mM TEA
30
10
−10

Figure 22. Block of SAK channels by external TEA. **a)** I/V curve for control (NS in pipette, circle) and for 10 (triangle, n = 2) and 20 mM (diamond, n = 3) TEA plus NS in pipette. Although slope conductances (determined by linear regression) were not significantly different (27 pS $\pm$ 0.7 pS ses, n = 7 and 27 pS $\pm$ 1.24 pS ses, n = 5 [TEA data combined], $p < .01$) it was clear in the range of physiological, depolarized voltages (-10 mV to 30 mV) that channel amplitude was decreased ~50% by TEA. **b)** Voltage dependency of TEA block. Slopes (δ) of linear regression fits to plots of $\ln(i_o/i - 1)$ *vs* V_m were -0.24 and -0.32 for 10 and 20 mM TEA respectively. These slopes were not significantly different from each other but were different from zero ($\alpha = 0.05$). Zero voltage dissociation constants ($K_d(0)$), derived from y-intercepts, for the two concentrations were 25 mM and 16 mM respectively.

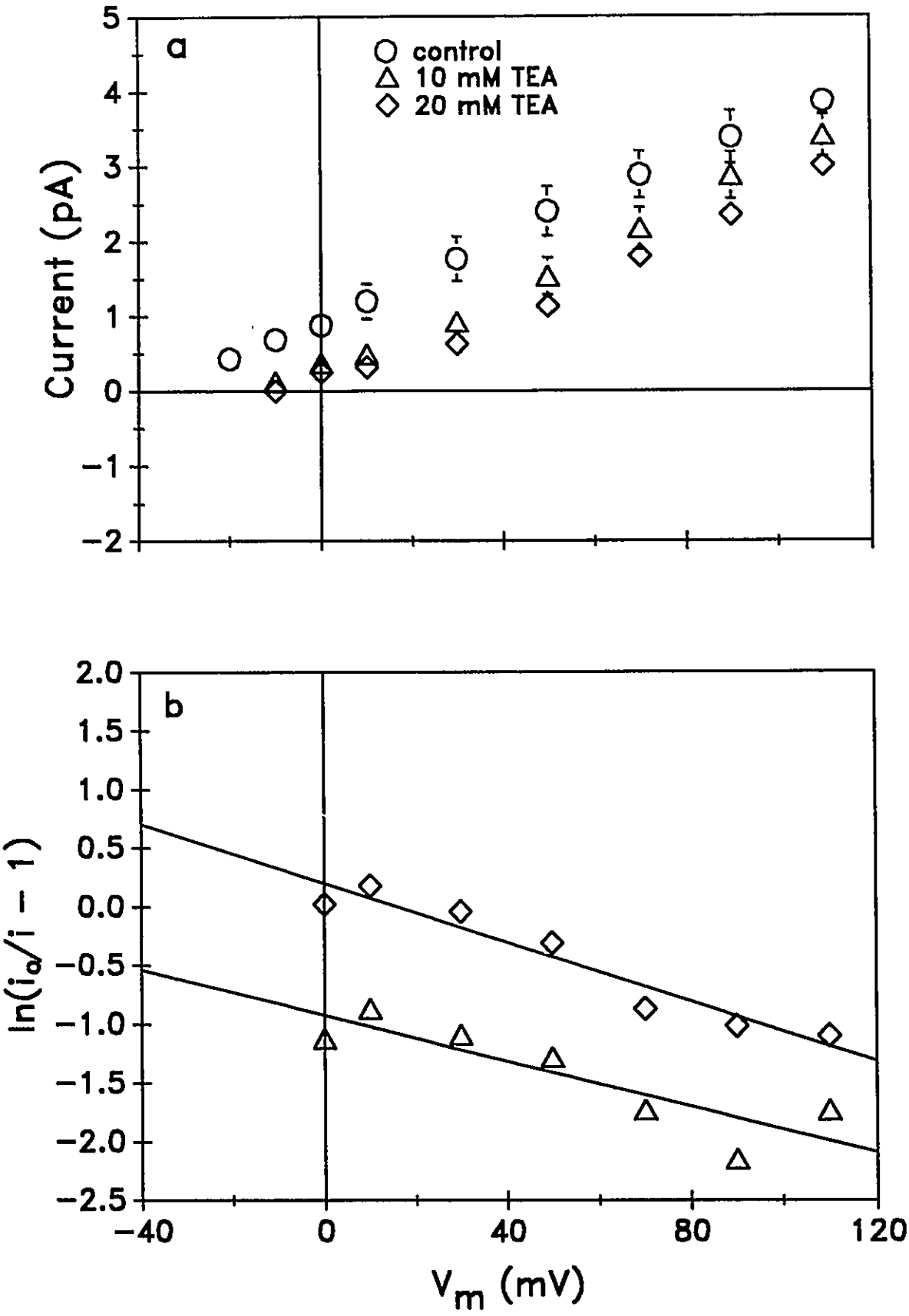
a
control
10 mM TEA
20 mM TEA
Current (pA)
5
4
3
2
1
0
−1
−2
b
$\ln(i_o/i - 1)$
2.0
1.5
1.0
0.5
0.0
−0.5
−1.0
−1.5
−2.0
−2.5
−40
0
40
80
120
V_m (mV)

Discussion

Potassium ion channels are both the most commonplace and diverse of all ion channel types, being expressed in virtually all cells, with each cell often containing several K^+ channel species (see Yellen, 1987). Stretch-activated K^+ selective channels constitute a K^+ channel subtype whose gating is regulated by membrane tension rather than by chemical ligands or voltage.

The *Lymnaea* heart SAK channel has essentially the same single-channel conductance as the neuron SAK channel (about 30 pS with physiological saline present; see Fig. 14) and the shifts in V_{rev} as external K^+ is increased are also similar, although the estimated P_{Na}/P_K ratio was marginally smaller (0.063 *vs* 0.083 for neurons) for the heart channel (Brezden et al., 1986). In different preparations containing SA K^+ channels (Sackin and Palmer, 1987; Bedard et al., 1988; Medina and Bregestovski, 1988; Zagotta et al., 1988), cell-attached conductance measurements range from 38 pS to 90 pS and will be dependent not only on channel properties, but also on the various ionic conditions used in the different studies. Selectivity of K over Na in mixed ionic conditions (12:1) was identical to that found by Sackin and Palmer (1987) in the renal K^+ channels which have subsequently been shown to be stretch-activated (Sackin, 1987; Sackin, 1989). The glial cell channel(s) appears to have a much larger conductance of ~200 pS (C. Bowman per. comm.).

Shifts in V_{rev} in response to changing K^+ gradients are good indicators of channel K^+ selectivity; the cell-attached and excised mixed ion experiments confirm this selectivity over Na^+. The 12 fold greater permeability of K^+ over Na^+ under mixed ionic conditions indicates that upon

stimulation the channel will act to hyperpolarize the cell provided V_{rest} is not at E_K (this appears to be the case since V_{rest} = -50 mV and estimated E_K is ~-85 mV). Whether these channels would produce membrane potential changes will depend on the channel's conductance, channel number and driving force for K^+. Brezden et al. (1986) determined that for a typical heart cell, a channel open probability of 0.5 would result in a turnover of about 1% of the internal K^+ in one second. Isolated neuron somatas tend to be quite spherical (see Sigurdson and Morris, 1989) permitting a good estimate of volume. By using an estimated channel density of 1 μm^{-2} (see Chapter 5), a typical cell diameter of 50 μm (giving about 7800 channels per cell assuming no membrane infolding), intracellular [K] equal to 50 mM (Sattelle, 1974), a channel P_o of 0.5 and a driving force sufficient to produce 0.5 pA per channel (17 mV), a similar estimate of total K^+ efflux is obtained (0.6% s^{-1}). Because of surface to volume ratio scaling, the effect of SAK channels on membrane potential in small structures, such as growth cones (see Chapter 5 and Sigurdson and Morris, 1989), may be accentuated. Choosing a half cylinder, 10 μm in diameter and length (see Appendix 2) as a model of growth cone shape, and using the same parameters for calculating somata K^+ efflux, in one second the growth cone could loose 4% of its K^+ (assuming constant K^+ driving force). These rough estimates of K^+ flux imply that SAK channel activation can have large effects on membrane potential, especially in those structures with large surface to volume ratios, provided the membrane potential is not at E_K. Under conditions of low extracellular [K^+] and continuous membrane tension (which might be expected during hyposmotic shock), channel activation could produce significant dumping of intracellular K^+.

The SAK channel possesses a large absolute permeability comparable to Ca^{2+}-activated K^+ channels. When P_K's of Ca^{2+}-activated K^+ channels from a number of different preparations are calculated from conductances in symmetrical K^+, the average P_K was $4.4 \times 10^{-13} \pm 1.03 \times 10^{-13}$ cm sec^{-1} (see Table 4), close to the SAK P_K of 4.9×10^{-13} cm sec^{-1}. This contrasts with the SA K^+ channel found in fish embryos, whose P_K was about a third this value (Medina and Bregestovski, 1988). The *Aplysia* S channel P_K also has P_K about one third that of the SAK channels, but shares with the SAK channel and other molluscan Ca^{2+}-activated K^+ currents a similar sensitivity to external TEA and lack of sensitivity to Ba^+ (Adams et al., 1980; Shuster and Siegelbaum, 1987). The SAK channel appears to have an optimized permeability, perhaps to balance the relatively low channel density.

Table 4. Absolute K^+ permeabilities of K^+ channels in different preparations.

Channel	P_K[a]	Cond. pS	[K] mM	Ref.
Ca^{2+}-activated K^+				
	4.5	200	126	Benham et al., 1986[b]
	5.23	300	150	Eisenman et al., 1986
	3.37	193	150	Gardner, 1986
	6.02	230	100	Cecchi et al., 1986
	4.33	240	145	Gallin, 1984
	5.45	300	144	Barrett et al., 1982
	3.75	208	145	Wong et al., 1982
	6.02	230	100	Latorre et al., 1982
	3.36	180	140	Marty, 1981
	3.5	187	140	Pallotta et al., 1981
	4.19	240	150	Methfessel and Boheim, 1983
Mean P_K	4.5 $\pm$ 1.02			
SR[c] K^+	3.4	130	100	Coronado et al., 1980
	3.93	150	100	Labarca and Miller, 1981
Lymnaea neuron SAK	4.9	91	50	
Cepaea neuron SAK	3.4			Bedard per. comm.
Aplysia S	1.45	200	360	Shuster and Siegelbaum, 1987
Fish embryo SA K^+	1.33	71	140	Medina and Bregestovski, 1988

[a] Calculated (except for Benham et al., 1986) by taking an arbitrary driving voltage (10 mV, near zero mV so as to avoid any non-linearities in I/V curves) and multiplying by the conductance to give I. This is substituted into equation 3.6 along with [K] and the voltage to obtain P_K which is given as x 10^{-13} cm s^{-1}

[b] value reported in publication

[c] Sarcoplasmic reticulum channel

The high conductance of SAK channels leads to questions concerning permeation mechanisms. These mechanisms may be analogous to those proposed for high conductance Ca^{2+}-activated K^+ channels, which achieve high selectivity concurrently with high rates of K^+ permeation. The SAK channel selectivity sequence is similar to other K^+ channels (Latorre and Miller, 1983; Hille, 1984) with Tl > K > Rb >> Na > Li; the P_{Na}/P_K and P_{Li}/P_K ratios may be actually underestimated due to the problems of obtaining reliable zero current potentials. It is evident, however, that Na does have a small permeability (small Na^+ currents were observed under biionic conditions (Fig. 16b), whereas Li^+ currents were never seen), larger than Li, that gives a sequence similar to Ca^{2+}-activated K^+ channels and different from that found in the snail neuron delayed rectifier which has Li > Na (Reuter and Stevens, 1980). Recently, Neyton and Miller (1988) have shown that a high conductance Ca^{2+}-activated K^+ channel can contain as many as 4 K^+ ions at one time, dramatically re-emphasizing the multi-ion nature of what was originally thought to be a single-ion channel (see Latorre and Miller, 1983; Yellen, 1984b; Eisenman et al., 1986). Although we have shown only that SAK current/voltage relations depart from independence, it has become clear that very few (only the skeletal muscle sarcoplasmic reticulum K^+ channel) K^+ channels are really single-ion channels (Miller et al., 1988; see Hill et al., 1989 for a multi-ion SR channel from cardiac sarcoplasmic reticulum). We can, therefore, expect complex permeation and blocking properties of SAK channels that will require further studies to be fully understood. The SAK channel manifests complexity typical of multi-ion channels in the departure from linearity at large depolarizations (seen in the symmetrical K^+ I/V curve, Fig. 16), and in

the reduction in conductance (compared to symmetrical K^+) seen in the presence of mixtures of K^+ and Na^+ (Fig. 15). More complex still is the discrepancy between the effect of Cs^+ on V_{rev} (suggesting that it is as permeable as K^+) and the total lack of any Cs^+ current. As suggested by Yellen (1984a), I/V curve sublinearities may be due to voltage-dependent block or diffusion-limited ion flow. It is perhaps dangerous to extrapolate Cs permeation properties of a single-ion channel (sarcoplasmic reticulum channel) to what is likely to be a multi-ion channel, but nonetheless, the SR channel also demonstrates a near unity permeability ratio but little conductance (Coronado and Miller, 1979). Cukierman et al. (1985) attribute this property to a deeper energy well in the permeation energy barrier profile for Cs than for K, causing Cs to bind to this site for a greater length of time.

Brezden et al. (1986) had previously shown that of three common K^+ channel blockers, only quinidine was effective on snail heart SAK channels and at 1 mM could completely eliminate SAK channel current in 75% of the patches and in the others reduce conductance by up to 90%. The block of neuron SAK channels by quinidine (in the same concentration range) implies that the two channels are very similar with respect to both their pharmacological sensitivity and permeation characteristics. It may be necessary however, to re-examine the TEA sensitivity of the heart SAK channel over a range of voltages to determine if at high concentrations TEA will produce a reduction in single-channel current comparable to that seen in the neuron SAK channels.

Although blockade by quinidine may have a voltage-dependent component, the variation of δ and $K_d(0)$ with concentration is not consistent

with the model on which the analysis was based (equation 3.9). This inconsistency may be related to the variation of block by 1 mM. Although this may be due to dilution of the pipette solution before seal formation (this seems unlikely, since positive pressure was applied up until the cell was touched), perhaps the membrane permeant nature of quinidine (Hermann and Gorman, 1984; Iwatsuki and Petersen, 1985) permits the drug to block from either side and/or from within the membrane. At pH 7.6 9% of the drug is neutral (Hermann and Gorman, 1984), a fraction that at higher concentrations such as 1 mM, may be large enough to have effects from within the membrane on sensitive hydrophobic sites in the channel protein. Therefore, quinidine is probably unsuitable for probing the SAK channel permeation pathway.

The increase in burst length caused by 10 μM quinidine is predicted for a single open state channel (Colquhoun and Hawkes, 1983). Quinidine apparently produces the type of block described as intermediate between slow and fast (Hille, 1984). The increased flicker (larger number of closings per burst) are hallmarks of blocking events having durations sufficient to be captured by the recording system. In contrast, externally applied TEA produced a fast type of block in SAK channels, comparable to the effects of TEA on Ca^{2+}-activated K^+ channels when the drug is applied to the internal side of the membrane (Yellen, 1984a; Villarroel et al., 1988).

Although SAK channels display a voltage-dependent TEA block with an electrical distance comparable to Ca^{2+}-activated K^+ channels, (Wong et al., 1982; Latorre and Miller, 1983; Blatz and Magleby, 1984; Yellen, 1984a; Villarroel et al., 1988) they differ from these channels in their sensitivity to external TEA (Ca^{2+}-activated K^+ channels typically have an external TEA

K_d < 1 mM). SAK channels possess sensitivity more in line with that described for the *Aplysia* S channel (K_d = 90 mM; Shuster and Siegelbaum, 1987). Effects of TEA on the internal side of the SAK channel remain to be examined. For the moment, TEA blocking characteristics appear to be intermediate between the S channel and Ca^{2+}-activated K^+ channels. TEA holds promise as a probe of the SAK channel permeation pathway, but would have to be used at concentrations that make it unsuitable for physiological studies of SAK channel function.

Are SAK channels fundamentally different from ligand and voltage-dependent K^+ channels or are they simply modifications of some basic K^+ channel motifs? SAK channels present few surprises regarding their permeation characteristics. The channels under physiological conditions will pass K^+ exclusive of all other available ion species. Input resistances of *Lymnaea* neuron cell bodies tend to be high (Byerly and Hagiwara, 1982; see Chapter 4), insinuating that even at low levels of activation, their large absolute permeability could significantly modify the whole cell conductance. This suggests that the channels have functions which specifically utilize the channels's mechanosensitivity. A possible role in osmoregulation will be examined in the following chapter.

Chapter 4. SAK channels and volume regulation during hyposmotic shock

Introduction

The presence of mechano-sensitive ion channels in cell types not involved in mechano-reception (see Sachs, 1984; Kullberg, 1987) leads to the obvious question - what physiological role, if any, are the channels playing? More specifically, what role does the SAK channel play in the physiology of a freshwater snail's heart cell or ganglionic neuron?

As suggested by Brezden et al. (1986), SAK channels could act in volume regulation, simply being conduits for the rapid exchange of osmolytes (in this case K^+) out of or into the cell. Under hypo-osmotic conditions, an increase in cell volume due to influx of water would exert tension on the cell membrane and associated cytoskeletal components. The tension transmitted to the SAK channel increases the channel's open probability. Potassium leaves the cell, moving down its electrochemical gradient (assuming a simple dilution of the extracellular medium, i.e. external $[K^+]$ is reduced thereby changing E_K), carrying with it osmotically obliged water. Activation of SAK channels would thus limit the degree of swelling, during acute hypo-osmotic stress. This mechanism assumes an associated Cl^- pathway, which may or may not be mechano-sensitive, in order to maintain electroneutrality.

Until recently, there has been little direct evidence for this type of mechanism in the literature although several authors have suggested that membrane conformational changes resulting in increased K^+ permeability would be considered a reasonable explanation for K^+ efflux observed during hypo-osmotic shock (HOS) (Hoffmann, 1976; Pichon and Treherne, 1976; Rorive and Gilles, 1979; Kevers et al., 1981). Hamill (1983) suggested this

as a possible function for a K^+ channel whose gating is sensitive to hypotonically induced swelling of frog red blood cells.

Evidence is now mounting that SA channels could play a role in cell-volume regulation being employed either directly, as proposed for the *Lymnaea* heart SAK channel (Brezden et al., 1986), or indirectly by passing a second messenger (Ca^{2+}) which activates other K^+ conductances. SAK channels found in *Necturus* kidney proximal tubule cells (Sackin and Palmer, 1987; Sackin, 1987), have been shown to be activated during cell swelling induced by HOS (Sackin, 1989). Ubl et al. (1988a) have also demonstrated activation of a non-selective SA channel found in opossum kidney cells during HOS. SACat channels, capable of passing Ca^{2+}, were activated during HOS concomitantly with Ca^{2+}-activated K^+ channels in *Necturus* choroid plexus cells. Christensen (1987) concluded that SACat activation could pass sufficient Ca^{2+} to activate Ca^{2+}-dependent K^+ conductances which would take part in volume regulatory decrease (RVD). In neuroblastoma, SACat channels were activated during HOS and as expected had reduced activity during the volume reduction phase of RVD (Falke and Misler, 1989). In all these examples, the lack of a suitable SA channel blocker (for either SAK or SACat channels) has frustrated attempts to obtain clear-cut answers concerning the involvement of these channels in osmoregulation. However, the transition element gadolinium, has recently been reported as a specific SACat channel blocker (Yang and Sachs, 1989). This cation holds promise as an investigative tool in cell types where SACat channels are suspected to be involved in volume regulation.

As a prelude to more detailed studies, several lines of investigation concerning *Lymnaea* SAK channels (heart and neuron) were attempted. The

questions addressed are simple ones, but should provide additional circumstantial evidence for a function of SAK channels in volume regulation. Are the cells simple osmometers or is swelling somewhat limited in hyposmotic media? Morris et al. (1989) have shown that *Lymnaea* heart, neuron and kidney cells exhibit limitation of cell swelling when under large (30% dilution) hyposmotic stress. Quinidine (a known SAK channel blocker) exacerbates swelling, making the cells more like osmometers. Although none of these cells exhibited RVD, the results were consistent with the idea that SAK channels could act to limit cell swelling. When stressed with a HOS, are the cells capable of recovery and resumption of normal physiological processes, i.e. has volume limitation been successful in preserving the cell machinery in a functional state? During HOS, K^+ efflux is expected which should be detectable as an hyperpolarization of V_m. Is SAK channel activity correlated with cell swelling and volume reduction during and after HOS?

Materials and Methods

Lymnaea collection and housing, as well as cell culture of heart and neurons, were performed as described in Brezden et al. (1986), Sigurdson et al. (1987a), Sigurdson and Morris (1989) and in chapter 3.

Single-channel recordings employed standard techniques (Hamill et al., 1981) and used recording pipettes of similar characteristics as described in Sigurdson and Morris (1989) and chapter 3. Intracellular voltage recordings were made using micropipettes filled with 2 or 3 M potassium acetate and having an average resistance of 39 MΩ $\pm$ 7 MΩ. Voltages were recorded using a WPI electrometer and Gould chart recorder. Input resistance

measurements were made by injecting positive or negative current with the same electrode used for V_m recording (for each electrode, the electrometer's bridge circuit was balanced to compensate for electrode resistance). Ideally, specific input resistances should be calculated from the voltage change induced by a known amount of injected current and the cell membrane area. Specific input resistances were not obtained for three reasons: 1) potential errors in measurement of cell diameter and hence membrane area (a 10% error in diameter measurement will result in a 17% area error, assuming a spherical neuron soma); 2) the unknown area of membrane in the form of pseudopods and neurites (which is quite variable between neurons); and, 3) any increase in cell diameter due to swelling will potentially expose an unknown amount of "new" membrane (formally residing in folds) that will contribute to the swelled cell diameter, but not to the normal diameter. Input resistances, which tended to be high (ranging from 75 to 475 kΩ), were compared for individual cells during pre-HOS, HOS and post-HOS..

Cells were exposed to HOS by dilutions (vol/vol) of normal saline (NS). Because diluted solutions have lower densities than 100% NS, care was taken to completely replace each solution by adding 2 to 3 times the culture dish volume and by thorough mixing. In experiments where intracellular or single-channels recordings were made, individual cells were exposed to the HOS shock by using a large-bore (> 50 μm) perfusion pipette (aimed at the cell of interest) containing the hyposmotic saline. This approach is required to prevent mechanical disruption of the recording preparation by large volumes of replacement saline and has the added benefit of producing saline changes much more rapidly. Perfusion flow-rates were adjusted by

visually monitoring cell-swelling, but the exact dilution was not known due to mixing with the bath saline. This meant that quantitative changes in cell volume for a given dilution could not be obtained.

Analysis of open probability (P_o) changes during HOS are described in Sigurdson et al. (1987a) and Sigurdson and Morris (1989).

Photographic records of cells were made using phase contrast or differential interference contrast optics (DIC) (Olympus inverted microscope).

Results

Preliminary experiments using *Lymnaea* heart cells, demonstrated qualitative changes in cell volume as a function of the degree of HOS. Cell-swelling was also shown to increase when the cells were exposed to quinidine concentrations known to be sufficient to block SAK channels (see Brezden et al., 1986). These results were used as the basis for more detailed studies (on neurons and kidney cells as well) which attempted to measure cell volume as a function of HOS and exposure time (see Morris et al., 1989). The different cell-types described in this study did not respond equally to similar HOS, i.e. the relative volume changes for a given dilution were not the same for heart, neuron and kidney cells. It is not known whether this is an intrinsic property of each cell type or due to the difficulty of determining accurate cell volumes (heart cells were approximated as cylinders, neurons and kidney cells as spheres). For all cell-types quinidine (1 mM) resulted in greater cell-swelling for a given HOS.

Neuron swelling and recovery after HOS

Kidney cells were shown to almost completely recover their pre-HOS cell volumes after ~20 minutes (Morris et al., 1989). Heart cells will also recover from severe HOS (30% dilution) and appear morphologically "normal" afterwards (not shown). During similar dilutions, *Lymnaea* neurons (which had formed pseudopods and neurite process, Fig. 23a), showed initially little swelling (4 min in 30% NS, Fig. 23b), but after 1 hr had increased their volume dramatically (Fig. 23c). The swelling appears primarily confined to the cell peripheries, but there is also an increase in soma diameter. Recovery began soon after removal of the HOS and was always accompanied by the formation of vesicles in pseudopods and neurites (Fig. 23d). As the recovery proceeded, the number of vesicles increased (Fig. 23e) often entirely filling these regions (Fig. 23f). Although best seen in the peripheral regions, vesicles were also observed in the cell body proper. Cell-volume recovery appeared complete after 1 to 2 hr (compare Fig. 23a to 1f), but the vesicles usually took longer to disappear. By the next day (Fig. 23g), the same cell appeared morphologically normal and had begun to extend neurite processes.

Figure 23. Cultured *Lymnaea* neurons exposed to severe HOS (30% NS), first swell and then volume regulate after HOS. **a)** Two *Lymnaea* neurons after 4 days in culture in 100% NS. Both cells have projected pseudopods and neurites around the cell body periphery. **b)** 4 minutes after exposure to 30% NS. During solution exchange, the cell on the right in (**a**) was washed away. Swelling appears to be confined to the peripheral membrane regions. **c)** After 1 hr in 30% NS the neuron has swelled dramatically, almost to the point of lysis. **d)** 8 min after replacement of bath saline with 100% NS. Volume regulation typically proceeded as shown in the next 4 plates. The first evidence of volume reduction was the appearance of vacuoles or vesicles within the cytoplasm (especially apparent in pseudopods). Such vacuoles were generally present within the soma cytoplasm, but were difficult to see. **e)** By 21 min post-HOS, vacuoles had proliferated and expanded in size. Formally swollen regions had begun to volume reduce. **f)** 55 min post-HOS. High magnification view of neuron showing vacuoles completely filling certain areas of the peripheral membrane regions. Vacuole morphology was dynamic; compare vacuole sizes, locations and numbers in **d, e** and **f** (focal planes throughout this series remained the same). **g)** By the next day (18 hr post-HOS), the cell appeared to have completely recovered; there was no evidence of any remaining vacuoles or residual swelling. There was evidence of new membrane extension (compare neurite extensions at right side of soma with those shown in **a**) and remodelling. DIC optics. Scale bar for plates **a, b, c, d, e** and **g** equals 54 μm; for plate **f**, 24 μm.

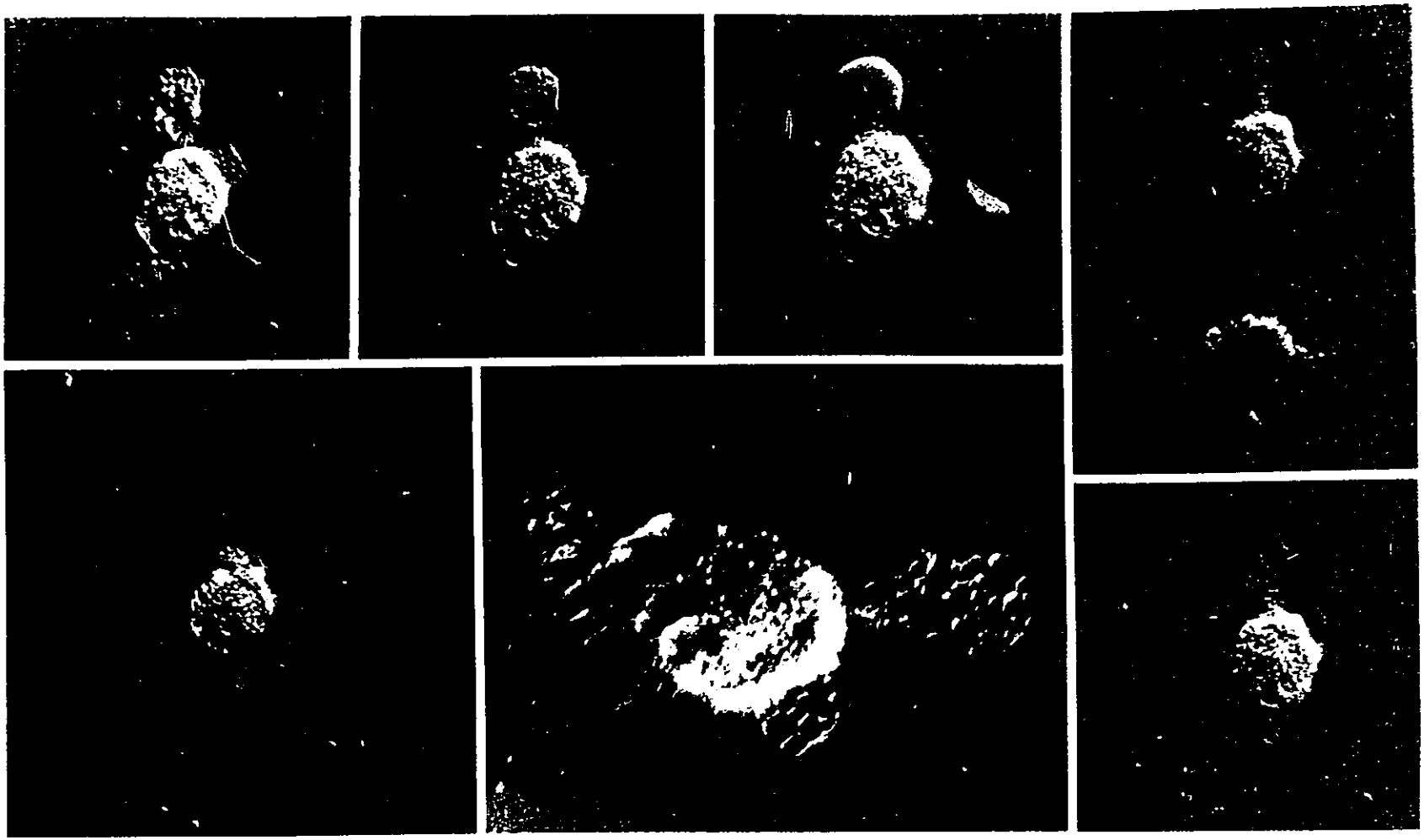

Neurons and heart cells assume normal morphologies after severe HOS

The observation that isolated neurons could recover from a large HOS and continue to grow (extend neurite processes) implied that the cells were still physiologically competent and had not sustained permanent damage. This notion was examined further by hyposmotically stressing heart cells and neurons when they likely to be most vulnerable; i.e., immediately after the enzymatic treatments used to dissociate the cells. Immediately after enzymatic treatment, both cell-types were exposed to HOS (60% and 30% NS) for 30 min, followed by plating out or in the case of neurons, a 30 min recovery period in 100% NS (this step was added for the neurons to prevent cell destruction during mechanical dissociation of the ganglia). Control batches of cells prepared from the same animals followed a parallel treatment, except for the HOS.

Figure 24. Cultured *Lymnaea* ventricular cells can recover from HOS received during the isolation procedure. **a)** Control (treated with 100% NS) heart cells 1 day after isolation. Once attached to the substrate, these cells do not change their morphology even after 3 to 4 days in culture. **b)** Heart cells (2 days post-isolation) which had been exposed to 60% NS HOS for 30 min immediately after enzymatic digestion and isolation. Following HOS, cells were gently centrifuged and resuspended with 100% NS before plating out. Cells have assumed a morphology similar to control cells. **c)** Heart cells (2 days post-isolation) which had been exposed to 30% NS HOS for 30 min following enzymatic treatment. Cells appear to be indistinguishable from control cells in **a.** DIC optics. Scale bar equals 54 μm.

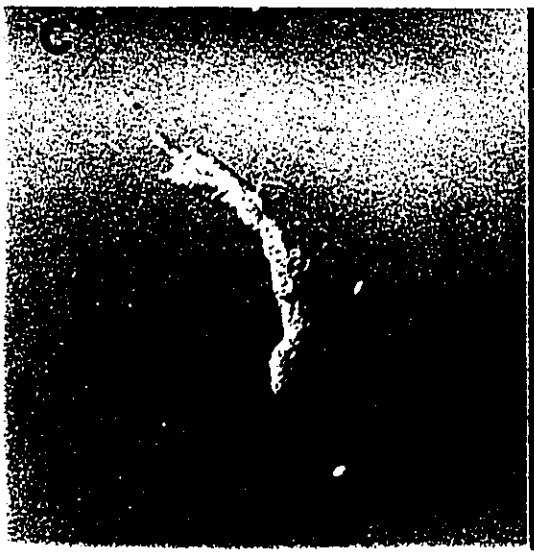

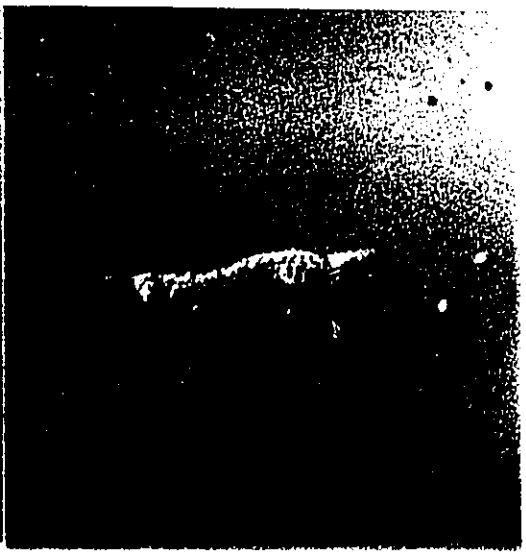

Lymnaea heart cells treated with 60% and 30% NS after enzymatic treatment (0.25% trypsin for 0.5 hr followed by 0.1% collagenase for 2 hr.; see Brezden et al., 1986) were morphologically indistinguishable from the control cells two days after isolation (Fig. 24a, b, c). Cell yield was not dramatically different between controls and HOS stressed cells, although the number of 30% NS stressed cells appeared to be slightly less. Reproducible quantification of cell number was hindered by its dependence on the number of attached cells, which is in turn dependent on substrate adhesion. Since there was variation in the number of attached cells between control culture dishes, determining cell yield differences was difficult.

Heart cells in culture for 3 or 4 days do not display any dramatic morphological changes (compare Fig. 1 Brezden et al., 1986 with Fig. 24) which might give clues to changes in their physiological status. *Lymnaea* neurons on the other hand (as shown by Sigurdson and Morris, 1989), can display extensive neurite development after 2 to 4 days in culture (initially only cell bodies and short axon stumps are isolated) thus allowing comparison with control cells. The degree of neurite arborization can only be subjectively analyzed, so comparisons with controls was made using "typical" cells. In Fig. 25, the development of neurite processes is followed from 1 to 4 days after isolation for cells treated with 100% NS and 30% NS. For both control cells (Fig. 25a, b, c) and 30% NS treated cells (Fig. 25d, e, f) neurites tipped with growth cones (see Fig. 25b and f) developed to approximately the same extent in both cases. Cells treated with 60% NS during the isolation procedure had a similar morphology.

Figure 25. *Lymnaea* neurons can recover from a HOS during isolation and then later produce morphological characteristics similar to those of control cells. Plates **a, b** and **c** show the progression of neurite outgrowth over 4 days in cells treated with 100% NS during isolation. The degree of neurite outgrowth is extremely variable in these cells; these plates show a "typical" amount of cell development for a given length of time in culture. **a)** A neuron 1 day after isolation displaying 3 extending neurites tipped with growth cones. **b)** A different neuron 3 days after isolation. **c)** Another control neuron 4 days after isolation displaying extensive neurite development. Plates **d, e** and **f** show the progression over 4 days of neurons which had been exposed to 30% NS for 30 min after the enzymatic treatment used during the isolation procedure. These cells were allowed a 30 min recovery period in 100% NS before mechanical dissociation and plating out. **d)** A *Lymnaea* neuron 1 day in culture displaying neurite extension comparable to that of the control neuron in **a**. **e)** Another 30% NS treated cell 3 days post-isolation showing extensive membrane spreading. **f)** By 4 days post-isolation many of the HOS cells had produced neurite development similar to this cell. Phase contrast optics. Scale bar equals 54 μm.

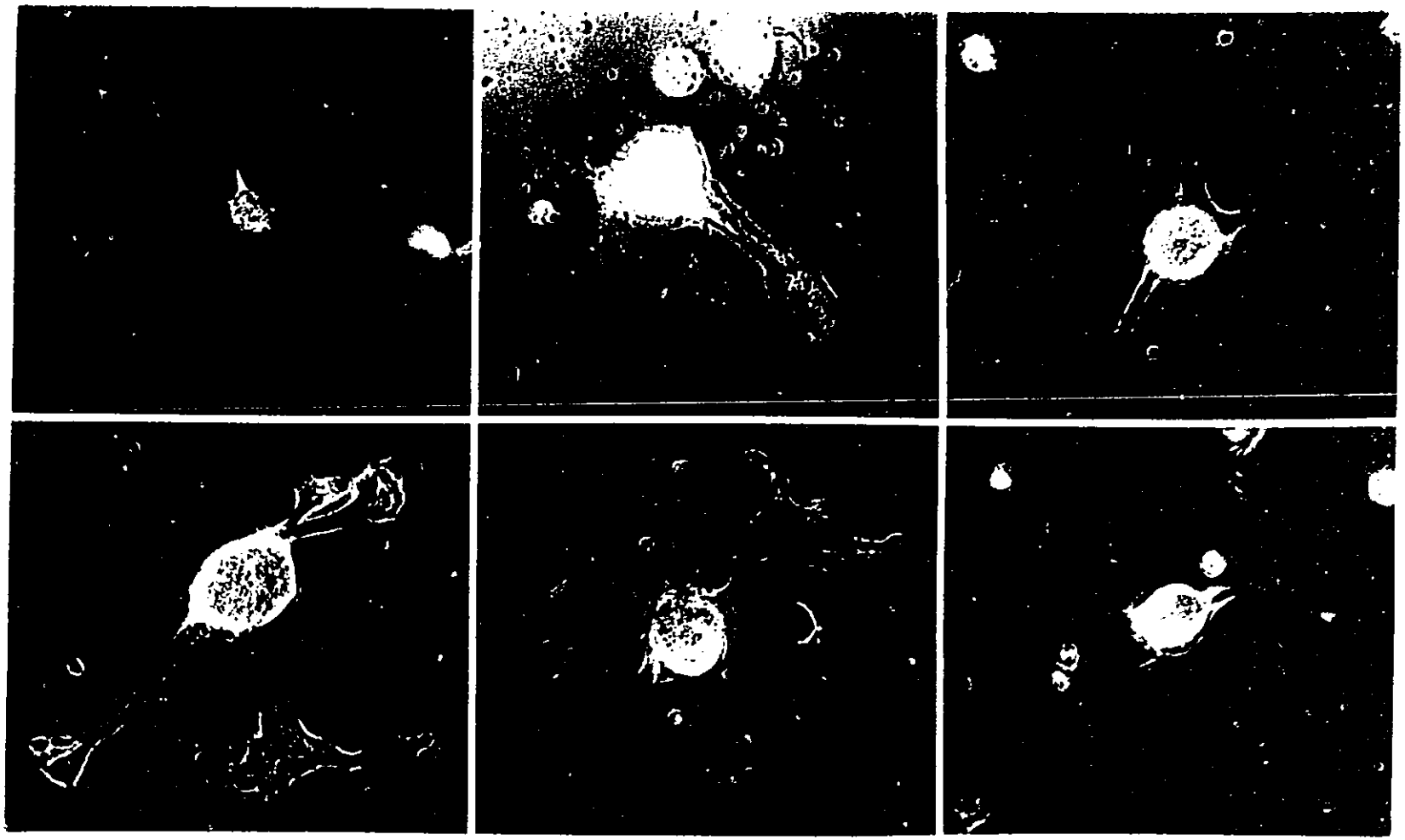

Lymnaea neurons hyperpolarize during HOS

The efflux of K^+ observed during HOS in various cell-types should result in changes in the resting potential (V_{rest}) of the cell, specifically a hyperpolarization (assuming that K^+ forms the basis of V_{rest}). Pichon and Treherne (1976) have reported hyperpolarizations of membrane potential (V_m) in marine invertebrates subjected to HOS. A similar response was expected in *Lymnaea* neurons, if K^+ conductances (including SAK channels) were being activated by cell-swelling.

This possibility was examined by intracellular voltage recording of neuron cell bodies before and during exposure to a HOS supplied by a nearby perfusion pipette. The possibility of "artifactual" voltage change by the perfusion stream was checked by using 100% NS in the perfusion pipette. In fact, perfusion did produce a consistent 4 mV $\pm$ 1 mV (std, n = 16) hyperpolarization (Fig. 26a) which may be due to activation of SAK channels by the perfusion stream. When 50% NS was perfused onto the cell (at a rate sufficient to cause swelling), V_m hyperpolarized by 14 mV $\pm$ 4 mV (std, n = 13, Fig. 26b) which was significantly different from the control perfusion (t test, α = 0.005). Correcting for the stream induced hyperpolarization, HOS resulted in an average 10 mV hyperpolarization of V_m. The hyperpolarization during HOS was sufficient in one cell to cause cessation of spontaneous action potentials (Fig. 26b_i).

Figure 26. HOS causes hyperpolarization in isolated *Lymnaea* neurons. Microelectrode recordings of membrane potentials recorded during exposure to 100% NS or 50% NS. For each voltage trace there is a current injection trace immediately above. Perfusion periods are indicated by a line above each voltage trace. At the upper part of each voltage trace is voltage that can be used as reference. For example, -3 mV in **a**, is represented by the top horizontal line of the trace. **a)** Perfusion of neurons with 100% NS produced a small, but reproducible hyperpolarization as shown by 3 consecutive perfusion episodes. Injection of -0.5 nA current produced ~40 mV hyperpolarizations before and during perfusion (see last perfusion episode). **b)** Three cells showing that when neurons were exposed to 50% NS (causing cells to swell), V_m recordings showed larger hyperpolarizations than observed during control perfusions (these cells were not exposed to 100% NS before HOS) **bi)** In this cell spontaneous action potential firing was interrupted during HOS, presumably because of the 10 mV hyperpolarization. **bii)** In another, non-spiking cell, perfusion of 50% NS resulted in a 10 mV hyperpolarization. Input resistance measurements, during this and other perfusion episodes on this cells, indicated that on average, input resistance decreased during exposure to HOS compared to pre-HOS periods. During this episode, average input resistances before HOS and during HOS were 370 MΩ $\pm$ 24 MΩ (std, n = 8) and 338 MΩ $\pm$ 12.5 MΩ (std, n = 9) respectively. **biii)** In yet another cell, HOS exposure resulted in 10 mV hyperpolarization. Input resistances were larger before HOS (300 MΩ $\pm$ 7 MΩ, std, n = 5) than during HOS (262 MΩ $\pm$ 11 MΩ, std, n = 20). Immediately following HOS, input resistance decreased for ~50 s, before stabilizing to about 270 MΩ. The mechanism for this increased conductance is not known, but was observed in about half the cells examined. Vertical scale; **a**, 1 nA and 20 mV; **bi and biii**, 0.4 nA and 50 mV; **biii**, 0.4 nA and 20 mV. Time scale equals 25 s.

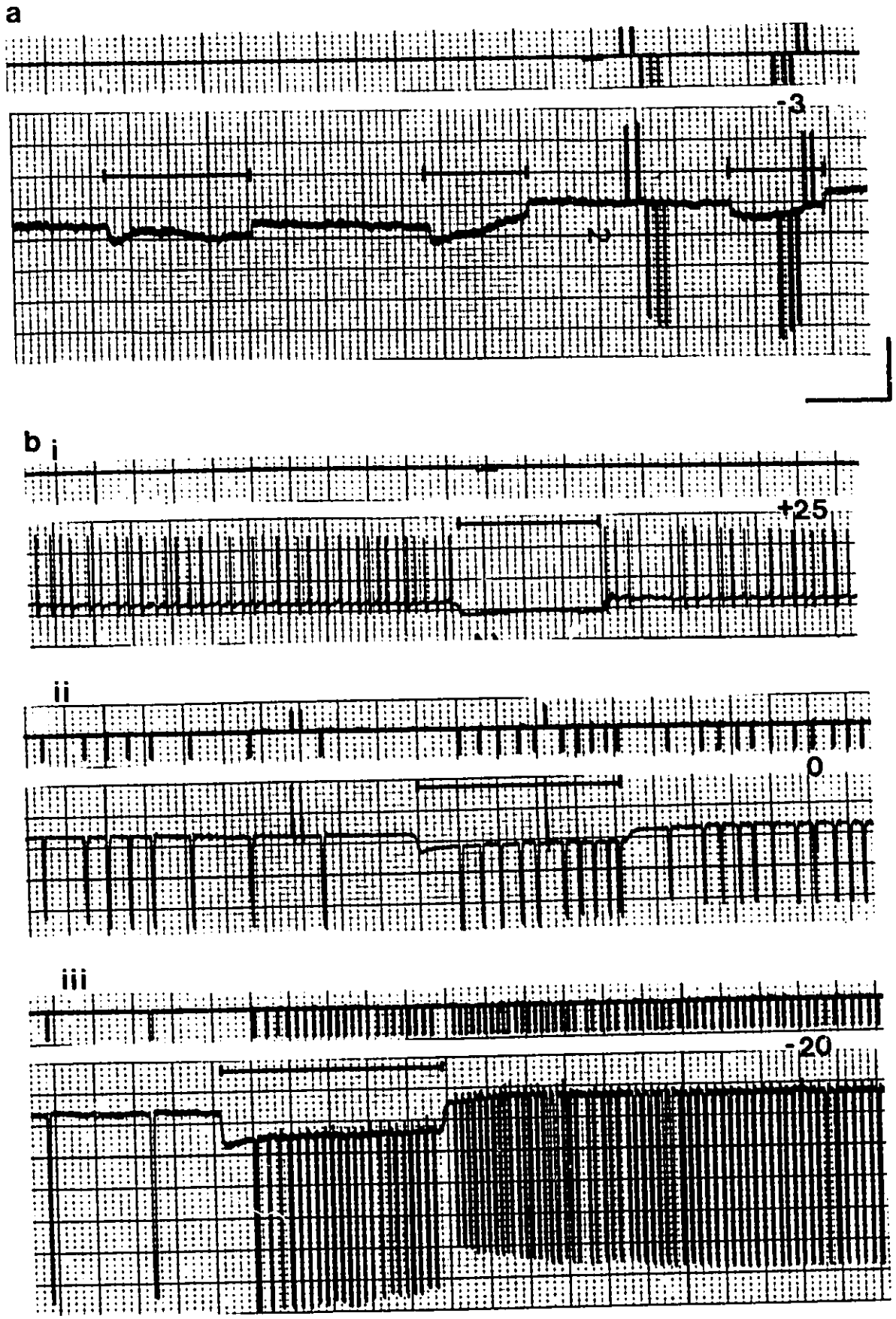
a
-3
b i
+25
ii
0
iii
-20

Increases in membrane conductance caused by the opening of SAK channels should be reflected in reductions of input resistance. The change, i.e. increase or decrease, in input resistance during HOS depended on whether the measurement was made before or after the HOS. Of 8 cells tested, 4 cells showed a decrease in membrane resistance after HOS; the rest were either the same (1 cell) or lower (3 cells). In all 4 cells, where measurements were made before HOS, the input resistance decreased by an average 27% (range of 10% to 63%) during HOS.

SAK channels can be activated during HOS associated cell-swelling

If SAK channels function to monitor membrane tension, then any change in tension should influence channel activity, whether due to cell-swelling during a HOS or during some other mechanical event. Directly monitoring SAK channel P_o during periods of increased membrane tension should provide a simple and unequivocal measure of the channel's ability to sense tension changes.

Single-channel recordings of 17 cell-attached patches revealed that in 35% (6) of these patches, SAK channel P_o increased during periods of HOS which were correlated with cell-swelling. In some patches (Fig. 27) P_o, reproducibly increased and decreased as the cells first swelled (during HOS) and then volume regulated (after HOS), but in other patches P_o increase was irreversible or occurred after the HOS was removed (while the cell was still swollen). In one patch (where this was examined), SAK channel reversal potential (-50 mV, NS in pipette), was the same before and after HOS indicating that the neuronal membrane physiology was not adversely affected, i.e. during volume-equilibration cell resting potential had been re-

established. For all patches, SAK channel presence was confirmed by application of pipette suction.

Discussion

The control of cell volume is divided into two processes, volume maintenance and volume regulation in anisosmotic media (Gilles, 1983). Volume maintenance under isosmotic conditions is necessary due to the presence of large impermeable anions within the cell and because membrane permeabilities to inorganic ions are much less than to water. The cell membrane may be regarded as approximately semipermeable such that the Gibbs-Donnan equilibrium theory predicts influx of water leading to high internal hydrostatic pressure (Hoffmann, 1976; Gilles, 1983). Cells should, therefore, act like perfect osmometers when exposed to changes in osmolarity. The fact that cells are not like osmometers, unless metabolically inhibited, implies an energy requiring component in volume maintenance (Rorive and Gilles, 1979).

Volume regulation under anisosmotic conditions is required to protect cells from exposures to external media which would induce severe swelling leading to lysis or cell-shrinking. Regulation must involve changes in the quantities of osmolytes, either by efflux or influx of inorganic ions or concentration changes in organic osmotic effectors such as amino acids. In vertebrates, inorganic ions appear to be the primary osmotic effectors (Rorive and Gilles, 1979), whereas in invertebrates both inorganic ions and amino acids are important (Gilles, 1979; Treherne, 1980).

Figure 27. Activation of SAK channels during HOS. A continuous record of index P_o (a measure of channel open probability not corrected for the number of channels in the patch) plotted against approximately equal time intervals. Before the start of perfusion with 50% NS (squares), P_o is near zero, but begins to increase when exposure to the hyposmotic saline begins (a, circles). During the first HOS episode (circles), maximum P_o is maintained even after the perfusion stream is stopped (b), but eventually decreases to pre-HOS levels. When the second HOS episode begins (c, triangles), P_o increases rapidly to a maximum that is correlated with the cessation of perfusion (d) and then rapidly falls to a level of activity slightly above that of pre-HOS levels.

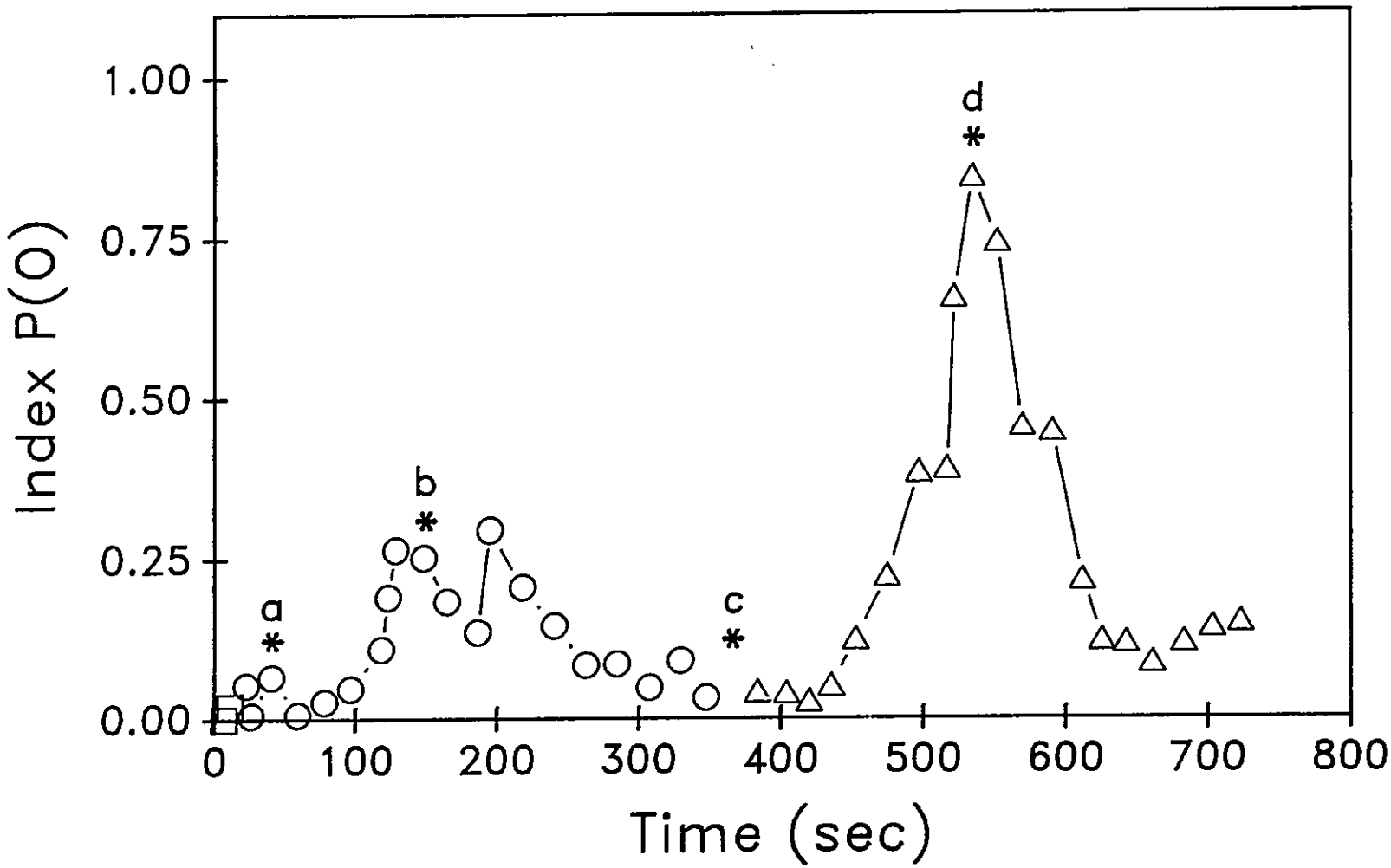
1.00
0.75
0.50
0.25
0.00
Index P(O)
a
b
c
d
0
100
200
300
400
500
600
700
800
Time (sec)

Cultured *Lymnaea* heart cells and neurons seem fully functional in the sense of volume maintenance; the cells survive in culture for several days without apparent ill effect. Neurons, in fact develop extensive morphological modifications indicative of healthy cells (Sigurdson and Morris, 1989). As shown in Morris et al. (1989), both cell-types can control cell volume under hyposmotic conditions by limiting swelling to amounts less than predicted for perfect osmometers. The ability of these cells to withstand short term media dilutions of 70% and then visibly continue normal physiological function (seen in neurons as neurite extension), is clear indication that acute volume limiting mechanisms are present.

K^+ efflux during HOS is a common mechanism of controlling cell volume, being found in cells known to have high internal [K^+], such as eurhyaline crustaceans, annelids and molluscs (Kevers et al., 1979, 1981; Treherne, 1980), human lymphocytes (Grinstein et al., 1982; Sarkadi et al., 1984), frog urinary bladder epithelium (Davis and Finn, 1985; Foskett and Spring, 1985), Amphiuma red blood cells (Cala, 1980; 1985) and Ehrlich ascites tumor cells (Hendil and Hoffmann, 1974; Hoffmann, 1985). Although *Lymnaea* cells did not display RVD (RVD is observed in the above preparations) when under HOS, the resting potentials of heart and neurons appear to be K^+ based (Sattelle, 1974; Brezden and Gardner, 1983) indicating a high internal [K^+]. Efflux of K^+ under HOS is therefore expected. By loading *Lymnaea* heart cells with ^{86}Rb and following tracer efflux, Morris et al. (unpublished results) have been able to show that K^+ efflux is likely occurring during HOS (recall that SAK channels, as other K^+ channels, are permeable to Rb^+).

Net K^+ efflux through ion channels is a dissipative process requiring an outwardly directed electrochemical gradient (Kregenow, 1981). If *Lymnaea* neurons have V_{rest} near E_K, net K^+ efflux will be negligeable under isosmotic conditions. Dilution of the external medium will lower external $[K^+]$, shifting E_K to more negative values and causing net K^+ efflux and V_m hyperpolarization (assuming all other non-K^+ membrane conductances remain constant). This is what Pichon and Treherne (1976) found in the axons of the spider crab which became hyperpolarized under hyposmotic conditions. The question then arises, is the resting K^+ permeability of *Lymnaea* neurons sufficiently large to allow enough K^+ efflux during HOS to prevent lysis, or are other normally quiescent conductances required? Given the large K^+ permeability of SAK channels (see Chapter 3), activation of large numbers of these channels could dramatically increase membrane conductance. I believe this is evident in the ability of an isosmotic perfusion stream to cause a small, but reproducible hyperpolarization in the neurons. In this case, SAK channels could be activated by the mechanical effects of the stream flowing across the membrane. It follows then, that the increased hyperpolarization observed during HOS, is the result of activation of more SAK channels since membrane tension increases with cell-swelling.

Input resistance measurements should reflect this increase in membrane conductance and although specific membrane resistance measurements were not obtained, it is instructive to calculate the changes in resistance which SAK channels could contribute. Input resistance measurements indicate that these cells have very large specific input resistances; for a typical 50 μm diameter cell specific membrane resistance was 15.7 kΩ-cm^2 (assuming a

spherical cell and a measured input resistance of 200 MΩ). This corresponds to a conductance of 64 μS cm^{-2}. SAK channel densities are on the order of 1 - 2 μm^{-2} (Sigurdson et al., 1987a) or about 100 million channels per cm^2. Activation of only 1% of the channels (or all channels having P_o = 0.1), each having a 30 pS conductance, would increase the resting conductance of the membrane by 50%. It is quite possible that the measured input resistances are in error due inaccuracies in the amount of injected current; i.e. the current injection circuit in the electrometer was malfunctioning. Even if the resistance measurements are off by a factor of 10, SAK channels having a P_o = 0.1 would contribute 5% to the resting conductance; a more realistic value for SAK channel P_o during HOS is perhaps 0.5, giving a 25% contribution.

It would seem initially, that an obvious way to resolve whether SAK channels are activated during HOS, would be to make single-channel recordings during periods of cell-swelling. Unfortunately, this approach will be dependent on the relationship between the membrane patch within the pipette and the surrounding "unpatched" membrane. Because tension is proportional to the radius of curvature (Laplace's Law for hemispherical elastic membranes)

$$T = Pd/4$$

for constant pressure, the patch membrane tension will be less than in the surrounding membrane. For large diameter cells, such as *Lymnaea* neurons, this means that patch tension will be as small as 2.5% of the whole-cell membrane tension (assuming a 2 μm diameter patch and 50 μm diameter cell,

typically the largest cells patched). The membrane patch is thought to have high mechanical stability which implies a certain degree of mechanical isolation from the rest of the native membrane. The best evidence for this is the ability to form excised patches; i.e. detaching the membrane patch from the cell without loosing the gigaseal. Since swelling is expected to create tension in parallel with the membrane, there is some question as to whether this tension will be transmitted to the membrane patch within the pipette. If membrane tension is transmitted to SAK channels via a sub-membranous cytoskeletal network (Guharay and Sachs, 1984; Sachs, 1988), during formation of the gigaseal the network within the patch may be decoupled from the surrounding cytoskeleton. This mechanical isolation may explain in part the low numbers of patches in which I observed SAK channel activation during HOS. Ubl et al. (1988a) have also noted that in only 50% of their patches did HOS result in SA channel (non-selective) activation, even though depolarizations of V_m occurred in all cells exposed to solutions of lower osmotic pressure. However, as shown in Fig. 27, it is clear that when SAK channel activation did occur, it could be closely correlated with cell-swelling in much the same way as shown by Sackin (1989) who observed similar activation of SAK channels in *Necturus* kidney cells. Unlike the *Lymnaea* SAK channels observed here (Fig. 25), Sackin (1989) was unable to correlate cell volume equilibration after HOS with a reduction in channel P_o.

None of the results presented here are inconsistent with SAK channels playing a major role in osmoregulation. However, there is still no direct evidence and this will likely remain the case until a specific SAK channel blocker is found. Whether SAK channels are important for volume regula-

tion may be a mute point in regard to questions of their activation during cell-swelling. The channels may simply have "no choice", but become activated. A mere 1 mOsm difference between the external media and cytoplasm is equivalent to 17 mmHg pressure. *Lymnaea* heart cell SAK channels were easily activated with 20 mmHg (Sigurdson et al., 1987a) and although neuron SAK channels are somewhat less sensitive (Sigurdson et al., 1987b; see Chapter 5), both channels should be activated by relatively small changes in osmotic pressure. Sackin (1989) has calculated that a 1% volume increase would be sufficient to activate SAK channels in *Necturus* kidney cells. Therefore, SAK channels may have only to be present in appropriate numbers to play a significant role in acute cell volume regulation.

Chapter 5: Gating characteristics of neuron cell-body SAK channels

Introduction

Ion channel gating has been extensively investigated for classical types of ion channels which have gating modes determined by transmembrane voltage or chemical agonists (Hille, 1984). A new class of ion channel, whose gating is primarily dependent on the input of mechanical energy in the membrane, has received little attention in this respect (Sachs, 1988). Except for the initial studies conducted by Guharay and Sachs (1984, 1985a), the gating properties of cation-selective stretch-activated (SACat) channels have not been examined in detail. Previous work has concentrated on demonstration of stretch-sensitivity and SA channel permeation properties (Cooper et al., 1986; Methfessel et al., 1986; Christensen, 1987; Lansman et al., 1987; Taglietti and Toselli, 1988; Kirber et al., 1988; Stockbridge and French, 1988; Falke and Misler, 1988; Moody and Bosma, 1989; Yang and Sachs, 1989). For stretch-activated K^+ selective (SAK) channels only 2 studies have attempted to describe channel gating properties in relation to stretch-sensitivity (Sigurdson et al., 1987a, see Chapter 2; Sigurdson and Morris, 1989, see Chapter 6), while other reports have, as in the SACat channels, demonstrated stretch-sensitivity and the K^+-selective nature of the channel (Brezden et al., 1986; Sackin, 1987; Ding et al., 1988; Medina and Bregestovski, 1988; Zagotta et al., 1988; Sackin, 1989).

This paucity of kinetic studies is not an accident; gating studies that relate channel mechano-sensitivity to changes in SA channel kinetics are problematic since precise measurement of stimulus magnitude (membrane tension) is dependent on patch geometry or other uncontrolled factors. This results in considerable heterogeneity of channel stretch-sensitivity

from patch to patch and makes comparisons between different preparations difficult. Kinetic studies are, nevertheless important, for they are the only means of testing the stretch-sensitivity model proposed by Sachs (Guharay and Sachs, 1984; Sachs, 1988; see Chapter 1).

Here I further the kinetic characterization of SAK channels begun in Chapter 3. I examine SAK channel stretch- and voltage sensitivity, kinetic stationarity and distributions of open, closed and burst dwell times. Analysis of mean dwell times suggests the neuronal SAK channel has at least 2 open states and 4 closed states. Of these 6 kinetic states only the long open and long closed time change as a function of pressure, and of these 2, only the changes in the long closed time are sufficient to explain the change in channel open probability as a function of pressure. The neuron SAK channel open probability was found to depend on the square of the stimulus intensity as dictated by the Sachs' model of SA channel activation.

Materials and Methods

Lymnaea collection and maintenance, as well as cell culture of neurons, were performed as described in Brezden et al. (1986), Sigurdson et al. (1987a), Sigurdson and Morris (1989) and in chapter 3.

Single-channel recordings were made using standard techniques (Hamill et al., 1981) and with recording pipettes as described previously (Sigurdson and Morris, 1989; chapters 3 and 6). For analysis of stretch- and voltage-sensitivity and kinetic stationarity, open probability (P_o) was determined as described in Sigurdson and Morris (1989) and in Chapter 6. Briefly, single-channel currents were digitized after filtering at 10 kHz (8

pole Bessel) and stored on video tape. For P_o analysis, currents were played back, filtered at 2 kHz and digitized at 0.1 ms point^{-1} (10 kHz, 5 times the filter cutoff frequency). P_o was calculated from either the time averaged currents or the proportion of time the channels spent open. For records with many open channels and little zero current baseline (encountered during periods high channel activity correlated with high negative pressure), P_o was determined by integration of the current record obtained from chart recordings. Because the number of SAK channels in each patch was not known, individual channel P_o was not determined. The P_o is instead reported as an index of open channel probability averaged over time and is given by

$$\text{Index } P_o = N_1P_1 + N_2P_2 + \ldots + N_nP_n$$

where N_i is the number of channels simultaneously open and P_i the proportion of time spent with N_i channels open. Dividing index P_o by n, were it known, would give P_o, the open probability for a single channel.

For analysis of channel kinetics, current records were filtered at 5 kHz and digitized at 50 μs point^{-1}. Event duration lists were constructed using half-threshold event detection software running on a DEC 11/23 computer. Mean open, closed and burst dwell times were extracted by curve fits (Marquardt non-linear least-squares algorithm) to frequency histograms by regression of the sum of probability density functions (see Sigurdson et al., 1987a; Chapter 3). Choice of the best fit to a particular function (one to four sums of exponentials) was made on the basis of three statistical criteria; the Schwarz criterion, the Akaike information criterion (AIC) and a form of the likelihood ratio test (*F* test) for nested models (see Landaw and DiStefano, 1984; Horn, 1987). The Schwarz criterion and

Akaike information criterion reward parameter parsimony; i.e. they indicate which model best fits the data with the fewest parameters, but do not provide any measure of statistical confidence for this "indication". The model with the lowest criterion is the best. The *F* test uses the residual sum of squares and the function order (1, 2, 3 or 4 exponentials) to compare two functions with an order difference of one. The calculated test statistic is distributed as an *F* distribution and large *F* values are evidence to reject the null-hypothesis, i.e. reject the lower order function (Landaw and DiStefano, 1984; Horn, 1987).

In most patches the number of events of long duration (closed dwell times) was quite small, preventing accurate simultaneous fitting of the function to the frequency histogram. This was particularly troublesome when P_o was low, where long closed times could be hundreds of ms long and subsequently few in number/unit time. In these cases, i.e. when simultaneous fitting of all exponentials was not possible, estimates of mean long closed durations were made by two approaches; the first simply widened the frequency histogram bin to 1 ms (as opposed to the sampling frequency bin size of 50 μs) thus increasing the number of events per bin at the expense of lumping all fast events into one or two bins. The second ignored all events faster than an arbitrary cutoff time (typically 2 to 5 times the next fastest mean dwell time) and assumed that the rest of closed dwell times belonged to a single exponential distribution. The average of these events minus the cutoff time gives the maximum likelihood estimate of the mean dwell time for a single exponential (Colquhoun and Sigworth, 1983). When estimates of mean long closed durations could be obtained by both approaches, the mean times estimated by the maximum likelihood

method was within the standard error limits of the least squares derived estimates.

Correlations between mean durations and applied pressure and P_o were checked by testing whether the linear regression slope estimate differed significantly from zero (Mendenhall, 1975).

Discrimination between models of stretch-activation

Comparison between the Sachs' model of pressure squared dependency (see Chapter 1; Sachs, 1988) and linear pressure dependency of SAK channel activation was made by normalizing index P_o values and fitting Boltzmann equations (equations 5.1 and 5.2) to a P_o *vs* pressure or pressure-squared plot respectively.

For a two-state reaction scheme

$$\text{Closed} \underset{\beta}{\overset{\alpha}{\rightleftharpoons}} \text{Open}$$

P_o is described as a Boltzmann distribution with an exponential dependency on pressure and channel stretch-sensitivity (see Cooper et al., 1986; Sachs, 1988). Plots of normalized P_o *vs* pressure (or pressure-squared) were fit to the following equations

$$P_o = 1/(1 + K_0\exp(-\Theta P)) \qquad (5.1)$$

and

$$P_o = 1/(1 + K_0\exp(-\Theta P^2)) \qquad (5.2)$$

where K_0 is an equilibrium constant describing P_o at zero pressure ($K_0 = \alpha/\beta_0$, where β_0 is the closing rate at zero pressure), Θ is channel stretch-sensitivity (Sachs, 1988) and P is pressure (Cooper et al., 1986; Sachs, 1988). Discrimination between non-nested models (equations 5.1 and

5.2) cannot employ the same techniques described above for nested models (sums of exponentials). Instead, a repeated sampling technique described in Horn (1987) was used to decide which of the models best fit the data. (I a.n grateful to R. Horn for his assistance in this analysis).

Results

SAK channel open probability increases with increasing pressure

During single-channel recording of isolated *Lymnaea* neurons, SAK channels were observed in practically every patch (>200 patches). Under normal recording conditions (normal saline, NS, in patch pipette and bath) SAK channels appeared as outward current typified as bursts, i.e. openings punctuated with several short closings (Fig. 28). When suction was applied to the pipette the probability that the channel was open (P_o) increased by augmenting the number of channel openings per unit time rather than by a dramatic increase in the time spent open for one channel (Fig. 29a-e). This implied that the time between openings (or more correctly, between bursts, since almost all "spikes" seen in Fig. 29 at low time resolution appear as bursts at high time resolution as seen in Fig. 28) decreases as suction is increased. All patches examined contained more than one SAK channel, as seen Fig. 29c-e where multiple channel openings occurred at higher negative pressures. Evidence of near maximal channel activation (Fig. 29e, -60 mmHg section) appears as the reduction in current variance compared to lower pressures (compare Fig. 29e and d) and the absence of any zero current. In all patches, release of suction resulted in an immediate decrease in channel P_o (Fig. 29e arrowhead), although zero pressure P_o often took several minutes to "relax" to pre-suction levels (Fig. 29f). The

time constant of this "relaxation" appeared to be dependent on the duration of the applied pressure stimulus, but was quite variable between patches and was not quantified.

Plots of SAK channel P_o (expressed as an index P_o, since individual channel P_o was not known) as a function of pressure show a rapid increase in P_o for small increments in pressure (Fig. 30). The response is non-linear showing saturating behavior at maximal P_o's and incremental P_o increases at pressures slightly below an apparent "threshold" pressure thus producing a sigmoidally-shaped curve. This threshold pressure was quite variable between patches and may represent a certain amount of mechanical slack in the membrane (possibly membrane infoldings) which absorb the initial increases in tension at lower pressures. SAK channels could be activated by both positive and negative pressure (Fig. 30).

The inset in Fig. 30 shows another P_o *vs* pressure plot taken from 5 different patches which were subsequently used for kinetic analysis of open, closed and burst durations.

Figure 28. Neuron SAK channels seen at high time resolution. In these and all other examples of current records of SAK channel activity, outward current is upward. Zero current is denoted by dotted line. Note that openings occur in bursts separated by closings which often exceed 25 ms. Single-channel currents filtered at 5 kHz for a cell-attached patch with NS in pipette, V_m = +70 mV and -60 mmHg suction. Scale, 2.5 pA and 25 ms.

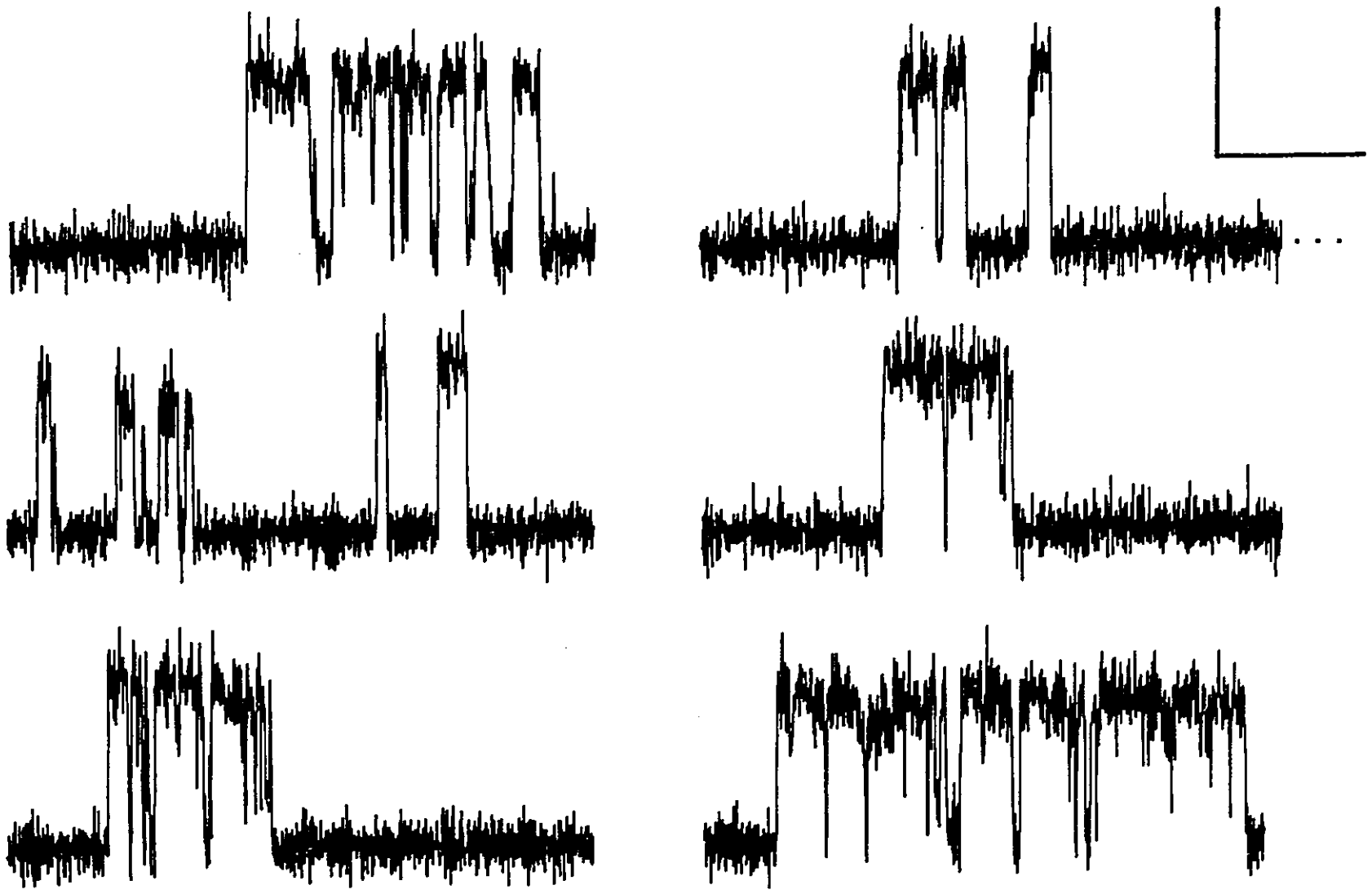

Figure 29. Pressure series showing SAK channel activity increasing as suction is increased. All records shown at reduced time resolution in order to show approximately 10 s of channel activity. Filtering by the oscilloscope display produced current amplitudes which did not appear unitary (compare with Fig. 28). **a)** SAK channel activity seen at nominal zero pressure, 0 mmHg applied suction. **b)** Channel activity at -20 mmHg suction. Frequency of openings had now increased and occasional multiple openings were seen. **c)** Channel activity at -40 mmHg showing increased channel P_o and instances of at least three simultaneously open channels. **d)** At -45 mmHg, SAK channel P_o had dramatically increased. Instances of zero current (indicated by dotted lines here and in **e)** had been significantly reduced with the record showing many multiple openings. **e)** SAK channel P_o near saturation at -60 mmHg. There were no zero current events and the current variance appeared reduced as expected if almost all channels were open. At arrowhead, suction was released with an immediate reduction in P_o. The rebound in channel activity seen after the release point was commonly seen in many patches. **f)** SAK channel activity at 0 mmHg following pressure series. This record was taken ~7 min. after the release of pressure shown in **e.** Typically, channel P_o required from several minutes to only a few seconds to reach pre-suction levels and appeared to be correlated with the length of time that suction was applied. SAK channel current record filtered at 2 kHz for a cell-attached patch with NS in pipette and V_m = +70 mV. Scale, 5 pA and 2.5 s.

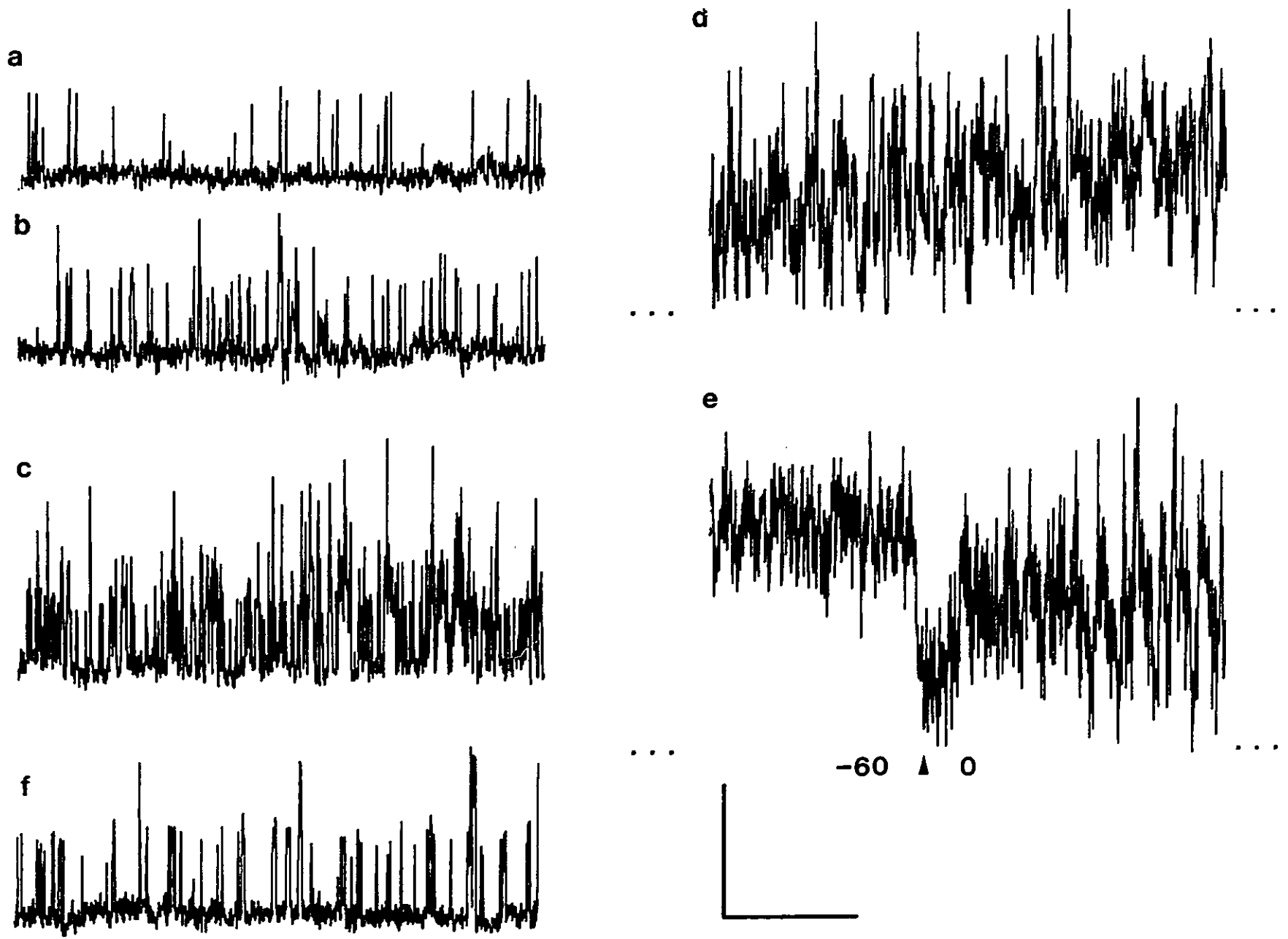
a
b
c
d
e
f
-60
0

Figure 30. SAK channel open probability as a function of positive and negative pressure. P_o shown as an index of true P_o which could be calculated if the true number of channels were known. **Main graph)** Curves determined for 4 different patches. Both positive and negative pressure could activate the channels and approximately to equal amounts (solid diamonds). There was considerable variability between patches as to the pressure where channel P_o began to rapidly increase, ranging from -30 mmHg to almost -90 mmHg. For 2 patches shown (open inverted triangles and closed diamonds), channel P_o could be forced to near saturation producing current records similar to that shown in Fig. 29e. Excised patches (inside-out) were also stretch sensitive (open triangles), but usually could not withstand pressures sufficient to cause P_o saturation. Open inverted triangles, open circles and solid diamonds are data from cell-attached patches with pipettes and bath containing NS and V_m = +70 mV. Open triangles were obtained from inside-out patches where the pipette contained 50 mM CsCl and the outside solution was 50 KCl, V_m = +80mV. **Inset)** Index P_o *vs* pressure curves from 5 different patches whose current records were later used for kinetic analysis. At these low pressures, changes in channel P_o were small but significant (slope of linear regression curve fit to the combined data was significantly different from 0, α = 0.01). All patches were cell-attached with NS in pipette and bath and V_m = +70 mV.

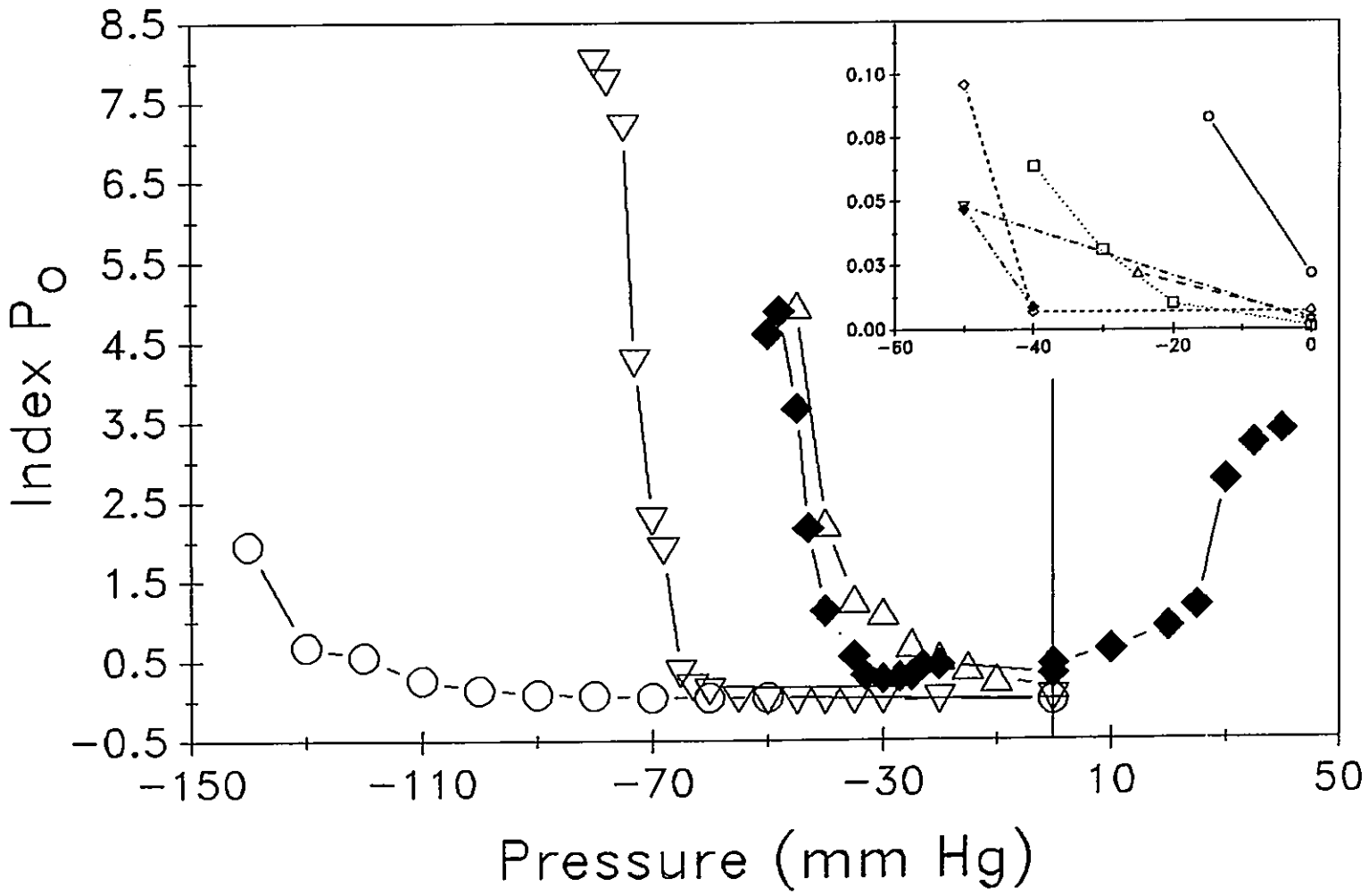
8.5
7.5
6.5
5.5
4.5
3.5
2.5
1.5
0.5
−0.5
Index P_O
−150
−110
−70
−30
10
50
Pressure (mm Hg)
0.10
0.08
0.05
0.03
0.00
−60
−40
−20
0

SAK channel voltage-sensitivity

Cursory examination of SAK channel gating at different transmembrane potentials (V_m) did not reveal a dramatic voltage-dependency. This was born out when analysis of channel P_o as a function of V_m was made (Fig. 31). Within a range of voltages, encompassing the physiological range of V_m (assuming $[K^+]_i$ = 50 mM and NS in bath), SAK channel mean sensitivity was 143 mV $\pm$ 26 mV (n = 4) per e-fold change in P_o (using a linearized fit, i.e. not a fit to a Boltzmann distribution). At extreme depolarizations, channels were more sensitive having a mean of 19 mV $\pm$ 9.2 mV (n = 3) per e-fold change in P_o. The lack of voltage-sensitivity was particularly evident when V_m was alternately switched from -50 mV to +70 mV (solid symbols in Fig. 31). Here, the overlapping standard errors for the mean P_o at the two voltages indicated little change in P_o over a 120 mV range.

SAK channel kinetic stationarity

Analyses of ion channel kinetics usually assume that the channel kinetics operate as a Markov process, where event durations are independent of the preceding event durations and the probability of being in a state does not depend on time (Colquhoun and Hawkes, 1977; Aldrich and Yellen, 1983; Colquhoun and Hawkes, 1983). This can only occur if the rate constants for transitions between different states are invariant with time. Time dependent changes in rate constants will be reflected by corresponding changes in P_o and state dwell times. In this case the channel kinetics will be non-stationary (state occupancy probabilities not constant with time) and invalidate the assumptions that dwell times will be exponentially distributed.

Figure 31. SAK channel voltage sensitivity. Normalized P_o *vs* V_m curves for 5 different patches. P_o was normalized for each patch such that the largest index P_o was set to 1. V_m was estimated by assuming V_{rest} = -50 mV and subtracting V_p. Open symbols represent patches where V_m was sequentially increased by 20 mV increments. Note that between V_m = -40 mV and +20 mV current amplitudes were too small for reliable estimates of P_o (pipette contained 30 mM K^+, bath was NS). Closed symbols are mean P_o for patches where voltage was repeatedly alternated between -50 mV and +70 mV (solid triangle 4 repetitions, solid diamond 3 repetitions). Slopes of curves in the physiological range of V_m gave a voltage-sensitivity of 143 mV $\pm$ 26 mV per e-fold change in P_o (n = 4, hollow arrowheads). Voltage-sensitivity at large depolarizations was much higher (19.3 mV $\pm$ 9.2 mV per e-fold change in P_o, n = 3, solid stars). For open triangles and circles and solid symbols, pipette contained 30 mM K^+ with NS in bath and 0 mmHg. Open squares are from one patch where the pipette solution and bath were NS and -30 mmHg suction was being applied.

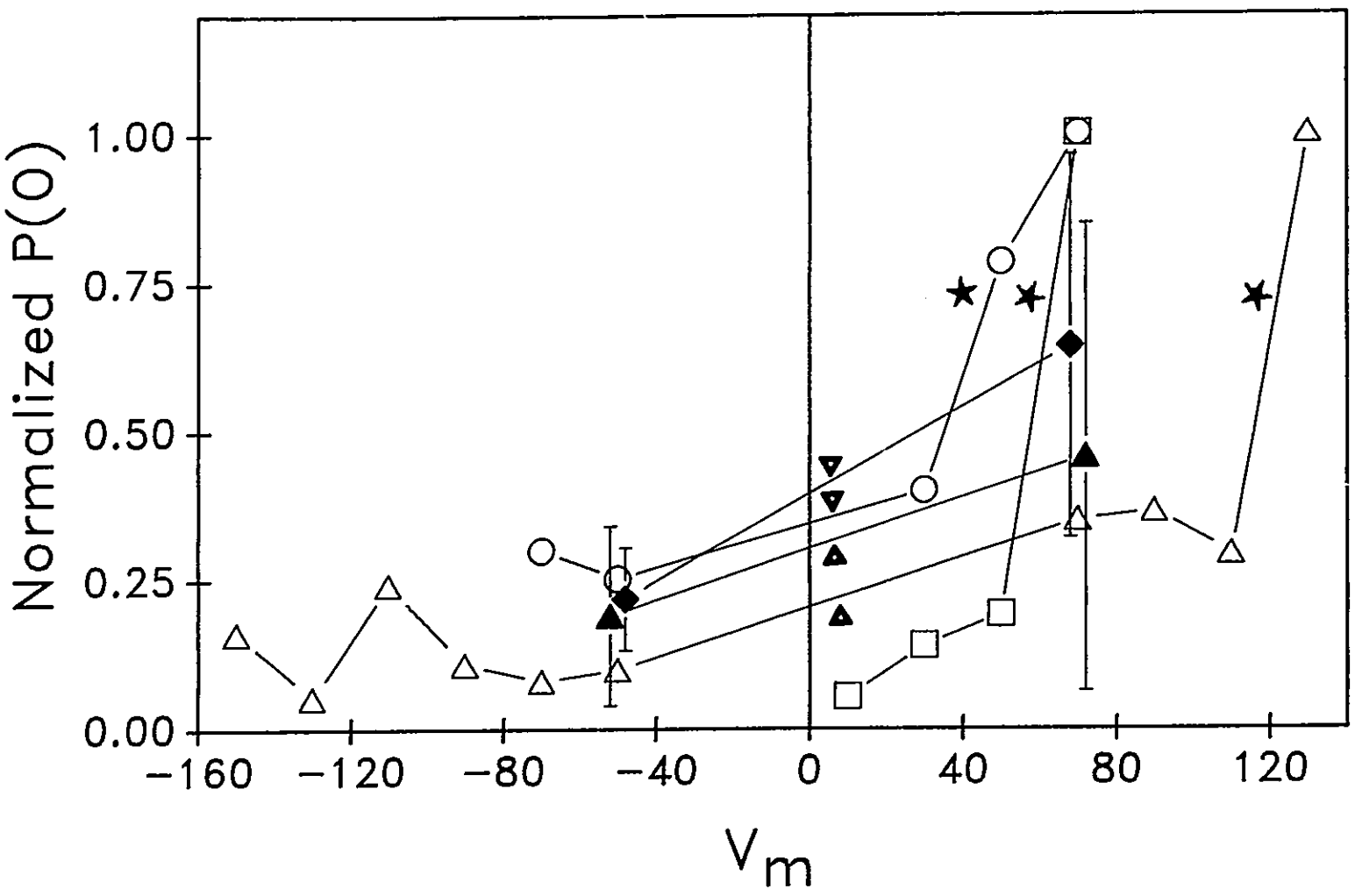
Normalized P(O)
1.00
0.75
0.50
0.25
0.00
−160
−120
−80
−40
0
40
80
120
Vm

SAK channels were tested for stationarity by determining channel P_o over ~10 s intervals and plotting P_o as a function of accumulated time. Comparison of three different patches (all at nominally zero membrane tension) revealed that P_o fluctuates over time even though the channels are not stimulated (Fig. 32). For two of the patches, P_o appeared to vary about the mean symmetrically, while the third patch clearly has P_o increasing with time. Kinetic stationarity during a stimulus was also tested on one patch, where channel P_o was monitored during periods of pipette suction (Fig. 33). Even though suction was constant over time, channel P_o did fluctuate; symmetrically about the mean for two of the pressures (-40 and -50 mmHg), but increasing for the other pressure (-70 mmHg). In the latter case, the P_o rise was observable in the raw data record.

Non-random fluctuations of P_o in time indicated either that the channel kinetics were inherently non-stationary or the stimulus was not constant. The former did not appear to be the case since other patches or pressures displayed stationary behavior. This implies that the pressure was changing (unlikely, since it was monitored during the experiment) or that the membrane tension does not immediately follow the pressure change (perhaps due to compliance in the membrane and underlying cytoskeletal structures) such that the steady-state tension had not been reached.

Figure 32. SAK channel kinetic stationarity at 0 mmHg, nominal 0 membrane tension. Single-channel current records from 3 different patches were sampled in ~10 s intervals and P_o determined. When plotted over accumulated time, these plots show the fluctuation in P_o when there was no applied suction. For 2 patches (circles in lower part of plot and triangles) this variation appeared to be symmetrically distributed about the mean which is indicated by dashed lines (lower circles mean P_o = 0.005, triangles mean P_o = 0.003). The other patch demonstrated a slow (accumulated time = 3 min.) rise in P_o (upper circles mean P_o = 0.061). All patches were cell-attached with NS in pipette and bath and V_m = +70 mV.

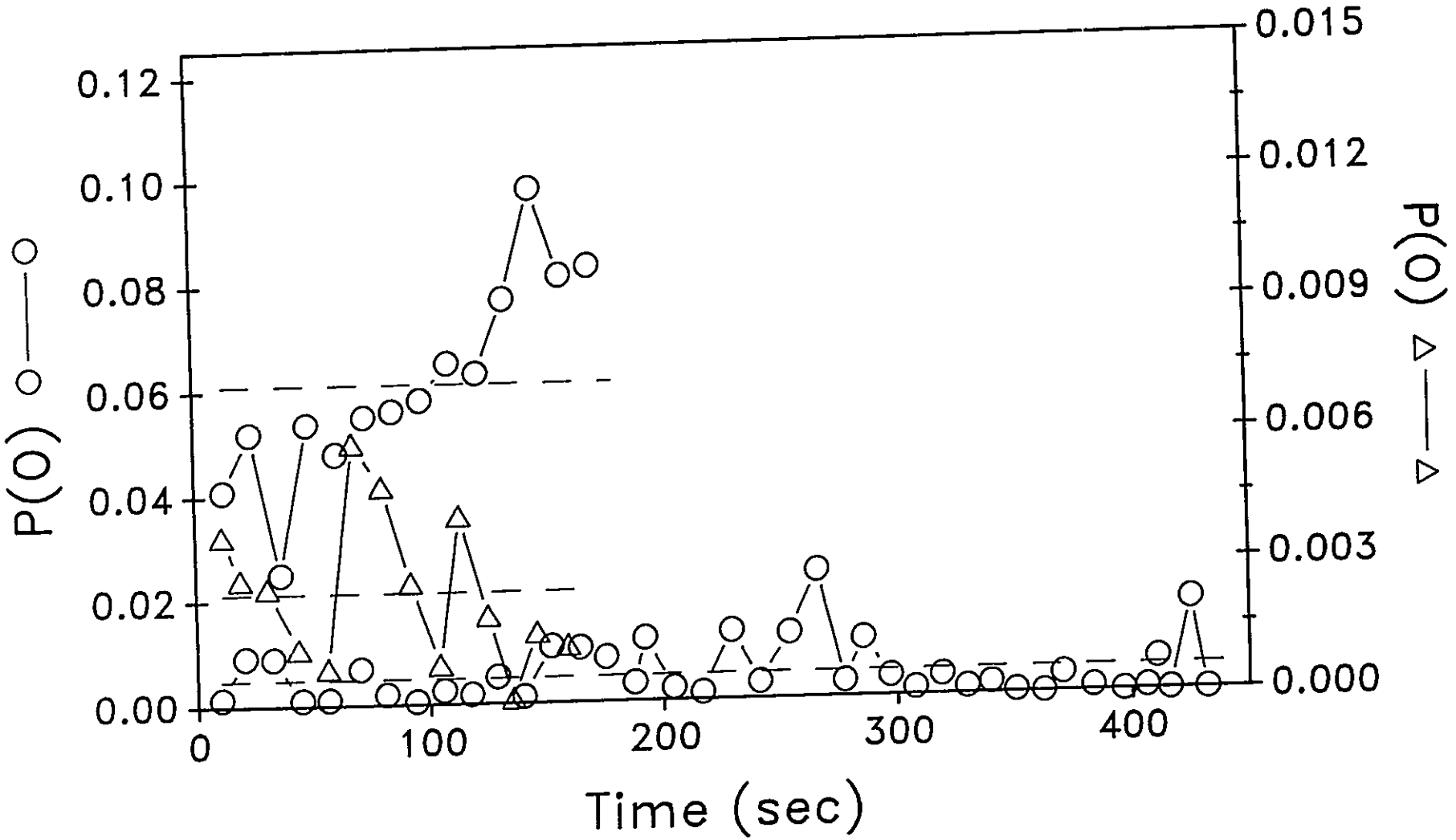
0.12
0.10
0.08
0.06
0.04
0.02
0.00
P(O) ○—○
0.015
0.012
0.009
0.006
0.003
0.000
P(O) △—△
0
100
200
300
400
Time (sec)

Figure 33. SAK channel kinetic stationarity at 3 different pressures for one patch. As in Fig. 32, P_o was determined for ~10 s intervals and plotted against accumulated time. For the 2 lower pressures, -40 and-50mmHg (diamonds and circles respectively), P_o fluctuated about the mean (dashed lines) in a random fashion indicative of stationary processes (mean P_o at -40 mmHg was 0.009; at -50 mmHg mean P_o was 0.047). At -70 mmHg however, P_o steadily rose during the 1 min. recording period (mean P_o was 0.037). Cell-attached patch with NS in pipette and bath, V_m = +70 mV.

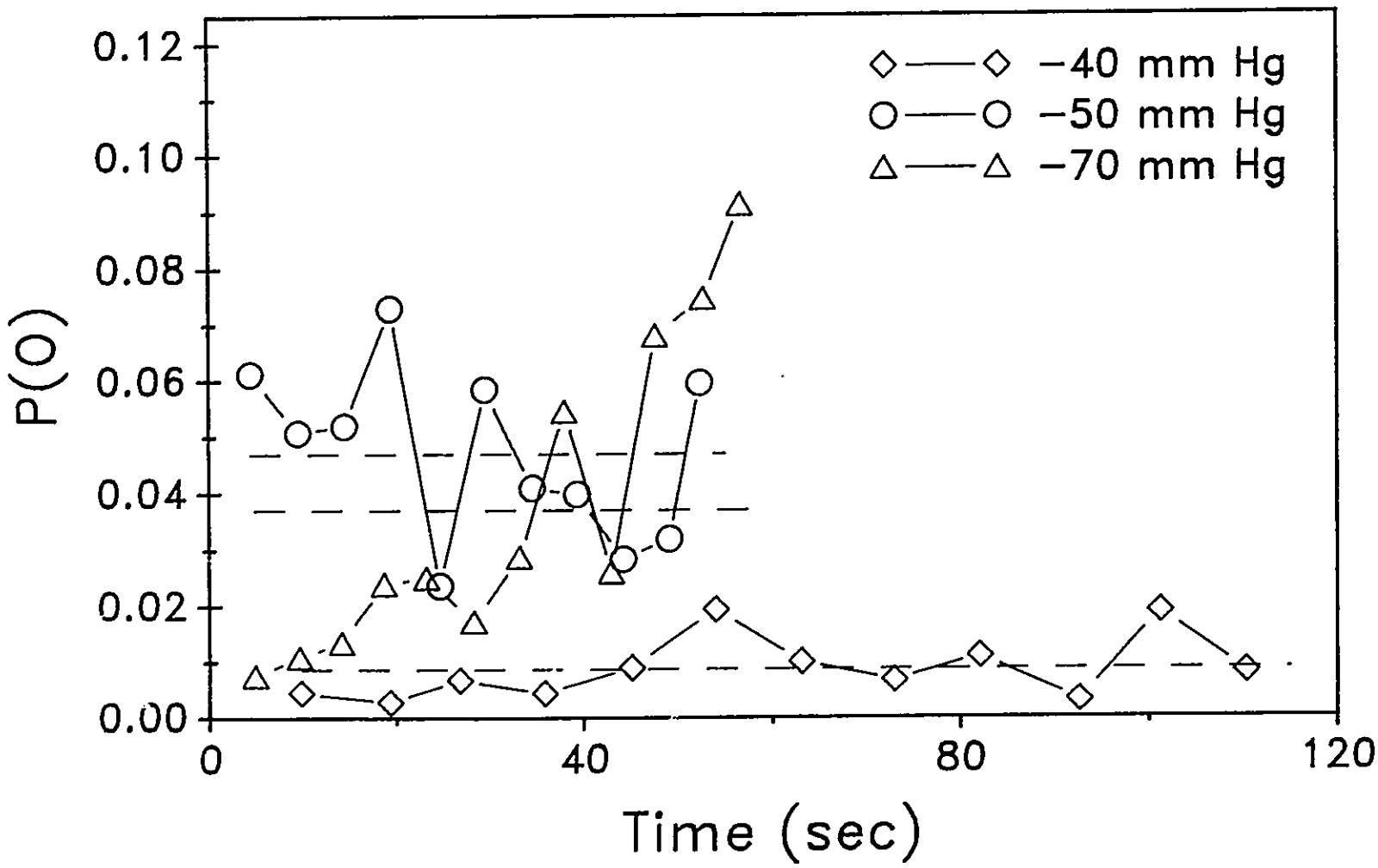
0.12
0.10
0.08
0.06
0.04
0.02
0.00
P(O)
0
40
80
120
Time (sec)
−40 mm Hg
−50 mm Hg
−70 mm Hg

SAK channel kinetics

The tension dependent increases in SAK channel P_o must arise from changes in the transition rates between different conformational states of the protein. Tension dependent changes in any or all of these rates would be reflected as changes in mean dwell times of the various states and probability of being in a particular state (Colquhoun and Hawkes, 1983). In a simple two-state kinetic scheme (one open and one closed state), P_o could increase by an increase in the rate for the transition from closed to open or by decrease in the rate of transition from open to closed. The former case would be revealed by a decrease in the mean closed time, while the latter in an increase of the open time. It is also conceivable that both rates change in opposite, but unequal amounts which would also result in changes in channel P_o. Although most ion channels studied to date possess more than two kinetic states, the same reasoning can be applied for SAK channels in distinguishing which of the dwell times are changing as a function of pressure. The extraction of mean dwell times from dwell time distributions relies on the assumption that these times are exponentially distributed; i.e. the channel gating kinetics are stationary and therefore are described as a Markov process (Colquhoun and Hawkes, 1983; Horn and Lange, 1983). Current records which did not appear stationary were not included in any kinetic analysis.

Dwell time histograms

The characteristics of the raw SAK channel current record (Fig. 28) immediately indicated that the channels' kinetic scheme could not be described as a simple two-state scheme. The channel activity appeared as a

series of bursts of openings, which by definition implied at least two closed states (Colquhoun and Hawkes, 1983). In fact, distributions of SAK channel open dwell times could be best fit by a sum of two exponentials, while closed times were best fit by a sum of four exponentials (for examples of dwell histograms for one patch at different pressures see Figs. 34 - 37). The channels therefore had at least 2 open states and 4 closed states represented by mean dwell open times τ_{O1} and τ_{O2} and mean closed times τ_{C1}, τ_{C2}, τ_{C3} and τ_{C4}, respectively. This was independent of suction, i.e. the number of states did not change as channel P_o increased. It was apparent, however, that only one of the mean dwell times changed dramatically as a function of pressure; for the patch described here (Figs. 34-37), the longest closed time (τ_{C4}) decreased by a factor of 4.6 when suction was increased and the resulting P_o increased by a factor of 6.4. A decrease in the long closed intervals as a function of pressure correlated with the appearance of the raw data; i.e. SAK channel open times did not appear to change, but the time between openings or bursts of openings decreased (increased opening frequency) resulting in an elevated P_o.

Figure 34. Open time frequency histogram obtained at 0 mmHg. This and all other open time distributions (obtained at different pressures or from different patches) were best fit with a sum of two exponentials. In this patch channel activity was very low (P_o = 0.0009), which meant that only a total of 178 openings were collected in a 3 min. period. All mean open dwell times (in this patch, τ_{O1} = 0.13 ms and τ_{O2} = 1.21 ms) were estimated from histograms constructed from bins equal to the sampling time (50 μs). Cell-attached patch, NS in bath and pipette, V_m = +70 mV.

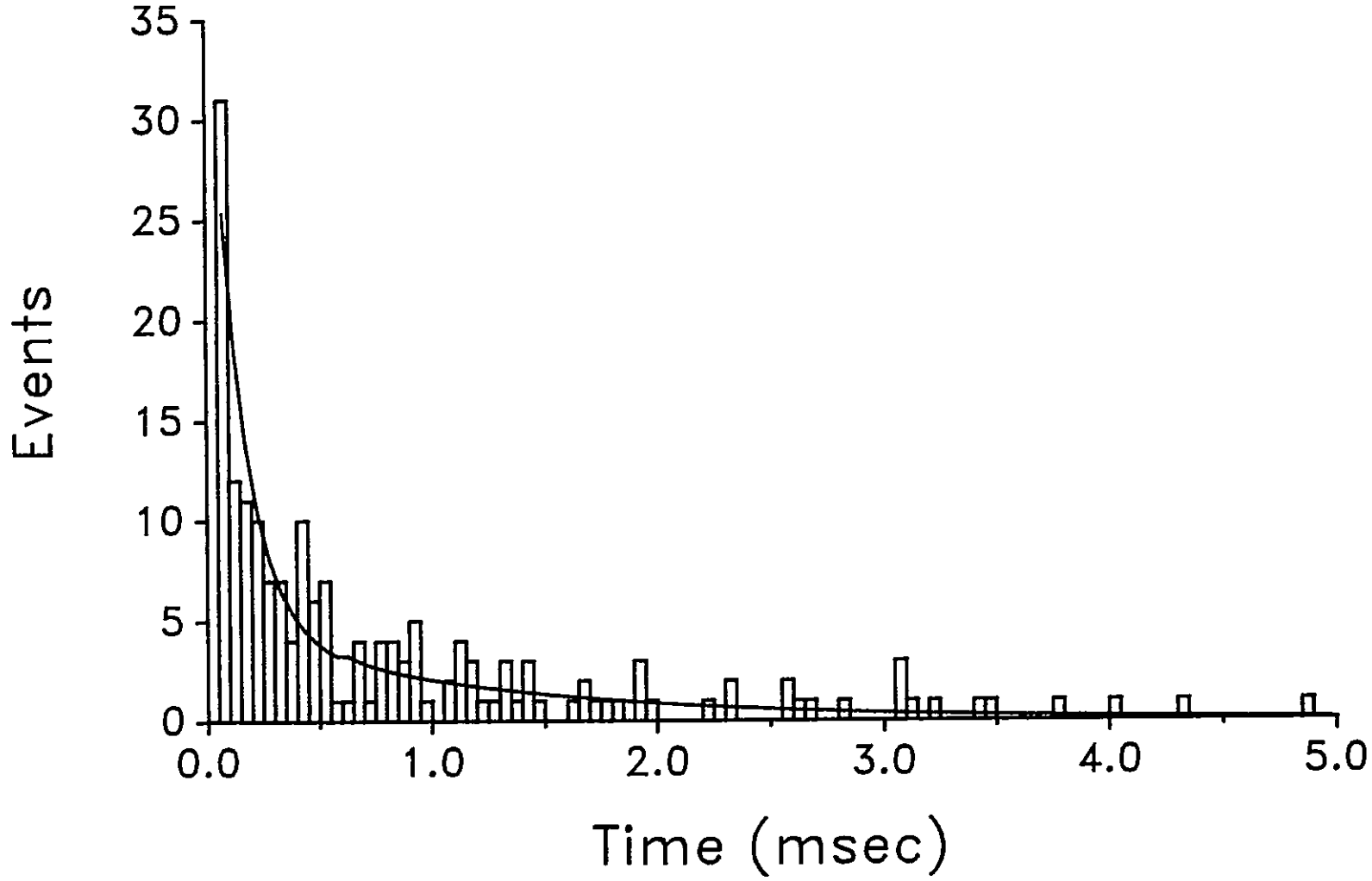
35
30
25
20
15
10
5
0
Events
0.0
1.0
2.0
3.0
4.0
5.0
Time (msec)

Figure 35. Open time frequency histogram obtained at -40 mmHg. Same patch as in Fig. 34, but now P_o = 0.064 (2133 open intervals were collected in 1 min.). Estimated mean dwell times were, τ_{O1} = 0.08 ms and τ_{O2} = 2.07 ms.

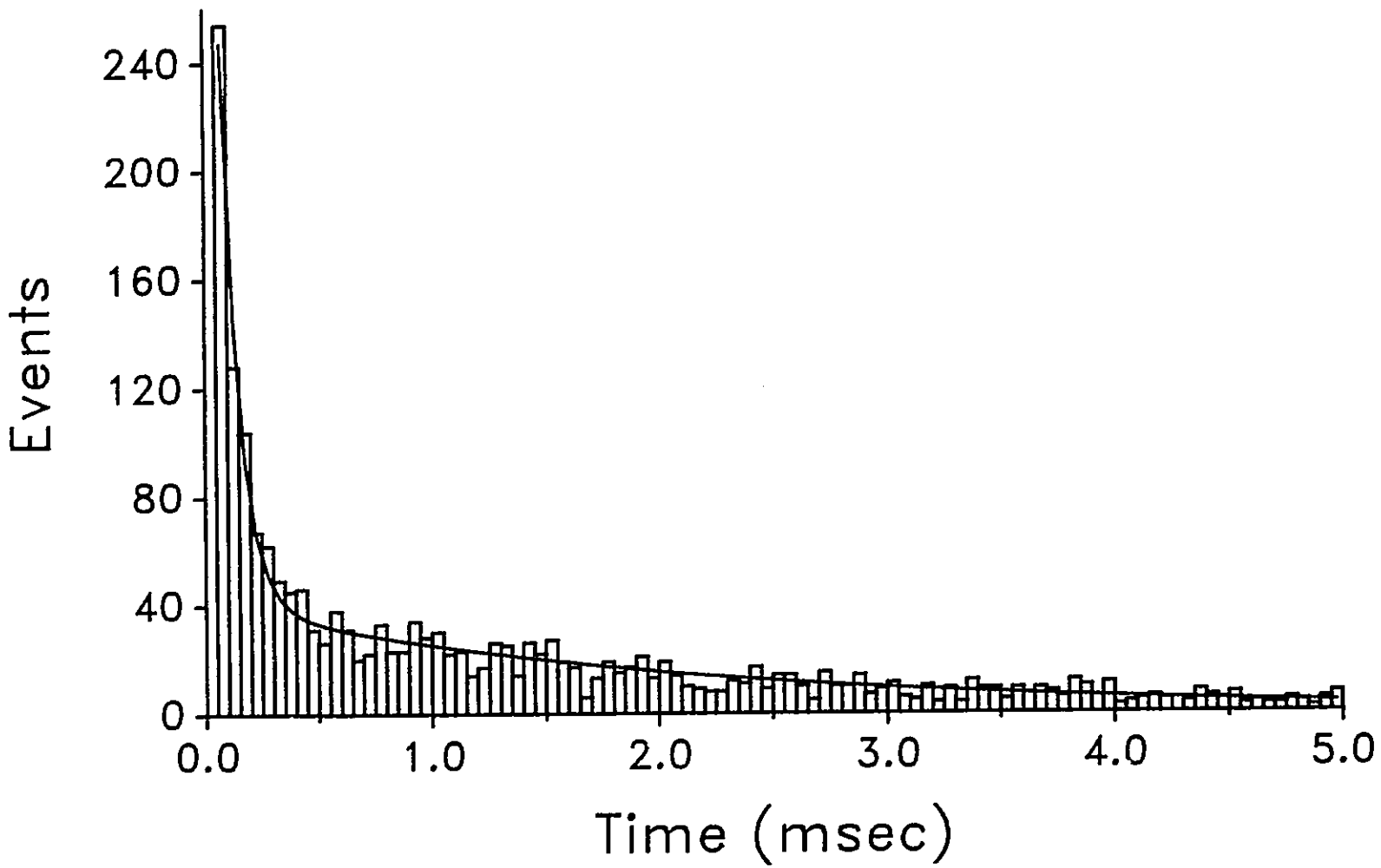
240
200
160
120
80
40
0
Events
0.0
1.0
2.0
3.0
4.0
5.0
Time (msec)

Figure 36. Closed time frequency histogram obtained at -20 mmHg. Same patch as in Fig. 34. In this and for all other patches the closed dwell time distribution was best fit by a sum of 4 exponentials. Channel activity was so low at 0 mmHg that too few events could be collected to simultaneously fit all 4 exponentials (see Fig. 34). At -20 mmHg P_o was 0.01 (983 closed intervals collected in 2.8 min.). Estimated closed mean dwell times were; τ_{C1} = 0.06 ms, τ_{C2} = 0.46 ms, τ_{C3} = 1.83 ms and τ_{C4} = 579 ms. τ_{C4} was estimated from histograms constructed with 1 ms wide bins. The shorter mean times were estimated from histograms constructed from bins equal to the sampling time (50 μs).

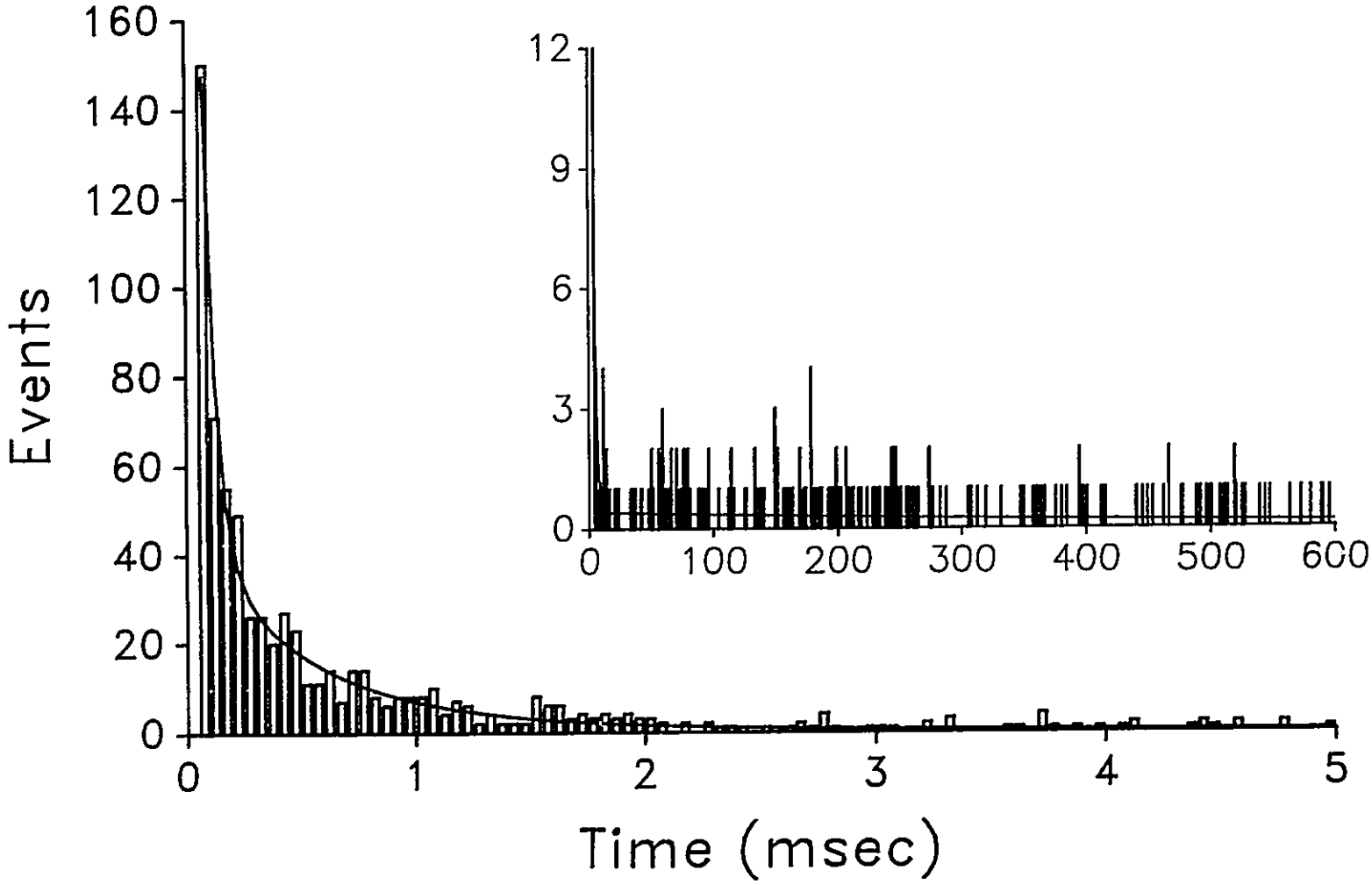
160
140
120
100
80
60
40
20
0
Events
0
1
2
3
4
5
Time (msec)
12
9
6
3
0
0
100
200
300
400
500
600

Figure 37. Closed time frequency histogram obtained at -40 mmHg. Same patch as in Fig. 34. Estimated mean closed times were; τ_{C1} = 0.06 ms, τ_{C2} = 0.57 ms, τ_{C3} = 2.02 ms and τ_{C4} = 125 ms. τ_{C4} was estimated from a frequency histogram constructed from 1 ms bins.

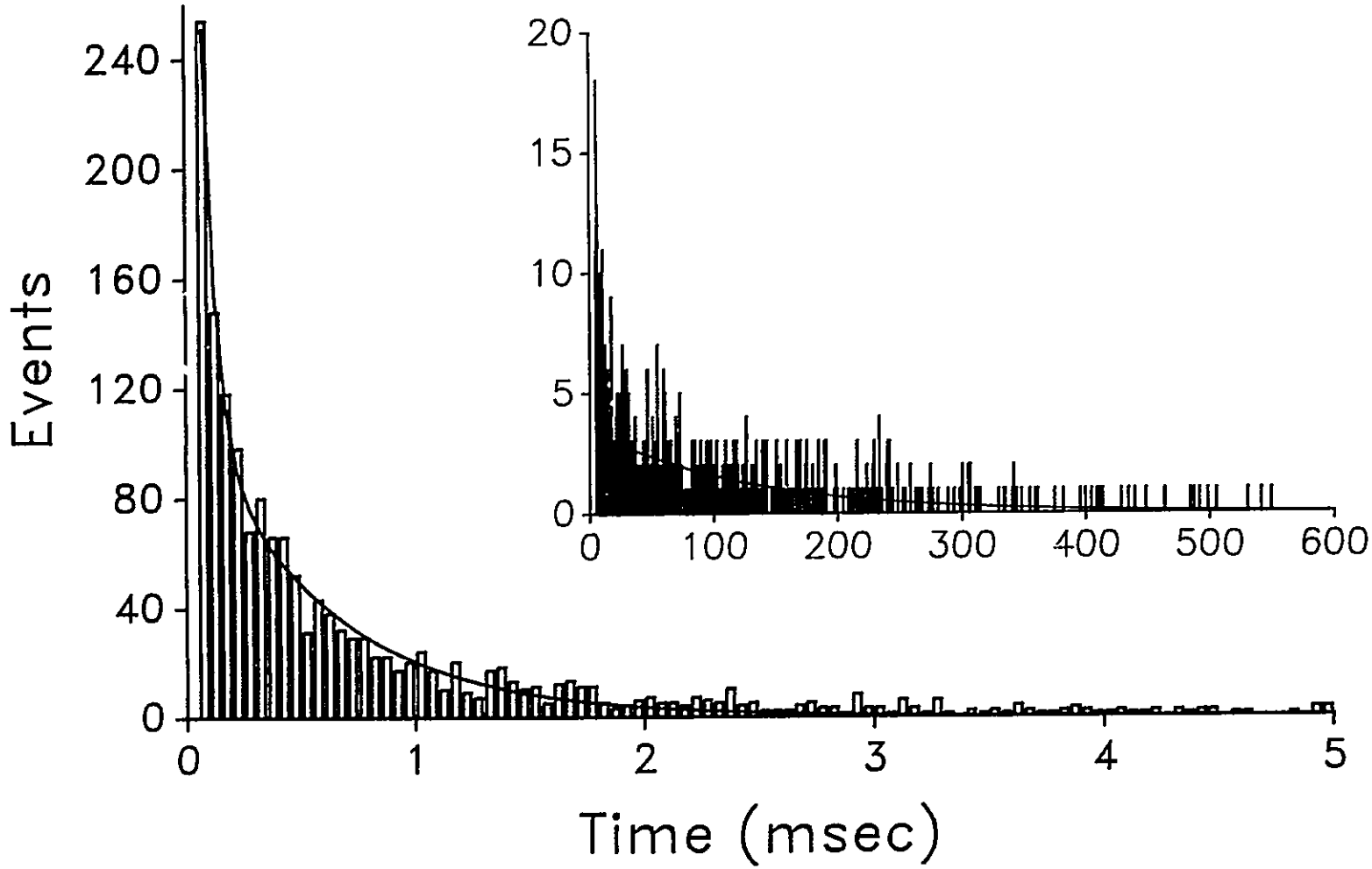
Events
240
200
160
120
80
40
0
0
1
2
3
4
5
Time (msec)
20
15
10
5
0
0
100
200
300
400
500
600

Mean open and closed dwell times as functions of pressure and P_o

When the previous analysis was repeated on 5 other preparations, a similar trend was found, but the interpretation was sometimes confused by inconsistent changes in τ_{C4} and other dwell times. The source of the inconsistencies was found to result from the individual patch P_o *vs* pressure curves, which did not always show a positive slope; i.e. for some pressures greater than nominal zero, P_o was less than at zero pressure (see inset Fig. 30). Ideally, the kinetic analysis would have been conducted on data where P_o is steeply dependent on pressure (Fig. 30), but the multiple channel nature of these patches dictated that only a low range of pressures and correspondingly low P_o's could be used. At higher pressures multiples of channel openings prevented kinetic analysis. If mean dwell times were instead plotted against SAK channel P_o, consistent patterns were observed. For comparison purposes, plots of dwell times against pressure and against channel P_o are presented.

Mean dwell times extracted from frequency histograms were plotted against applied suction or P_o and fit with linear least squares. Linear dependence between dwell times and pressure or P_o were determined by testing for a slope significantly different from zero (Figs. 38 - 40). (Although the Sachs' model of stretch sensitivity predicts a logarithmic relation between mean dwell times and pressure, for the limited range of pressures examined a linear relationship was a reasonable assumption.) Of the 6 mean dwell times required to adequately fit the open and closed distributions, only 2 were significantly correlated with changes in pressure or P_o (slopes significantly different from zero, $\alpha = 0.05$); the long open time, τ_{O2} and the aforementioned long closed time, τ_{C4}. The average

Table 5. The average of mean dwell times (ms) from 5 patches (6 pressure series) which were not linearly dependent on pressure or P_o*.

Open time	Closed times		
τ_{O1}	τ_{C1}	τ_{C2}	τ_{C3}
0.15 $\pm$ 0.08	0.06 $\pm$ 0.032	0.46 $\pm$ 0.16	1.82 $\pm$ 0.57

*Extracted mean times are expressed as averages (ms) and standard deviations from 17 different "conditions" (n = 17), i.e. data was from different patches and different pressures were lumped together.

Figure 38. Mean open dwell times as functions of pressure or P_o. Mean open dwell times were extracted from frequency histograms from 5 other preparations in addition to the histograms shown in Figs. 34-37. Because P_o did not always smoothly increase as suction increased in all patches (see inset Fig. 30), dwell times were plotted against both pressure or P_o. This allowed a clearer resolution of which dwell times altered as the P_o and pressure changed. Changes in mean dwell times were checked by testing if linear regression slope estimates were significantly different from zero. **a)** τ_{O1} was not significantly related to pressure or **b)** P_o. Solid and dotted lines here and in Figs. 39 and 43 represent mean and standard deviation of estimated time constants (see Table 5 for values). When τ_{O2} was plotted as function of pressure, **c**, the slope was not significantly different from 0. Note however, that in all patches except one (medium dashed line) τ_{O2} increased when pressure was changed from 0 mmHg to some new pressure value. In this figure and all following, data from individual patches may be identified by the line type, i.e. solid, dotted, short dash, long dash, dash-dot and dash-dot-dot which connect data points. **d)** The slope of τ_{O2} plotted as a function of P_o was significantly different from 0 (α = 0.05) thus implying a relation between the two. All patches were cell-attached with NS in pipette and bath and V_m = +70 mV.

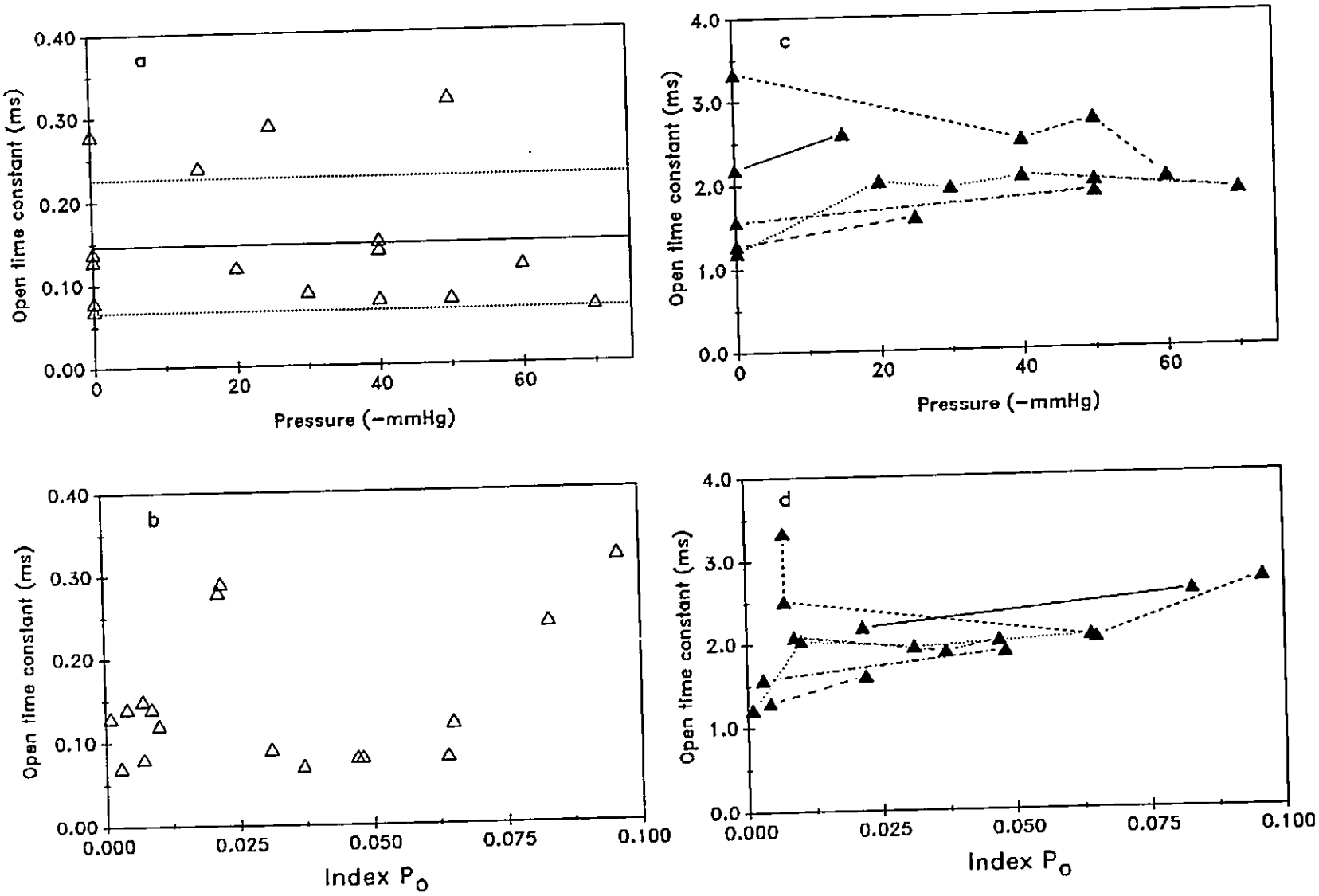
a
b
c
d
Open time constant (ms)
Pressure (−mmHg)
Index P_o
0.00
0.10
0.20
0.30
0.40
0.0
1.0
2.0
3.0
4.0
0
20
40
60
0.000
0.025
0.050
0.075
0.100

Figure 39. Mean closed times as functions of pressure or P_o. There were no significant correlations between pressure a) or P_o b) for the short closed times τ_{C1} (circles) and τ_{C2} (triangles). In a, only the mean and standard deviation for τ_{C2} is shown. The same result was obtained for τ_{C3} (diamonds), i.e. slope was not significantly different from 0. See Table 5 for means and standard deviations of time constants combined from all patches.

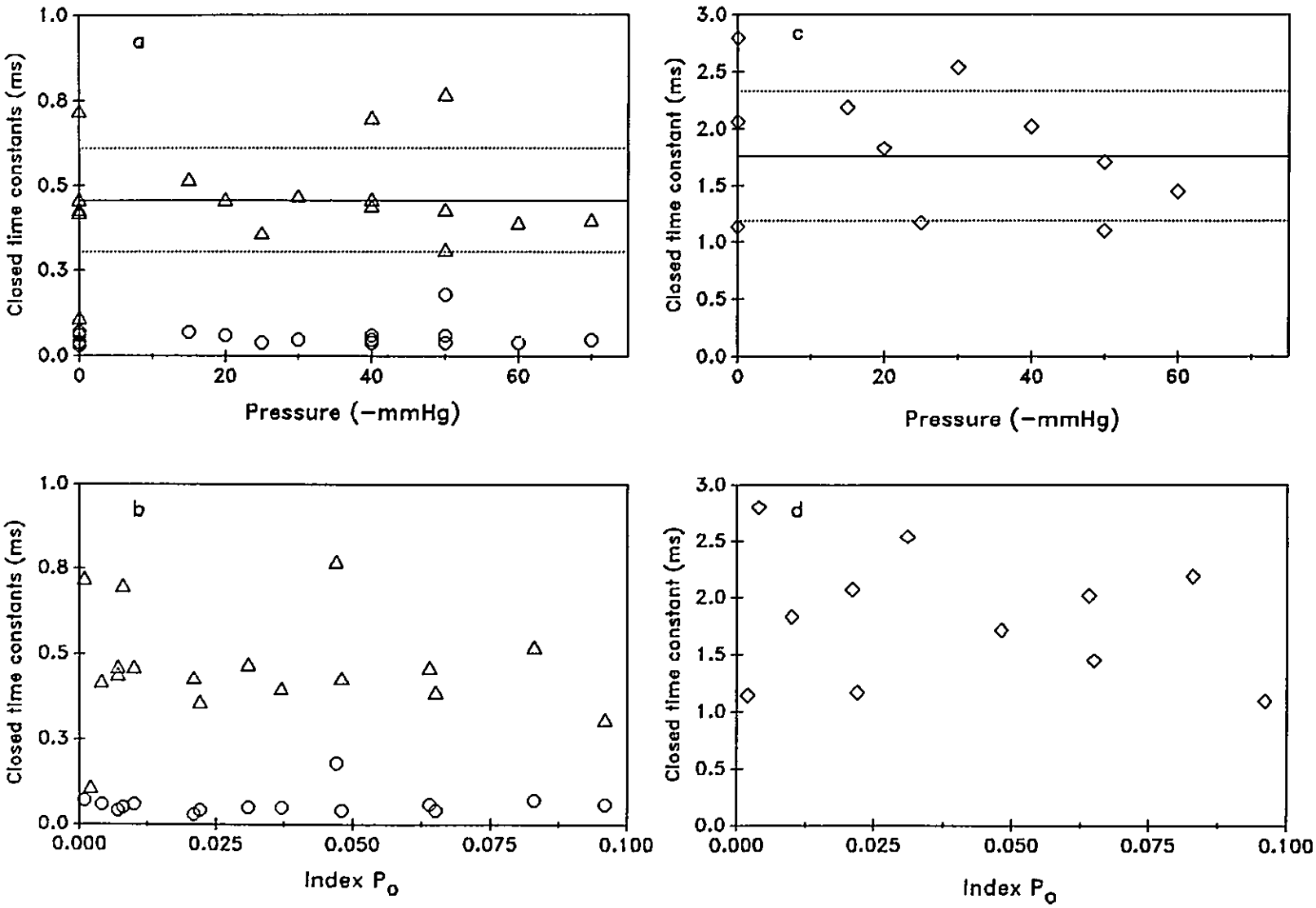
a
b
c
d
Closed time constants (ms)
Closed time constant (ms)
Pressure (−mmHg)
Index P_o
1.0
0.8
0.5
0.3
0.0
3.0
2.5
2.0
1.5
1.0
0.5
0.0
0
20
40
60
0.000
0.025
0.050
0.075
0.100

Figure 40. Long closed dwell time (τ_{C4}) as a function of pressure or P_o. Since estimates of τ_{C4} could not always be made from simultaneous fits of 4 exponentials to frequency histograms (due to paucity of events, especially at low pressures), mean τ_{C4} was determined in all patches by assuming that all long closings belonged to a single exponential distribution and then averaging all intervals greater than a cutoff time (4 ms or 10 ms) which was at least 4 times greater than τ_{C3}. The cutoff time was then subtracted from the average to give maximum likelihood estimate of τ_{C4} (open symbols). For patches where fits to 4 exponentials was possible, these estimates (solid symbols, obtained from histograms with 1 ms bins) are include along with their standard errors. The close agreement between the 2 methods (estimates overlap for each patch) gives some measure of confidence in estimates obtained using the maximum likelihood method alone. Slopes of plots of τ_{C4} *vs* pressure (**a**) or P_o (**b**) were significantly different from 0 (α = 0.05 and 0.005 respectively) decreasing in all patches as pressure or P_o increased. The extent of τ_{C4} decrease in some patches is emphasized by need for a log time scale in order to adequately display all τ_{C4} values.

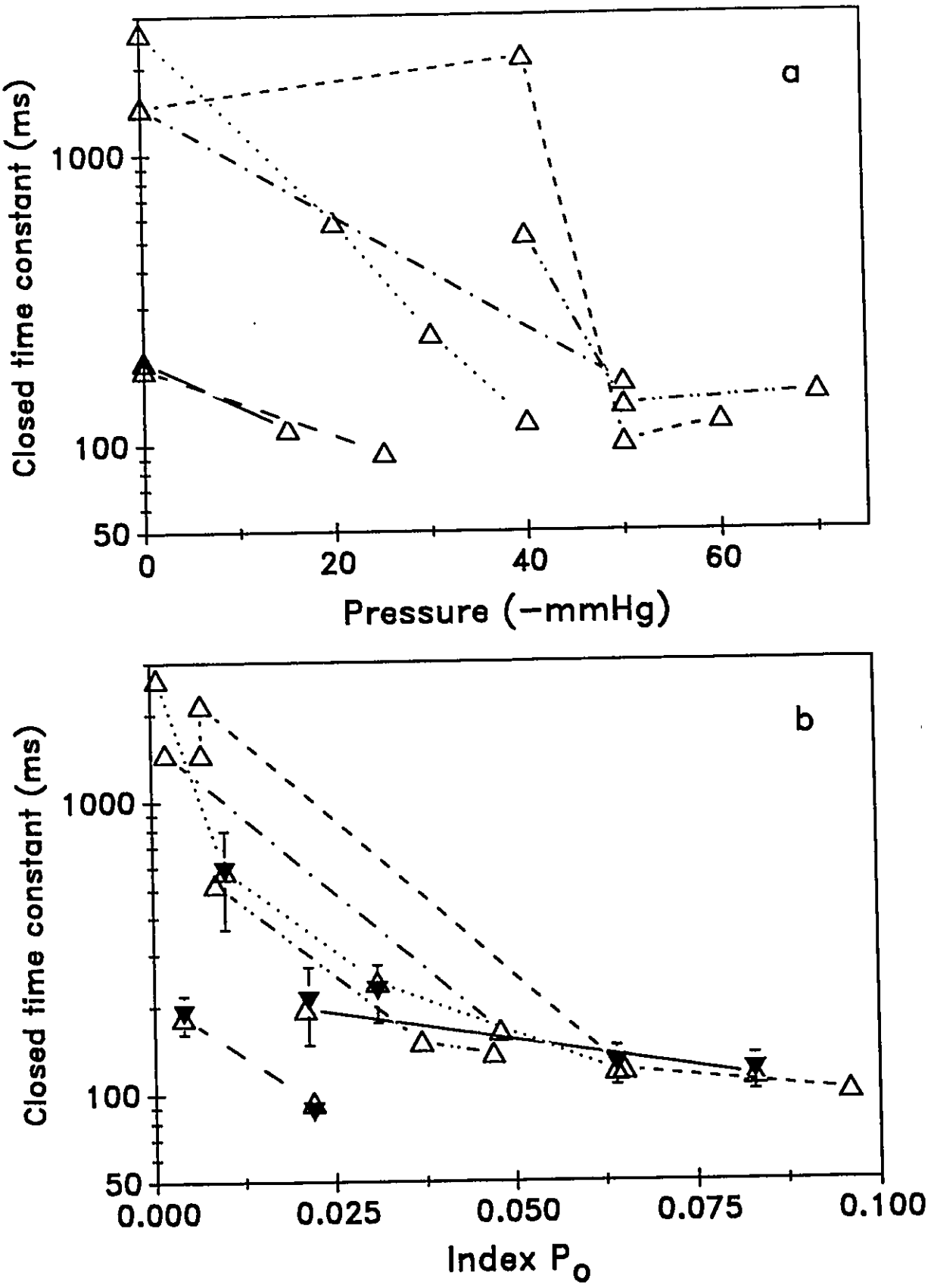
a
Closed time constant (ms)
1000
100
50
0
20
40
60
Pressure (−mmHg)
b
Closed time constant (ms)
1000
100
50
0.000
0.025
0.050
0.075
0.100
Index P_o

values of the other dwell times are given in Table 5.

The changes in τ_{O2} and τ_{C4} were opposite and not of the same magnitude; τ_{O2} increased (Fig. 38d), while τ_{C4} decreased (Fig. 40a, b). For the largest increases in P_o determined during the analysis, the maximum relative changes in τ_{C4} and τ_{O2} were very different (Table 6). In one patch where P_o increased 77 times when suction was applied, τ_{C4} decreased to about one-twentieth the zero pressure τ_{C4}, while τ_{O2} only increased by a factor of 1.7. In all patches, the increased P_o could be attributed primarily to decreases in τ_{C4}, since no other dwell times changed significantly enough to account for the changes in P_o (Figs. 38 - 40, Table 6).

Estimates of τ_{C4} and τ_{IB} cannot be accurate since all patches contained multiple channels. If channel number (N) were known, τ_{C4} could be directly scaled to N. Producing conditions of saturating P_o will give estimates for N, provided the channel has only 2 kinetic states and the unitary current are known. For state diagrams having more than 2 states (some of which having stretch-independent transition rates), P_o can never be forced to 1, meaning an estimate of N will always be underestimated. In Fig. 30, one patch appears to be near saturated activity, with index P_o reaching 8.5. N in this case is at least 9. N for other patches was in the range of 3 to ~10, but often the gigaseal was lost before maximum activation was achieved.

SAK channel burst kinetics

Characteristics of SAK channel burst kinetics were obtained using the same empirical approach used on SAK channels described in *Lymnaea* heart cells (Sigurdson et al., 1987a; see Chapter 2). Analysis of burst duration

and interburst intervals allowed an independent inquiry as to whether the tension dependent change in SAK channel P_o, was primary expressed as a decrease in the long closed time. If SAK channels currents appeared as well separated bursts of openings (see Fig. 28), then it was likely that the long closed events would occur between the bursts. Whether SAK channel openings occurred in bursts was examined by plotting burst duration (at several different pressures for the same patch) as a function of the inter-burst interval (Fig. 41a).

Figure 41. SAK channel burst analysis. Burst duration, proportion of time open in burst and number of closings per burst determined for one patch for 5 different pressures. **a)** The burst durations formed a plateau region between interburst intervals 2 ms and 10 ms, indicating that the channel openings occurred in bursts which were well separated in time. The burst duration (between 2 ms and 10 ms) was seen to increase as suction was increased (see figure for symbol key) followed by a reduction in the post-pressure (0 mmHg) records. Increases in burst duration seen at interburst intervals greater than 10 ms, are due to coalescing of groups of bursts. **b)** Proportion of time spent open in a burst remains constant over the pressure range examined in this patch. At long interburst intervals, proportion of time spent open decreases since the amount of closed time increases as interburst closed intervals are included in the burst duration. **c)** Number of closings per burst shows an increase as pressure is increased (in the 2 ms to 10 ms interburst interval range) as would be expected if the burst duration was also increasing.

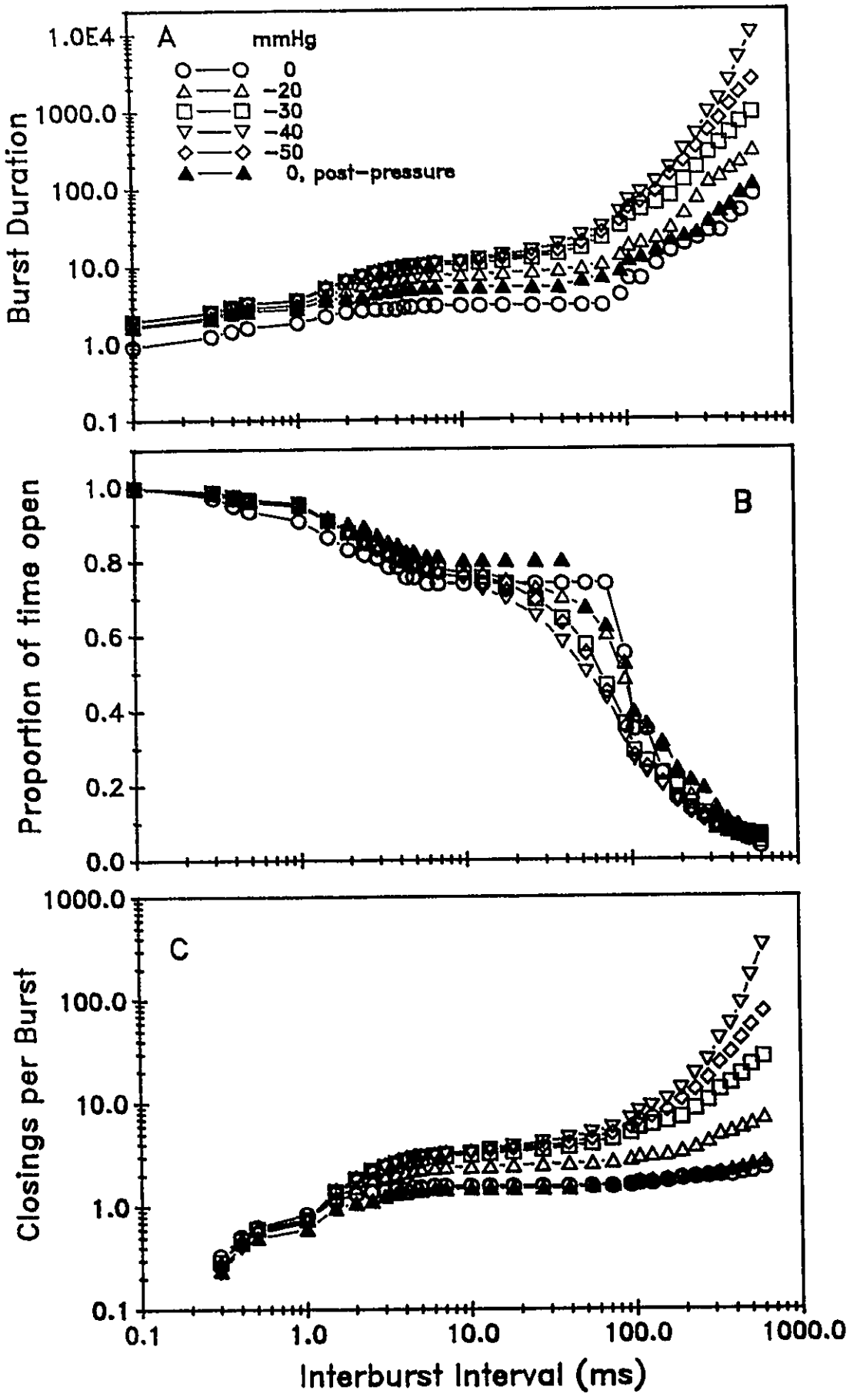
A
mmHg
0
−20
−30
−40
−50
0, post−pressure
Burst Duration
1.0E4
1000.0
100.0
10.0
1.0
0.1
B
Proportion of time open
1.0
0.8
0.6
0.4
0.2
0.0
C
Closings per Burst
1000.0
100.0
10.0
1.0
0.1
0.1
1.0
10.0
100.0
1000.0
Interburst Interval (ms)

For any channel which has a clearly defined, i.e. sufficiently long interburst closed-interval, there should be a range of interburst intervals over which the burst duration should change relatively little (Sigurdson et al., 1987a). As seen in Fig. 41a such a range exists (extending from 2 to 10 ms) where the burst duration plots form a plateau. An interburst interval was chosen from the middle of this range and was then used as a filter to construct a new events list consisting of bursts separated by closed intervals of 6 ms or more (all closed events less than 6 ms, were considered part of the burst). This new events list was used to form a burst frequency histogram from which the mean burst duration was extracted. Typically these histograms were best fit by a sum of 2 exponentials (Fig. 42a), the burst duration (τ_{B2}) and a much faster component (τ_{B1}) which was less than 0.3 ms in duration (these may be isolated openings separated by the chosen interburst discriminating time). The mean interburst duration (τ_{IB}) was similarly determined from a curve fit to a single exponential (Fig. 42b). In addition to burst durations, the proportion of time spent open per burst and the number of closing (of any duration less than the discriminating interburst time) were examined at different pressures (Fig. 41b, c).

For the patch presented in Fig. 41, burst duration seemed to increase as function of pressure. The accumulated data from 5 patches indicated the slope of the plot of mean burst duration (τ_{B2}) *vs* pressure or P_o was significantly different from zero ($\alpha = 0.05$; Fig. 43). Interburst duration was also significantly correlated with pressure or P_o, decreasing as pressure or P_o increased (Fig. 44). The maximum relative changes in τ_{B2} were slightly larger than those observed for τ_{O2}, but were all (except for patch #1) smaller than the changes found for τ_{IB} (Table 6).

Figure 42. Burst duration and interburst closed time frequency histograms. Construction of histograms was made by choosing an interburst interval cutoff time (6 ms) from the middle of the plateau region described in Fig. 41. **a)** Burst duration histograms could be best fit by the sum of 2 exponentials in all patches except one. The fast burst time τ_{B1}, is probably due to contamination by isolated short openings which occurred in closed intervals greater than the cutoff time. For this patch, τ_{B1} was 0.1 ms while the mean burst duration, τ_{B2} was 17 ms. **b)** Interburst closed time (τ_{IB}) histograms were best fit by a single exponential, although in most patches at low pressure there were too few events for generation of a frequency histogram suitable for curve fitting. Maximum likelihood estimates were made instead. In this patch, τ_{IB} was 92.2 ms. Cell-attached patch with NS in pipette and bath, V_m = +70 mV and suction at -50 mmHg.

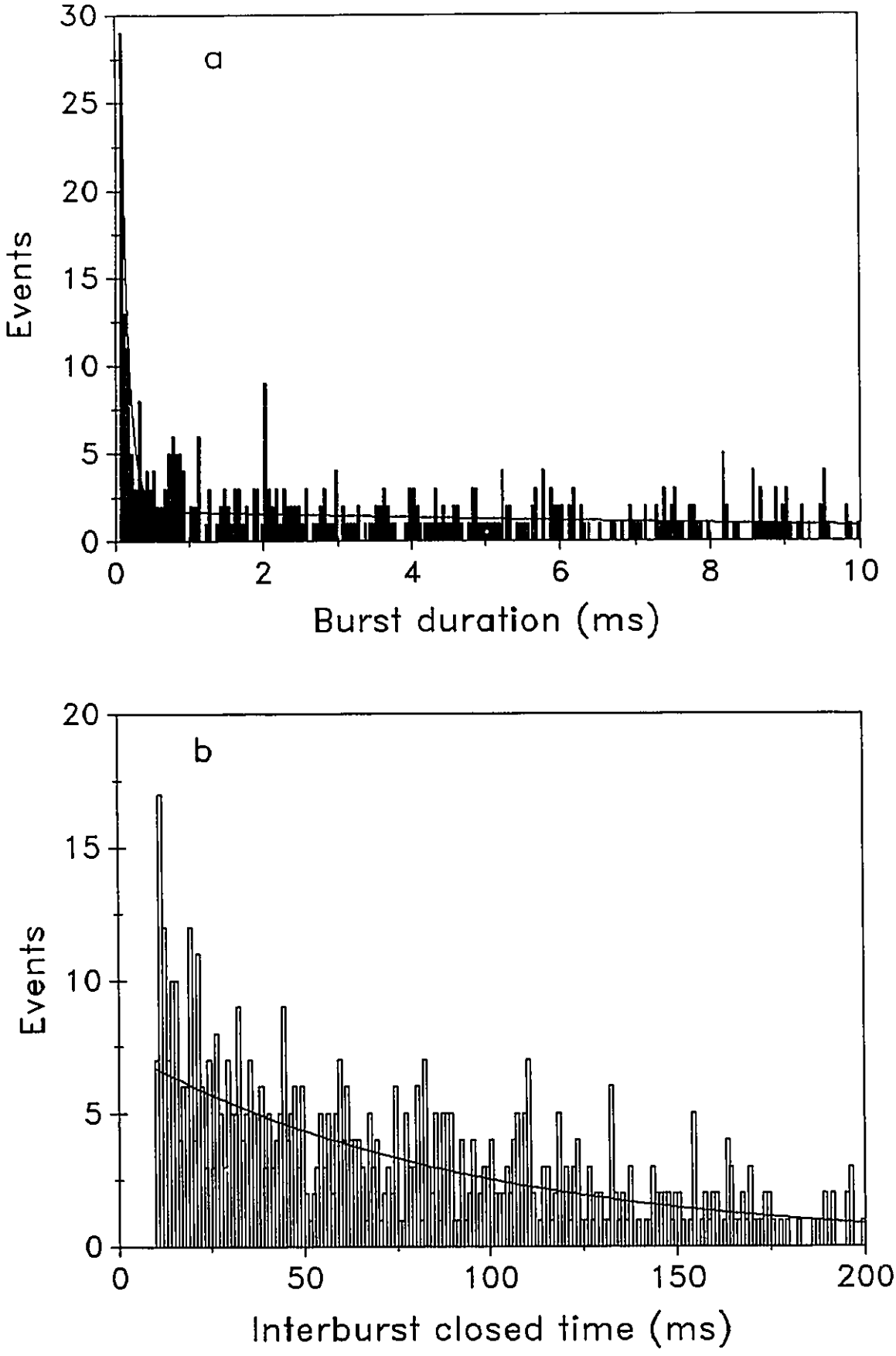
a
Events
Burst duration (ms)
0
5
10
15
20
25
30
0
2
4
6
8
10
b
Events
Interburst closed time (ms)
0
5
10
15
20
0
50
100
150
200

Figure 43. Mean burst duration as a function of pressure or P_o. As might be expected for random inclusions of brief openings into the burst duration distribution, the short time constant (τ_{B1}) of the burst duration frequency histogram was not correlated with pressure (**a**) or P_o (**b**). **c**) τ_{B2} did increase as pressure or P_o (**d**) increased (slope significantly different from 0, $\alpha = 0.05$ and 0.01 respectively).

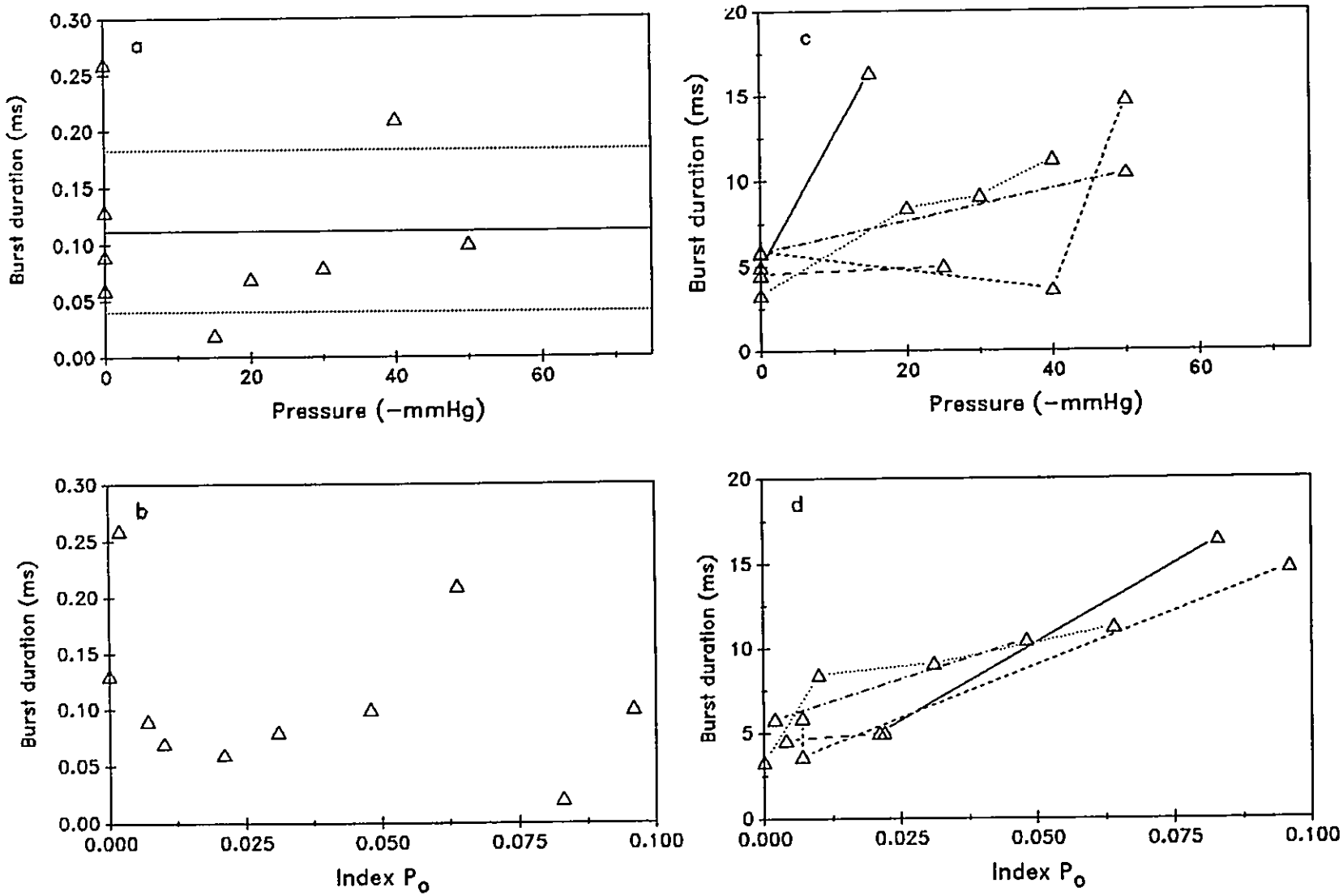
a
Burst duration (ms)
0.30
0.25
0.20
0.15
0.10
0.05
0.00
0
20
40
60
Pressure (−mmHg)
c
Burst duration (ms)
20
15
10
5
0
0
20
40
60
Pressure (−mmHg)
b
Burst duration (ms)
0.30
0.25
0.20
0.15
0.10
0.05
0.00
0.000
0.025
0.050
0.075
0.100
Index P_o
d
Burst duration (ms)
20
15
10
5
0
0.000
0.025
0.050
0.075
0.100
Index P_o

Figure 44. Interburst closed time (τ_{IB}) as a function of pressure or P_o. Open symbols obtained from maximum likelihood estimates using a 10 ms cutoff. Filled symbols are estimates based on a single exponential curve fit. τ_{IB} decreased significantly (slopes different from 0, $\alpha = 0.05$) as pressure (**a**) or P_o (**b**) increased.

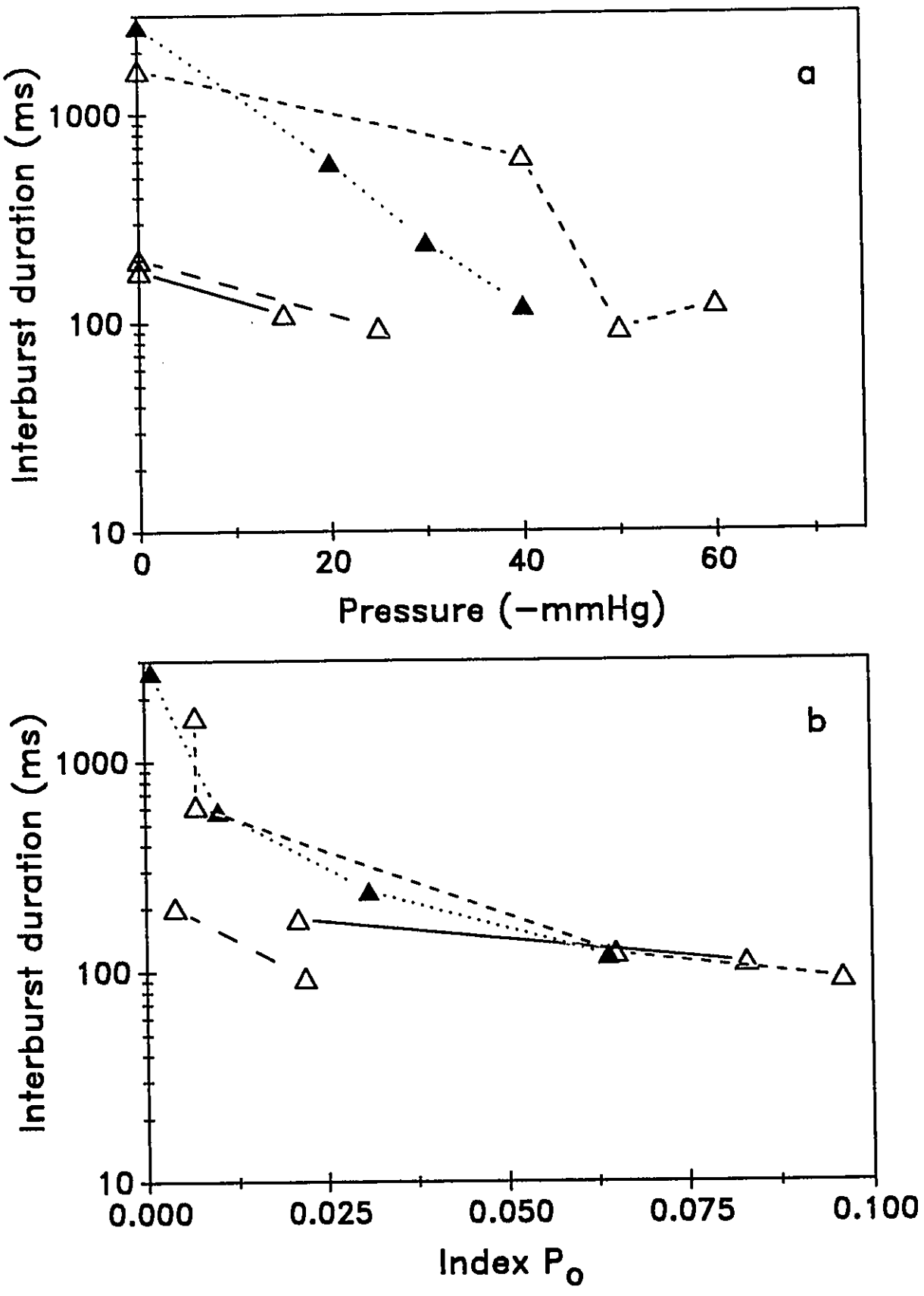
a
Interburst duration (ms)
1000
100
10
0
20
40
60
Pressure (−mmHg)
b
Interburst duration (ms)
1000
100
10
0.000
0.025
0.050
0.075
0.100
Index P_o

Table 6. Maximum relative changes in τ_{O2}, τ_{B2}, τ_{C4} and τ_{IB} as a function of increased suction.

Patch	Pressure Change[1]	P_o	Relative increase[2] τ_{O2}	τ_{B2}	τ_{C4}	τ_{IB}
1	15	3.9	1.2	3.3	1.7	1.7
2	25	5.4	1.2	1.1	2.0	2.0
3	10	5.4	1.0	-	3.8	-
4	50	13.7	0.8	2.5	14.5	17.8
5	50	17.1	1.2	1.8	9.0	-
6	40	71.1	1.7	3.3	22.3	22.6

[1] For all patches except number 3, this range was from 0 mmHg to the pressure which produced the greatest increase in P_o and was still amenable to kinetic analysis. Given as mmHg.

[2] Ratio of the maximum and minimum (0 mmHg) values of P_o, τ_{O2}, τ_{B2}, τ_{C4} and τ_{IB}. Blank values indicate patches where data were insufficient to determine burst parameters.

Discrimination of the Sachs' model of stretch-sensitivity

The central premise of the Sachs' model of ion channel mechano-sensitivity, is the pressure-squared dependence of channel P_o via a stretch-dependent transition rate (Guharay and Sachs, 1984; Sachs, 1988). The model treats the ion channel as a Hooke's law spring which implicitly describes the free energy change required for channel gating in terms of tension or pressure-squared. Deciding whether the SAK channel P_o as a function of pressure plots (Fig. 30) were best described by a pressure or pressure-squared relation (Equations 5.1 and 5.2, and henceforth models 1 and 2), required fitting equations 5.1 and 5.2 to the data and then deciding which of the models best fit the data. The assumption of a 2-state channel is clearly wrong for both neuron and heart SAK channels, but given that only one mean dwell time changed significantly with pressure (τ_{C4} in neurons and τ_{C3} in heart cells, Chapter 2) implied that only one transition rate was changing as a function of pressure and that simplification to a 2-state kinetic state diagram could be made. Fitting the data to model 2 allowed extraction of the stretch-sensitivity term Θ, thus permitting comparison of SAK channel stretch-sensitivity with other channels.

Surprisingly, adequate curve fits could be made for both models for all patches examined from both neuron and heart SAK channels (Figs. 45 and 46). (I have included data from the *Lymnaea* heart cells to permit comparison with the neuron data presented in this chapter. At the time when the heart data was analyzed and published, this analysis had not been available.) A preliminary discrimination of model 1 *vs* model 2 using the AIC criteria (Horn, 1987) showed that model 2 (pressure-squared) best fit the data. Subsequent model discrimination analysis performed by R. Horn

on this data showed that only the neuron data was best fit by model 2 ($p > 0.95$); the heart data was best fit by the null hypothesis (model 1, pressure). θ for neuron SAK channels was 0.278 $\pm$ 0.192 $cm^{-2}Hg$ (n = 6, range 0.044 - 0.54 $cm^{-2}Hg$) and 17.6 $\pm$ 18.2 $cm^{-2}Hg$ (n = 4, range 1.9 - 42.5 $cm^{-2}Hg$). Both cell-attached and inside-out patches were included in these means. For one neuron patch (see Fig. 30, solid diamonds), θ was quite similar when determined for both negative and positive pressures (0.36 $cm^{-2}Hg$ and 0.4 $cm^{-2}Hg$ respectively).

Figure 45. Comparison of the Sachs' pressured-squared model of stretch-sensitivity to a linear model in *Lymnaea* heart cell SAK channels. P_o *vs* pressure curves were obtained from Chapter 2, and then the normalized P_o fit to either equation 5.1 or 5.2. Fits to either the pressure-squared (**a**) or linear (**b**) model were quite good for this patch. Estimated stretch-sensitivity, θ, was 1.9 $cm^{-2}Hg$. There was however, considerable scatter of the estimated stretch-sensitivity parameter θ when data from all heart patches was pooled (mean θ = 17.6 $\pm$ 18.2 $cm^{-2}Hg$, n = 4). Although the AIC measure of goodness of fit chose the pressure-squared model, R. Horn's discrimination analysis for non-nested models chose the linear model for this patch. Cell-attached patch with 30 mM K^+ in pipette and NS in bath, V_m = +50 mV.

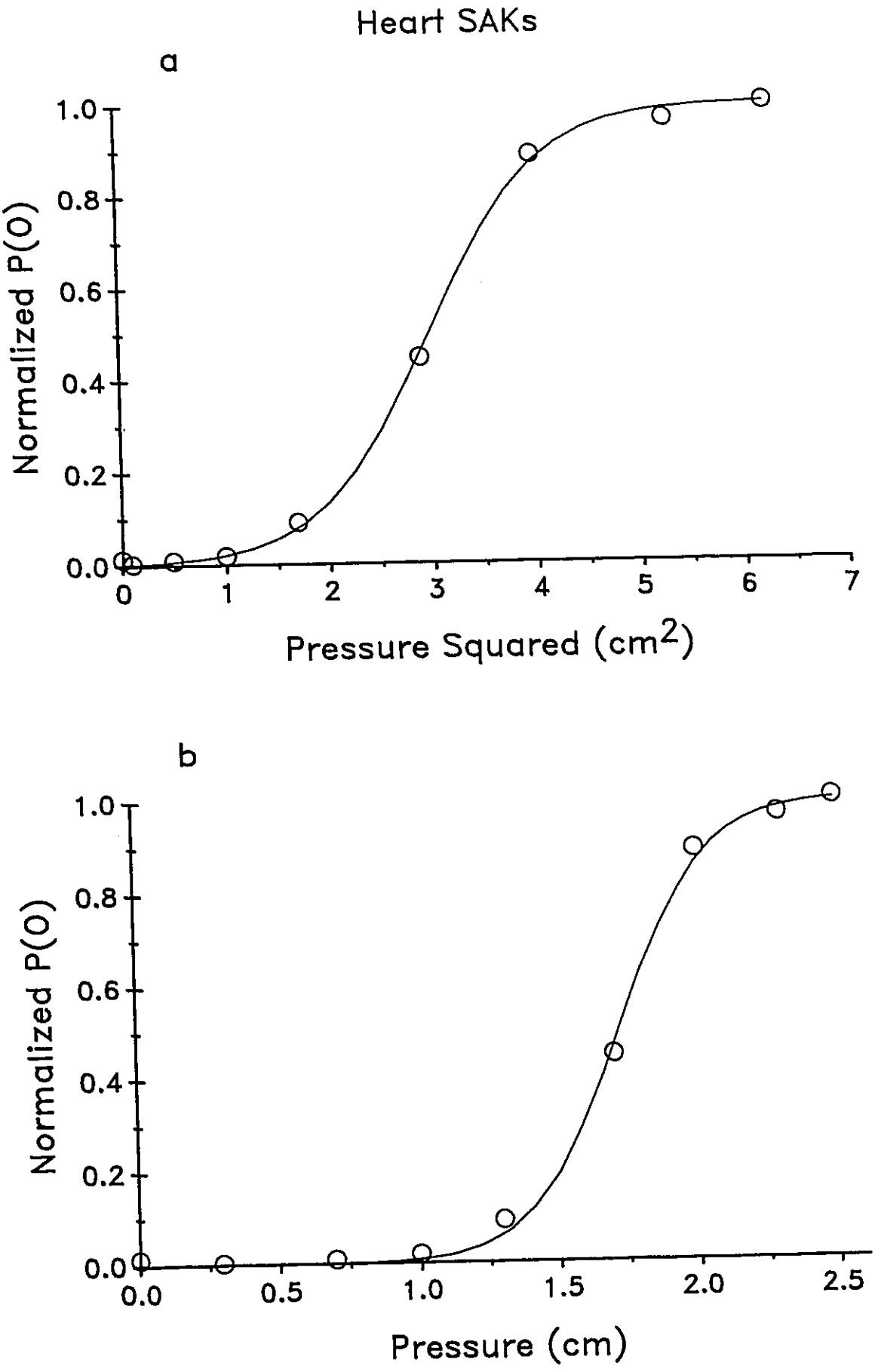
Heart SAKs
a
Normalized P(O)
1.0
0.8
0.6
0.4
0.2
0.0
0
1
2
3
4
5
6
7
Pressure Squared (cm2)
b
Normalized P(O)
1.0
0.8
0.6
0.4
0.2
0.0
0.0
0.5
1.0
1.5
2.0
2.5
Pressure (cm)

Figure 46. Comparison of the Sachs' pressured-squared model of stretch-sensitivity to a linear model in *Lymnaea* neuron SAK channels. As in for the heart SAK channels, both models fit the data, but the estimated mean θ for the pooled neuron was much less variable (0.278 $\pm$ 0.192 $cm^{-2}Hg$, n = 6). For this patch θ was 0.04 $cm^{-2}Hg$. Both AIC and the Horn discrimination analysis chose the pressure-squared model for this patch. Cell-attached patch with NS in pipette and bath and V_m = +70 mV.

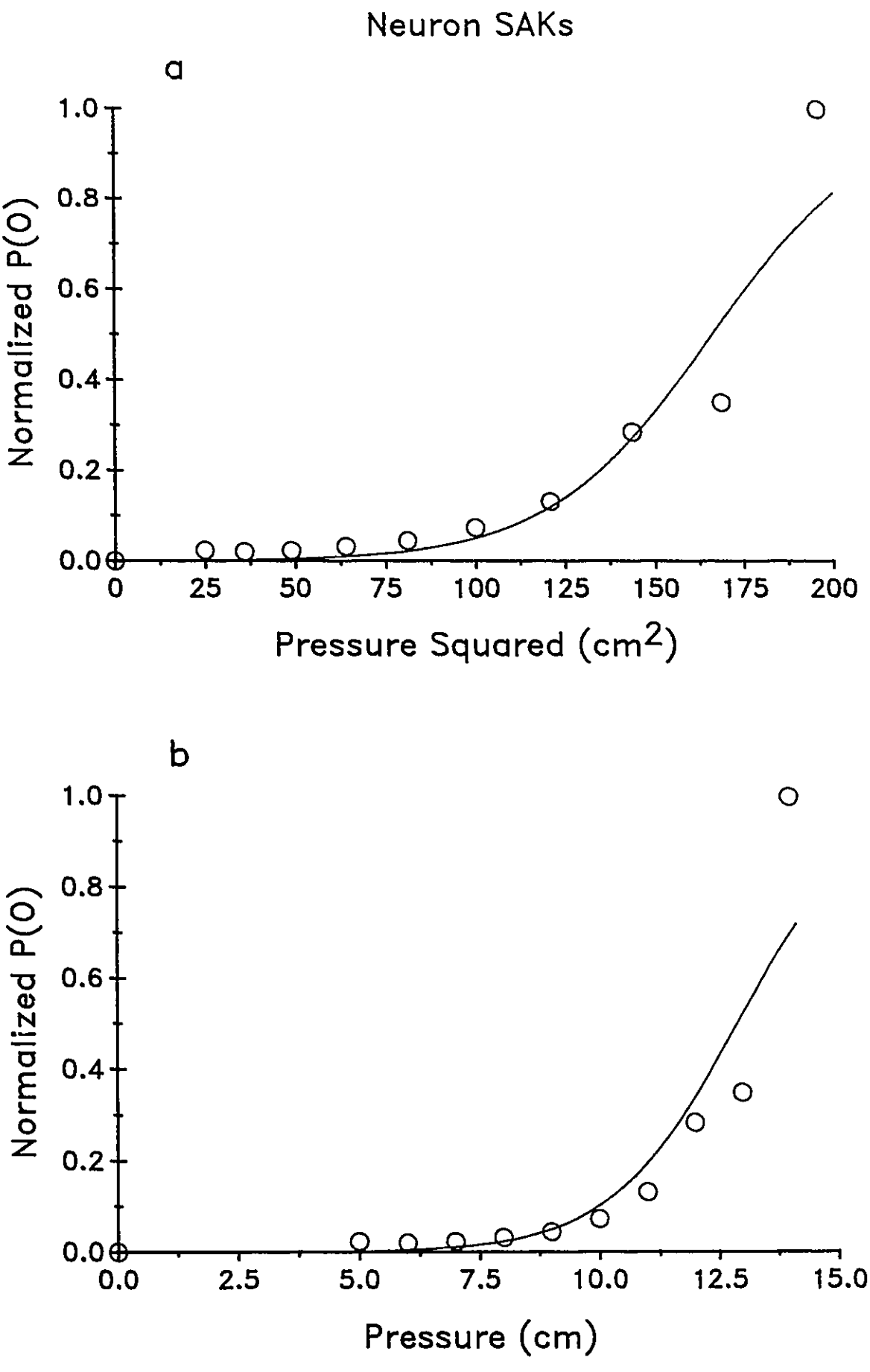
Neuron SAKs
a
Normalized P(O)
1.0
0.8
0.6
0.4
0.2
0.0
0
25
50
75
100
125
150
175
200
Pressure Squared (cm2)
b
Normalized P(O)
1.0
0.8
0.6
0.4
0.2
0.0
0.0
2.5
5.0
7.5
10.0
12.5
15.0
Pressure (cm)

Discussion

Mechanically-gated ion channels may still seem somewhat of a novelty, but this channel type has now been described animals, plants, fungi and bacteria (Sachs, 1988; Morris, 1989). While it is unlikely that the underlying transduction mechanisms are similar in all channels from this diverse group, it is reasonable to postulate similar mechanisms within any one of the groups. A mechanism was postulated by Guharay and Sachs (1984) for SACat channels in chick skeletal muscle (see Howard et al., 1988 for a dissenting view), but relatively little data is available to test or confirm the model.

The SAK channels in neuron somas examined here displayed a reproducible activation in response to negative or positive pressure. The general features of this response were so consistent between different patches from different cells that I feel there is no question that these channels can transduce membrane tension when measured as single-channel current using the patch clamp technique. However, quantification of channel stretch-sensitivity and channel gating characteristics were compromised by two main factors: 1) heterogeneity of "threshold" pressure between patches (Fig. 30); and 2) all patches contained multiple and unknown number of SAK channels.

Heterogeneity of threshold pressure may be a result of membrane slack, which must be first reduced before the channels begin to "feel" increases in membrane tension. By adding a offset pressure (P_{off}) term to equation 5.2,

$$P_o = 1/(1 + K_0 \exp(-\theta (P - P_{off})^2)) \qquad (5.3)$$

Sachs (1988) was better able to fit his average current (equivalent to P_o) *vs* pressure curves. When equation 5.3 was fitted to the neuron data in Fig. 30, the estimated P_{off} ranged from 1 to 5 cmHg which correlated with the pressure needed to reach "threshold" in each patch (Interestingly, addition of the P_{off} term did not significantly improve the fit of equations 5.1 or 5.2 to the P_o data as based on the AIC test). Perhaps a more unpleasant explanation of "threshold" heterogeneity, is that the pressure-squared relation does not hold for channels in some of the patches examined. It was possible to fit some of the neuron data to a pressure-cubed relation, although the fit was statistically poorer than for the pressure-squared fit. Higher order relations imply complex underlying processes, ones which could not be accounted for by a Hooke's Law spring. At present, the membrane slack explanation is the simplest and the most testable hypothesis.

In a more general sense, the "threshold" heterogeneity problem is founded on the unknown geometry of the membrane patch, which is presently assumed to be a hemispherical structure (Guharay and Sachs, 1984). At small pipette pressures, membrane tension and pressure may not be closely related. Other factors such as capillary forces, adhesion between the membrane and glass, drift in the manipulator or intracellularly generated forces may generate membrane tensions which exceed those at small pipette pressures. Conversely, such effects could potentially relieve the tension created by small pressure changes. This could explain the non-uniform changes in channel P_o seen at low pressures in the inset in Fig. 30 and highlights the difficulty in knowing the true magnitude of the stimulus.

Given this uncertainty, the mean stretch-sensitivity (Θ) for the neuron SAK channels is quite similar to Θ determined for SACat channels in skeletal muscle (0.66 $cm^{-2}Hg$, Guharay and Sachs, 1985a) and lens epithelium (0.51 $cm^{-2}Hg$, Cooper et al., 1986). The reason for the wide range of Θ's found for heart SAK channels is not clear. It was also apparent that SAK channels (within the physiological voltage range) are quite voltage-insensitive requiring 143 mV to change P_o e-fold. In general, SA channels tend to be either voltage-independent or show low voltage-sensitivity, with activation increasing upon depolarization (Morris, 1989). An exception is the SAK channel found in the basolateral membranes of kidney cells which increase P_o upon hyperpolarization (Sackin and Palmer, 1987).

Given the difficulty in knowing what the true membrane tension is, P_o was the best measure available for use in detecting changes in time constants of dwell time distributions. P_o (a dependent variable) is determined by the underlying rate constants which are indirectly measured by the average dwell times. (For a 2-state diagram, $P_o = k_{21}/k_{21} + k_{12}$ and $\tau_O = 1/k_{21}$; Colquhoun and Hawkes, 1981, 1983.) Therefore the measured changes in P_o are the result of changes in the underlying rate constants, some of which in turn depend (by definition of a stretch-activated channel) on the membrane tension. Simply put, if P_o changes, then a rate constant must have changed. If P_o is clearly correlated with pressure (at least at higher pressures) then comparable changes should have occurred in the same rate constant.

Table 6 shows that there is little relation between the degree of increase in SAK channel activity (ratio between P_o at 0 mmHg and the largest P_o examined for a particular patch) and the change in burst

durations and open times. Although τ_{O2} did increase as pressure increased, the change was slight, but perhaps sufficient to account for the increase in burst duration. SACat channels have a pressure-insensitive open time (Guharay and Sachs, 1984), but a SAK channel in fish embryos showed an apparent increase (see Morris, 1989) in burst duration as function of pressure (Medina and Bregestovski, 1988)

Table 6 does show that τ_{C4} and τ_{IB} are closely related to SAK channel P_o; i.e. the larger the increase in pressure and corresponding increase in P_o, the greater the decrease in τ_{C4} and τ_{IB}. This is comparable with the kinetic changes found in *Lymnaea* heart cells (Sigurdson et al., 1987; Chapter 2) and the SACat channels described in chick skeletal muscle (Guharay and Sachs, 1984). In these examples, both channels had at least 3 closed states with the longest mean dwell time stretch-dependent. If a linear reaction scheme is assumed, then the transition rate for leaving the long state is the only rate significantly stretch-dependent, which is what Guharay and Sachs (1984) had determined after directly determining the rates. Because all patches had multiple and unknown numbers of channels, the change in τ_{C4} provides, at best, a measure of the underlying transition rate change. It is reassuring, however, that the results from *Lymnaea* heart cells (Sigurdson et al., 1987), neuron somas and growth cones (Sigurdson and Morris, 1989), chick skeletal muscle (Guharay and Sachs, 1984) and fish embryos (Medina and Bregestovski, 1988) all show the same phenomena of a long closed interval decreasing in response to membrane tension. This implies the possibility of a common mechano-transducing mechanism among SA channels.

Confirmation of the Sachs' pressure-squared transduction model is still lacking. What is needed is an experimental preparation in which membrane tension can be accurately measured. The correspondence between *Lymnaea* heart and neuron SAK channels in ion selectivity and kinetics, leads me to believe that the failure to select the pressure-squared dependence model partially stems from our ignorance of the true membrane tension rather than any fundamental difference between transduction mechanisms. The ease in which models 1 and 2 could be fit to the data from neuron and heart cells, also points to the poor discriminatory power of this sort of experiment. If proteins, at the molecular level, indeed act like macroscopic Hooke's Law springs, the Sachs model must apply. The larger problem then becomes one of characterizing the mechanical properties of SA channels and identifying any associated cytoskeletal proteins.

Chapter 6: Stretch-activated ion channels in growth cones of snail neurons

Introduction

The idea that cells which are not specialized mechano-sensors should possess stretch-sensitive ion channels still seems novel, but following the first observation of such channels in skeletal muscle (Guharay and Sachs, 1984), similar channels have been described in cells as diverse as bacteria, yeast, plant protoplasts, lens epithelium, smooth muscle, endothelial cells, (reviewed by Kullberg, 1987; Sachs, 1988) and teleost embryos (Medina and Bregestovski, 1988).

Here I report that molluscan neurons contain stretch-activated channels. These channels occurred in the cell body, but more interestingly yet, in the mechanically-active part of the cell, the growth cone. They were ubiquitous rather than confined to identified neurons. Isolated in culture, *Lymnaea* neurons actively put out new processes with growth cones which, like those in other gastropod neurons (Siegelbaum et al., 1986) are large enough for single channel recording.

Neurite elongation and cell locomotion are related processes, probably using the common underlying mechanisms of exocytosis and actin-myosin contractions (Lackie, 1986; Bray, 1987; Kater et al., 1988). Models of these processes, therefore, require that Ca^{2+} concentrations be controlled within narrow limits (Kater et al., 1988). Snail neurons have been instrumental in showing how neurotransmitters and electrical activity, through indirect effects on intracellular Ca^{2+}, control growth cone motility. Given the strong precedent for regulation of neuronal Ca^{2+} levels by K^+ channels (Siegelbaum et al., 1986), stretch-activated channels that are K^+ selective would naturally be of special interest in growth cones. Growth cone

motility, by definition, is a mechanical process, so that neurite membranes should experience tension changes during growth. Stretch-sensitive channels in growth cones could provide a link between this membrane tension and - via membrane voltage - transmembrane Ca^{2+} fluxes.

Preliminary communications describing stretch-activated channels in snail neurons (Sigurdson et al., 1987b; Bedard et al., 1988) and in neuroblastoma (Falke and Misler, 1988; Falke and Misler, 1989) have appeared.

Materials and Methods

Lymnaea stagnalis were collected locally or purchased from Blades Biological, Edenbridge, England. Sterile isotonic normal saline (NS) (50 mM NaCl, 1.6 mM KCl, 3.5 mM $CaCl_2$, 2.0 mM $MgCl_2$, 5 mM HEPES, 5 mM glucose, pH 7.6, adjusted with NaOH) supplemented with penicillin (500 I.U. ml^{-1}) and streptomycin (500 μg ml^{-1}) was used as the culture medium. Pipette solutions were either antibiotic-free NS or 50 mM KCl saline (50 mM KCl, 1 mM $CaCl_2$, 5 mM HEPES, pH 7.6). A low Ca^{2+} saline (buffered to 10^{-8} M Ca^{2+}; 60 mM KCl, 2 mM $MgCl_2$, 0.2 mM $CaCl_2$, 2.2 mM EGTA, 5 mM HEPES, pH 7.6) was used to perfuse inside-out patches in some experiments. Neurons from the circumoesophageal ganglia were isolated by first loosening the connective tissue sheath in 0.25% protease (Sigma) (40 min agitation) followed by mechanical dispersion. Neurons from individual ganglionic masses were then dispersed directly onto coverslips (recording chamber bottoms). Chambers were detergent-washed, rinsed thoroughly with distilled water, surface sterilized with 70% ethanol and then dried in a 60° C oven for at least 2 hours before use. Cell adhesion and spreading on the

glass substratum was generally good provided the amount of cellular debris was minimized during dispersal.

Standard single-channel recording techniques were employed (Hamill et al., 1981) to record from the neuron cell membrane. Patch electrodes were pulled (Kopf 750 pipette puller) from Corning 7052 capillary tubes (Garner Glass Co, Claremont, CA ID=0.8 mm, OD=1.65 mm), fire-polished and filled with NS, with NS plus 1 mM quinidine (Sigma) or 50 mM KCl saline. Pipette tip openings were estimated to be a maximum of 2 μm in diameter prior to fire-polishing and had a mean bubble number of 4 $\pm$ 0.6, n=5 (Corey and Stevens, 1983). Suction applied to the patch pipette through the sidearm of the electrode holder was monitored by a Bio-Tek pressure transducer (Bio-Tek Instruments, Burlington, VT).

Single-channel currents were recorded using a patch clamp amplifier (Axon Instruments, Burlingame, CA), filtered at 10 kHz and stored on video tape using a PCM-1 (Medical Systems, Greenvale, NY) digitizing unit. For analysis of current amplitudes, data were filtered at 1 or 2 kHz, displayed on a digital storage oscilloscope and the amplitudes of at least 10 individual events directly measured from the display. For analysis of open probabilities (P_o) and for mean open and closed times, data were filtered at 2 kHz and digitized at 0.1 msec point^{-1} (five times the filter cutoff frequency). An event-detection program run on a DEC 11/23 computer produced an idealized record of the open and closed times thus allowing determination of the proportion of time the channels spent open. When intense channel activity precluded accurate event detection, an index of P_o was determined by integrating the current record over a known time interval and dividing by the single channel current. The true number (n) of channels in the patch

is unknown, hence, in both approaches, P_o is reported as (Sigurdson et al., 1987a):

$$\text{Index } P_o = N_1P_1 + N_2P_2 + \ldots + N_nP_n$$

where N_i is the number of channels simultaneously open and P_i the proportion of time spent with N_i channels open. Dividing index P_o by n, were it known, would give P_o, the open probability for a single channel.

Curve-fitting procedures used to determine time constants associated with the open and closed times have been described previously (Sigurdson et al., 1987a).

For current/voltage (I/V) relations of cell-attached patches, the membrane voltage (V_m) was taken to be:

$$V_m = V_{rest} - V_p$$

where V_p is the pipette holding potential and V_{rest} the assumed resting potential of the cell. V_{rest}, obtained from intracellular measurements, was -50 mV $\pm$ 1.9mV (SEM, n=32).

Photomicrographs were made using an Olympus IMT-2 inverted microscope employing phase contrast or Nomarski differential interference contrast (DIC) optics. Cells were cultured and all recordings made at room temperature (18-23° C).

Results

Rearborization of the isolated neurons

Isolation disrupted the *in vivo* structure of neurons. Freshly dissociated, neurons consisted only of a cell body, sometimes bearing a short axon stump (Fig. 47a,b). For my purposes, this was advantageous, because the subsequent rearborization provided an opportunity to record from

membrane which, I could assume, was newly-elaborated. To illustrate some of the dynamics of regrowth of isolated *Lymnaea* neurons under the minimal culture conditions used (see Kater and Mattson, 1988), Fig. 47b-g follows a cell for 68 hr post-dissociation. The axon remnant (Fig. 47b) became the first attachment site 20 min after isolation. In the next hour a lamella appeared (Fig. 47c), then spread extensively. The cell became firmly attached (Fig. 47d, 21.5 hr), as indicated by its stability during jarring movements of the culture dish. Over the same period, small neurites with microspikes began to extend from the opposite side of the soma (Fig. 47d). One of these neurites rapidly broadened into a growth cone (Fig. 47e, 24 hr) which extended for ~70 μm before retracting (not shown). By 46 hr another neurite had formed and produced a much larger growth cone (Fig. 47f) which continued to elongate and branch (Fig. 47g, 68 hr). Meanwhile the neurite (Fig. 47e) which had retracted, re-extended. Throughout the neuron's regrowth process, the large lamella established from the axon remnant was relatively stable, with major neurite and growth cone formation occurring on the opposite side of the soma.

Most, but not all isolated cells attached and began spreading within minutes; Fig. 48a shows two cells five days in culture, one which merely persisted, another which rearborized. The gamut of rearborization patterns was wide. At one extreme (Fig. 48b,c), cell bodies had multiple neurites with sub-branches. Some cells were dominated by two long neurites (Fig. 48d,e), whereas others were essentially monopolar (Fig. 48f). As the figures show, neurites were terminated by growth cones from which extended microspikes (Fig. 48b,e) and/or lamellae (Fig. 48b,f). Recordings were made from cell bodies and growth cones in neurons of all morphological types.

Figure 47. Time course of neurite growth. **a)** Freshly isolated unidentified *Lymnaea* neurons. DIC optics; scale bar = 106 μm. **b-g,** Neurite development of one cell from isolation until day 3. **b)** 20 min. **c)** 1 hr. **d)** 21.5 hr. **e)** 24 hr. **f)** 45.5 hr. **g,** 68 hr. Phase contrast optics; scale bar, 54 μm.

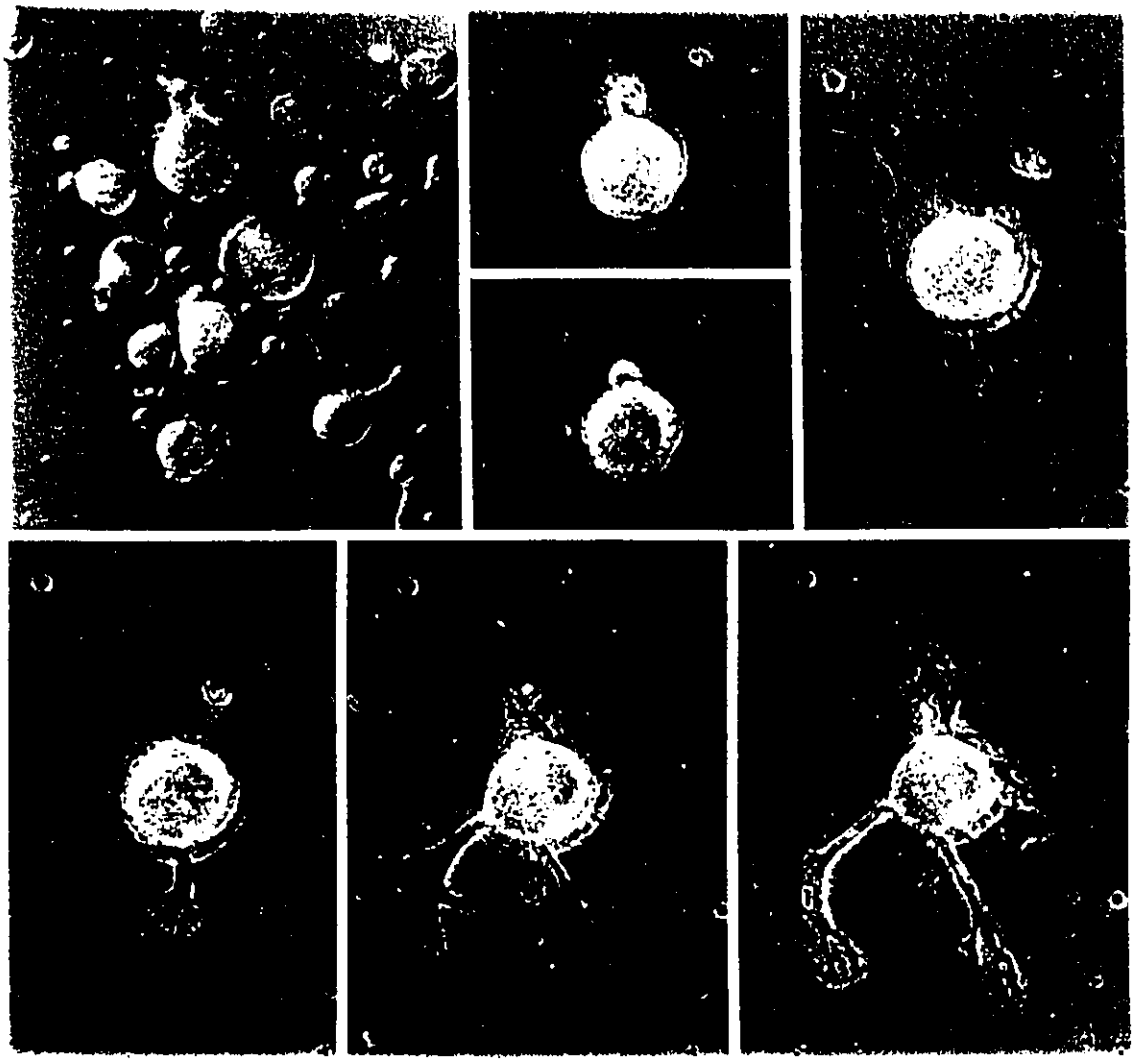

Figure 48. *Lymnaea* neurons several days in culture. **a)** Neurons 5 days after isolation. Note patch pipette (arrowhead) located on a process close to the cell body. SAK channels were observed during recordings made at this point. **b)** Patch pipette on growth cone from the cell in **c**. Recordings from this patch exhibited SAK channels. **c)** Day 3 cell with numerous neurites terminated by growth cones with lamellae and microspikes. Arrowhead marks the location of the patch pipette pictured in **b**. **d)** A very long (>720 μm) day 3 neuron. Patch recordings from the growth cone (lower part of plate) and the cell body both showed SAK channels (see Fig. 49). **e** Higher magnification view of the patched growth cone (with numerous microspikes) in **d**. Patch location indicated by arrowhead. **f** Day 5 neurons showing extensive neurite development with overlapping of processes. As in other cells, growth cones are well-developed, many contain large veil areas with protruding microspikes. DIC optics for **a**, **c**, **d**, **e**; Phase contrast optics for **b**, **f**. Scale bar for **a**, **b**, **c**, **f**, 54 μm; for **d**, 208 μm; for **e**, 36 μm.

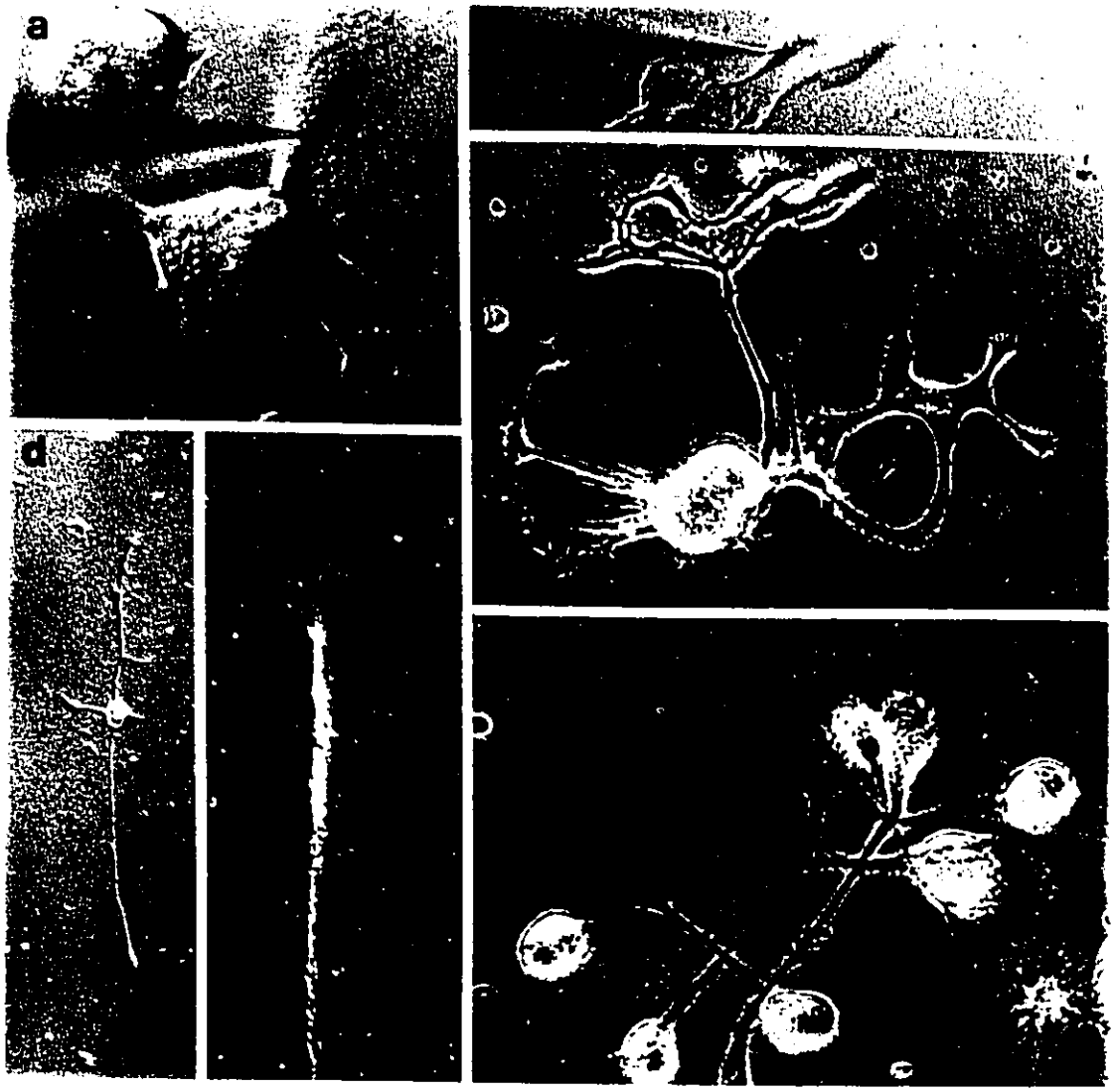
a
d

Stretch-activated K^+ (SAK) channel distribution

Stretch-activation of the (SAK) channel was observed in cell-attached and excised (inside-out) patches. Except where specifically noted data were obtained from cell-attached patches using pipettes containing antibiotic-free NS.

SAK channels were ubiquitous. They were observed in each of 6 freshly-isolated neurons tested at 0.3-2.0 hr post-dissociation as well as in the cell bodies of all older neurons tested. They were observed in broad dilations near the cell body (Fig. 48a) in older, spread-out cells. They were observed in regions of extensive neurite and growth cone formation (Fig. 48b,c). Fig. 48d shows an actively advancing growth cone approximately 370 μm from the cell body; SAK channels were recorded from both the cell body and growth cone of this cell (Fig. 49a,b). This growth cone (Fig. 48e) and that in Fig. 48b,c approach the minimum size from which single-channel recordings were successfully made. Patch recordings were not made on lamellae or microspikes, but note that growth cone recordings were obtained only a few micrometers from these structures (see Fig. 48b,c,e) where the cell thickens slightly.

Figure 49. Stretch increases the open probability of SAK channels from the cell body and growth cone. **a)** Cell body and **b)** growth cone of the neuron pictured in Fig. 48d. Bars indicate suction of ~-50 to -70 mm Hg, which was submaximal for this patch. V_m = 70 mV for both patches.

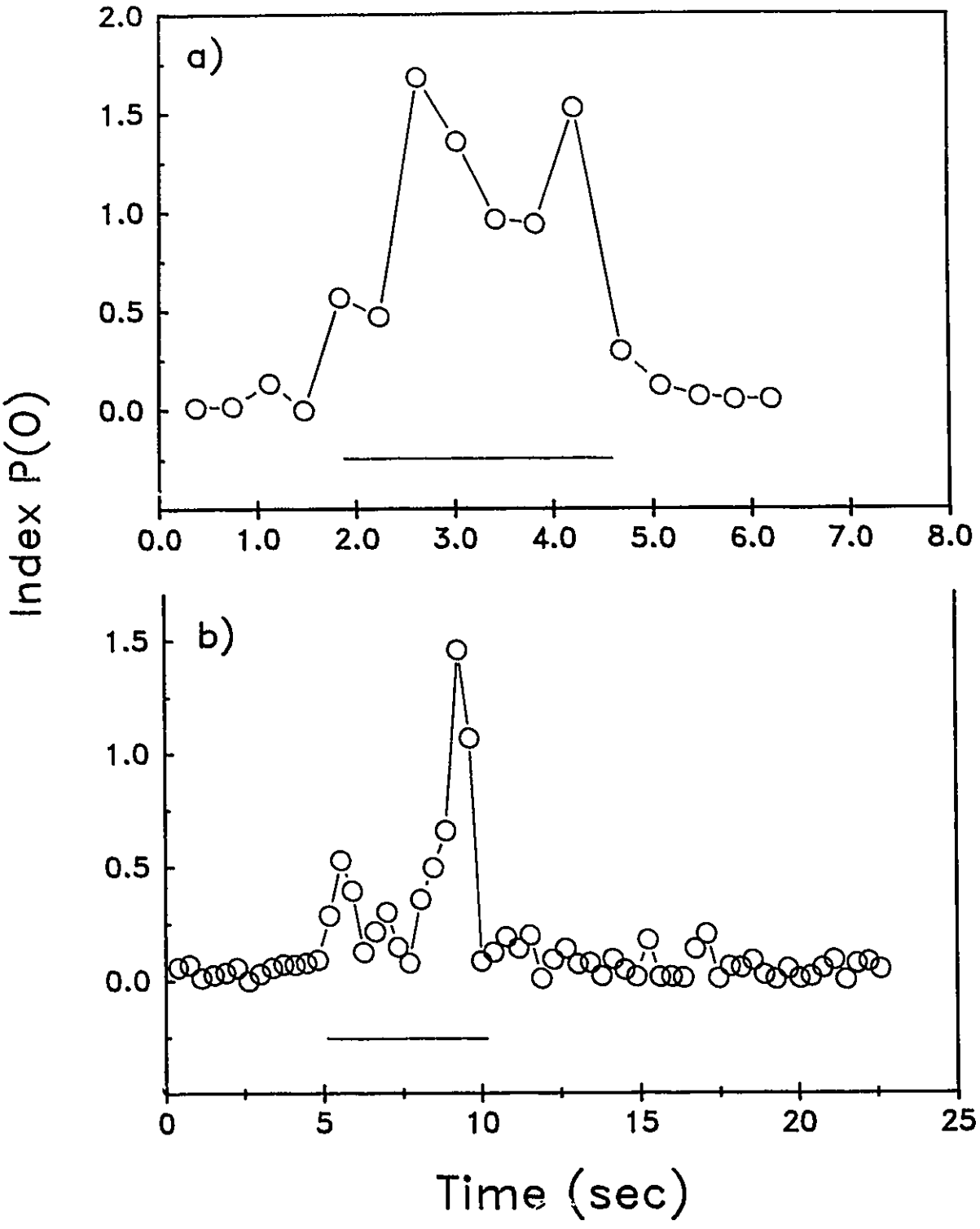
a)
b)
Index P(O)
Time (sec)
2.0
1.5
1.0
0.5
0.0
0.0
1.0
2.0
3.0
4.0
5.0
6.0
7.0
8.0
0
5
10
15
20
25

Growth cone SAK channel stretch-sensitivity

SAK channel openings generally occurred in bursts as illustrated in the lower trace of Fig. 50. A typical response to suction is demonstrated in the upper trace, where, on this time scale, individual channel openings (outward current) appear as spikes. During suction, with the increased membrane tension, the rate of opening and the probability of multiple open channels (up to three channels in this case) increased. Upon release, activity subsided to the pre-suction level. Other channels recorded from the growth cones displayed no stretch-activation under the range of recording conditions (i.e. pressure and voltage excursions and various salines) described here. We have, however, recently observed a low conductance K^+ channel inactivated by stretch (Morris and Sigurdson, 1989); it occurs in growth cones as well as cell bodies.

The lower trace of Fig. 50 contains several low conductance events that appear as small outward current shifts from the baseline. Such events were routinely excluded from the quantitative analyses described below.

Fig. 51a shows single-channel recordings with no applied suction, as well as suction sufficient to begin activating the channels. Such data were used to construct the curve shown in Fig. 51b. The open probability increased steeply beyond a "threshold" pressure. Thresholds in the range ~-50 to -100 mm Hg were observed for various patches. Usually P_o curves are expected to saturate at higher pressures when all channels are recruited (see Sigurdson et al., 1987b), but in the example shown in Fig. 51b, the membrane ruptured at -140 mm Hg. The index P_o at this highest experimental pressure is a reflection of the average channel activity seen over a period of about 15 sec, but is deceptively low as an indicator of the

number of SAK channels present. As many as eight channels (as opposed to the average of 1.8) were open simultaneously at some points indicating that at least 8 channels must have been present in this patch. In general, patches from growth cones had similar SAK channel density to those from cell bodies (~4-8 patch^{-1}; corresponding to a density of ~1-2 μm^{-2} (see Guharay and Sachs, 1984; Sigurdson et al., 1987a).

The SAK channel of *Lymnaea* heart cells is insensitive to intracellular Ca^{2+} (Sigurdson et al., 1987a), as is the neuronal cell body SAK channel (Sigurdson and Morris unpublished observation). Ca^{2+} insensitivity of growth cone SAK channels was confirmed using inside-out patches (50 mM KCl saline in pipette) which contained both Ca^{2+}-activated K^+ channels (Lux et al., 1981) and SAK channels. When these patches were perfused with a low Ca^{2+} solution (not shown) which silenced the Ca^{2+}-activated K^+ channels, the SAK channels remained activatable by suction.

Figure 50. Recordings of SAK channel activity. Upper trace, suction (bar, ~-70 mm Hg) produces simultaneous activation of up to 3 channels. C indicates the zero current (all channels closed) baseline, O_1-O_3 indicate successive open levels. Lower trace, higher resolution recording showing the bursty nature of SAK channel openings. Upper trace filtered at 1 kHz; V_m = 30 mV; scale 5 pA and 2.5 sec. Lower trace, 2 kHz; V_m = 70 mV; scale 5 pA and 50 msec.

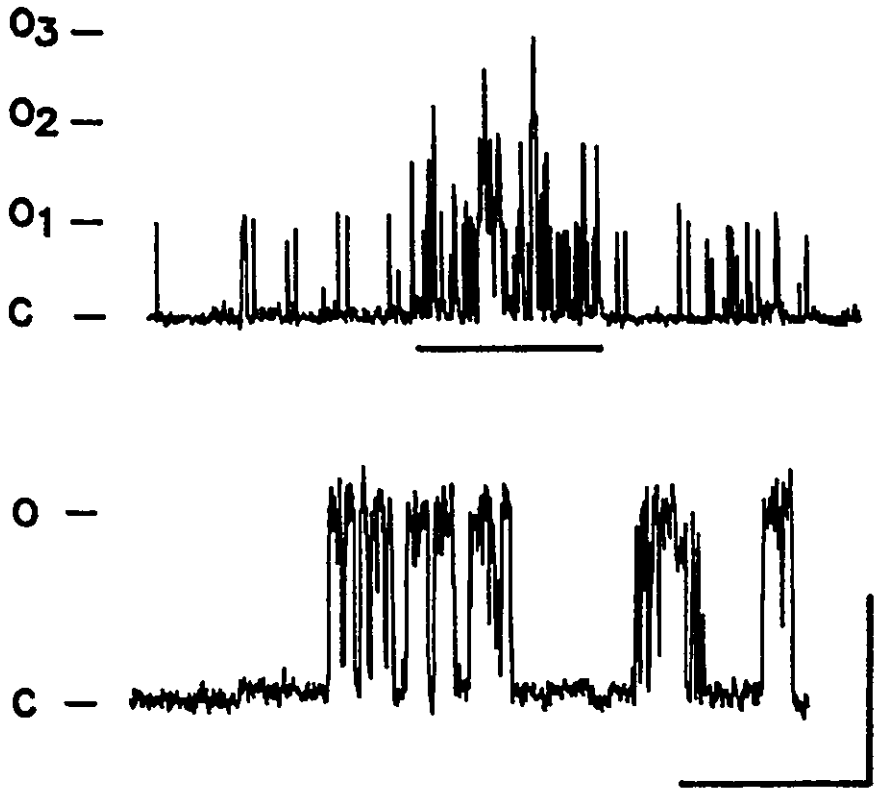
O3
O2
O1
C
O
C

Figure 51. Effect of pressure on SAK channel activity. **a)** Recordings at indicated suction (mmHg) applied by the pressure transducer. Note that channel open probability appears to increase by a reduction of closed intervals, yielding more openings per unit time. V_m = 70 mV. Scale, 5 pA and 50 msec. **b)** Open probability data for the same patch shown in **a.**

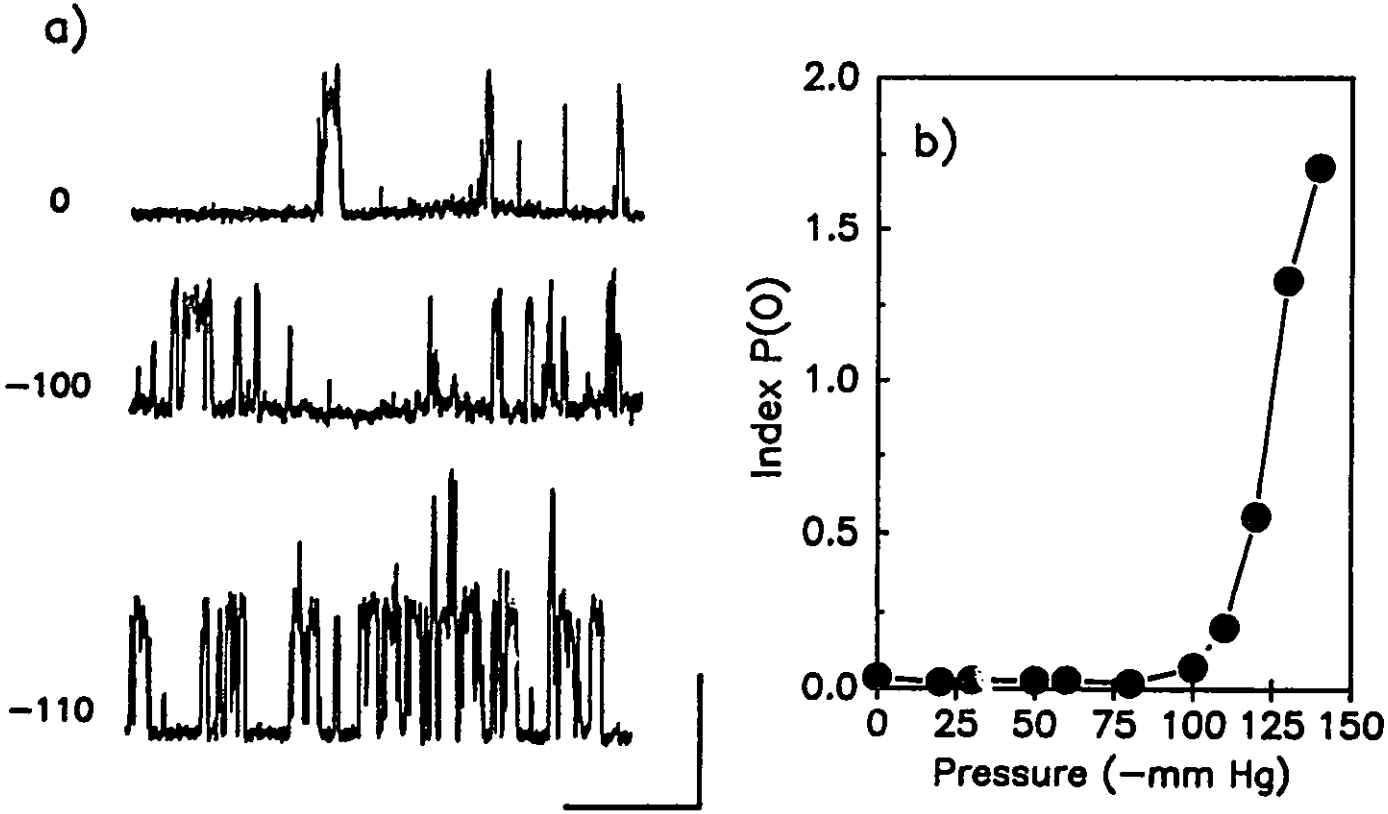
a)
0
−100
−110
b)
2.0
1.5
1.0
0.5
0.0
Index P(O)
0
25
50
75
100
125
150
Pressure (−mm Hg)

More detailed kinetic analysis of the recordings used to generate Fig. 51b was possible for 0, -100, -110 and -120 mm Hg. This allowed us to ask which of the kinetic parameters contributes to the stretch-induced increase in P_o. At all pressures, open time distributions were best fit to a sum of two exponentials (Fig. 52), while closed times (histogram not shown) were best fit to a sum of three exponentials (see Table 7). The number of open and closed times and the values of their constants (mean dwell times) are in good accord with those reported for *Lymnaea* heart SAK channels (Sigurdson et al., 1987a). In principle, increased open times and/or decreased closed times could be responsible for increased P_o. A pronounced effect of increasing tension is the progressive decrease of the longest closed time. This coincides with what has been observed for other stretch-sensitive channels, where a between-bursts closed time is most affected by stretch (Guharay and Sachs, 1984; Sigurdson et al., 1987a).

Figure 52. Open time histogram of growth cone SAK channels. Superimposed on the histogram (for -100 mm Hg) are best fit curves for a sum of 2 exponentials to the 0 mm Hg data (solid line; histogram not shown; total number of events was 788) and to the -100 mm Hg data (dashed line; total number of events was 1168). Error bounds for the indicated open time constants are given in Table 7.

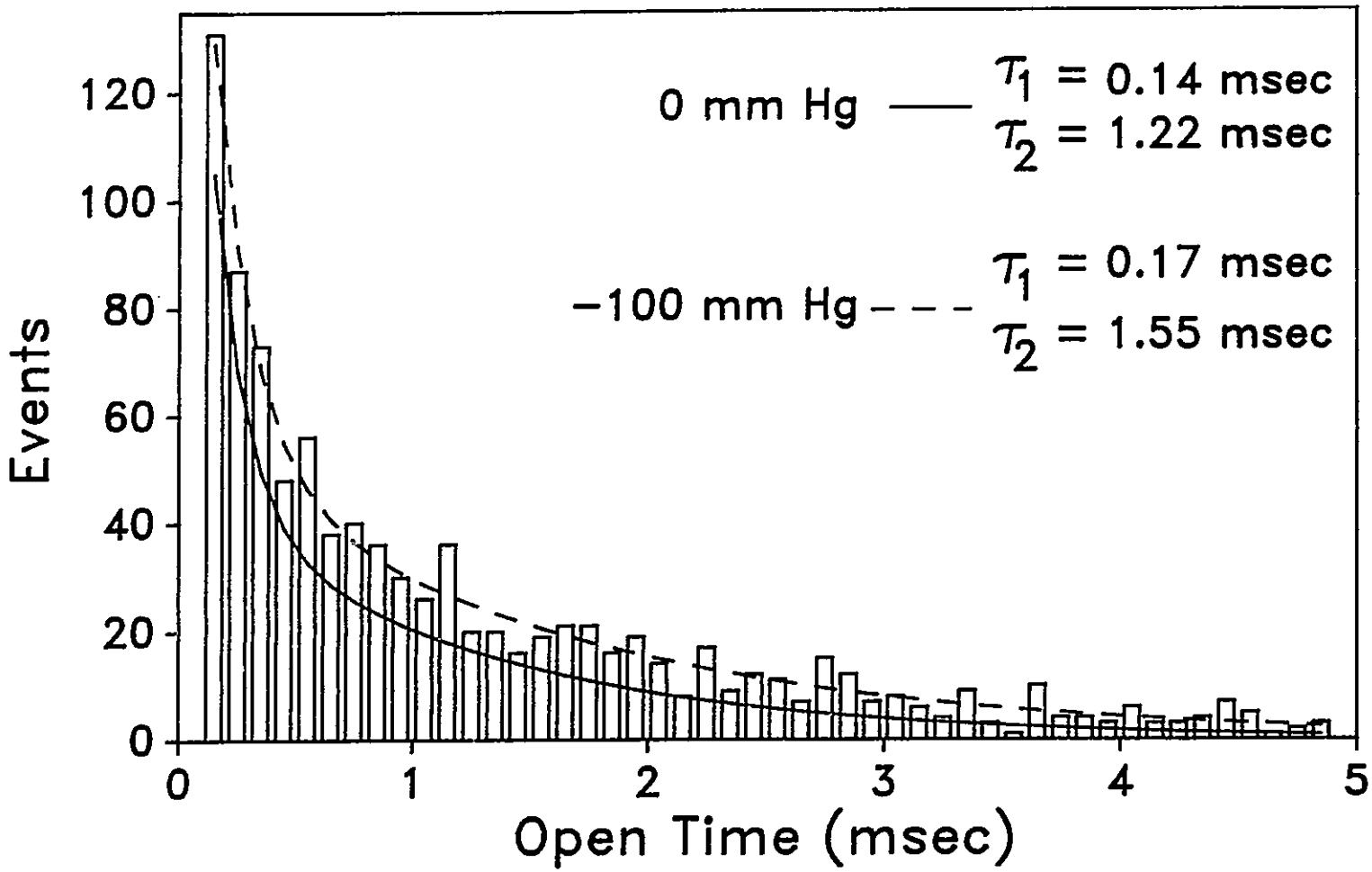
0 mm Hg
τ_1 = 0.14 msec
τ_2 = 1.22 msec
−100 mm Hg
τ_1 = 0.17 msec
τ_2 = 1.55 msec
Events
120
100
80
60
40
20
0
0
1
2
3
4
5
Open Time (msec)

Table 7. Kinetic analysis of growth cone SAK channels[a]

Pressure (mm Hg)	Index P_o	Open times τ_1 (msec)	Open times τ_2 (msec)	Closed times[b] τ_1 (msec)	Closed times[b] τ_2 (msec)	Closed times[b] τ_3 (msec)
0	0.038	0.14±0.03	1.22±0.12	0.3±0.05	1.29±0.32	57.2±8.5 (57.9)
-100	0.073	0.17±0.02	1.55±0.09	0.18±0.02	1.46±0.12	37.2±4.5 (40.6)
-110	0.203	-	-	-	-	(20.0)
-120	0.555	-	-	-	-	(6.8)

[a] Same patch as used for Fig. 50. N.B. Ratios of P_os relative to 0 mm Hg are 1.92, 5.34 and 14.5 for -100, -110 and -120 mm Hg respectively.

[b] Beyond -100 mm Hg the records contained too many multiple openings for generating the histograms needed for curve fitting. Instead, an approximation to τ_3 was obtained by averaging the closed (zero current) intervals greater than 2 msec and subtracting this cutoff time from the average (equation 50 in Colquhoun and Sigworth, 1983). Note that when both approaches are used where P_o is low (0 and 100 mm Hg), the estimated average (given in brackets) falls within the error bounds of the values obtained by fitting.

SAK I/V relations

I/V relations of the stretch-sensitive channel in growth cones were determined under near-physiological ionic conditions (cell-attached, NS in pipette and bath) as well as with high K^+ saline (Fig. 53). For each voltage, suction was applied to activate the channels and thus unambiguously distinguish the SAK channels from stretch-insensitive channels. With NS in the pipette, the zero current potential for stretch-activated currents was near the resting potential of the cell. With 50 mM KCl saline in the pipette, the zero current potential shifted approximately 50 mV to the right, a shift that would be in accord with the altered K^+ equilibrium potential. As expected for a K^+ selective channel, when excised patches were exposed to symmetrical NS and suction was applied, no channel activity was observed. Conversely, excised patches exposed to 50 mM KCl in the pipette with NS in the bath (symmetrical Cl^-, asymmetrical K^+ and Na^+) demonstrated stretch activated inward current, but not outward current. This is consistent with a channel permeable to K^+ and not to Na^+ or Cl^-. Non-linearities in single K^+ channel I/V relations, such as those seen in Fig. 53 (except for the nonlinearity at the foot of the NS curve, which is predicted by electrodiffusion for a K^+ channel under asymmetric K^+), can generally be attributed to effects of voltage on ion permeation through a multi-ion channel (Yellen, 1987; Yellen, 1984a) and to apparent attenuation produced by high frequency flickering at large polarization (Yellen, 1984b).

Figure 53. I/V relations for growth cone SAK channels. Triangles, NS in pipette; circles, 50 mM KCl saline in pipette. Each curve (lines fit by eye) incorporates data from 4 patches; error bars are standard errors and where not shown are contained within the symbols. The steepest portions of the NS and 50 mM KCl curves correspond to slope conductances of 44 pS and 80 pS respectively.

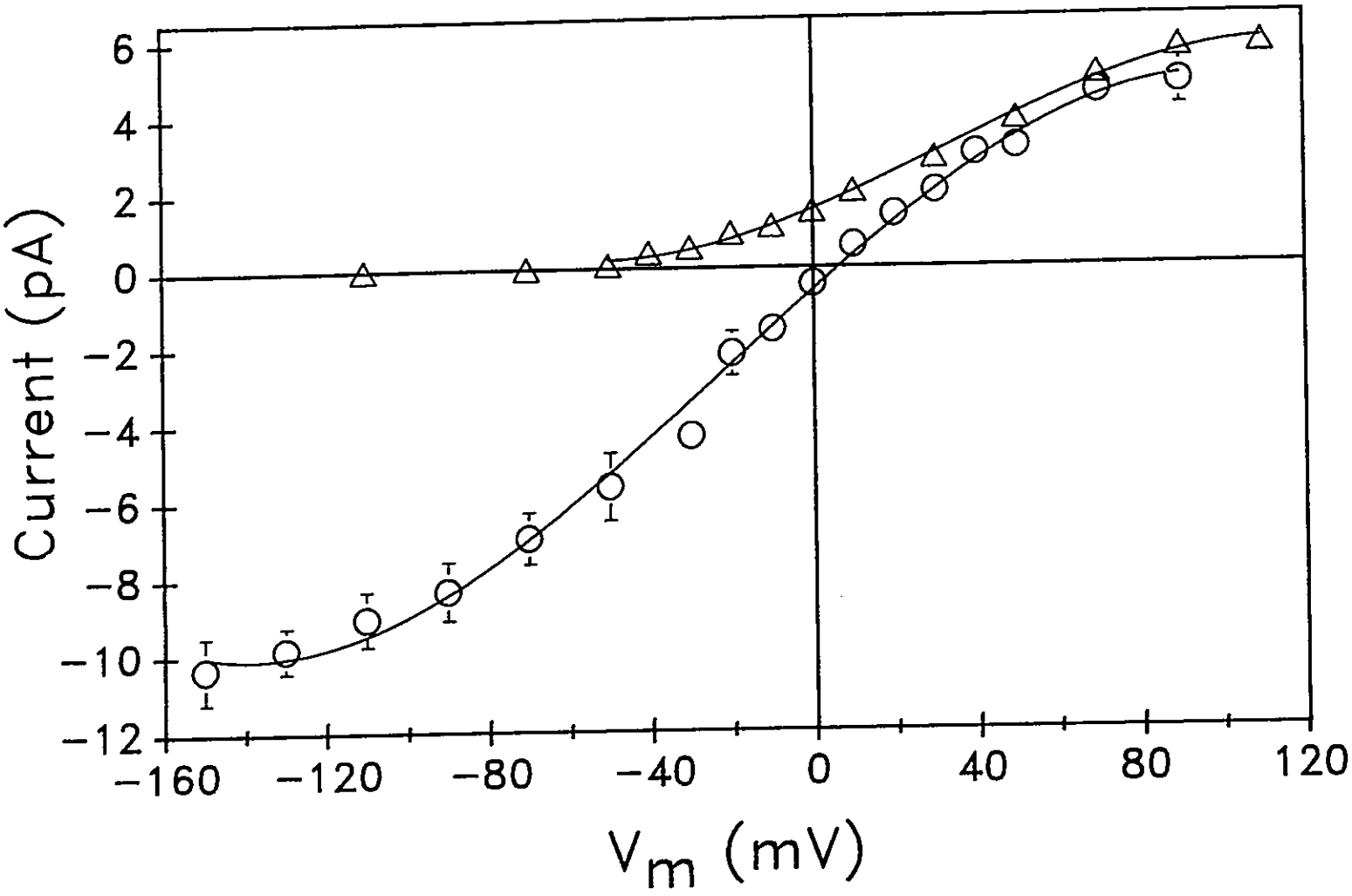
Current (pA)
6
4
2
0
−2
−4
−6
−8
−10
−12
−160
−120
−80
−40
0
40
80
120
V_m (mV)

Quinidine blocks SAK channels

The K^+ channel blocker, quinidine, blocks cell body SAK channels in a dose-dependent manner (Sigurdson et al., 1987b); 1 mM produces a flickery block (Yellen, 1984b), or in some cases, a full block of SAK channel currents. For growth cone SAK channels, this concentration of quinidine induced flickery block in 3 of 4 patches. The fourth patch was silent.

Discussion

It has been demonstrated that growing neurites, like fibroblastic cells, experience varying degrees of tension associated with their motility (Bray, 1987; Letourneau et al., 1987; Dembo and Harris, 1981). Accordingly, some models of neurite elongation and neurogenesis incorporate tension as a regulatory element (Bray, 1984; Gordon and Brodland, 1987; Letourneau et al, 1987; Bray and White, 1988; though see Goldberg and Burmeister, 1986, 1988). The model of growth cone generated tension influencing neurite elongation appears to have been confirmed (Lamoureux et al., 1989). Yet in spite of the clearly mechanical nature of neurite motility, no mechanism has been identified by which tension could be sensed. Stretch-activated channels would seem to be ideally suited for this role.

Although the mechanism by which stretch-sensitive channels transduce membrane tension is still speculative, there is evidence that the channels are tied into the underlying cortical cytoskeleton. In particular, Guharay and Sachs (1984) showed that cytochalasin increased the stretch-sensitivity of SA channels in skeletal muscle. Their interpretation (Sachs, 1988) was that normally, actin filaments relieve tension on the membrane cytoskeletal elements which directly apply tension to the channels. These unknown

elements may involve spectrin/ankyrin; the density of Na^+ channels and glutamate receptors has recently been shown to be controlled by anchorage to these proteins (Siman et al., 1985; Srinivasan et al., 1988). For stretch-activated channels, one could envisage that such connections were specialized to render the channels sensitive to membrane tension.

A question that was addressed by recording from growth cones was whether newly-incorporated membrane would contain stretch-sensitive channels. If the channel's tension sensing elements were not in place, then even if the channel were present, stretch would not activate it. Incorporation of plasmalemma by exocytosis is believed to take place in the main body of the growth cone (Tosney and Wessells, 1983; Goldberg and Burmeister, 1986). Since SAK channels were found in all growth cones examined, the simplest conclusion is that newly-incorporated membrane contains the channel and its tension-sensing element(s) as an already-functional unit, or at least in a state which allows rapid acquisition of full function.

If SAK channels play a role in regulation of neurite extension, the membrane tensions exerted during growth cone movement should match the range of tensions required for activation. Traction forces produced by fibroblast locomotion can exceed 10^{-3} dyn μm^{-1} (Harris et al., 1980), while forces needed to move particles over the cell surface are much smaller (10^{-8} dyn μm^{-1}; Dembo and Harris, 1981). The experimental tensions applied to the growth cone membrane in this study fall within this range (6.7×10^{-4} dyn μm^{-1} for -100 mm Hg in a typical patch, based on the calculations of Guharay and Sachs, 1984), but it is not yet possible to relate this tension to traction and/or other forces experienced by growth cones. Evidence that physiologically-relevant tensions affect stretch-sensi-

tive channels comes from a recent report on teleost embryos (Medina and Bregestovski, 1988), in which tensions generated during cytokinesis activate SAK channels.

The potential role of any channel is constrained by its ion-selectivity; K^+ channels typically hyperpolarize, whereas (non-selective) cation or Na^+ channels depolarize the membrane. The I/V relations show that the growth cone stretch-activated channel is essentially identical to that in the soma, namely, K^+ selective (Sigurdson et al., 1987b). Invertebrate (Zagotta et al., 1988) and vertebrate SAK channels have been identified (Sackin, 1987; Ding et al., 1988; Medina and Bregestovski, 1988; Sackin, 1989), but the most-studied vertebrate stretch-sensitive channel is a cation channel which allows K^+, Na^+ (Cooper et al., 1986; Sachs, 1987) and Ca^{2+} (Christensen, 1987; Kirber et al., 1988) to permeate. Activation of either class of channel could profoundly affect local intracellular Ca^{2+} concentrations (Lipscombe et al., 1988). The cation channels would act to increase Ca^{2+}, indirectly by depolarizing the membrane and directly by passing Ca^{2+} ions. Activation of K^+ channels, on the other hand, would stabilize the membrane potential near E_K, thereby decreasing influx of Ca^{2+} through its voltage-gated channels. Motile growth cones in *Helisoma* have recently been shown to have higher free Ca^{2+} levels than those which have stopped growing (Cohan et al., 1987). This Ca^{2+}-driven motility could employ tension-sensitive K^+ channels as a negative feedback mechanism.

In a recent summary scheme of "known and suspected pathways of Ca^{2+} regulation in the growth cone", Kater et al. (1988) feature a variety of ion channels. SA channels can probably now be added to this scheme under the heading "suspected". Much of the work which lead to the

present picture of Ca^{2+} regulation was done on *Helisoma*, a snail of the same suborder (Basommatophora) as *Lymnaea*. Since SAK channels also occur in neurons of a more distantly-related gastropod (*Cepaea nemoralis*, from the same family as *Helix* in the Suborder Stylommatophora) (Bedard et al., 1988), there is some justification in presuming that the stretch-activated channels are widely distributed in pulmonate snails. It would be surprising if they were not found in *Helisoma* neurons.

The presence of mechano-sensitive integral membrane proteins in the growth cone (see also Morris and Sigurdson, 1989) raises the possibility that additional (perhaps electrically-silent) proteins might likewise possess mechanotransduction machinery, giving them access to information about growth cone motility which could help them govern the pace and/or direction of neurite elongation.

Chapter 7: Stretch-inactivated ion channels coexist with stretch-activated ion channels

Introduction

Stretch-activated (SA) channels have been studied in diverse cell types including animal, plant, bacterial and fungal cells where the channels are implicated in mechanotransduction and osmoregulation (Guharay and Sachs, 1984; Sachs, 1986; Christensen, 1987; Falke et al., 1987; Gustin et al., 1987; Kullberg, 1987; Martinac et al., 1987; Sigurdson et al., 1987; Kirber et al., 1988; Sachs, 1988; Stockbridge and French, 1988). Although there are numerous examples of ion channels activated by mechanical means, this may not be the only form of mechanically induced gating possible. A new class of channel is described here; it is stretch-inactivated (SI). The channel occurs in neurons, where it coexists with SAK channels. The SI channel (or SIK channel) is K^+ selective and has a different stretch sensitivity than the SAK. This may have implications regarding control of membrane potential in response to membrane tension and the resulting effect on voltage-dependent channels.

Materials and Methods

Lymnaea stagnalis neurons were isolated from circumoesophageal ganglia (45 min in 0.25% protease), plated on glass coverslips, and used for up to 4 days post-dissociation. Cells were maintained in NS (50 mM NaCl, 1.6 mM KCl, 3.5 mM $CaCl_2$, 2 mM $MgCl_2$, 5 mM Hepes, pH 7.6) supplemented with 5 mM glucose, 50 i.u. ml^{-1} penicillin, and 50 μg ml^{-1} streptomycin. All recordings were made on cells bathed in this solution (exception noted in legend of Fig. 56) at room temperature. Patch clamp

recordings of single channel activity were made with standard cell-attached gigaseal techniques (Hamill et al., 1981); pipettes were made from Corning 7052 glass. Suction, applied through a port in the microelectrode holder, was measured and controlled with a Bio-tek transducer. Cell body membrane potentials are calculated on the assumption of V_{rest} = -50 mV (from intracellular recordings, V_{rest} = -51$\pm$1.9mV (SEM), n=32).

For kinetic analysis, data were filtered at 2.5 kHz and digitized at 20 kHz. Point by point amplitude histograms (Fig. 55) were constructed from data filtered at 1 kHz and sampled at 10 kHz. Open probabilities (P_o) were obtained from time- or current-averaged single-channel records filtered at 1 or 2.5 kHz and digitized at 10 or 20 kHz.

Results and Discussion

In snail neurons, under conditions used previously to study SAK channels (Sigurdson et al., 1987b; Sigurdson and Morris, 1989), some membrane patches were observed in which suction through the recording pipette not only activated the ubiquitous SA channels, but simultaneously inhibited a class of lower conductance, spontaneously-active channels (Fig. 54). In a single channel recording where SA channel activity was abolished by quinidine, spontaneous currents (multiples of ,1 pA) were evident in the absence of external membrane tension and were abolished by suction (Fig. 54a). By contrast, more typical patches of membrane did not exhibit

Figure 54. Currents inhibited and activated by membrane stretch coexist. a) Activity of SI channels in a cell body patch abolished by application of ,-40 mmHg. Normal saline (NS) plus 1 mM quinidine (Brezden et al., 1986) in pipette; membrane potential, V_m = +70 mV. b) SA channel activity stimulated by -40 mmHg. NS in pipette; V_m = +70 mV. Sustained responses in (A) and (B) were typical; note different amplitude calibration. c) SA channel (arrowhead) and SI channel activity in the same patch, -70 mmHg, NS in pipette, V_m= +70 mV. d) Higher resolution trace of SA channel and SI channel events from a growth cone, 0 mmHg, 50 mM K^+ in pipette, patch V_m = V_{rest} + 120 mV (the resting potential, V_{rest}, was unknown for growth cones). e) SI and SA channels in a growth cone patch. Suction (mmHg) is indicated adjacent to each segment of record; at the arrowheads, suction was abruptly released. Note that between about -20 and -50 mmHg, neither channel type was active. 50 mM K^+ saline in the pipette; patch held at V_{rest}. Calibration: (a) 1 pA, 2 s; (b) 4 pA, 2 s; (c) 2 pA, 1 s; (d) 2 pA, 40 ms; (e) 4 pA, 2 s. Traces (a), (b), (d) and (e) filtered at 1 kHz, (c) at 500 Hz. Solid bars below traces (here and in Fig. 56) indicate suction.

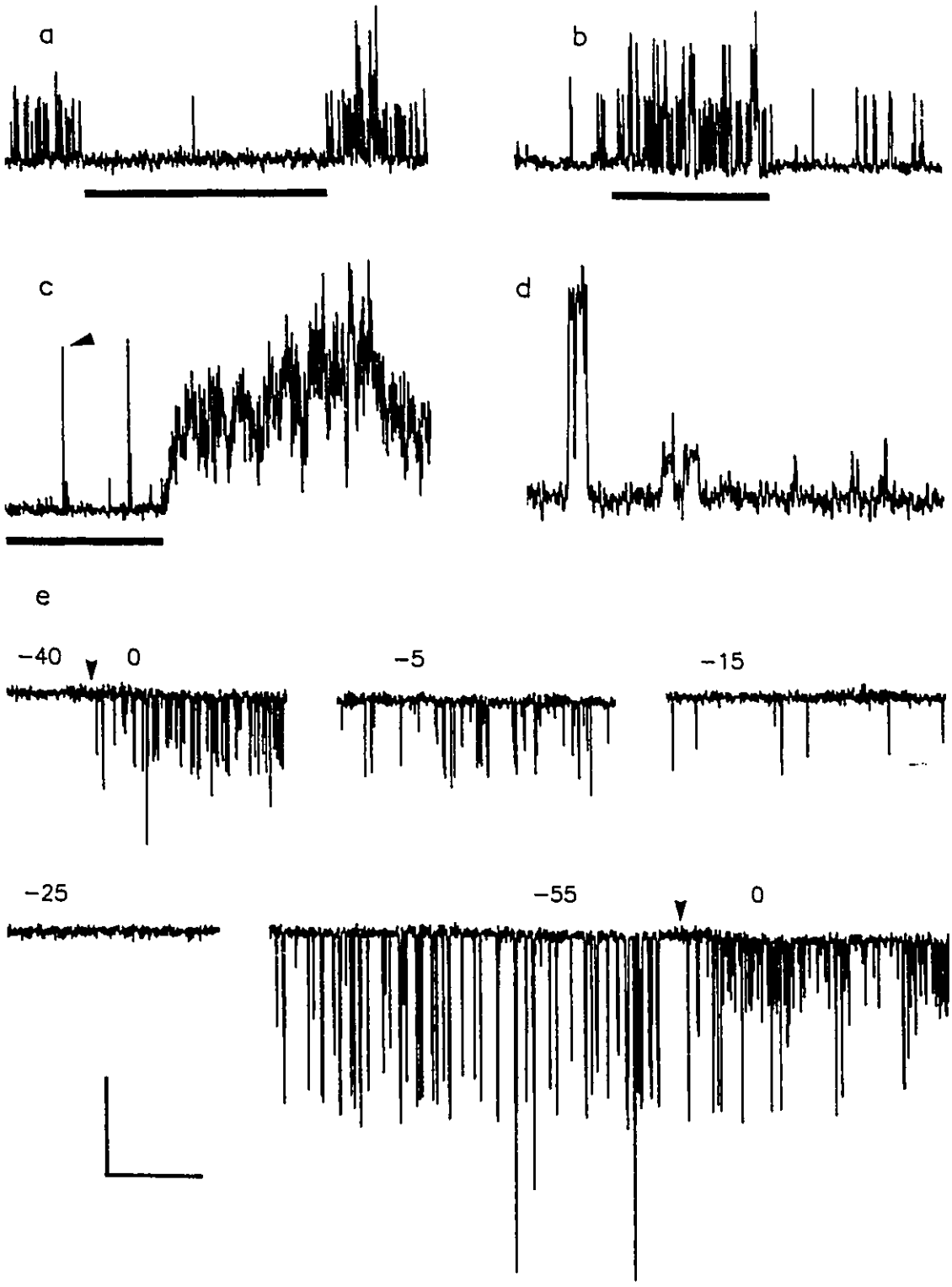
a
b
c
d
e
−40
0
−5
−15
−25
−55
0

stretch-inactivated (SI) currents but were nearly quiescent until stretch evoked SA channel activity (Fig. 54b). It is possible that even with the pipette tip tension nominally at zero, there was often sufficient residual suction (from capillarity) to inactivate the SI channels. This would explain why it was sometimes possible to stimulate activity by applying 3 to 5 mmHg of positive pressure; this activity subsided with further positive pressure, as expected for a SI channel (see Fig. 57, left). SI channels were however, observed in 13 out of 219 patches made on cell bodies with pipettes made from small bore (outside diameter, 1.65 mm; inside diameter, 0.85 mm) tubing. When such pipettes were used on growth cones, SI channel activity was not observed (15 patches), but with wider bore pipettes (outside diameter, 1.65 mm; inside diameter, 1.15 mm), 3 of 11 successfully-patched growth cones exhibited SI channels. This frequency of occurrence represents a minimum; it is likely that patches were discarded as being merely "noisy" when in fact they were displaying multiple spontaneously-active SI channels. On two cells in which SI channels were noted, second and third patches were obtained. All showed SI and SA currents, indicative, for these cells at least, of a homogeneous channel distribution.

The occurrence of SI and SA currents together (Figs. 1 c, d and e) in a single patch from cell bodies or growth cones demonstrates that distinct populations of channels with reciprocal responses to mechanical tension can coexist within a membrane area of several square micrometers.

To exclude the possibility that suction inhibits channel activity not because of increased membrane tension but because the channel-bearing membrane is drawn against the inner wall of the pipette, amplitude histograms were examined for the presence of attenuated events. Under condi-

tions where suction sharply decreased the open probability (P_o) for SI channels, the distribution of single channel amplitudes was unchanged (Fig. 55). Calcium-related artifacts (for example, Ca^{2+}-inactivation induced by inward leak of calcium) are ruled out by the observation of SI events in Ca^{2+}-free conditions (Fig. 56). Even with such artifacts eliminated, do membranes in fact encounter tensions comparable to those applied through the patch pipette? Probably they do; for a semipermeable membrane, a mere 1 mOsm equals 18 mmHg. Moreover, at the advancing tip of crawling cells, motility generates forces ranging from 10^{-8} to 10^{-3} dyn/μm (Harris et al., 1980; Dembo and Harris, 1981), so that experimental tensions [on the order of 10^{-5} to 10^{-4} dyn/μm for -10 mmHg in a typical patch (Guharay and Sachs, 1984) are not excessive.

For the SI channel, as for the SA channel (Sigurdson et al., 1987b), analysis of single-channel current voltage relations indicates that K^+ is the physiologically permeant species. With normal saline (NS) in the pipette (Fig. 56), the zero-current potential for the SI channel was near the resting potential and, as expected for a channel with negligible Na^+ and intracellular anion permeability, the channel did not pass inward current. When Na^+ was replaced with K^+ (making no Cl^- changes), inward SI currents were seen at rest (three patches) and the reversal potential (V_{rev}) shifted to ,0 mV. The current voltage relations of a Cl^- channel would not be altered by this cation substitution. Since inward and outward SI currents were seen with thallium acetate (TlAc) in the pipette (Fig. 56), the possibility that the SI channel is anion-selective is ruled out unless extracellular TlAc inexplicably induces permeability to intracellular anions. SI currents were also observed with 50 mM RbCl in the pipette; as with K^+ and Tl^+, V_{rev} shifted

in the depolarizing direction (to -12 mV), with 0.5 pA SI inward Rb^+ currents at the resting membrane potential (V_{rest}) and outward K^+ currents at positive potentials. These permeation characteristics (that is, substantial conductance for Tl^+ followed by K^+ and Rb^+, and sparing or zero permeability to Na^+ and anions) are consistent with properties shown for other highly K^+ selective channels (Yellen, 1987) including *Lymnaea* SA channels (Sigurdson et al., 1987b). Recently, SA channels with similar permeation properties have been described in vertebrate cells (Sackin, 1987; Medina and Bregestovski, 1988; Sackin, 1989).

Figure 55. Suction does not affect elementary SI channel current amplitude. a) Patch in which multiple openings were rare (same as Table 8); histogram (constructed from events used in kinetic analyses) for 0 mmHg is shown. Overlying lines are Gaussian fits to this data and to histograms (not shown) for four other pressures. Suction did not decrease the mean amplitude and tests for skewness and kurtosis indicated no deviations from Gaussian distributions. b) Patch in which multiple openings were the norm (same as Fig.4, cell body); family of amplitude histograms for six pressures ranging from 0 to -30 mmHg show that both within a given histogram and from one pressure to the next, amplitude peaks occur at multiples of 0.6 pA.

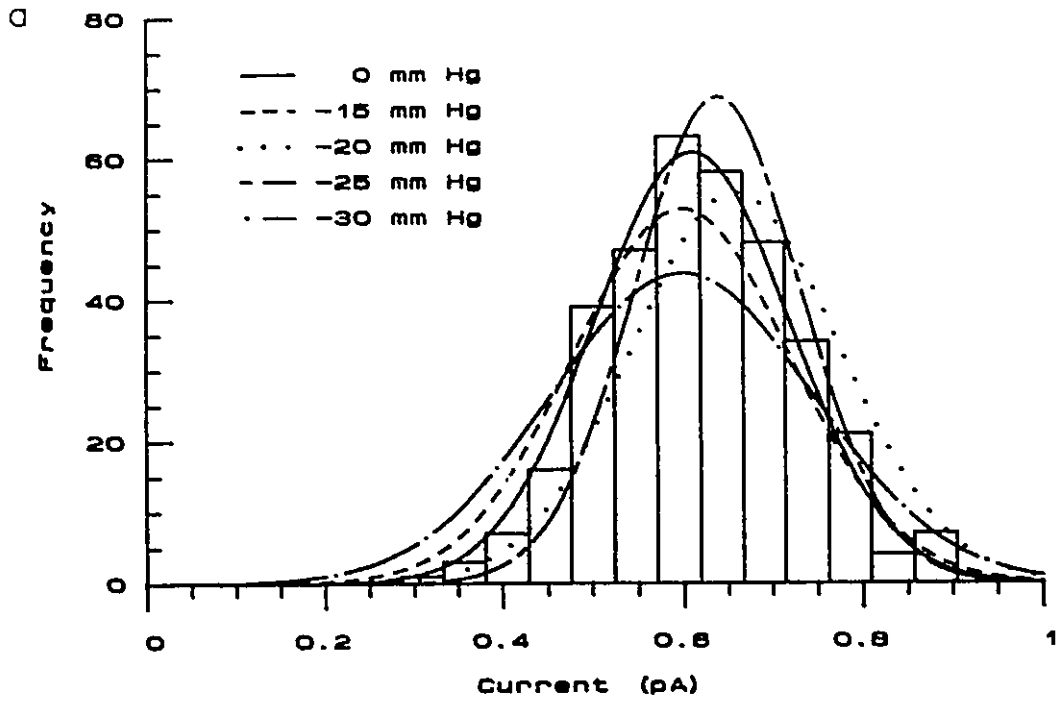
a
0 mm Hg
-15 mm Hg
-20 mm Hg
-25 mm Hg
-30 mm Hg
Frequency
0
20
40
60
80
0
0.2
0.4
0.6
0.8
1
Current (pA)

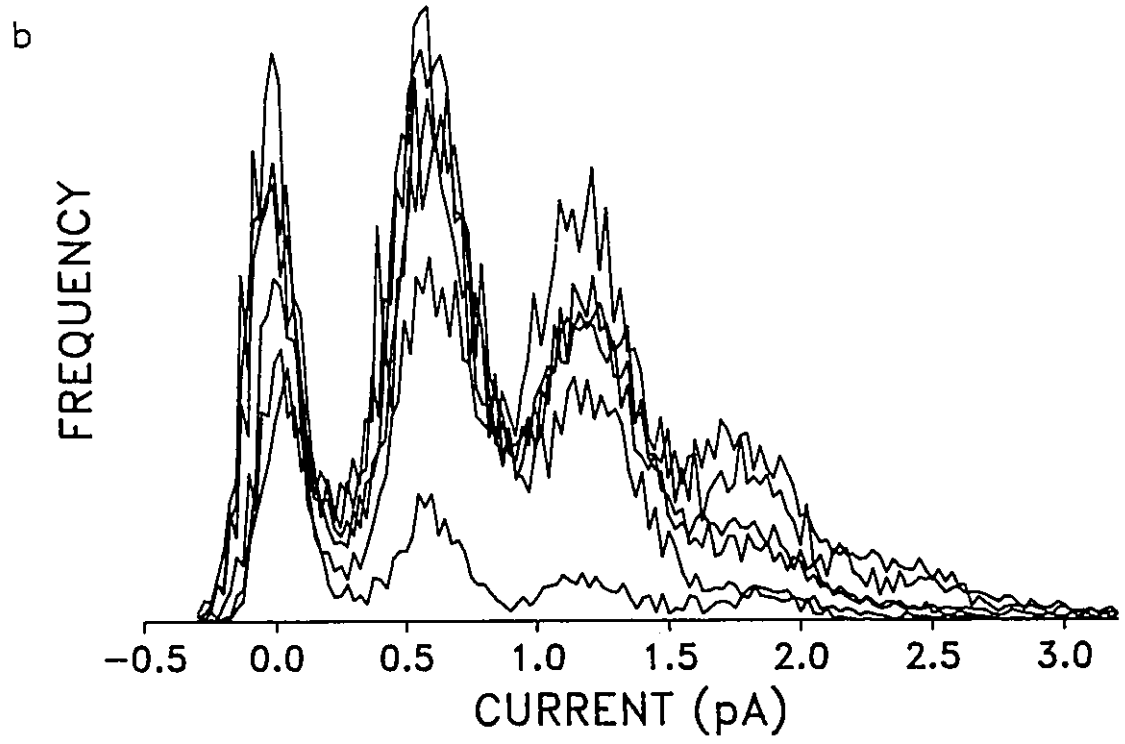
b
FREQUENCY
-0.5
0.0
0.5
1.0
1.5
2.0
2.5
3.0
CURRENT (pA)

Figure 56. SI channel current voltage relations. Open circles, NS in the pipette; conductance, 6.6 pS (linear regression to all points), zero-current intercept, -66 mV. Solid circles, 50 mM thallium acetate (TlAc) in the pipette, 50 mM KCl in bath, both solutions Ca^{2+}-free (2.2 mM EGTA in bath only) and buffered with Hepes (5 mM), V_{rest} assumed to be 0 mV. Slopes (fit by eye) of linear portions are 38 pS (lower quadrant) and 5.6 pS (upper quadrant), V_{rev} = +7 mV. Note that the outward current conductances with NS and TlAc in the pipette are similar, suggesting that intracellular K^+ carries the current in both cases. **Inset)** Stretch-inactivation (,40 mmHg) of outward and inward currents (TlAc experiment), and (bottom), at higher time resolution, a record from the NS experiment, V_m as indicated. Cell body patches for both experiments. Calibration: 2 pA, 4 s (top traces), 40 ms (bottom trace).

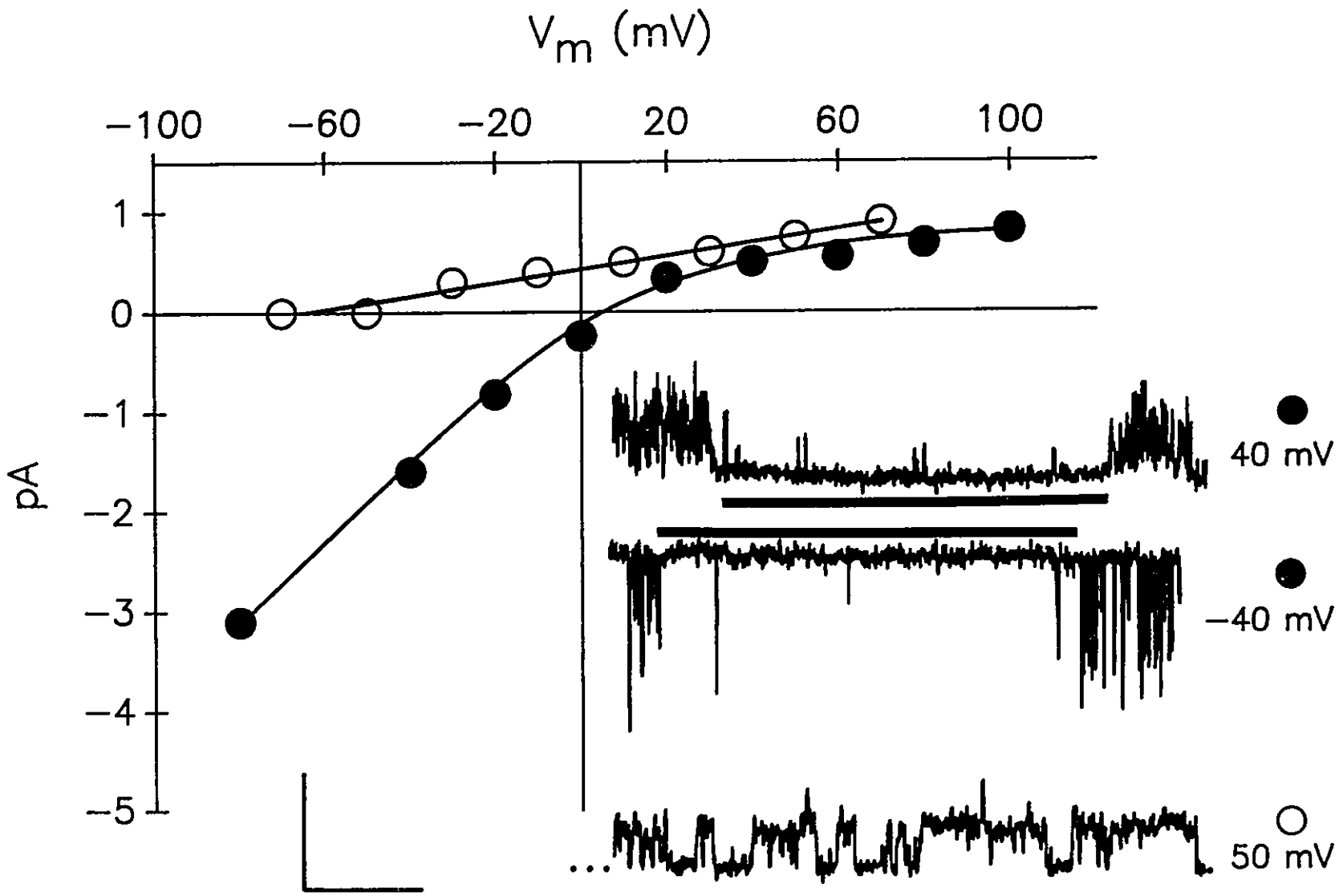
V_m (mV)
−100
−60
−20
20
60
100
1
0
−1
−2
−3
−4
−5
pA
40 mV
−40 mV
50 mV

On three cell body patches (different cells), P_o was measured for SI channels at four or more pressures. In each case, P_o decreased to 50% or less (compared to 0 mmHg) by -15 mmHg. By contrast, SA channel activation in *Lymnaea* neurons seldom attained a half maximal level before -30 mmHg. Fig. 57 quantifies the stretch sensitivity of SI and SA channels in a cell body patch and in two growth cone patches. The "notch-filter" appearance of the paired curves (that is, SI/SA activity from the same patch) of Fig. 57 is particularly noteworthy, because it shows how intermediate tensions minimize K^+ permeability, thereby maximizing the likelihood of membrane excitation and the attendant entry of Ca^{2+} through voltage-gated Ca^{2+} channels. Given the central role of Ca^{2+} in the control of exocytosis, of cytoskeletal structure, and of growth cone motility (Cohan et al., 1987; Augustine et al., 1988; Kater et al., 1988), membrane tension effects on SI and SA channel activity could have important feedback consequences for local motility and for morphology. It is plausible that reduced adhesion to the substrate would activate SI channels, whereas excessively rapid growth or abutment against a surface would recruit SA channels. A widespread utilization of mechanosensitive K^+ channels in morphogenesis is suggested by the finding that SA K^+ channels are activated cyclically in dividing vertebrate embryonic cells (Medina and Bregestovski, 1988).

Stretch-dependent decreases in the SI channel P_o could stem either from stretch-induced increases in the rate of leaving an open state (yielding briefer open sojourns) or from decreases in the rate of leaving a closed state (longer closed sojourns). Open time histograms for SI events could be fit with a single exponential whereas multiple exponentials were

required for the closed times, the longest of which could be ascribed to a between-bursts state. Table 8 provides evidence that the channel open time is insensitive to membrane tension. In contrast, the long closed time lengthens with increasing stretch as P_o declines. Interestingly, SA K^+ channels (Sigurdson et al., 1987a) and other stretch-activated channels (Guharay and Sachs, 1984; Lansman et al., 1987) conform to this same basic pattern: stretch acts on the between-bursts closed time, without substantially altering either open times or brief closed times. In stretch sensitive channels, therefore, slow mechanical transduction processes and fast kinetic processes may represent modes of gating arising from spatially distinct regions of the channel.

Several additional observations on SI channels are worth noting. The maximum number of SI channels in any patch was ten and the minimum in patches which exhibited SI events was two, a range corresponding to that for SA channels in *Lymnaea* neurons. (Density per patch is obtained from the maximum number of stretch sensitive elementary amplitudes, as seen in Fig. 55b). SI channels, like SA channels, showed no obvious voltage dependence; spontaneous SI channel activity at V_{rest} was evident with K^+, Tl^+, or Rb^+ in the pipette and no inactivation occurred with depolarization. Normal-looking SI events were observed with both 10 mM tetraethylammonium and 1 mM quinidine (for example, Fig. 54a) in the pipette. The phenomenon of channel inactivation by stretch is not unique to this preparation; SI channels have recently been observed in mammalian astrocytes (C. Bowman, per. comm.).

Figure 57. SI and SA channels coexist in patches from cell body and growth cone. Ordinate, P_o normalized to the maximum value for each type of channel in each patch; solid symbols refer to SI channels, open symbols to SA channels. Circles represent paired curves for a cell body patch (same patch as Fig. 54c), diamonds, paired curves for a growth cone patch. Triangles, as explained in text, represent growth cone SI channels with activity that was suppressed by the residual pipette suction (,10 mmHg); note inactivity at nominally zero and negative pressures. Circles, NS in pipette, V_m = +70 mV. Diamonds, 50 mM K^+ in pipette, patch at V_{rest}. (Same patch as Fig. 54c). Triangles, 50 mM K^+ in pipette, patch $V_m = V_{rest} - 60$ mV.

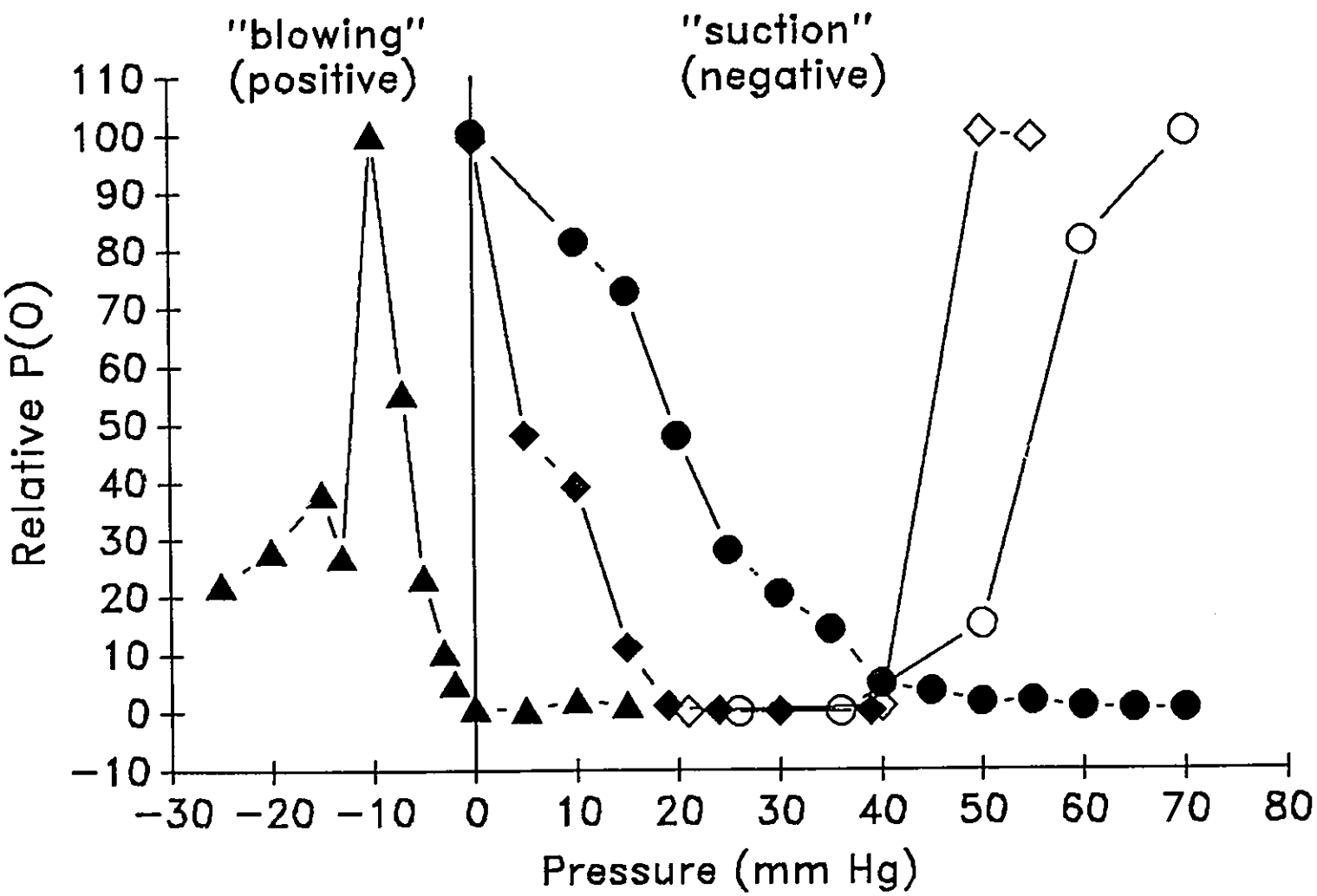
"blowing"
(positive)
"suction"
(negative)
110
100
90
80
70
60
50
40
30
20
10
0
−10
Relative P(O)
−30
−20
−10
0
10
20
30
40
50
60
70
80
Pressure (mm Hg)

Table 8. Kinetics for SI channels at three pressures. Time constants[1] (τ_{open} and τ_{closed}) obtained from a cell body patch in which the SI channel activity was appropriate for kinetic analysis over a range of pressures including 0 mmHg.

Pressure (mmHg)	Relative P_o[2]	τ_{open}[3] (ms)	τ_{closed}[4] (ms)
0	1	0.85 ± 0.07 (0.87)	109
-15	0.16	1.12 ± 0.29 (0.87)	294
-30	0.068	0.75 ± 0.23 (0.85)	559

[1] Insufficient events precluded multiexponential fits to the closed-time data in this patch, so measurements are restricted to closed times which should belong to the slowest component. NS plus 1 mM quinidine in pipette, V_m = +90 mV.

[2] P_o relative to value at 0 mmHg, which was 0.024.

[3] Given both as inverse rate constant (± sem, the error associated with the fit) to a single exponential fit (events ≥ 0.1 ms) and (in brackets) as a maximum likelihood estimate (that is, average open time minus cutoff time of 0.1 ms ; see Equation 50, (Colquhoun and Sigworth, 1983).

[4] Average closed time minus cutoff time of 5 ms (Colquhoun and Sigworth, 1983).

A number of properties shared by the two stretch sensitive channels (the parallel kinetic effects of stretch on a between-bursts closed state in both, the similarities in membrane densities, the concurrent changes of SI and SA activity in a given patch) are consistent with the possibility that the channels are linked to a common transduction mechanism. A good candidate is the submembranous filament network proposed by Sachs (Sachs, 1986; Sachs, 1988;). The discovery of a SI channel in parallel with the SA channel also raises the interesting prospect that yet other integral membrane proteins - ones implicated in cell motility, cell compliance or osmoregulation, but whose "outputs" are not necessarily measurable with a patch clamp (carriers, enzymes) - might also be influenced by membrane tension.

Summary and General Conclusions

Mechano-sensitive ion channels have been identified and characterized in the isolated cells of a freshwater snail (*Lymnaea stagnalis*). In ventricular cells the stretch-sensitivity and kinetic properties of a K^+ selective channel are described. In neurons isolated from the circumoesophageal ganglia, a similar channel was found and subsequently examined in greater detail with respect to permeation properties, stretch-sensitivity, kinetics, spatial distribution and physiological function.

In neuron cell bodies, under physiological conditions, the stretch-activated K^+ (SAK) channel has a 30 pS conductance and passes only outward K^+ current (no inward Na^+ current). Raising extracellular K^+ concentration caused a positive shift in the reversal potential of current/voltage (I/V) relations, indicative of K^+-selective channel. This is comparable to the results reported by Brezden et al. (1986) for *Lymnaea* heart SAK channels (see Table 9). Biionic I/V relations established that K^+ is at least 10 times more permeable than Na^+ and that the channel has a selectivity sequence not unlike other K^+ selective channels [Tl^+ (1.61) > K^+ (1) > Rb^+ (0.49) > Na^+ (0.154) > Li^+ (0.027)]. Absolute K^+ permeability for the channel was 4.9×10^{-13} cm s^{-1}, a value comparable to Ca^{2+}-activated K^+ channels. Current/voltage curve non-linearities and deviations from the Goldman-Hodgkin-Katz current equation demonstrated that the channels do not follow the independence assumption; i.e. the channel permeation mechanism is complex, implying a multi-ion permeation pathway. This should not be surprising in light of the fact that essentially all ion channels appear to be multi-ion channels; i.e. more than one ion can occupy the permeation pathway at once.

As shown by Brezden et al. (1986) heart SAK channels are blocked by quinidine. This observation was extended to neuron SAK channels where significant blockade was observed with 0.1 and 1 mM quinidine and 10 and 20 mM tetraethylammonium (TEA). Quinidine produced an intermediate type of block, typified by an increase channel flicker. TEA block was much faster; block appeared only as a amplitude reduction with no appreciable effect on channel kinetics. Both drugs displayed voltage-dependence of block, with the TEA binding site located between 24 to 32 % across the voltage field. Extracellularly applied Ba^+ (100 mM) did not block or permeate neuron SAK channels.

Given the absence of specific SAK channel blockers (both quinidine and TEA block other K^+ channels), a physiological role for SAK channels was (and still is) difficult to establish. Correlative evidence was obtained in an attempt to determine if SAK channel activation during hyposmotic shock induced cell-swelling, could act as a volume-limiting mechanism. Neuron cell bodies and heart cells were very resistant to severe hyposmotic shock (30% dilution) and were capable of resuming "normal" development (in culture) after such shocks. Intracellular recordings indicated cell membrane hyperpolarization during hyposmotic shock. In 35% of patches, cell-swelling was correlated with increased SAK channel activity. Although not conclusive, these results are consistent with SAK channel activation playing a role in cell volume limitation during hyposmotic shock.

Stretch-sensitivity and kinetics of SAK channels was studied in heart and neuron cell bodies and in somewhat less detail in growth cones. In both cell types, stretch-sensitivity was variable; the "threshold" pressure for patches encompassed a range of 20 to 70 mmHg suction. This may be the

result of membrane slack; i.e. infoldings which must first be unfolded before the membrane tension reaches levels sufficient for channel activation. SAK channel kinetics were somewhat similar in heart and neurons; heart SAK channels possessed at least 2 open and 3 closed states, while the neuron channels were best described as having at least 2 open and 4 closed states (based on curve fits of sums of exponentials to duration frequency histograms) (see Table 9). In both cell types, the changes in open probability (P_o) as a function of pressure, were related to the decrease in the average closed time separating bursts of openings rather than by increasing the duration of openings. This was observed, whether by determining mean dwell times by extraction of rate constants from frequency histograms or by analysis of burst duration and interburst closed intervals.

SAK channel spatial distribution within neurons was examined by recording from growth cones from actively extending neurite processes. These SAK channels did not differ dramatically from the cell body channels, having similar selectivity, stretch-sensitivity and kinetics. Since freshly isolated neuron cell bodies have been stripped of dendritic and axonal structures, the presence of SAK channels in newly developed growth cones ($>$ 100 μm from cell body) indicated the channels had been newly synthesized (at least since isolation).

During recordings of SAK channels in neuron cell bodies and growth cones, a new class of mechano-sensitive channel was discovered having an opposite gating property and differing stretch-sensitivity than the SAK channel. This channel had only one-fifth the SAK channel conductance, but had a similar selectivity ($Tl^+ > K^+ > Rb^+ > Na^+$). In response to increased membrane tension, the stretch-inactivated K^+ (SIK) channel decreased its P_o

and did so at pressures lower than those required to activate SAK channels. This P_o decrease was associated with an increase in the estimate of the mean long closed time, an analogous, but opposite result obtained for the SAK channel. The SIK channel stretch-sensitivity properties in combination with coexisting SAK channels, resulted in P_o *vs* pressure curves (for the two channels) resembling those of a "notch filter"; i.e. for certain intermediate membrane tensions, membrane K^+ permeability should be minimized. It is postulated that voltage-dependent Ca^{2+} channels present in the growth cone cell membrane would be activated at these pressures resulting in increased intracellular Ca^{2+}. Given the central role of Ca^{2+} in the control of exocytosis, of cytoskeletal structure, and of growth cone motility SIK and SAK channel activity could have important feedback consequences for local motility and for morphology.

We still know very little about how mechano-sensitive ion channels operate. We are beginning to establish that these channels can have a wide variety of permeation and conduction characteristics which gives the impression that the stimulus for gating the channel has little to do with what the channel conducts. This is quite surprising because a mechanical perturbation might be expected to distort the channel's permeation pathway producing stretch-dependent permeation properties. This gives a clue to the protein structure; the permeation pathway must be quite stiff to avoid being influenced by the membrane tension. Another surprising observation is that there is only one significantly stretch-dependent rate constant in SACat, SAK and SIK channels. This implies a similar transduction and gating mechanism and also says that the protein must be very rigid in the other closed and open states. The small changes in the neuron SAK channel τ_{O2}

and τ_{B2} are simply not large enough to account for the P_o changes observed and may be a sign that the SAK channel protein is not quite as stiff in the open conformation as the SACat channels.

Functionally, SAK and SIK channels can only signal changes in membrane tension by passing K^+ ions. Under physiological conditions this means passing outward K^+ current causing a membrane hyperpolarization or merely inducing increased K^+ conductance when the resting potential is at E_K thereby stabilizing V_{rest} against voltage shifts. Although the heart cells were not described as having SIK channels, another look is probably in order. When dealing with very small conductance channels such as these, experience plays a large role in knowing what is noise and what is bona fide channel activity. The heart experiments were performed during the early phases of this work, so SIK channels were likely overlooked. The occurrence of two ion channels of the opposite and differing mechano-sensitivity within the same membrane immediately leads one to speculate on channel function. The possibility that neuron growth cones modulate membrane potential in a tension dependent manner via the interaction of SAK and SIK channels is seductive, but unproven. A role for SAK channels in volume regulation is supported by correlative data, but also awaits direct demonstration. In a mechanically active organ such as the heart, SAK channels could have a number of functions, ranging from negative feedback during ventricular overfilling (overfilling would hyperpolarize cells causing relaxation) to control over beat frequency (setting pacemaker potentials). None of these ideas have been examined in the context of SA channels in snail or vertebrate heart cells. As far as a physiological role for *Lymnaea* mechano-sensitive channels, all that can be said for certain, is that cells

which are not normally thought of as mechano-sensory structures have ion channels capable of transducing membrane tensions. Demonstration of a functional role for mechano-sensitive ion channels must await a pharmacological agent capable of blocking or disabling the channel's stretch-sensitivity.

Is the mechano-sensitivity of *Lymnaea* SAK and SIK channels artifactual? First, it must be established that the membrane tensions required to activate these channels are realistic, physiological ones. 10 mmHg represents 10^{-4} dyn/μm (Guharay and Sachs, 1984) which is easily within range of tensions cell membranes experience during motility (10^{-8} to 10^{-3} dyn/μm; Harris et al., 1980; Dembo and Harris, 1981). These are reasonable values, given the uncertainty of the membrane tension, and indicate that the channels do not require outlandish amounts of mechanical energy for gating. Possible activation by chemical agonists and second messengers can only be ruled out for the case of Ca^{2+} which has been shown to be ineffectual.

If the Sachs model of transduction is correct, I expect that the membrane cytoskeleton will be closely associated with mechano-sensitive channels. The homogeneous distribution of SAK and SIK channels already gives hints of this; i.e. the channels are evenly spaced by virtue of their cytoskeletal attachments. A legitimate concern is that this association, by accident of design, results in mechano-sensitive channels which really have other undisclosed gating properties and functions. There presently is no way of discerning this possibility, which would involve disrupting the channel's mechano-sensitivity and determining what physiological function was no longer operating. A more straightforward method is to simply block

these channels, but again we come up against the major stumbling block of this research, the lack of specific pharmacological agents. We therefore must wait for ingenious experimentation and perhaps a little serendipity before we can positively link mechano-sensitive ion channels with specific physiological functions.

Table 9. Comparison of properties of *Lymnaea* neuron and heart SAK channels.

Property	Neuron	Heart
Conductance (physiological saline)	30 pS	33 pS
Selectivity (P_{Na}/P_K)	0.083	0.063
Selectivity Sequence	$Tl^+ > K^+ > Rb^+ > Na^+ > Li^+$	$K^+ > Na^+$
Channel block by externally applied agents		
Quinidine (1 mM)	yes	yes
TEA (10 and 20 mM)	yes	no
4-aminopyridine	?	no
apamin	?	no
cetedil	?	no
Cs^+	no	?
Ba^+	no	?
Kinetics		
# of open states	2	2
# of closed states	4	3
Mean dwell times (ms)		
τ_{O1}	0.15 ± 0.08	0.21
τ_{O2}	SS*	2.5
τ_{C1}	0.06 ± 0.032	0.13
τ_{C2}	0.46 ± 0.16	0.69
τ_{C3}	1.82 ± 0.57	SS
τ_{C4}	SS	-
τ_{B1}	< 0.3	0.07
τ_{B2}	SS	4.2
τ_{IB}	SS	SS
Suction required to reach threshold activation (mmHg)	-30 to -70	-5 to -15

* Stretch sensitive

References

ABE, H. & OGATA, N. (1982). Ionic mechanism for the osmotically-induced depolarization in neurons of the guinea-pig supraoptic nucleus in vitro. J. Physiol. 327, 157-171.

ADAMS, D.J., SMITH, S. & THOMPSON, S.H. (1980). Ionic currents in molluscan soma. Ann. Rev. Neurosci. 3, 141-167.

ALDRICH, R.W. & YELLEN, G. (1983). Analysis of nonstationary channel kinetics. In Single-channel Recording. Eds. B. Sakmann and E. Neher. Plenum Press, New York , 287-299.

ALLISON, P. & BENJAMIN, P.R. (1985). Anatomical studies of central regeneration of an identified molluscan interneuron. Proc. R. Soc. Lond. B. 226, 135-157.

ALMERS, W. & STIRLING, C. (1984). Distribution of transport proteins over animal cell membranes. J. Membrane Biol. 77, 169-186.

ANDERSON, C.R. & STEVENS, C.F. (1973). Voltage clamp analysis of acetylcholine produced end-plate current fluctuations at frog neuromuscular junction. J. Physiol. 235, 655-691.

AUERBACH, A. & SACHS, F. (1984). Patch clamp studies of single ionic channels. Ann. Rev. Biophys. Bioeng. 13, 269-302.

AUGUSTINE, G.J., CHARLTON, M.P. & HORN, R. (1988). Role of calcium-activated potassium channels in transmitter release a the squid giant synapse. J. Physiol. , -.

BARRETT, J.N., MAGLEBY, K.L. & PALLOTTA, B.S. (1982). Properties of single calcium-activated potassium channels in cultured rat muscle. J. Physiol. 331, 211-230.

BEAN, R.C., SHEPHERD, W.C. & EICHNER, J. (1969). Discrete conductance fluctuations in lipid bilayer protein membranes. J. Gen. Physiol. 53, 741-752.

BEDARD, E., SIGURDSON, W.J. & MORRIS, C.E. (1988). Stretch-activated (SA) channels in the neurons of Cepaea (Helicideae) and Lymnaea. Biophys. J. 53, 154a.

BELARDETTI, F., KANDEL, E.R. & SIEGELBAUM, S.A. (1987). Neuronal inhibition by the peptide FMRF-amide involves opening of S K+ channels. Nature 325, 153-156.

BENHAM, C.D., BOLTON, T.B., LANG, R.J. & TAKEWAKI, T. (1986). Calcium-activated potassium channels in single smooth muscle cells of rabbit jejunum and guinea-pig mesenteric artery. J. Physiol. 371, 45-67.

BLATZ, A.L. & MAGLEBY, K.L. (1984). Ion conductance and selectivity of single calcium-activated potassium channels in cultured rat muscle. J. Gen. Physiol. 84, 1-23.

BRAY, D. & WHITE, J.G. (1988). Cortical flow in animal cells. Science **239**, 883-888.

BRAY, D. (1984). Axonal growth in response to experimentally applied mechanical tension. Developmental Biol. **102**, 379-389.

BRAY, D. (1987). Growth cones: do they pull or are they pushed?. Trends Neurosci. **10**, 431-434.

BREHM, P., KIDOKORO, Y. & MOODY-CORBETT, F. (1984). Acetylcholine receptor channels properties during development of Xenopus muscle cells in culture. J. Physiol. 357, 203-217.

BREZDEN, B.L. & GARDNER, D.R. (1983). The effect of the molluscide Frescon on the smooth and cross-striated muscles of Lymnaea stagnalis and Helix aspersa. Pestic. Biochem. Physiol. **20**, 259-268.

BREZDEN, B.L. & GARDNER, D.R. (1984). The ionic basis of the resting potential in a cross-striated muscle ofthe aquatic snail Lymnaea stagnalis. J. exp. Biol. **108**, 305-314.

BREZDEN, B.L., GARDNER, D.R. & MORRIS, C.E. (1986). A potassium selective channel in isolated Lymnaea stagnalis heart muscle cells. J. exp. Biol. 123, 171-189.

BROWN, H.M., OTTOSON, D. & RUDQVIST, B. (1978). Crayfish stretch receptor: an investigation with voltage clamp and ion-selective electrodes. J. Physiol. (Lond.) 284, 155-179.

BROWN, A.M. (1981). What barorecptors tell the brain in hypertension. In Central Nervous System Mechanisms in Hypertension. Edited by J.D.Buckley and C.M. Ferrario. Raven, 1-7.

BYERLY, L. & HAGIWARA, S. (1982). Calcium currents in internally perfused nerve cell bodies of Lymnaea stagnalis. J. Physiol. **322**, 503-528.

BYERLY, L. & MOODY, W.J. (1984). Intracellular calcium ions and calcium currents in perfused neurones of the snail, Lymnaea stagnalis. J. Physiol. 352, 637-652.

BYERS, T. & BRANTON, D. (1985). Visualization of the protein associations in the erythrocyte membrane skeleton. Proc. Natl. Acad. Sci. U.S.A. **82**, 6153-6157.

BYERS, M.R. (1985). Sensory innervation of peridontal ligament of rat molars consists of unencapsulated ruffini-like mechanorecptors and free nerveendings. J. Comp. Neurol. 231, 500-518.

CALA, P.M. (1980). Volume regulation by Amphiuma red blood cells: The membrane potential and its implications regarding the nature of the ion-fluxpathways. J. Gen. Physiol. **76**, 683-708.

CALA, P.M. (1985). Volume regulation by Amphiuma red blood cells: strategies for identifying alkali metal/H^+ transport. Fed. Proc. **44**, 2500-2507.

CECCHI, X., ALVAREZ, O. & WOLFF, D. (1986). Characterization of a calcium-activated potassium channel from rabbit intestinal smooth muscle incorporated into planar bilayers. J. Membrane Biol. **91**, 11-18.

CHRISTENSEN, O. (1987). Mediation of cell volume regulation by Ca^{2+} influx through stretch-activated channels. Nature **330**, 66-68.

COHAN, C.S. & KATER, S.B. (1986). Suppressor of neurite elongation and growth cone motility by electrical activity. Science **232**, 1638-1640.

COHAN, C.S., CONNOR, J.A. & KATER, S.B. (1987). Electrically and chemically mediated increases in intracellular calcium in neuronal growth cones. J. Neurosci. **7**, 3588-3599.

COLQUHOUN, D. & HAWKES, A.G. (1977). Relaxation and fluctuations of membrane currents that flow through drug-operated channels. Proc. R. Soc. Lond. B. **199**, 231-262.

COLQUHOUN, D. & HAWKES, A.G. (1983). The principles of the stochastic interpretation of ion-channel mechanisms. In Single-channel Recording, Eds. B. Sakmann and E. Neher. Plenum Press , 135-175.

COLQUHOUN, D. & SAKMANN, B. (1985). Fast events in single-channel currents activated by acetylcholine and its analogues at the frog muscle end-plate.. J. Physiol. **369**, 501-557.

COLQUHOUN, D. & SIGWORTH, F. (1983). Fitting and statistical analysis of single-channel records. In Single-channel Recording. Eds. B. Sakmann and E. Neher, Plenum Press, New York. , 191-263.

COOPER, K.E., TANG, J.M., RAE, J.L. & EISENBERG, R.S. (1986). A cation channel in frog lens epithelium responsive to pressure ans calcium. J. Membrane Biol. **93**, 259-269.

COREY, D.P. & HUDSPETH, A.J. (1979). Ionic basis of the receptor potential in a vertebrate hair cell. Nature **281**, 675-677.

COREY, D.P. & STEVENS, C.F. (1983). Science and technology of patch-recording electrodes. In Single-channel Recording. Eds. B. Sakmann and E. Neher. Plenum Press, pp 53.

CORONADO, R. & MILLER, C. (1979). Voltage-dependent Cs^+ block of a K^+ channel from sarcoplasmic reticulum. Nature **280**, 807-810.

CORONADO, R., ROSENBERG, R.L. & MILLER, C. (1980). Ionic selectivity, saturation, and block in a K^+-selective channel from sarcoplasmic reticulum. J. Gen. Physiol. **76**, 425-446.

CUKIERMAN, S., YELLEN, G. & MILLER, C. (1985). The K^+ channel of sarcoplasmic reticulum: A new look at Cs+ block. Biophys. J. **48**, 477-484.

DAVENPORT, P.W. & THOMPSON, F.J. (1987). Mechanosensitive afferents of femoral-saphenous vein. Am. J. Physiol. **252**, R367-R370.

DAVIS, C.W. & FINN, A.L. (1985). Cell volume regulation in frog urinary bladder. Federation Proc. **44**, 2520-2525.

de BOLD, A.J., BORENSTEIN, H.B., VERESS, A.T. & SONNENBERG, H. (1981). A rapid and potent natriuretic response to intravenous injection of atrial myocardial extracts in rats. Life Sci. **28**, 89-94.

DEITMER, J.W. (1981). Voltage and time chararcteristics of the potassium mechanoreceptor jcurrent in the ciliate Stylonychia. J. Comp. Physiol. **141**, 173-182.

DEMBO, M. & HARRIS, A.K. (1981). Motion of particles adhering to the leading lamella of crawling cells. J. Cell Biol. **91**, 528-536.

DING, J., YANG, X., BOWMAN, C.L. & SACHS, F. (1988). Stretch-activated ion channels in rat astrocytes in primary culture. Soc. Neurosci. Abst. **425**, 5.

ECKERT, R. & RANDALL, D. (1983). Animal Physiology: Mechanisms and adaptations. W.H. Freeman and Company.

ECKERT, R. (1972). Bioelectric control of ciliary activity. Science **176**, 473-481.

EISENMAN, G., LATORRE, R. & MILLER, C. (1986). Multi-ion conduction and selectivity in the high-conductance Ca^{2+}-activated K^+ channel from skeletal muscle. Biophys. J. **50**, 1025-1034.

EWALD, D.A., WILLIAMS, A. & LEVITAN, I.B. (1985). Modulation of single Ca^{2+}-dependent K^+ channel activity by protein phosphorylation. Nature **315**, 503-506.

FALKE, L. & MISLER, S. (1988). Ion channel acitvity during osmoregulation in clonal neuroblastoma (N1E115) cells. Biophys. J. **53**, 412a.

FALKE, L.C. & MISLER, S. (1989). Activity of ion channels during volume regulation by clonal N1E115 neuroblastoma cells. Proc. Natl. Acad. Sci. USA **86**, 3919-3923.

FALKE, L., EDWARDS, K.L., PICKARD, B.G. & MISLER, S. (1987). A stretch-activated anion channel in cultured tobacco cells. Biophys. J. **51**, 251a.

FLYNN, T.G. & DAVIES, P.L. (1985). The biochemistry and molecular biology of atrial natriuretic factor. Biochem. J. **232**, 313-321.

FOSKETT, J.K. & SPRING, K.R. (1985). Involvement of calcium and cytoskeleton in gallbladder epithelial cell volume regulation. Am. J. Physiol. **248**, C27-C40.

FRENCH, A.S. (1985). After-hyperpolarization and receptor potential attenuation following bursts of action potentials in an insect mechanoreceptor. Can. J. Physiol. Pharmcol. **63**, 18-22.

GALLIN, E. (1984). Calcium- and voltage-activated potassium channels in human macrophages. Biophys. J. **46**, 821-825.

GARDNER, P.I. (1986). Single-channel recordings of three K^+-selective currents in cultured chick ciliary ganglion neurons. J. Neurosci. **6**, 2106-2116.

GELETYUK, V.I. & KAZACHENKO, V.N. (1985). Single Cl^- channels in molluscan neurones: Multiplicity of the conductance states. J. Membrane Biol. 86,]9-15.

GILLES, R. (1983). Volume maintenance and regulation in animal cells: Some features and trends. Mol. Physiol. **4**, 3-16.

GLAVINOVIC, M.I. & TRIFARO, J.M. (1988). Quinine blockade of currents through Ca^{2+}activated K^+ channels in bovine chromaffin cells. J. Physiol. **399**, 139-152.

GOLDBERG, D.J. & BURMEISTER, D.W. (1986). Stages in axon formation: Observations of growth of Aplysia axons in culture using video-enhanced contrast- Differential interference contrast microscopy. J. Cell Biol. **103**, 1921-1931.

GOLDBERG, D.J. (1988). Local role of Ca^{2+} in formation of veils in growth cones. J. Neurosci. **8**, 2596-2605.

GORDON, R. & BRODLAND, G.W. (1987). The cytoskeletal mechanics of brain morphogenesis. Cell Biophysics **11**, 177-238.

GRINSTEIN, S., DUPRE, A. & ROTHSTEIN, A. (1982). Volume regulation by human lymphocytes. J. Gen. Physiol. **79**, 849-868.

GRINSTEIN, S., ROTHSTEIN, A., SARKADI, B. & GELFAND, E.W. (1984). Responses of lymphocytes to anisotonic media: volume-regulating behavior. Am. J. Physiol. **246**, C204-C215.

GUHARAY, F. & SACHS, F. (1984). Stretch-activated single ion channel currents in tissue-cultured embryonic chick skeletal muscle. J. Physiol. 352, 685-701.

GUHARAY, F. & SACHS, F. (1985a). Mechanotransducer ion channels in chick skeletal muscle: The effects of extracellular pH. J. Physiol. **363**, 119-134.

GUHARAY, F. & SACHS, F. (1985b). Mechano-receptor ion channels are not nicotinic. Biophys. J. **47**, 203a.

GUSTIN, M.C., ZHOU, X.L., MARTINAC, M.R., CULBERTSON, M.R. & KUNG, C. (1987). Stretch-activated cation channel in yeast. Biophys. J. **51**, 251a.

GUSTIN, M.C., ZHOU, X., MARTINAC, B. & KUNG, C. (1988). A mechano-sensitive ion channel in the yeast plasma membrane. Science **242**, 762-765.

HAMILL, O.P., NEHER, M.E., SAKMANN, B. & SIGWORTH, F.J. (1981). Improved patch-clamp techniques for high resolution current recording from cells and cell-free membrane patches. Pflugers Arch. **391**, 85-100.

HAMILL, O.P. (1983). Potassium and chloride channels in red blood cells. In Single-channel Recording. Eds. B. Sakmann and E. Neher, Plenum Press, New York, 451-471.

HARRIS, A.K., WILD, P. & STOPAK, D. (1980). Silicone rubber substrata: A new wrinkle in the study of cell locomotion. Science **208**, 177-179.

HAYDON, P.G., MCCOBB, D.P. & KATER, S.B. (1984). Serotonin selectively inhibits growth cone motility and synaptogenesis of specific identified neurons. Science **226**, 561-564.

HELFRICH, W. (1973). Elastic properties of lipid bilayers: Theory and some possible experiments. Z. Naturforsch. **28C**, 6933-703.

HENDIL, K.B. & HOFFMANN, E.R. (1974). Cell volume regulation in Ehrlich ascites tumor cells. J. Cell. Physiol. **84**, 115-126.

HERMANN, A. & GORMAN, A.L.F. (1984). Action of quinidine on ionic currents of molluscan pacemaker neurons. J. Gen. Physiol. **83**, 919-940.

HILL, J.A., CORONADO, R. & STRAUSS, H.C. (1989). Potassium channel of cardiac sarcoplasmic reticulum is a multi-ion channel. Biophys. J. **55**, 35-46.

HILLE, B. (1970). Ionic channels in nerve membrane. In Progress in biophysics and molecular biology **21**, 1-32.

HILLE, B. (1984). Ionic Channels of Excitable Membranes. Sinauer Associates Inc, Sunderland Mass.

HOFFMANN, E.K. (1976). Control of cell volume. In Transport of Ions and Water in Animals, edited by B.L. Gupta, R.B. Moreton, L. Oschmann and B.J. Wall, Academic Press, New York. pp232-285.

HOFFMANN, E.K. (1985). Role of separate K^+ and Cl^- channels and of Na^+/Cl^- cotransport in volume regulation in Ehrlich cells. Federation Proc. 44, 2513-2519.

HORN, R. & LANGE, K. (1983). Estimating kinetic constants from single channel data. Biophys. J. **43**, 207-223.

HORN, R. (1987). Statistical memthods for model discrimination: Application t gating kinetics and permeation of the acetylcholine receptor channel. Biophys. J. 51, 255-263.

HOWARD, J., ROBERTS, W.M. & HUDSPETH, A.J. (1988). Mechanoelectrical transduction by hair cells. Ann. Rev. Biophys. Biophys. Chem. **17**, 99-124.

HUDSPETH, A.J. & COREY, D.P. (1977). Sensitivity, polarity, and conductance change in the response of vertebrate hair cells to controlled mechanical stimuli. Proc. Natl. Acad. Sci. USA **74**, 2407-2411.

HUGUES, M., SCHMID, H., ROMEY, G., DUVAL, D., FRELIN, C. & LAZDUNSKI, M. (1982). The Ca^{2+}-dependent slow K^+ conductance in cultured rat muscle cells: characterization with apamin. EMBO J. 1, 1039-1042.

IWATSUKI, N. & PETERSEN, O.H. (1985). Inhibition of Ca^{2+}-activated K^+ channels inpig pancreatic acinar cells by Ba^{2+}, Ca^{2+}, quinine and quinidine. Biochim. Biophys. Acta **819**, 249-257.

JACOBSON, S.L. (1977). Culture of spontaneously contracting myocardial cells from adult rats. Cell Struct. Funct. **2**, 1-9.

KATER, S.B. & MATTSON, B.M. (1988). In Cell Culture Approaches in Invertebrate Neuroscience. D.J. Beadle, G. Lees and S.B Kater, eds. Academic Press, Toronto. pp1.

KATER, S.B., MATTSON, M.P., COHAN, C. & CONNOR, J. (1988). Calcium regulation of the neuronal growth cone. Trends Neurosci. **11**, 315-320.

KATZ, B. (1950). Depolarizations of sensory terminals and the initiation of impulses in the muscle spindle. J. Physiol. (Lond.) **111**, 261-282.

KAZACHENKO, V.N. & GELETYUK, V.I. (1984). The potential-dependent K+ channel in molluscan neurones is organized in a cluster of elementary channels. Biochim. Biophys. Acta **773**, 132-142.

KEVERS, C., PEQUEUX, A. & GILLES, R. (1979). Effects of an hypo-osmotic shock on Na+, K+, and Cl- levels in isolated axons of Carcincus maenas. J. Comp. Physiol. 129, 365-371.

KEVERS, C., PEQUEUX, A. & GILLES, R. (1981). Roles of K+ in the cell volume regulation response of isolated axons of Carcinus maenas submitted to hypo-osmotic conditions. Mol. Physiol., 1-13.

KIRBER, M.T., SINGER, J.J. & WALSH JR., J.V. (1987). Stretch-activated channels in freshly dissociated smooth muscle cells. Biophys. J. **51**, 252a.

KIRBER, M.T., WALSH JR., J.V. & SINGER, J.J. (1988). Stretch-activated ion channels in smooth muscle: a mechanism for the initiation of stretch-induced contraction. Pflugers Arch **412**, 339-345.

KOSTENKO, M.A., GELETYUK, V.I. & VEPRINTSEN, B.N. (1973). Completely isolated neurons in the mollusc Lymnaea stagnalis. A new objective for nerve cell biology investigation.

KREGENOW, F.M. (1981). Osmoregulatory salt transporting mechanisms. Ann. Rev. Physiol. **43**, 493-505.

KULLBERG, R. (1987). Stretch-activated ion channels in bacteria and animal cell membranes. Trends Neurosci. **10**, 387-388.

LABARCA, P.P. & MILLER, C. (1981). A K^+-selective, three-state channel from frgmented sarcoplasmic reticulum of frog leg muscle. J. Membrane Biol. **61**, 31-38.

LACKIE, J.M. (1986). Cell Movement and Cell Behavior. Allen and Unwin, Boston.

LAMOUREUX, P., BAXBAUM, R.E. & HEIDEMANN, S.R. (1989). Direct evidence that growth cones pull. Nature **340**, 159-162.

LANDAW, E.M. & DISTEFANO III, J.J. (1984). Multiexponential, multicompartmental, and noncompartmental modelling. II. Data analysis and statistical considerations. Am. J. Physiol. **246**, R665-R677.

LANSMAN, J.B., HALLAM, T.J. & RINK, T.J. (1987). Single stretch-activated ion channels in vascular endothelial cells as mechano-transducers?. Nature **325**, 811-813.

LATORRE, R. & MILLER, C. (1983). Conduction and selectivity in potassium channels. J. Membrane Biol. **71**, 11-30.

LATORRE, R., VERGARA, C. & HIDALGO, C. (1982). Reconstitution in planar lipid bilayers of a Ca^{2+}-dependent K^+ channel from transverse tubule membranes isolated from rabbitskeletal muscle. Proc. Natl. Acad. Sci. U.S.A. **79**, 805-809.

LEESON, C.R. & LEESON, T.S. (1976). Histology. W.B. Saunders Company, Toronto , 533-535.

LETOURNEAU, P.C., SHATTUCK, T.A. & RESSLER, A.H. (1987). "Pull" and "push" in neurite elongation: Observations on the effects on different concentrations of cytochalasin B and taxol. Cell Motil. Cytoskel. **8**, 193-209.

LIPSCOMBE, D., MADISON, D.V., POENIE, M., REUTER, H., TSIEN, R.W. & TSIEN, R.Y. (1988). Imaging of cytosolic Ca^{2+} transients arising from Ca^{2+} stores and Ca^{2+} channels in sympathetic neurons. Neuron 1, 355-365.

LOWENSTEIN, W.R. & SKALAK, R. (1966). Mechanical transmission in a pacinian corpuscle. An analysis and a theory. J. Physiol. 182, 346-378.

LUX, H.D., NEHER, E. & MARTY, A. (1981). Single channel activity with the calcium dependent outward current in Helix pomatia. Pflugers Arch. 389, 293-295.

MAGELBY, K.L. & PALLOTTA, B.S. (1983). Interpretation of the distributions of the open and shut intervals of the calciumm-activated potassium channel in terms of molecular mechanism. Biophys. J. **41**, 280a.

MARTINAC, B., BUECHNER, M., DELCOUR, A.H., ADLER, J. & KUNG, C. (1987). Pressure sensitive ion channel in Escherichia coli. Proc. Natl. Acad. Sci. U.S.A. 84, 2297-2301.

MARTY, A. (1981). Ca-dependent K channels with large unitray conductance in chromaffin cell membranes. Nature **291**, 497-500.

MATTSON, M.P. & KATER, S.B. (1987). Calcium regulation of neurite elongation and growth cone motility. J. Neurosci. **7**, 4034-4043.

MEDINA, I.R. & BREGESTOVSKI, P.D. (1988). Stretch-activated ion channels modulate the resting membrane potential during early embryogenesis. Proc. R. Soc. Lond. B 235, 95-102.

MEECH, R.W. & STRUMWASSER, F. (1970). Intracellular calcium injection activates potassium conductance in Aplysia nerve cells. Fed. Proc. 29, 834.

MENDENHALL, W. (1975). Introduction to probability and statistics. Wadsworth Publishing Co, Belmont, CA , 260-261.

METHFESSEL, C., WITZEMANN, V., TAKAHASHI, T., MISHINA, M., NUMA, S. & SAKMANN, B. (1986). Patch clamp measurements on Xenopus laevis oocytes: currents through endogenous channels and implanted acetylcholine receptor and sodium channels. Pfleugers Arch. **407**, 577-588.

MILLER, C., STAHL, N. & BARROL, M. (1988). A thermodynamic analysis of monovalent cation permeation through a K^+-selective ion channel. Neuron 1, 159-164.

MILLET, B. & PICKARD, B.G. (1988). Gadolinuium ion is an inhibitor suitable for testing the putative role of stretch-activated ion channels in geotropism and thigmotropism. Biophys. J. **53**, 155a.

MOODY, W.J. & BOSMA, M.M. (1989). A nonselective cation channel activated membrane deformation in oocytes of the ascidian Boltenia villosa. J. Membrane Biol. **107**, 179-188.

MORETON, R.B. & GARDNER, D.R. (1976). Frescon: Neurophysiological action of a molluscide. Experientia **32**, 611-612.

MORRIS, C.E. (1989). Mechanosensitive ion channels. J. Membrane Biol. In press.

MORRIS, C.E. & SIGURDSON, W.J. (1989). Stretch-inactivated ion channels coexits with stretch-activated ion channels. Science **243**, 807-809.

MORRIS, C.E., WILLIAMS, B. & SIGURDSON, W.J. (1989). Comp. Biochem. Physiol. **92A**, 479-483.

MORRIS, C.E., MONTPETIT, M.R., SIGURDSON, W.J. & IWASA, K. (1989). Activation by curare of acetylcholine receptor channels in a murine skeletal muscle cell line. Can. J. Physiol. Pharmacol. **67**, 152-158.

MUELLER, P.R.D.O., RUDIN, D.O., TIEN, H.T. & WESCOTT, W.C. (1962). Reconstitution of excitable cell membrane structure in vitro. Circulation **26**, 1167-1171.

NAKACHE, M. & GAUB, H.E. (1988). Hydrodynamic hyperpolarization of endothelial cells. Proc. Natl. Acad. Sci. U.S.A. **85**, 1841-1843.

NEHER, E. & SAKMANN, B. (1976). Single-channel currents recorded from membrane of denervated frog muscle fibers. Nature **260**, 799-802.

NEHER, E., SAKMANN, B. & STEINBACH, J.H. (1978). The extracellular patch clamp: A method fro resolving currents through individual open channels in biological membranes. Pfleugers Archiv. **375**, 219-228.

NEYTON, J. & MILLER, C. (1988). Discrete Ba^{2+} block as a probe of ion occupancy and pore struture in the high-conductance Ca^{2+}-activated K^+ channel. J. Gen. Physiol. **92**, 569-586.

NIER, K. (1975). Stabilization phenomena in synchronous neural activity of vibrissa receptors. In The Somatosensory System. Edited H.H. Kornhuber. Georg Thiem Publishers, Suttgart. 204-207.

OHMORI, H. (1984). Mechanoelectrical transducer has discrete conductances in the chick vestibular hair cell. Proc. Natl. Acad. Sci. USA **81**, 1888-1891.

OHMORI, H. (1987). Gating properties of the mechano-electrical transducer channel in the dissociated vestibular hair cell of the chick. J. Physiol. **387**, 589-609.

OLESEN, S.P., CLAPHAM, D.E. & DAVIES, P.F. (1988). Haemodynamic shear stress activates a K^+ current in vascular endothelial cells. Nature 331, 168-170.

PALLOTTA, B.S., MAGLEBY, K.L. & BARRETT, J.N. (1981). Single channel recordings of Ca^{2+}-activated K^+ currents inrat muscle cell culture. Nature **293**, 471-475.

PASZTOR, V.M. & BUSH, B.M. (1987). Peripheral modulation of mechano-sensitivity in primary afferent neurons. Nature **326**, 793-795.

PICHON, Y. & TREHERNE, J.E. (1976). The effects of osmotic stress on electrical properties of the axons of a marine osmoconformer (Maia squinado. Brachyara: Crustacea). J. exp. Biol. **65**, 553-563.

PIOMELLI, D., VOLTERRA, A., DALE, N., SIEGELBAUM, S.A., KANDEL, E.R., SCHWARTZ, J.H. & BELARDETTI, F. (1987). Lipoxygenase metabolites of arachidonic acid as second messengers for presynaptic inhibition of Aplysia sensory cells. Nature **328**, 38-43.

REUTER, H. & STEVENS, C.F. (1980). Ion conductance and ion selectivity of potassium channels in snail neurones. J. Membrane Biol. **57**, 103-118.

RORIVE, G. & GILLES, R. (1979). Intracellular inorganic osmotic effectors. In Mechanisms of Osmoregulation in Animals, edited by R. Gilles. John Wiley & Sons , 83-109.

SACHS, F. (1986). Biophysics of mechanoreception. Membr. Biochem. **6**, 173-195.

SACHS, F. (1987). Barorecptor mechanisms at the cellular level. Fed. Proc. **46**, 12-16.

SACHS, F. (1988). Mechanical transduction in biological systems. CRC Critical Reviews in Biomedical Engineering **16**, 141-169.

SACKIN, H. & PALMER, L.G. (1987). Basolateral potassium channels in renal proximal tubule. Am. J. Physiol. **253**, F476-F487.

SACKIN, H. (1987). Stretch-activated potassium channels in renal proximal tubule. Am. J. Physiol. **253**, F1253-F1262.

SACKIN, H. (1989). A stretch-activated K^+ channel sensitive to cell volume. Proc. Natl. Acad. Sci. U.S.A **86**, 1731-1735.

SAKMANN, B. & NEHER, E. (1983). Geometric parameters of pipettes and membrane patches. In Single-channel Recording Eds. B. Sakmann and E. Neher. Plenum Press, New York , 37-51.

SAMI, Y., MARTINAC, B., GUSTIN, M.C., CULBERTSON, M.R., ADLER, J. & KUNG, C. (1988). Ion channels in Paramecium, yeast and Escherichia coli. Trends Neurosci. **13**, 304-309.

SARKADI, B., MACK, E. & ROTHSTEIN, A. (1984). Ionic events during the

volume response of human peripheral blood lymphocytes to hypotonic media. J. Gen. Physiol. **83**, 497-512.

SATTELLE, D.B. (1974). Electrophysiology of the giant nerve cell bodies of Limnaea stagnalis (L) (Gastropoda: Pulmonta). J. exp. Biol. **60**, 653-671.

SCHREINER, W., KRAMER, M., KRISCHER, S. & LANGSAM, Y. (1985). Nonlinear least-squares fitting. PC Tech. J. **3**, 170-190.

SHUSTER, M.J. & SIEGELBAUM, S.A. (1987). Pharmocological characterization of the serotonin-sensitive potassium channel of Aplysia sensory neurons. J. Gen. Physiol. **90**, 587-608.

SHUSTER, M.J., CAMARDO, J.S., SIEGELBAUM, S.A. & KANDEL, E.R. (1985). Cyclic AMP-dependent protein kinase closes the serotonin-sensitive K^+ channels of Aplysia sensory neurons in cell-free membrane patches. Nature **313**, 392-395.

SIEGELBAUM, S.A., CAMARDO, J.S. & KANDEL, E.R. (1982). Serotonin and cyclic AMP close single K^+ channels in Aplysia sensory neurones. Nature **299**, 413-417.

SIEGELBAUM, S.A., BELARDETTI, F., CAMARDO, J.S. & SHUSTER, M.J. (1986). Modulation of the serotonin-sensitive potassium channel in Aplysia sensory neurone cell body and growth cone.. J. exp. Biol. **124**, 287-306.

SIGURDSON, W.J. & MORRIS, C.E. (1989). Stretch-activated ion channels in growth cones of snail neurons. J. Neurosci. **9**, 2801-2808.

SIGURDSON, W.J., MORRIS, C.E., BREZDEN, B.L. & GARDNER, D.R. (1987a). Stretch activation of a K channel in molluscan heart cells. J. exp. Biol. **127**, 191-209.

SIGURDSON, W.J., BEDARD, E. & MORRIS, C.E. (1987b). Stretch-activated (SA) channels in molluscan neurons. Biophys. J. **51**, 50a.

SIMAN, R., BAUDRY, M. & LYNCH, G. (1985). Regulation of glutamate receptor binding by the cytoskeletal protein fodrin. Nature **313**, 225-228.

SMITH, S.J. (1988). Neuronal cytomechanics: The actin-based motility of growth cones. Science **242**, 708-715.

SOKAL, R.R., ROHLF, F.J. (1981). Biometry. W.H. Freeman and Company. pp499-508.

SRINIVASAN, Y., ELMER, L., DAVIS, J., BENNETT, V. & ANGELIDES, K. (1988). Ankyrin and spectrin associate with voltage-dependent sodium channels in brain. Nature **333**, 177-180.

STOCKBRIDGE, L.L. & FRENCH, A.S. (1988). Stretch-activated cation channels in human fibroblasts. Biophys. J. **54**, 187-190.

TAGLIETTI, V. & TOSELLI, M. (1988). A study of stretch-activated channels in the membrane of frog oocytes: Interactions with Ca^{2+} ions. J. Physiol. 407, 311-328.

TIVEY, D.R., SIMMONS, N.L. & AITON, J.F. (1985). Role of passive potassium fluxes in cell volume regulation in cultured HeLa cells. J. Membrane Biol. 87, 93-105.

TOSNEY, K.W. & WESSELLS, N.K. (1983). Neuronal motility: The ultrastructure of veils and microspikes correlates with their motile activities. J. Cell Sci. 61, 389-411.

TREHERNE, J.E. (1980). Neuronal adaptations to osmotic and ionic stress. Comp. Biochem. Physiol. 67B, 455-463.

UBL, J., MURER, H. & KOLB, H.A. (1988a). Ion channels activated by osmotic and mechanical stress in membranes of opossum kidney cells. J. Membrane Biol. 104, 223-232.

VIERCK, C.J. (1975). Proprioceptive deficits after dorsal column lesions in monkeys. In The Somatosersory System, ed. H.H. Kornhuber, Stuttgart, Thieme , 310-317.

VILLARROEL, A., ALVAREZ, O., OBERHAUSER, A. & LATORRE, R. (1988). Probing a Ca^{2+}-activated K^+ channel with quaternary ammonium ions. Pfleugers Arch. 413, 118-126.

WONG, B.S., LECAR, H. & ADLER, M. (1982). Single calcium-dependent potassium channels in clonal anterior pituitary cells. Biophys. J. 39, 313-317.

WOODHULL, A.M. (1973). Ionic blockage of sodium channels in nerve. J. Gen. Physiol. 61, 687-708.

YANG, X.C. & SACHS, F. (1987). Stretch-activated channels in several tissues. Biophys. J. 51, 252a.

YANG, X. & SACHS, F. (1989). Block of stretch-activated ion channels in Xenopus oocytes by gadolinium and calcium ions. Science 243, 1068-1071.

YANG, X.C., GUHARAY, F. & SACHS, F. (1986). Mechanotransducing ion channels: Ionic selectivity and coupling to visoelastic components of the cytoskeleton. Biophys. J. 49, 373a.

YAZEJIAN, B. & BYERLY, L. (1989). Voltage-independent barium-permeable channel activated in Lymnaea neurons by internal perfusion or patch excision. J. Membrane Biol. 107, 63-75.

YELLEN, G. (1982). Single Ca^{2+}-activated nonselective cation channels in neuroblastoma. Nature 296, 357-359.

YELLEN, G. (1984a). Ionic permeation and blockade in Ca^{2+}-activated K^+ channels of bovine chromaffin cells. J. Gen. Physiol. 84, 157-186.

YELLEN, G. (1984b). Relief of Na^+ block of Ca^{2+}-activated K^+ channels by external cations. J. Gen. Physiol. **84**, 187-199.

YELLEN, G. (1987). Permeation in potassium channels: Implications for channel structure. Ann. Rev. Biophys. Biophys. Chem. **16**, 227-246.

ZAGOTTA, W.N., BRAINARD, M.S. & ALDRICH, R.W. (1988). Single-channel analysis of four distinct classes of potassium channels in Drosophila muscle. J. Neurosci. 8, 4765-4779.

Appendix 1. Dependence of stretch-sensitivity on SA channel density

As described by Guharay and Sachs (1984) and Sachs (1988) the effective SA channel radius must be greater than any "reasonably" sized protein. This implies that cytoskeletal structures link the channels into a tension sensing network. The effective channel radius will determine channel density (D), total channel number (N) and therefore the magnitude of the whole cell current (I) (equation A1.1; equations 9-12 have been reproduced here for ease of reference).

$$I = gNP_oV_m \qquad \text{(A1.1)}$$

Channel open probability (P_o) is given by,

$$P_o = 1/(1 + K_{eq}\exp(-\theta P^2) \qquad \text{(A1.2)}$$

where θ is the channel's stretch sensitivity parameter as defined by

$$\theta = \frac{d^2A}{32K_AkT} \qquad \text{(A1.3)}$$

and k is the Boltzmann constant, T is absolute temperature, d is patch diameter (μm), A is channel area (Å), P is pressure (cmHg) and K_{eq} is the ratio of opening and closing rates at zero tension for a simple two state system (Cooper et al., 1986). Equation A1.3 reduces to

$$\theta = \frac{1.73 \times 10^{-3}r^2}{K_A} \qquad \text{(A1.4)}$$

when the d is 2 μm. Θ is therefore dependent on channel radius and area elasticity, K_A. For any given operating tension and channel K_A, there will an optimum D; high tensions allow greater densities while stiff channels (high K_A's) require lower densities (effective radius must be larger in order to gather more mechanical energy).

Density optima (in terms of whole cell current calculated from equations A1.1 and A1.2) may be derived analytically (see Sachs, 1988) or, as I have done here (Fig. A1), graphically presented for a range of D's (from channel radii) at one tension. These curves (Fig. A1) implicitly show that stretch-sensitivity (Θ) varies with D and in turn with K_A. Reasonable estimates of protein area elasticities (K_A = 10,000 dyn/cm) show optimal channel densities of 1 to 10 μm^{-2}.

Figure A1. Maximum patch current is dependent on channel density. Curves were generated for a range of effective channel radii (from 100 to ~30,000 Å) giving a range of channel densities of <0.03 to >3,000 μm^{-2}. Stretch-sensitivity was calculated for each channel radius assuming a patch diameter of 2 μm and a temperature of 20°C (equation A1.3 and A1.4). Θ was then used to calculate P_o (equation A1.2) at an arbitrary pressure (2 cmHg, K_{eq} = 1000). Whole patch current was then determined using equation A1.1 (V_m = 20 mV). When four such curves are plotted, each differing only by the value of K_A (ranging from 500 dyn/cm to 50,000 dyn/cm), it is clearly shown that a maximum current occurs at specific D's. As the channels are "made" stiffer, the optimum D decreases; soft channels (K_A = 500 dyn/cm) allow greater densities. Because D's were not constrained, i.e. some densities were calculated that produced a total area (total channel number x channel radius) which could exceed the membrane area, a secondary current increase occurs at high densities.

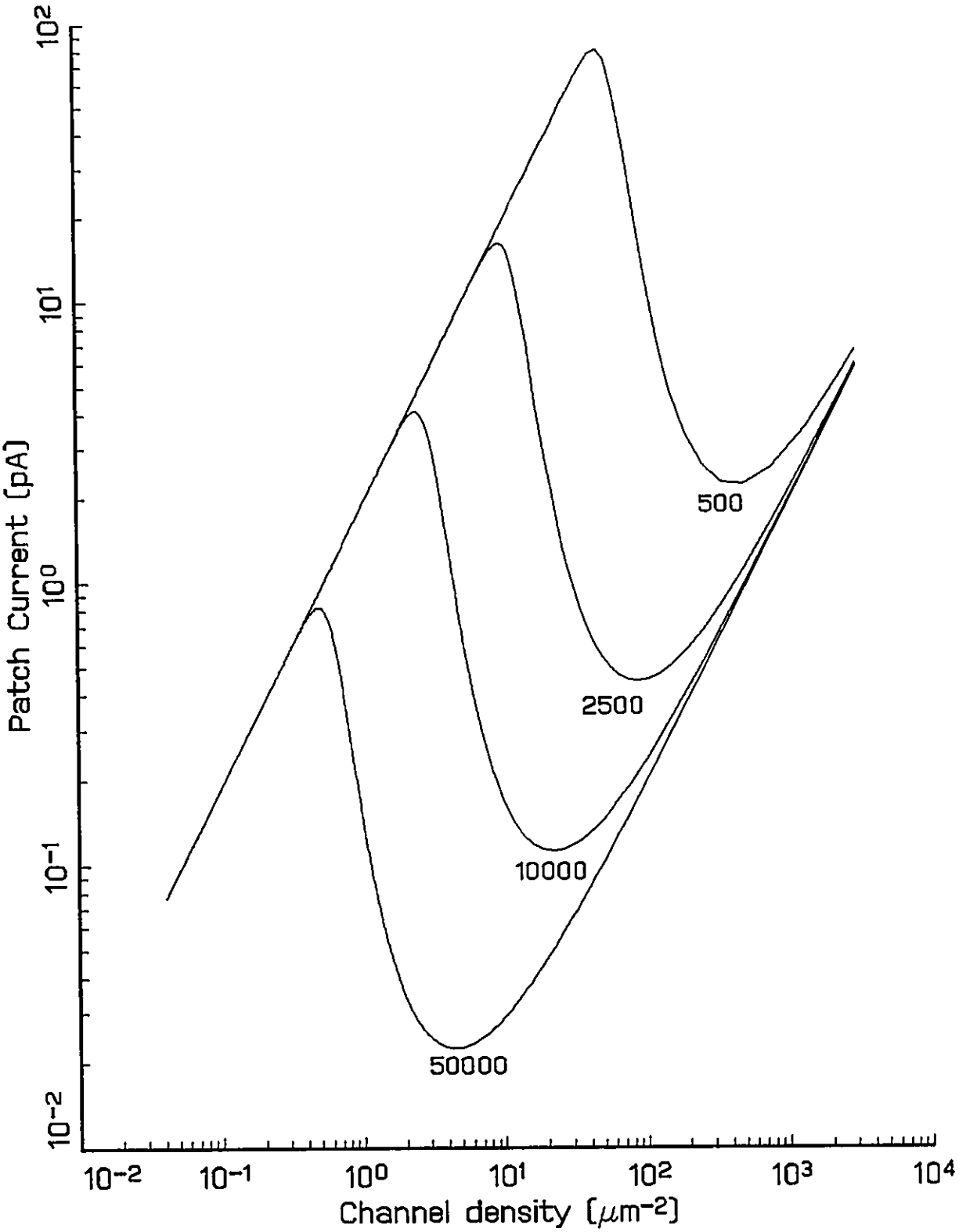
Patch Current [pA]
10^{2}
10^{1}
10^{0}
10^{-1}
10^{-2}
500
2500
10000
50000
10^{-2}
10^{-1}
10^{0}
10^{1}
10^{2}
10^{3}
10^{4}
Channel density [μm^{-2}]

Appendix 2. Voltage-dependent block

Woodhull (1973) proposed a simple mechanism to explain voltage-dependent block of ion channels with charged blockers. The model is based on several assumptions of which the most pertinent are: 1) There is a single blocking site within or near the ion channel's permeation pathway, that when occupied by the blocker, prevents passage the "normal" ionic species, i.e., there will be no current flow; 2) The blocker has negligible channel permeability, i.e., it does not pass through the channel; 3) The blocker binding site may reside within the electric field across the membrane which will cause the binding and unbinding rates to be exponential functions of the electric field felt at that site.

This would mean that an externally applied, positively charged blocker will block less effectively when the membrane potential is made more positive (in cell-attached patches this is done by making the patch pipette more negative relative the inside of the cell). The degree of voltage-dependency is dependent on where the binding site is located with respect to the electric field across the membrane, i.e. the fraction of the voltage field the blocker "sees" when at the binding site. The fractional electrical distance, δ, will be unity when the blocker experiences the entire voltage field or will be zero if the binding site is not within the electric field.

Coronado and Miller (1979) and Yellen (1984a) employed the following function (after Woodhull, 1973) to describe the fractional decrease in current in terms of the zero-voltage dissociation constant ($K_d(0)$) and δ.

$$i = \frac{i_o}{1 + [B]/K_d(0)\exp(zF\delta V/RT)} \qquad (A2.1)$$

which, rearranged and linearized gives

$$\ln(i_o/i - 1) = \ln \frac{[B]}{K_d(0)} + \frac{F\delta V}{RT} \qquad (A2.2)$$

where i_o is the unblocked single-channel current, i the blocked current, [B] blocker concentration, V the voltage, z the blocker valence and F, R and T have their usual meanings. A linear regression plot of $\ln(i_o/i - 1)$ *vs* voltage gives the slope as δ and the y-intercept which yields $K_d(0)$ (where $K_d(0)$ = [B]/exp(y-intercept). Alternatively, equation A1 may be fit to the data using a non-linear curve-fitting routine which extracts estimates of δ and $K_d(0)$ directly. The form of equation A1 dictates that for positively charged blockers, δ will be negative when the blocker is present on the extracellular (outside) side of the membrane. Conversely, δ will be positive if the blocker were negatively charged or positively charged and on the intracellular (inside) side.

Examples of the expected voltage-dependency of block can easily be obtained by generating I/V curves (using the GHK current equation to produce i_o) and calculating i from equation A1 for different δ's and $K_d(0)$'s. Fig. A2 gives 4 examples of I/V relations created in this way. In all examples the blocker is assumed to be positively charged unless otherwise indicated. The first 3 figures (Fig. A2 a,b,c) demonstrate the effects of changing both the sign and magnitude of δ (with constant $K_d(0)$ and [B]) under hypothetical symmetrical (Fig. A2a) and asymmetrical ionic conditions (Fig. A2b,c); the latter are comparable to the cell-attached, NS in pipette conditions used to study the effects of quinidine and TEA on SAK channels.

As shown in Fig. A2a, when the blocker is positively charged and is on the external side of the membrane, the blocked current becomes almost equivalent to the unblocked current at positive membrane potentials (δ = -0.5), but is greatly accentuated at negative potentials. When blocker is on the internal side (δ = 0.5) the converse is true. In Fig. A2b, under conditions of outward current rectification, block voltage-dependency is seen at large positive potentials where block is attenuated (δ = -0.5). If the blocker were negatively charged or on the inside (δ = 0.5), block is accentuated. Fig. A2c shows too extremes of the degree of voltage-dependent block, i.e. when δ is near -1 (-0.99) or near zero (-0.01).

In Fig. A2d, values for δ and $K_d(0)$ extracted from TEA voltage-dependent block of SAK channels were used for the calculation of i (i_o was calculated as in Figs. A2b and c). The similarity of the shape of these curves (those with δ negative, circles and triangles) with those of the real TEA data (see Fig. 22a) lends some confidence to my conclusion that SAK channel block by external TEA is voltage dependent, with the binding site between 0.22 and 0.31 into the electric field and a $K_d(0)$ of about 20 mM. It does not appear that TEA, which is positively charged, permeates the channel or membrane and blocks from the inside, since curves for positive δ's (pluses and crosses) are unlike those for the real data.

Figure A2. Calculated I/V relations demonstrating the effects of voltage-dependent block. **a)** i_o current (solid line in this and **b**, **c** and **d**) calculated from GHK current equation using P_K = 4.9 x 10^{-13} cm s^{-1} and $[K]_o$ and $[K]_i$ = 50 mM. Blocked current, i, calculated from equation A1 using δ equal to -0.5 (circles) and 0.5 (triangles), $K_d(0)$ = 2 mM and [B] = 1 mM. **b)** I/V curves generated as in **a**, except that $[K]_o$ = 1.6 mM. I_o outward rectification is more symbolic of the data obtained in cell-attached recording conditions used in during the quinidine and TEA experiments described in Chapter 3. **c)** Comparison of the calculated blocked current obtained with strong (δ = -0.99) and weak voltage-dependence (δ = -0.01). I_o calculated as in **b**. **d)** When values for δ and $K_d(0)$ obtained from TEA block I/V curves (Chapter 3) are inserted in equation A1 (circles, [B] = 10 mM, $K_d(0)$ = 25 mM, δ = -0.24; triangles, [B] = 20 mM, $K_d(0)$ = 16 mM, δ = -0.32), the resulting I/V curves are quite similar in shape to I/V curves constructed from the real data (current magnitudes are not the same). Reversal of δ's sign (pluses and crosses, δ = 0.24 and 0.32 respectively) produces curves quite unlike those of the real data (compare with Fig. 22a in Chapter 3).

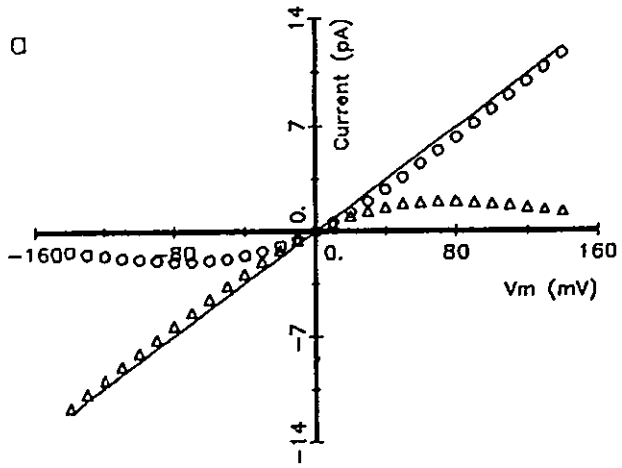
a
Current (pA)
14
7
0.
-7
-14
-160
-80
0.
80
160
Vm (mV)

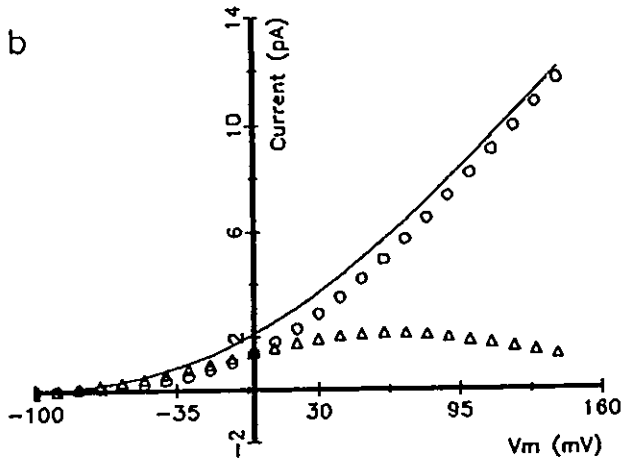
b
Current (pA)
14
10
6
2
-2
-100
-35
30
95
160
Vm (mV)

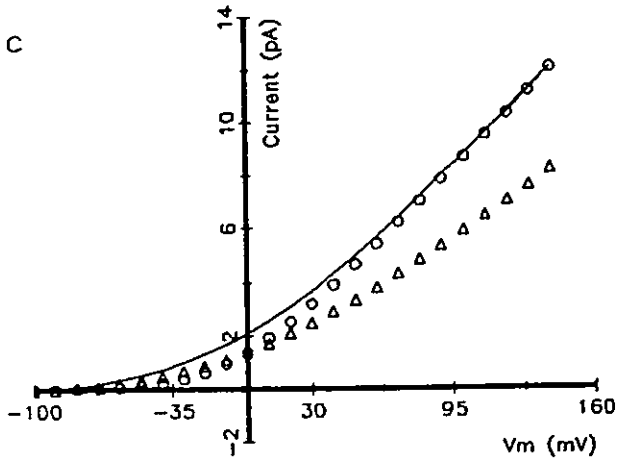
c
Current (pA)
14
10
6
2
-2
-100
-35
30
95
160
Vm (mV)

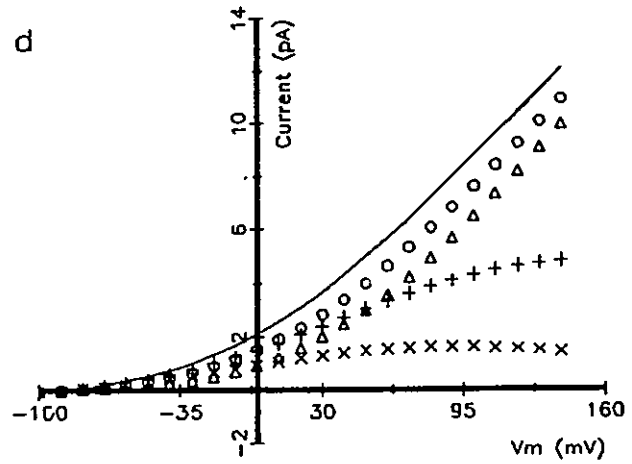
d
Current (pA)
14
10
6
2
-2
-100
-35
30
95
160
Vm (mV)

Appendix 3. Selection of models for growth cone shape

Calculations of whole-cell current flux are dependent not only channel, membrane and solution properties, but also on the shape and size of the cell. The number of channels in a cell is dependent on channel density and total membrane area, which is in turn related to cell shape and size, since scaling of surface to volume ratios (S:V) depend on the geometric model used to simulate the cell. For neuron cell bodies, a sphere appears to be a good approximation. Growth cones, on the other hand, are more like cylinders, but are not completely circular in cross section (see Chapter 5). A half-cylinder (split length-wise) is a better approximation of growth cone shape.

How do the choices of cell-shape affect the calculations of K^+ efflux made in Chapter 3? Recall that the area of a sphere is

$$A_s = 4\pi r^2$$

and the volume

$$V_s = 4\pi r^3/3$$

For cylinders (including both ends)

$$A = 2\pi rl + 2\pi r^2$$

and volume

$$V = \pi r^2 l$$

For a half-cylinder, area is

$$A_c = \pi rl + \pi r^2/2 + 2rl$$

and volume

$$V_c = \pi r^2 l/2$$

For a sphere, area scales with volume as

$$A_s = 3V_s/r$$

whereas the area of a half-cylinder scales with volume as

$$A_c = 2V_c/r + V_c/l + 2rl$$

where r is radius and l cylinder length. For spheres, a 10 fold increase in radius results in a 10 fold decrease in the S:V ratio; in half-cylinders this is a 7 fold decrease.

Growth cones have diameters of about 10 μm. The area which is known to contain SAK channels (see Chapter 5) extends back at least 10 μm from the growth cone tip, so that an estimate of a 10 μm growth cone length is reasonable. Volumes and areas for these dimensions for spheres and half-cylinders are 0.52 pl, 314 μm^{-2} and 0.4 pl, 296 μm^{-2} respectively (S:V ratios of 604 and 740 respectively). This means that the sphere model underestimates the amount of membrane area, the number of channels and therefore the potential increase in K^+ conductance. When K^+ loss/second is calculated for the two models, the half-cylinder looses 4% of its K^+ and the sphere 3.2%.